

A Comprehensive Dynamical Model for Human $\text{Ca}_v1.2$ Ion Channel:
Structural and Functional Studies

by

Tianhua Feng

A thesis submitted in partial fulfillment of the requirements for the degree of

Master of Science

in

Pharmaceutical Sciences

Faculty of Pharmacy and Pharmaceutical Sciences
University of Alberta

© Tianhua Feng, 2019

ABSTRACT

Human Cav1.2 is a voltage-gated calcium channel (VGCC), which plays an essential role to maintain a normal cardiac function. Any abnormalities in Cav1.2 can lead to serious cardiac diseases (e.g. cardiac arrhythmias and Timothy syndrome). Thus, understanding the structure-function-dynamics relationships of Cav1.2 is important to avoid and develop treatments of these diseases. Several small molecules (e.g. dihydropyridines and phenylalkylamine) have been identified and designed to modulate the activity of Cav1.2. Yet, their mode and site of action within the Cav1.2 channel are still unclear. In order to understand how these drugs interact with Cav1.2, a detailed three-dimensional structure of the human Cav1.2 channel is necessary. However, such structures have not been resolved yet.

Toward this goal, this thesis employed computational molecular modeling techniques to model the transmembrane α_1 -subunit three-dimensional (3D) structure of the open and closed Cav1.2 channel. We used a combination of homology modeling and threading approaches along with classical and advanced molecular dynamics simulations to explore the conformational transitions between the closed and the open states of the channel. The ultimate goal was to predict the binding orientation and critical interactions for known Cav1.2 modulators.

Our molecular dynamics simulations revealed many conformational changes in the pore and voltage-sensing domains of the Cav1.2 channel. The mode-of-binding of Amlodipine, Diltiazem, and Verapamil were also identified to the atomic level. Our binding affinity calculations suggest that both Amlodipine and Verapamil have a high potential to block the Cav1.2 channel. The conformational dynamics and the interactions reported from our binding mode analysis will be useful for understanding the structure-function-dynamic relationship in the Cav1.2 channel and guiding future drug design efforts.

PREFACE

A version of Chapter 1 has been published as a book chapter: *Feng Tianhua, Subha Kalyaanamoorthy, and Khaled Barakat. "L-Type Calcium Channels: Structure and Functions." Ion Channels in Health and Sickness. IntechOpen, 2018 Oct 10:127-148.*

A version of Chapter 2 has been published as a research article: *Feng Tianhua, Aravindhana Ganesan, Subha Kalyaanamoorthy, and Khaled Barakat. "Atomistic modeling and molecular dynamics analysis of human Cav1.2 channel using external electric field and ion pulling simulations." Biochim Biophys Acta Gen Subj. 2019 Jun;1863(6):1116-1126.*

A version of Chapter 3 has been submitted as a research article to the Journal of Molecular Modeling as *Feng Tianhua and Khaled Barakat. "Effects of Drug Binding on The Ion Permeation Through The Human Cav1.2 Ion Channel: A Computational Study".*

A version of Appendix A and Appendix B has been published as a book chapter: *Tianhua Feng and Khaled Barakat. "Molecular Dynamics Simulation and Prediction of Druggable Binding Sites." Methods Mol Biol. Springer, 2018;1762:87-103.*

ACKNOWLEDGEMENTS

I would like to express my sincere gratitude to my supervisor, Dr. Khaled Barakat, who enabled my research for his support and motivation throughout the course of my degree. His guidance helped me in all the time of research and writing from the beginning of my thesis. This project couldn't be completed without his generous kindness and gracious blessings. I also wish to thank my committee members Dr. Arno Siraki, Dr. Ayman El-Kadi, and Dr. Carlos A. Velázquez-Martínez.

I acknowledge my other mentors, Dr. Subha Kalyaanamoorthy, Dr. Aravindhan Ganesan, and Dr. Marawan Ahmed, for their invaluable help and time in completing my research projects. I also acknowledge my other labmates Horia Jalily Hasani, Rui Chen, Yasser Tabana, and Farag Mosa. The spiritual encouragement from my parents supports me in everyday of my life.

Last but not least, I would like to thank the financial assistance from the University of Alberta, the computational resources from the Compute Canada, as well as financial support from the Shoppers Drug Mart Graduate Scholarship.

TABLE OF CONTENTS

CHAPTER 1: INTRODUCTION	1
1.1: Introduction.....	3
1.2: Voltage-Gated Calcium Channel.....	4
1.2.1: Cardiac action potential and voltage-gated calcium channels.....	4
1.2.2: Classification of calcium channels.....	6
1.3: L-Type Calcium Channels.....	10
1.3.1: Distribution of LTCC.....	10
1.3.2: L-type calcium channel subunits.....	12
1.3.3: Current state of LTCC structural research.....	14
1.3.4: Current State of LTCC Structural and Modelling Research.....	20
1.4: Human Cav1.2 Channel.....	28
1.4.1: Cav1.2 channel properties and structure.....	28
1.4.2: Cav1.2 channel regulation	29
RATIONAL, HYPOTHESIS, AND OBJECTIVES	32
CHAPTER 2: MODELING THE CARDIAC CAV1.2 ION CHANNEL	34
2.1: Introduction.....	34
2.2: Homology Modeling of Human Cav1.2 Alpha Subunit.....	36
2.3: Molecular Dynamic Simulations on Human Cav1.2.....	42
2.4: External Electric Field MD Simulation on Human Cav1.2.....	47
2.5: Conformational States of Human Cav1.2.....	49
2.6: Steered MD Simulation on Cav1.2	51
2.7: Ion Permeation.....	52
2.8: Open-State Conformation Cav1.2.....	59
2.9: Conclusion.....	61
CHAPTER 3: SMALL MOLECULES DOCKING ON HUMAN CAV1.2 CHANNEL	63
3.1: Introduction.....	63
3.2: Methods.....	68
3.2.1: Ligand preparation for docking.....	68
3.2.2: Flexible docking.....	69

3.2.3: MM-GBSA scoring.....	70
3.2.4: Classical MD simulations: parameters and protocol.....	71
3.2.5: MD-based MM-PBSA.....	72
3.2.6: Steered molecular dynamics simulations.....	73
3.2.7: Visualization and analysis.....	73
3.3: Results and Discussion.....	74
3.3.1: Rosetta flexible docking.....	76
3.3.2: Classical MD studies.....	83
3.3.3: MM-PBSA analysis.....	84
3.3.4: Modes of binding.....	85
3.3.5: Steered MD studies.....	90
3.4: Conclusion.....	95
CHAPTER 4: GENERAL DISCUSSION.....	97
CHAPTER 5: FUTURE PERSPECTIVES.....	103
BIBLIOGRAPHY.....	105
APPENDIX A: PREDICTION OF DRUGGABLE BINDING SITES.....	126
A.1: Introduction.....	126
A.2: Binding site identification and druggability evaluation	128
A.2.1: Binding site identification methods.....	128
A.2.2: Druggability evaluation methods.....	131
A.3: Importance of Protein Flexibility.....	133
A.3.1: Generation of conformation ensemble.....	134
A.3.2: Cosolvent molecular dynamics simulations.....	135
A.3.3: Site identification by ligand competitive saturation.....	136
A.3.4: WaterMap.....	137
A.4: Cases Studies.....	138
A.4.1: A catalytic site problem: Viral Neuraminidase.....	138
A.4.2: An allosteric site problem: G-Protein Coupled Receptor (GPCR)	139
A.4.3: A cryptic site problem: Bcl-xL protein.....	140
A.5: Conclusion.....	141
A.6: References.....	143

APPENDIX B: MOLECULAR DYNAMIC SIMULATIONS	147
B.1: Introduction.....	147
B.2: Classical MD Simulations.....	148
B.2.1: Limitations of classical MD.....	149
B.3: Enhanced MD Simulations.....	151
B.3.1: External electric field MD simulations.....	151
B.3.2: Steered MD simulations.....	152
B.4: References.....	153

LIST OF FIGURES

Figure 1.2.1. A). Cardiac action potential (top). B). Activities of three types cation channels during phase 2 (below).

Figure 1.2.2. Phylogenetic tree showing the evolutionary relationship among the members of the VGCCs.

Figure 1.3.1. The major tissue distribution and physiological functions of the four LTCC isoforms in human body.

Figure 1.3.2. The topology structure of LTCC complex.

Figure 1.3.3. The secondary structure topology of the α_1 -subunit of LTCCs.

Figure 1.3.4. The domain architecture and topology of β_1 -subunit (bottom), $\alpha_2\delta_1$ -subunit (top right) and γ_1 -subunit (left bottom).

Figure 1.3.5. The homo-tetramer architecture of CavAb includes six transmembrane segments, including voltage-sensor domain (VSD: S1-S4) and pore-forming domain (PFD: S5-S6).

Figure 1.3.6. The missing residues in the rabbit Cav1.1- α_1 subunit (PDB ID: 5GJV) shaded in grey.

Figure 1.3.7. A) The bottom view and B) the side view of pore-forming domain (S5-S6) in the human Cav1.2 α_1 homology model.

Figure. 1.4.1. The secondary structure topology of the hCav1.2 α_1 -subunit.

Figure 2.2.1. The sequence alignment between Human Cav1.2 α_1 (111-1527) and Rabbit Cav1.1 α_1 .

Figure 2.2.2. A) The Ramachandran plot, and B) protein structure of second hCav1.2 α_1 -subunit model.

Figure 2.2.3. The Ramachandran plots on hCav1.2 α_1 -subunit first, third, fourth, and fifth models.

Figure 2.2.4. A) The structure and position of the AID segment (yellow) in the hCav1.2 model. B) The Rabbit AID structure (cyan) superimposes with the AID of hCav1.2 model.

Figure 2.2.5. Classical MD simulation system on hCav1.2 channel, including solvent, ions, lipid bilayers, and transmembrane domain of human Cav1.2 channel.

Figure 2.2.6. A) The structure and position of the AID segment (yellow) in the hCav1.2 model. B) The Rabbit AID structure (cyan) superimposes with the AID of hCav1.2 model.

Figure 2.3.1. A) RMSD of ~100 ns length classical molecular dynamic of human calcium channel with 1) all-atom, 2) transmembrane helix, and 3) backbone of transmembrane helix. B) The CA-

RMSD of four transmembrane domains, DI, DII, DIII, and DIV from the last 50 ns of the simulation is shown in blue.

Figure 2.3.2. A) The RMSF and B) the structure of hCav1.2 α_1 -subunit with different colored domains and selectivity filter.

Figure 2.3.3. A) Three calcium ions (yellow) located close to the negatively charged ASP residues on the outer vestibule of the selectivity filter, B) Three calcium ions (yellow) on protein electrostatic surface (negatively charged shown as red, vice versa), and C) Distance between the three calcium ions and the corresponding carboxyl oxygen of the ASP residues.

Figure 2.3.4. Water molecules permeated into the center-cavity and SF after 100 ns MD and the changes pore-radius of hCav1.2 along 100 ns classical MD.

Figure 2.4.1. A) The pore domain of hCav1.2 embedded in the membrane with asymmetric ionic concentrations. B) Electrostatic potential map over a cross section of the system normal to the membrane averaged over the last 5 ns of the simulation trajectory. C) Electrostatic potential normal to the plane of membrane average along the Z-axis.

Figure 2.4.2. A) Overall ~300 ns-length RMSD plot, including ~100 ns of classical MD and 200 ns EEMD. B) 200 ns-length RMSD plot of EE-MD referred on the last frame of MD. C) The RMSF of residues in cMD and EE-MD. D) Pore-radius of simulation comparing with Cav open.

Figure 2.5.1. A) Clustering analysis for the classical MD (left) and external electric MD (right) trajectories. B) Heatmap based on the RMSD of classical (left) and external electric (right) MD clustered conformations.

Figure 2.7.1. Calcium ion permeation as seen in the SMD simulation of R6 replica A) Intracellular view and B) Z-axis view.

Figure 2.7.2. The force profile of SMD trajectories from R0 to R9 and the open Cav model.

Figure 2.7.3. Key residues in three SF-sites, site-1(left), site-2(middle), and site-3(right) of NOC simulation. Distances of residues and ion-residue pairs are showing the table below.

Figure 2.7.4. Water molecules and calcium ion forms H-bond with residues at the three Ca^{2+} binding sites in the selectivity filter, A) the site-1, B) the site-2, and C) the site-3.

Figure 2.7.5. Water molecules within 3.5Å of Ca^{2+} in the selectivity filter, central cavity, and internal gate of NOC.

Figure 2.8.1. A) Pore radius along Z-axis of NOC, Rabbit-based close and Eel-based open hCav1.2. B) Comparison of bending angle in NOC and eel-based open-state hCav1.2 model.

Figure 2.8.2. The pore-radius plot based on the last frame of three SMD simulation (black) with error bars (light blue).

Figure 2.8.3 A) Comparison of bending angles in the NOC (orange) and Eel-based (blue) open-state hCav1.2 model. B) The selectivity filter (orange) and S4 helix before cMD (red), after cMD (white) and NOC (blue).

Figure 3.2.1. The chemical structures of representative DHP and PAA calcium channel blockers. A) representative DHP antagonists. B) Representative PAA antagonists.

Figure 3.3.1. The permeation pathway (grey) of human Cav binds with calcium ion (yellow), nifedipine (blue), and verapamil (Orange). The binding sites of DHPs and PAAs are shaded in blue and orange.

Figure 3.3.2. The correlation between MM-GBSA binding energy and experimental binding affinity (IC_{50}) of, amlodipine, nifedipine, Isradipine, nifedipine, nimodipine, and verapamil ($R_{\text{perason}} = 0.7919$).

Figure 3.3.3. The RMSD value of human Cav1.2 complex with calcium channel blockers calculate along the ~10 ns length classical MD trajectory based on the initial conformation of the complex.

Figure 3.3.4. The comparison of RMSF value between protein (black) and complex (red), A) nifedipine, B) nimodipine. C) clevidipine, D) verapamil, and E) Br-verapamil. The underline indicates the region in complex are more flexible (yellow) or stable (blue) during the MD simulation.

Figure 3.3.5. The heatmap of residues in A) electrostatic interaction and B) Van der Waals interaction in DHP-binding complex, nifedipine, nimodipine, and clevidipine, and PAA-binding complex, verapamil and Br-verapamil.

Figure 3.3.6. A) The H-bond and B) the distance between residues and ligand in the DHP-type complex, including nifedipine, nimodipine, and clevidipine, and PAA-type complex, verapamil and Br-verapamil.

Figure 3.3.7. A) The force profiles of SMD on human Cav1.2, and B) The NOC conformation of human Cav1.2 channel. The force profile and structure align on the Z-axis direction. The calcium ion passed through the selective filter, central cavity, and internal gate.

Figure 3.3.8. The force profiles of SMD simulations on A) DHP-type inhibitors, including nifedipine (Orange), nimodipine (Blue), and clevidipine (Grey) B) PHE-type inhibitors, including Br-verapamil (Orange) and verapamil (Blue).

Figure A.1.1 Different types of binding sites include the active site (a), allosteric site (b), which can change their conformation before (pink) and after (blue) binding with allosteric modular, and cryptic binding site(c), which keep in continuous changing (blue and pink).

Figure A.2.1 Geometric-based binding site identification mechanism. The methods scan the grid points outside the protein for protein-solvent-protein and surface-solvent-surface events.

Figure A.2.2 Energy-based binding site identification mechanism. Different types of drug-like fragments dock on the protein surface. And, after two turns of cluster process, multiple fragments are gathering around the Consensus Sites.

Figure A.3.1 Surface representation of Bcl-xL in unbound and bound conformation. Based on the geometric feature, the binding site can be recognized as high druggability in bound conformation with Bak peptide (A). However, the same binding site of unbound Bcl-xL is identified as low druggability (B).

Figure A.3.2 The free-energy surface of protein. During the MD simulation, conformations of targeted protein are sampled. The local and global minimums are separated by energy barriers. The conformations may gather around local minimums and cannot reach global minimum, which leads to the insufficient sampling.

Figure A.4.1 2D chemical structure of Oseltamivir(a) and Zanamivir(b). They are both orthosteric inhibitors bind to the active site of Neuraminidase. Generated by Maestro.

Figure B.2.1 The free-energy surface of protein. During the MD simulation, conformations of targeted protein are sampled. The local and global minimums are separated by energy barriers.

LIST OF TABLES

Table 1.2.1. Blocker sensitivities of different HVA channels.

Table 2.1.1. The amino acid sequence comparison among human $\text{Ca}_v1.2$ α_1 -subunit, rabbit $\text{Ca}_v1.1$ α_1 -subunit, Eel $\text{Nav}1.2$ α_1 -subunit, and bacteria Ca_vAb channel.

Table 2.2.1. Structural quality scores of five hCaV1.2 homology models estimated from different structure evaluation programs.

Table 3.1.1. Common L-type calcium channel antagonists. The list of drugs and their 2D structures are obtained from the Drugbank database.

Table 3.3.1. The scores of Rosetta flexible docking between small molecules and human $\text{Ca}_v1.2$.

Table 3.3.2. The MM-GBSA binding free energy of complexes, between small molecules and human $\text{Ca}_v1.2$.

LIST OF ABBREVIATIONS

CaM	Calmodulin
VGIC	Voltage-Gated Ion Channel
VGCC	Voltage-Gated Calcium Channel
MD	Molecular Dynamics
SMD	Steered Molecular Dynamics
EE-MD	External Electric-Field Molecular Dynamics
Nav	Voltage-Gated Sodium Channel
Cav	Voltage-Gated Calcium Channel
Kv	Voltage-Gated Potassium Channel
NMR	Nuclear Magnetic Resonance
PDB	Protein Data Bank
PIP2	Phosphatidylinositol 4,5-bisphosphate
POPC	palmitoyl-oleoyl-phosphatidylcholine
RMSD	Root Mean Square Deviation
RMSF	Root Mean Square Fluctuations
SQTS	Short QT Syndrome
LQTS	Long QT Syndrome
hCav1.2	Human Cav1.2 Channel
NOC	Near-Open Conformation
cMD	Classical Molecular Dynamics
AID	Alpha Interacting Domain
SSR/SST	Sum of Squares Regression/ Total Sum of Squares
DBI	Davies-Bouldin Index
PCA	Principal Component Analysis
VSD	Voltage-Sensor Domain
PFD	Pore-Forming Domain
SF	Selectivity Filter
Cryo-EM	Cryogenic Electron Microscopy
HVA	High-Voltage-Activated
LVA	Low-Voltage-Activated

CHAPTER 1: INTRODUCTION¹

In 1953, Paul Fatt and Bernard Katz discovered the existence of calcium-conducting ion channels in the crustacean muscle Fatt and Katz (1953). Following this initial discovery, several reports confirmed the expression of these channels in various mammalian cell types including, skeletal, cardiac muscles and all excitable cells (Zamponi, Striessnig et al. 2015). In addition, the German physiologist Albrecht Fleckenstein discovered that Phenylalkylamine-related molecules, such as verapamil, closely mimicked the cardio-depressant actions of β -receptor antagonists while their action could not be explained through binding to β -adrenergic receptors (Dolphin 2006). Later, it became evident that the pharmacological actions of these molecules could be fully explained through their ability to block the “so-called” voltage-gated Ca^{2+} channels (VGCCs) in the nanomolar concentration range.

The normal functioning of ion channels involves numerous intricate details that have been the subject of research for many years. As one of the three main types of cation channels (i.e. calcium, potassium, and sodium channels), calcium ion channels participate in maintaining the heart rhythm (Striessnig, Pinggera et al. 2014). Voltage-gated calcium channels open in response to membrane depolarization and allow Ca^{2+} ions to enter the cells throughout its 10,000-fold chemical gradient across the membrane (Adiban, Jamali et al. 2016). Their dynamical action potentials are further translated into contractions and relaxations of the heart muscle. The critical role of VGCCs in the normal functioning of the heart is further emphasized by the number of diseases that result from mutations within these proteins. This makes it crucial to understand how they work. Thusly motivated, this thesis is focused on this complicated process, taking one calcium

¹ A version of this chapter has been published as a book chapter: *Feng Tianhua, Subha Kalyaanamoorthy, and Khaled Barakat. "L-Type Calcium Channels: Structure and Functions." Ion Channels in Health and Sickness. IntechOpen, 2018 Oct 10:127-148.*

channel as an example, namely the Cav1.2 calcium channel. This thesis employed several computational techniques to understand the structure, function, and dynamics of this channel. Furthermore, the models generated in this thesis illustrate the mode of action of known Cav1.2 modulators and predict their effects on ion passage through the channel.

As Cav1.2 channel is a voltage-gated ion channel, it is directly linked to the change of the membrane potential. It plays a significant role in controlling the depolarization phase of the cardiac action potential and its duration. This is important to maintain the normal pace of the heart. Furthermore, mutations in the cardiac Cav1.2 ion channel is a leading cause of heritable long QT syndrome (LQTS) (Giudicessi and Ackerman 2016), Short QT syndrome (SQTS) (Kim 2014), and cardiac arrhythmias (Striessnig, Pinggera et al. 2014), seizures (Ortner and Striessnig 2016), and sudden death (Abriel, Rougier et al. 2015).

The primary goal of this thesis is to develop a much-needed comprehensive structural model for the Cav1.2 ion channel in its active form as well as to understand the ion conduction mechanism and modes of drug binding. Our literature review identified many limitations and gaps in previous research, which we aimed to fulfill in the current model. With that in mind, the model for Cav1.2 ion channel was developed with the extensive inclusion of available experimental information as described. Our methodologies combined several cutting-edge modeling techniques. These included homology modeling to develop the initial Cav1.2 protein structure, classical as well as external electric field molecular dynamic (MD) simulation techniques to mimic the calcium channel under depolarization transmembrane potential. Multiple conformations of human Cav1.2 (hCav1.2) gathered from simulation trajectories to represent Cav1.2. These conformations were used for ion-pulling through the channel and ligand-docking to obtain ion conduction and drug-bound structures studies.

This thesis is organized as follows. Chapter 1 presents background information about the different types of calcium ion channels. This will be followed by a focus on the Cav1.2 ion channel, describing its structural properties, its role in controlling the action potential and its regulation by other cellular components. Chapter 1 also includes a literature review on the current state-of-art in this area and provides a detailed description of the research objectives and questions of this thesis. Chapter 2 describes our efforts in developing a comprehensive homology model for the Cav1.2 protein using computational techniques. In this chapter, we employ steered MD simulations to study ion permeation in Cav1.2. At the end of this chapter, we also report an open conformation for the human Cav 1.2 channel. Chapter 3 is focused on protein-drug binding simulations and the utilization of the model generated in Chapter 2 to study drug binding interactions and their effect on the ion influx through the channel. The overall findings are summarized in Chapter 4 with implications for future studies. Appendices of the Thesis describe the methods and parameters used in Chapters 2 and 3.

1.1 Introduction

Voltage-gated calcium channels (VGCCs/Cavs) regulate the permeation of calcium ion through the cellular cytoplasmic membrane (Catterall 2011, Dolphin 2016, Hering, Zangerl-Plessl et al. 2018). The voltage-sensor structure of the protein helps VGCCs to detect any change in the membrane potential and respond to this change during depolarization (as shown in Fig.1.2.1 and Fig.1.3.2). As calcium ions enter the cytoplasm through VGCCs, they serve as secondary electrical signal messengers and initiate multiple cellular events. In cardiac and neuronal cells, the excitation of VGCCs initiates cellular contraction and gene expression (Hofmann, Flockerzi et al. 2014). The depolarization of transmembrane potential can also stimulate VGCCs to control the secretion of hormones in the pancreatic and adrenal gland. On the other hand, VGCCs respond to alternative

depolarized potential to regulate neuronal excitability. Additionally, each type of calcium channel can be divided into different subtypes to control detail physiological functions

This section serves as the first part of the introduction chapter and begins with a general classification of the calcium channels and describes their main types and subtypes. The following section describes the distribution of calcium ion channels in the human body. Then, the chapter focuses on L-type calcium channels, which are largely expressed in the cardiac system and describes their associated cardiac currents. This chapter lays the background for the next chapters.

1.2 Voltage-Gated Calcium Channels

1.2.1 Cardiac action potential and voltage-gated calcium channels

The cardiac action potential is a classic example of the voltage-dependent mechanism. During the action potential, the ion channels undergo several conformational transitions and regulate the exchange of ions across the membrane. When the intracellular gates of the channel are open, the channel is referred to as conducting. The smooth passage of ions through the open-pore of the channel generates the electrical current across the membrane. More than 20 types of ion channels are expressed in the cardiac tissue, giving rise to several types of currents, each of which possesses specific characteristics (Grant 2009). The electrical charge on both sides of the cardiac cell membrane is altered even when a single ion channel is activated. This difference in the membrane charge is called membrane potential, which creates an activation signal and propagates throughout the heart. The action potential can be divided into five phases (Phase 0–4, shown in the Fig.1.2.1) and the concerted activities of various ion channels in the heart help in maintaining the cardiac rhythm. Cardiac action potential represents the changes in the voltage of a single cardiac cell plotted over time. It can be broken down into different phases that are the

result of atomic level changes in the ion channels. Below, we provide a simplistic view of how Cav channels play a role in pacing the cardiac cycle.

During phase 0, the membrane is initially at the resting potential (-90 mV, phase 4), where the VGCCs are in a closed-state (no Ca^{2+} ion passage). When depolarization occurs, and the membrane potential reaches a threshold voltage of -70 mV, the inward sodium ion (Na^+) channels are activated allowing the flow of the I_{Na} current. This current flow further increases the membrane potential to a more positive value and reaches a peak, when the activation of LTCCs are initiated, and the sodium channels are inactivated. At the end of the depolarization phase, the membrane potential is reaching at about +30 mV.

In Phase 1, which is called the initial/early repolarization, the Na^+ channels close as rapidly as they opened. This leads to a short and quick decline of the action potential. The potassium channels then open slowly, causing K^+ ions to move out of the cell and return the membrane voltage to approximately 0 mV. Early and rapid repolarization occurs by the brief activation of K^+ channels and the LTCCs remain in a pre-open state. After phase 1, the opening of the calcium channel (open/activated state) slows the repolarization down. This phase of the cardiac action potential, phase 2, is called a plateau phase and is maintained by the balancing act of the Ca^{2+} and K^+ ions (shown in figure 1.2.1B). This Ca^{2+} influx that occurs during phase 2 initiates the contractile function of the cardiac cells. Close to the end of phase 2, when more Ca^{2+} ions are released an auto-inhibitory signal is triggered resulting in a non-conducting state or closed state of the calcium channel. During phase 3, the cell tries to return to the resting state by the gradual inactivation of the calcium channels (inactivated state) and continued efflux of K^+ ions (Di Virgilio, Milani et al. 1987). This brings the membrane voltage back to -90 mV. At the end of Phase 3 inward rectifying K^+ channels are activated to reset the membrane potential to the resting state.

The last phase of the action potential, in phase 4, the membrane returns to resting potential (-90 mV). In this phase, most Na^+ , K^+ , and Ca^{2+} ion channels are in the closed/inactivated state. This resting potential of the membrane is maintained by the continued leak of the K^+ ions. The VGCCs to transit from the inactivated state to the closed state for the next cycle of events.

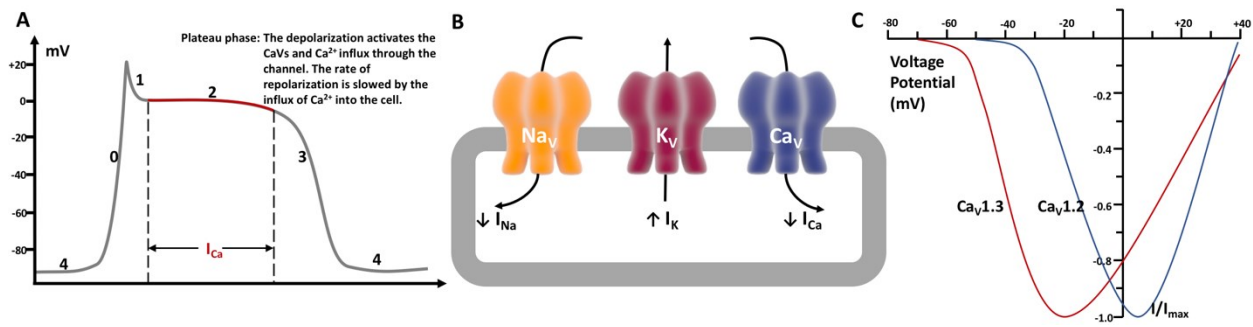


Figure 1.2.1. A) Cardiac action potential (left). B) Activities of three types cation channels during phase 2. The inward sodium and calcium current decays with time; the outward potassium current is activated allowing the cell to move to resting state. C) $\text{CaV}1.2$ and $\text{CaV}1.3$ voltage potential amplitude. Plot re-generated from Xu and Lipscombe data (Lipscombe, Helton et al. 2004).

1.2.2 Classification of voltage-gated calcium channels

VGCCs were initially classified into two main types, namely high-voltage-activated (HVA) and low-voltage-activated (LVA) calcium channels (Dolphin 2006). This classification was based on their activation voltage and conductance. HVA and LVA channels have distinct gating properties and pharmacological profiles (Dolphin 2006, Catterall 2011). For example, Hess et al. found that HVA channels are sensitive to 1,4-dihydropyridine (DHP) derivatives that stabilize the close-conducting state of HVA channels. This kind of compounds are calcium channel blockers, also known as calcium antagonists, which disrupt the movement of calcium ion through calcium channels (Hess, Lansman et al. 1984). There are also DHP derivatives belong to calcium channel agonists, which increase calcium influx into calcium channel. The calcium channel agonists can stabilize the open-conducting state of HVA channels for a prolonged time (Zhao, Huang et al.

2019). Interestingly, some of the identified HVA calcium channels exhibited preferences to different tissues and different sensitivity to DHP and other toxin antagonists, which led to the identification and classification of various HVA channels (Dolphin 2006). The DHP-sensitive HVA channels were found to be present in various cells and exhibited a long-lasting activation length and hence were termed as the DHP channel or the L-type calcium channel (LTCC) (Tang, Gamal El-Din et al. 2014, Tang, Gamal El-Din et al. 2016). ω -CTX-sensitive calcium channels were pronounced for their roles in the nervous system and were thus classified as N-type (non-L or Neuronal) channels. These ω -AGA-sensitive channels were initially found in the Purkinje cells of the cerebellum and were, therefore, named as P-type channels. Another close homolog of the P-type channels, which can be produced by alternative splicing of the CACNA1A gene, was found and was referred to as the Q-type calcium channel. In addition to these three types of HVA, some calcium-conducting channels were found to be insensitive to any of these antagonists and have been classified as R-type (resistant) channels (as **Table 1.2.1**).

	Antagonists Sensitivity					Reference
	1,4-DHP	PAA	BZZ	ω -CTX	ω -AGA	
L-type	blocks	Blocks	blocks	resistant	resistant	(Godfraind 2017)
P/Q-type	resistant	Resistant	resistant	resistant	blocks	(Protti and Uchitel 1993)
N-type	resistant	Resistant	resistant	blocks	resistant	(Zamponi, Striessnig et al. 2015)
R-type	resistant	Resistant	resistant	resistant	resistant	(Zamponi, Striessnig et al. 2015)

Table 1.2.1. The voltage-gated calcium channels are sensitive to different calcium channel blockers.

On the other hand, only one type of calcium channels has been reported among the LVA channels, namely, the transient-opening calcium channel (also called T-type channel). T-type channels are similar to L-type channels in their diverse expression and antagonist resistant

properties (Hansen 2015, Morton and Valenzuela 2016). However, their small single-channel conductance and ability to be activated at lower membrane potentials made them distinct from the L-type channels.

The prevalence of N-, P/Q-, and R- channels in neurons, and L- and T- channels in broad cellular types, shows the distinctive functional roles of the calcium channels. Besides their role in the characterization of the homologous channels, the calcium channel antagonists remain promising for their ability to specifically-modulate the different types of channels (Teng, Goto et al. 2008). The different sensitivities of the HVA and LVA channels to different antagonists show the potential for engineering these antagonists to selectively-alter the calcium conduction in different cells for various functions.

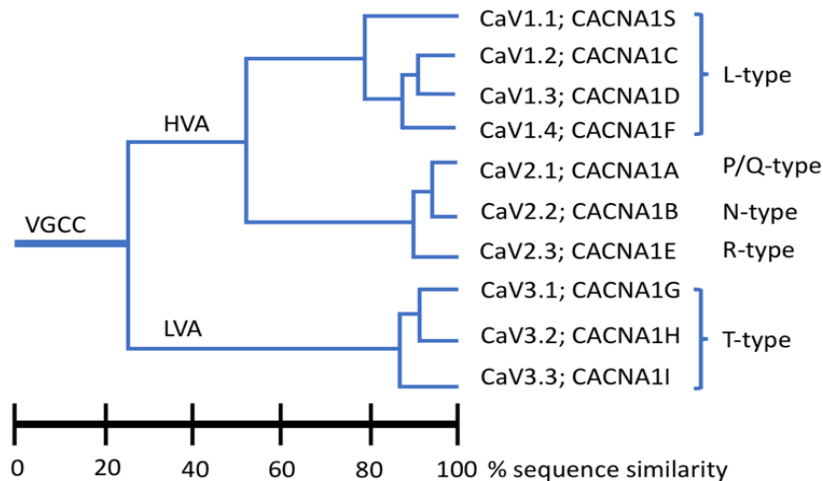


Figure 1.2.2. Phylogenetic tree showing the evolutionary relationship among the members of the VGCCs. The tree was constructed using the Clustal Omega. The scale in the figure shows the percentage of sequence identity in the $Ca_v\alpha_1$ subunit of different channels.

Ten mammalian VGCCs have been identified, of which the L-type calcium channel includes four members, $Ca_v1.1$ - $Ca_v1.4$, the P-/Q- type includes $Ca_v2.1$, the N-type includes $Ca_v2.2$, the R-type includes $Ca_v2.3$, and the T-type includes three members, $Ca_v3.1$ - 3.3 (Catterall,

Perez-Reyes et al. 2005). The members of the three families (Cav1, Cav2, and Cav3) share high sequence similarity (above 80%). Their sequence similarity and evolutionary relationship are shown in figure 1.2.1. In particular, Cav1 and Cav2 families have relatively high sequence similarity, when compared with that of the LVA Cav3 family.

L-type calcium channels

L-type of calcium channels (LTCCs), also known as the Cav1 family, contain four subtypes channel, including Cav1.1 (CACNA1S), Cav1.2 (CACNA1C), Cav1.3 (CACNA1D), and Cav1.4 (CACNA1F). The L-type channels were named based on their long-lasting inward currents during depolarization. And, they are all sensitive toward three types of L-type calcium channel blockers, including dihydropyridine, benzothiazepine, and phenylalkylamine. However, each of LTCCs channels have their different distributions and biophysical properties (Zamponi, Striessnig et al. 2015). Additionally, four members of LTCCs have their own preferences to auxiliary subunits, which will be discussed later.

Other types of voltage-gated calcium channels

As the other group of HVA, the Cav2 family is encoded by three genes (CACNA1A, CACNA1B, and CACNA1E) that encode Cav α_1 subunits Cav2.1, Cav2.2, and Cav2.3, respectively. Each member of the Cav2 family represents one type of calcium channel. Cav2.1 channel gives rise to both P-type and Q-type currents that were described in neurons, with this distinction is likely being caused by a combination of associated the Cav β subunit and alternative splice events in the Cav2.1 subunit (Etemad, Obermair et al. 2014). Cav2.2 and Cav2.3 underlie neuronal N-type and R-type currents, respectively.

T-type calcium channels are represented by three genes (CACNA1G, CACNA1H, and CACNA1I) that encode three different types of Cav3 α_1 subunit: Cav3.1, Cav3.2, and Cav3.3. The Cav3 group

of channels was the last to be cloned, and a comparison of their homology shows that these channels are divergent from the HVA regarding their structure (Hansen 2015). Expression of these subunits gives rise to the T-type currents with distinct electrophysiological and pharmacological properties (Zamponi, Striessnig et al. 2015). Unlike members of the high voltage-activated channel; Cav1 and Cav2 families, Cav3 calcium channels do not require co-assembly with auxiliary calcium channel subunits.

1.3 L-Type Calcium Channels

1.3.1 Distribution of LTCC channels

The distribution of LTCCs varies widely across its' members as their functions vary in different excitable cells (as **Fig. 1.3.1**) (Zamponi, Striessnig et al. 2015). Transcripts for all L-type channel isoforms have been detected in lymphocytes for endocrine functions (Gomes, Savignac et al. 2004). Among the four LTCCs types, Cav1.1 is mainly distributed in skeletal muscle and plays a role in muscle contraction. It is co-expressed with ryanodine receptors (RYRs) in GABAergic neurons, which produces gamma-Aminobutyric acid (GABA) (Hofmann, Flockerzi et al. 2014). Cav1.2 and Cav1.3 show a highly overlapping expression pattern in many tissues and are mostly present in same cell types, such as in adrenal chromaffin cells, cardiac and neuronal cells. Cav1.2 and Cav1.3 are predominantly located post-synaptically on the cell soma and in the spine and shaft of dendrites in the neurons (Striessnig, Pinggera et al. 2014). Cav1.2 and Cav1.3 are also expressed in the sinoatrial node (SAN) and atrial cardiomyocytes and play a role in cardiac pacemaker activity (Mangoni, Couette et al. 2003, Temme and Murphy 2017). In cardiomyocytes, Cav1.2 is mainly involved in the excitation-contraction coupling. Cav1.3 are found in the pancreas and kidney, where it correlates with endocrine secretion, and in the cochlea to regulate the auditory transduction. Cav1.4 is primarily expressed in the retinal cells and helps in normal visual functions

(Baumann, Gerstner et al. 2004). In addition to the expression of the LTCCs, the auxiliary subunits of the isoforms are also differentially distributed, which will be discussed in the later section of this chapter.

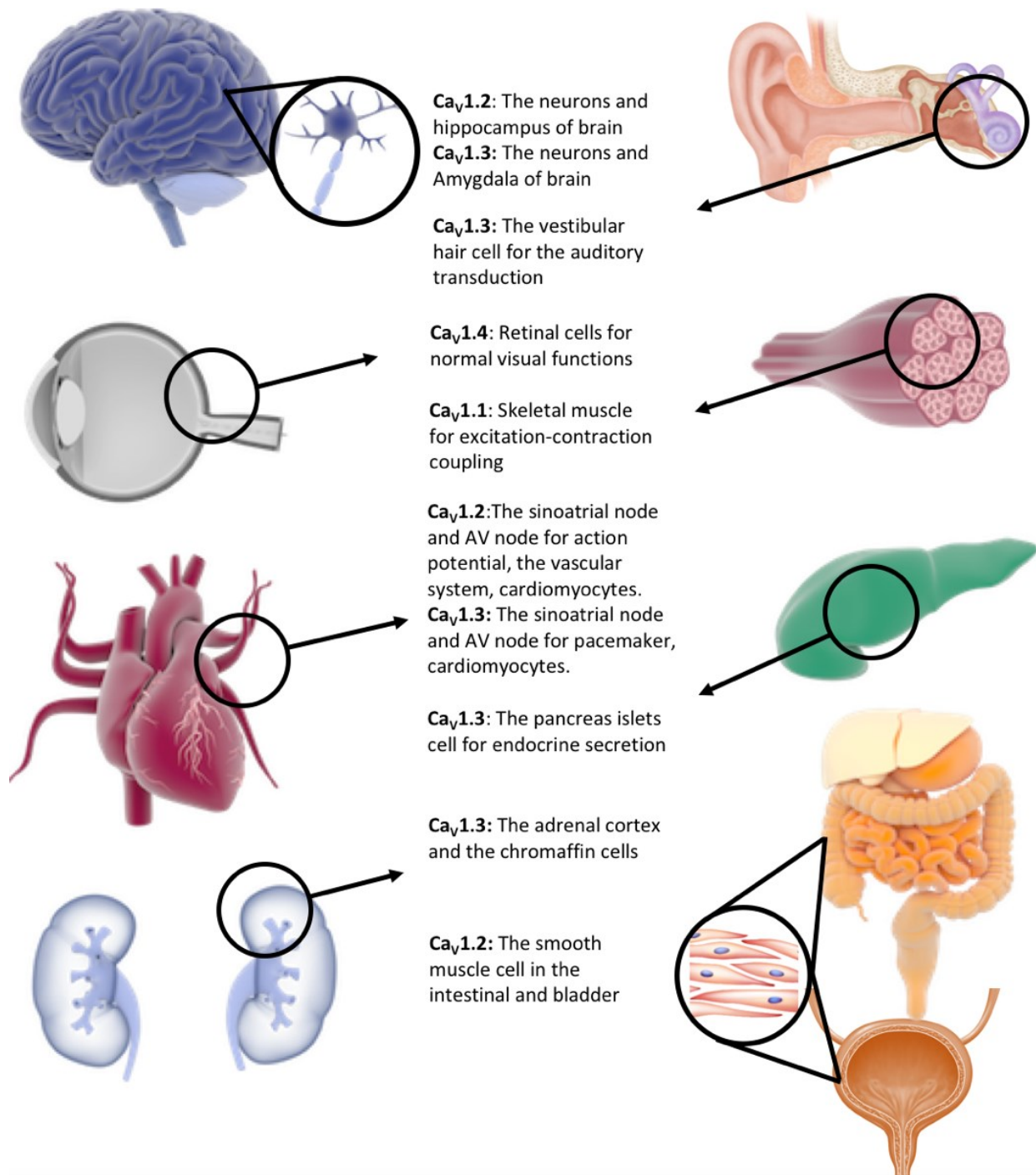


Figure 1.3.1. The major tissue distribution and physiological functions of the four LTCC isoforms

in human body. Except for skeletal muscle Ca^{2+} channels ($\text{Cav}1.1\alpha_1$ associated with β_1 , $\alpha_2\delta$, and γ_1 -subunit) and the working myocardium ($\text{Cav}1.2\alpha_1$ associated with β_1 and $\alpha_2\delta$ -subunit), their subunit composition is not known for other tissues. These sites represent actual and potential sites for action of selective LTCC blockers.

1.3.2 L-type calcium channel physiology and pathophysiology

When the LTCCs detect the electrical signal on the cell membrane, they transform these signals into other physiological activities, such as the contraction of the muscle, secretion of hormones, and regulation of genes expression (Artalejo, Adams et al. 1994, Karaki, Ozaki et al. 1997). These processes can generally be summarized as excitation-contraction (Karaki, Ozaki et al. 1997), excitation-secretion (Artalejo, Adams et al. 1994), and excitation-transcription coupling (Hofmann, Flockerzi et al. 2014), respectively. The activities of the LTCCs and their interaction with cell signaling pathways remain essential for governing these physiological processes. During depolarization, LTCCs detect the changes in the membrane potential and initiate the release of intracellular Ca^{2+} (also referred to as the Ca^{2+} spark) from the sarcoplasmic reticulum to perform the excitation-contraction coupling function. During this process, the associated ryanodine receptor (RyR) channels are activated, and the Ca^{2+} from sarcoplasmic reticulum are released resulting in contraction of the skeletal muscles (Bidaud, Mezghrani et al. 2006).

In many endocrine cells, such as pancreatic islet cells, adrenal chromaffin cells, and aldosterone-producing cells in the adrenal cortex, the Ca^{2+} influx mediated by LTCCs trigger the secretion of hormones (Striessnig, Pinggera et al. 2014). For example, activating LTCCs showed increased insulin secretion in the absence of glucose, while its' blockade showed significant inhibition of the insulin levels. Similarly, the Ca^{2+} ions released from LTCCs help in the release of neurotransmitters at specialized ribbon synapses in sensory-transduction neurons.

LTCCs are also known to regulate expression of genes (excitation-transcription coupling), by modulating the Ca^{2+} dependent pathways. In the brain, Cav1.2 and Cav1.3 are located on the postsynaptic membrane, where they interact with the members of the cell signaling pathway and influence the expression of genes (Berger and Bartsch 2014, Ortner and Striessnig 2016). Compared to other types of VGCCs, LTCCs show a privileged role in the regulation of gene transcription in the neurons. For example, Hippocampus and neocortex-specific deletion of the CACNA1C gene (Cav1.2) impair nuclear gene transcription and weakens the long-term potentiation and spatial learning capabilities (Oliveria, Dittmer et al. 2012). In addition to the direct involvement of pore-forming domains of LTCCs in gene regulation, the auxiliary subunits of LTCCs are also known to interact with several proteins that can alter the gene transcription process.

The LTCCs are considered as an important target for the treatment of various diseases (Bidaud, Mezghrani et al. 2006, Berger and Bartsch 2014, Striessnig, Ortner et al. 2015, Zamponi, Striessnig et al. 2015, Ortner and Striessnig 2016). As the major isoform of the skeletal LTCCs, the Cav1.1 is reported to correlate with hypokalemic periodic paralysis, which is characterized by muscular weakness or paralysis (Bidaud, Mezghrani et al. 2006). Cav1.2 and Cav1.3, being more expressed in the heart and the brain, their dysfunction results in severe disease states, such as Timothy's syndrome, cardiac arrhythmia, bipolar disorder, and autism (Berger and Bartsch 2014, Ortner and Striessnig 2016). Any abnormality in the cardiac LTCCs leads to Long-QT Syndrome (LQTS), where the QT interval of the cardiac action potential is prolonged, a condition that causes heart arrhythmias or sudden cardiac death (SCD) (Giudicessi and Ackerman 2016). The Timothy Syndrome (TS), is an extremely rare multisystem LQTS subtype, that is mainly caused by the dysfunctions of LTCC and Ca^{2+} handling proteins. The TS has two distinctive types (I and II), and both of them are related to mutations in CACNA1C gene. As the only LTCC subtype in the retinal

cells, mutations in the $Cav1.4$ gene are known to weaken the normal visual functions and cause night blindness (Striessnig, Bolz et al. 2010). Modulating LTCCs, therefore, remains to be an important avenue for the treatment of several diseases (Hofmann, Flockerzi et al. 2014).

1.3.3 L-type calcium channel complexes

LTCC pore-forming α_1 -subunit

The LTCC polypeptide forms a heterotetramer and includes the pore-forming transmembrane α_1 -subunit, the intracellular β subunit, and an extracellular $\alpha_2\delta$ subunit (as **Fig.1.3.2**). Most of the pharmacological and gating properties of LTCCs are accomplished by their α_1 -subunits. The structural topology of the α_1 -subunits is highly conserved among the members of the LTCCs and is made up of the cytoplasmic N- and C-terminal domains and four intervening transmembrane domains (DI-DIV). Each transmembrane domain is composed of six transmembrane α -helices (S1-S6), where S1-S4 helices are known as the voltage sensing domain (VSD), and S5-S6 forms the pore domain (Tuluc, Yarov-Yarovoy et al. 2016). VSD detects the changes in the membrane potential and PD helps in the selective passage of calcium ions through the channel pore. The S4 helix of the VSD encompasses several conserved positively charged residues, whereas, the S1-S3 helices are dominated by negatively charged amino acids. When the membrane is depolarized, the movement of the S4 helices is transmitted to the cytoplasmic ends of the S5 and S6 helices, through the S4-S5 linkers, resulting in the opening of the activation gate formed by the S6 helices on the inner side of the channel (Catterall 2011, Striessnig, Pinggera et al. 2014).

The membrane-associated P-loop in each domain between the two helices, S5 and S6, form the selectivity filter of the channel. The selectivity of calcium channels relies on the P-loops domains and their calcium ion binding sites. The selectivity filter of VGCC includes conserved

glutamate residues (E-E-E-E) in the P-loop region (Tang, Gamal El-Din et al. 2014). Their side chains can restrain Ca^{2+} at the right coordination and let Ca^{2+} enter into the pore region. The recent research identified three aspartic acid residues along the selectivity filter from extracellular to intracellular. Amino acid substitution and X-ray structure has helped in locating the three binding sites for the Ca^{2+} ions (Adiban, Jamali et al. 2016). Although the bacterial calcium channel is different from the mammalian LTCCs in their amino acid sequence and structural features, the structure of CavAb has provided valuable insights into calcium ion selectivity conferred by the selectivity filter.

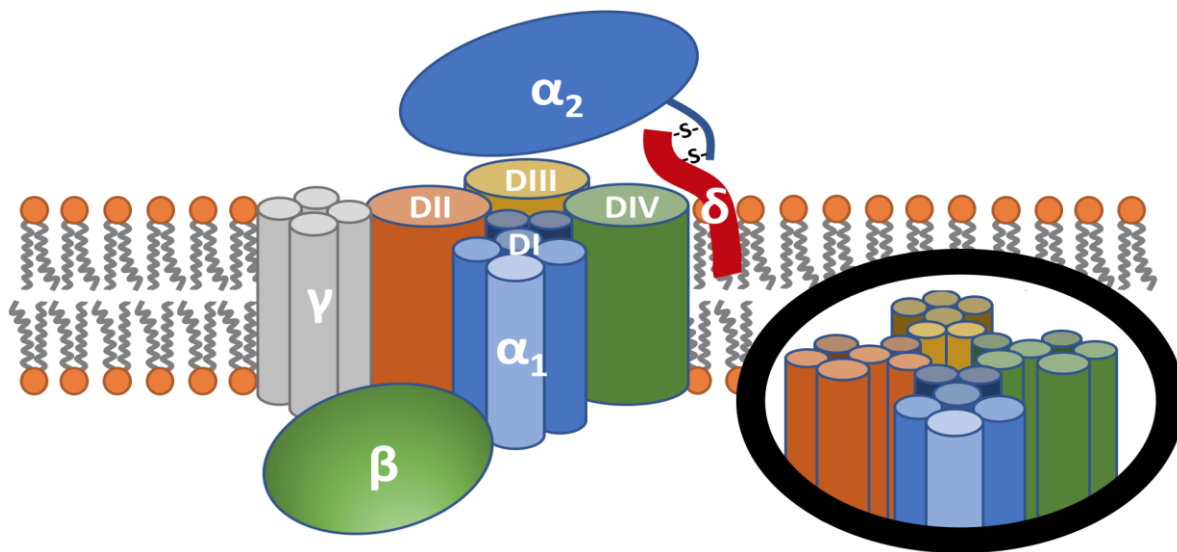


Figure 1.3.2. The topology structure of LTCC complex. The pore-forming transmembrane α_1 -subunit, the intracellular β -subunit, the extracellular α_2 -subunit co-linked with the transmembrane δ -subunit, and the transmembrane γ -subunit are shown. The α_1 -subunit contains four homologous domains (DI-DIV), each composed of six transmembrane helices. The detailed structure of α_1 -subunit transmembrane segments has been shown in the black circle. The β subunit binds the DI-DII linker of α_1 subunit. The δ subunit anchors the $\alpha_2\delta$ subunit on the cell membrane, and the α_2 interacts with the α_1 subunit extracellularly. The γ -subunit contains four transmembrane helices, which directly binds to the DIII of the α_1 subunit.

The N-terminus and C-terminus region of LTCC are both located in the cytosolic space. Although the major sequence of the N-terminus is composed of random loops, it also includes a calmodulin interaction domain, known as N-terminal spatial Ca^{2+} transforming elements (NSCaTE) (Liu and Vogel 2012). The length of the C-terminus is much longer than N-terminus and contains several binding sites for various proteins that modulate the LTCCs activity (shown in figure 1.3.3). Proteolytic cleavage of the C-terminal domain generates two fragments, the proximal C-terminal regulatory domain (PCRD) and the distal C-terminal regulatory domain (DCRD) (Catterall 2011). The upstream sequence of the cleaved site contains the PCRD, IQ domain, pre-IQ domain, and the EF-hand motif. This region is important for Ca^{2+} /CaM binding and regulation. The downstream sequence from the cleavage site includes the A-kinase-anchoring-protein (AKAP) binding domain (ABD) and DCRD. When the DCRD is proteolytically cleaved, the cleaved fragment can remain non-covalently bound to the PCRD, thus allowing the two regions of the C-terminal domain to interact with each other and perform the auto-inhibitory function for the LTCCs. The DCRD serves as an effective auto-inhibitory domain for the LTCCs or as a transcriptional modular when it enters the nucleus (Hulme, Yarov-Yarovoy et al. 2006). The ABD of the distal C-terminus plays a vital role in PKA-induced phosphorylation of the DCRD. The AKAP binds with the ABD and helps PKA identify the phosphorylation sites in the cleaved fragment. The phosphorylation shuts down the auto-inhibition of LTCC and facilitates the Ca^{2+} influx (Striessnig, Pinggera et al. 2014).

LTCC auxiliary β -, γ - and $\alpha_2\delta$ -subunits.

Co-expression and co-assembly of $\text{Cav}\beta$ and $\text{Cav}\alpha_2\delta$ subunits with $\text{Cav}\alpha_1$ have a significant role in LTCCs trafficking (Simms and Zamponi 2012). The $\text{Cav}\beta$ subunit, which belongs to the membrane-associated guanylate kinase (MAGUK) protein family is composed of three domains similar to that of the MAGUK family, except for the missing PDZ in the N-terminus. The two

conserved structural domains of the Cav β , the SH3 and the guanylate-kinase (GuK) like domain are linked together by a domain, which looks like a shape of the hinge, named as HOOK domain. The HOOK domain has been reported from different eukaryotic organisms. It has variable lengths in the Cav β isoforms and share a relatively low overall amino acid identity and plays an important role in the Cav β interaction with other proteins (Van Petegem, Clark et al. 2004). Similar to the DCTD, the HOOK domain possesses sites for phosphorylation and alters the conduction state of LTCCs. The Cav β subunit interacts with the 18-residue long DI-II linker (or the alpha interaction domain (AID)) of the α_1 subunit. The α -binding pocket (ABP), a hydrophobic groove formed by the surrounding α -helices, in the GuK domain of the Cav β subunit interacts with the AID (Almagor, Chomsky-Hecht et al. 2012). The high-affinity association between AID and ABP markedly influences the cell surface expression of functional channels (Van Petegem, Clark et al. 2004).

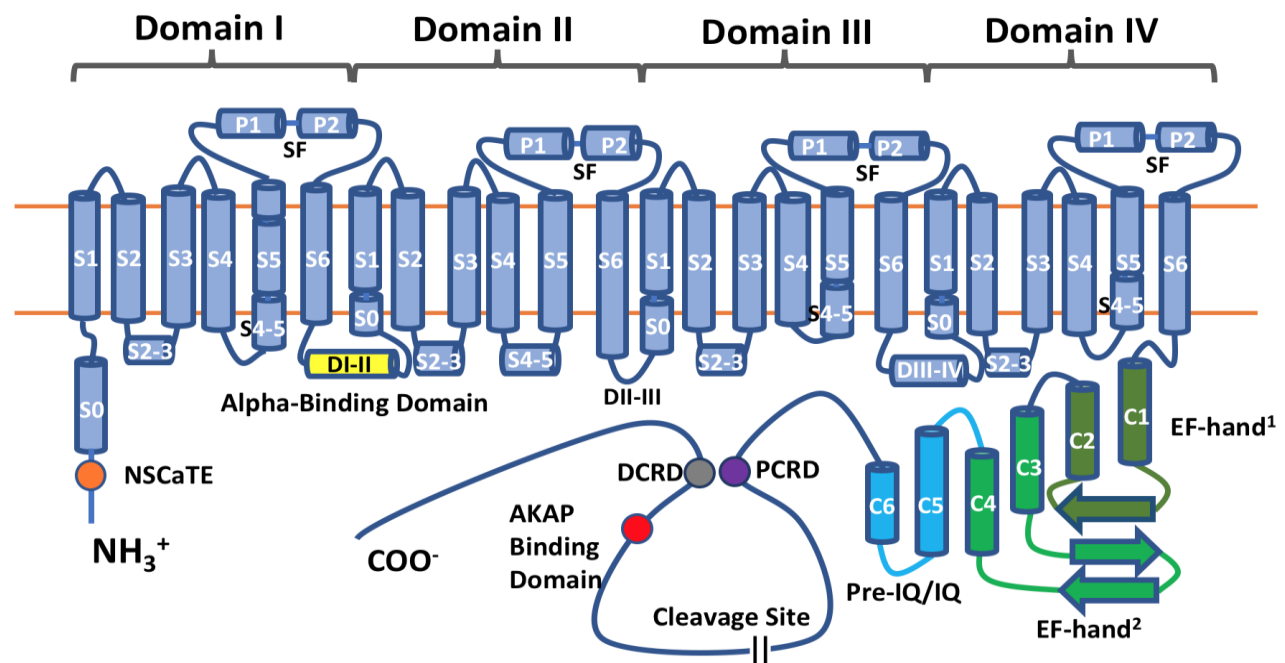


Figure 1.3.3. The secondary structure topology of the α_1 -subunit of LTCCs. The N-terminal domain is followed by four homologous transmembrane domains and the C-terminal domain. Each of the transmembrane domains is made of six helices and a membrane associated P-loop. The

orange, purple, red, and grey dots indicate the location of NSCaTE, PCRD, AKAP binding domain, and DCRD, respectively. The linker of DI and DII, colored in yellow, is the alpha-binding domain (ABD). The sequence from C1 to C2 and from C3 to C4 shows the two EF-hand motifs. Sequence from the end of C4 to the end of C6 colored in light blue is Pre-IQ and IQ domain. The cleavage site is located in the sequence between DCRD and PCRD. The secondary structure is based on the PDBsum database.

Another important co-expressed protein component of the LTCC complex is the $\text{Cav}\alpha_2\delta$ subunit. The $\alpha_2\delta$ subunit remains to be a promising target for the treatment of neuropathic pain and mutations that affect the function of $\text{Cav}\alpha_2\delta_1$ were found to cause cardiac dysfunctions (Simms and Zamponi 2012). The $\text{Cav}\alpha_2\delta$ subunit is a disulfide-linked polypeptide that interacts with the α_1 subunit on the extracellular space through its' α_2 segment, while the δ segment serves as an anchor fixing the subunit to the membrane. The $\text{Cav}\alpha_2\delta$ contains a similar domain arrangement to various plasma proteins, which includes Von Willebrand factor type-A (VWFA) and the calcium channel and chemotaxis (CACHE) domain (shown in figure 1.3.4) (Briot, D Avanzo et al. 2016). The VWFA domain found in $\text{Cav}\alpha_2$ promotes the trafficking of the α_1 subunit to the membrane and acts as a receptor for the extracellular ligands, such as thrombospondins. This VWFA domain also contains a metal ion-dependent adhesion site (MIDAS), which allows precise coordination of the VWFA domain with bound protein ligand (Eroglu, Allen et al. 2009). Mutation of this site can result in the loss of $\text{Cav}\alpha_2\delta$ subunits' regulatory function to the $\text{Cav}1.2$, $\text{Cav}2.1$, and $\text{Cav}2.2$. Nevertheless, the $\text{Cav}\alpha_2\delta$ subunit can still help in trafficking the $\text{Cav}\alpha_1$ subunit to the cytoplasmic membrane. The CACHE domain is located at the downstream sequence of VWFA domain in the extracellular side. This domain is known to have a possible role in small-molecule recognition (Dolphin 2013, Briot, D Avanzo et al. 2016).

The γ protein belongs to the PMP-22/EMP/MP20 family of the integral membrane protein superfamily (Chen, Deng et al. 2007). As a transmembrane protein, the γ -subunit contains the

intracellular N- and C-terminal intervened by four transmembrane helices (shown in figure 1.3.4). The cytoplasmic C-terminus of Cav γ -2, Cav γ -3, Cav γ -4, and Cav γ -8 have a PDZ binding motif, which was named based on the first three proteins, PSD96, Dlg1, and Zo-1, discovered to share it (Kennedy 1995). The PDZ binding motif, also known as TARPs, regulates the synaptic transmission function of alpha-amino-3-hydroxy-5-methylisoxazole-4-propionic acid (AMPA) receptor in neurons. The neuronal Cav γ -5 and Cav γ -7 lacks the PDZ binding motif. They have also been shown to vary based on their location of expression, for example, the γ subunit expressed in skeletal muscles have a shorter C-terminal domain when compared to those expressed in the neuronal cells. These γ subunits interact with PDZ domain-containing proteins, some of which help in the assembly of the calcium channels.

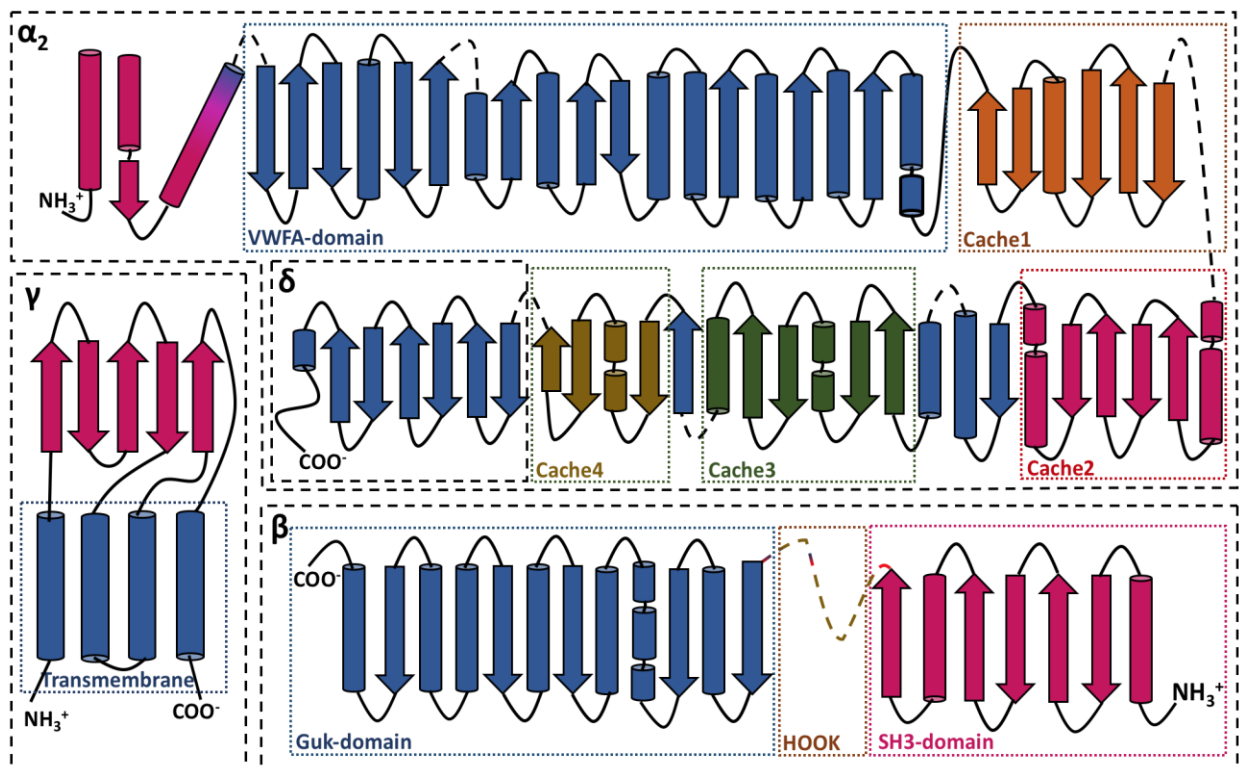


Figure 1.3.4. The domain architecture and topology of β_1 -subunit (bottom), $\alpha_2\delta_1$ -subunit (top right) and γ_1 -subunit (left bottom). The dotted line represents the missing sequence. The structural topology was retrieved from PDBsum Database.

1.3.4 Current State of LTCC Structural and Modelling Research

Crystallography of LTCC

The crystal structures of three isoforms of Cav β have been resolved in complex with AID (i.e., short polypeptides from the DI-II linker of Cav α_1) from different species. The 2.2 Å resolution structure of rabbit Cav β_2 isoform was crystallized in complex with an 18-residue long polypeptide, corresponding to the AID of Cav1.1 α_1 (PDB ID:1T3L). The core region of rat Cav1.2 β_3 isoform was crystallized (PDB ID:1VYV) with a polypeptide (49 AAs) at 2.6 Å resolution. Chen et al., crystallized the single structure of Cav β_4 isoform at 3Å resolution (PDB ID:1VYU) (Chen, Li et al. 2004). Their core structures, which includes the SH3 and GuK domains, exhibit high similarity. A chimeric complex of rat Cav β_2 isoform and first sixteen residues of human Cav1.2 AID region was crystallized at 1.97Å resolution (PDB ID: 1T0J) (Van Petegem, Clark et al. 2004). Mutation analysis showed that three Cav1.2 AID residues, Tyr447, Trp440, and Ile441 are important for the interaction between the Cav β subunit and the AID (Chen, Li et al. 2004, Van Petegem, Clark et al. 2004).

In 2012, a 2.0 Å resolution crystal complex of rabbit Cav1.2 DI-DII linker and Cav β_2 isoform was determined (Almagor, Chomsky-Hecht et al. 2012). Not until recently, the 3D structure of the last isoform of Cav β subunit, the Cav β_1 , has been identified in a complex with the complete cryo-EM model of Rabbit Cav1.1. The mechanism that Cav β regulates Cav α_1 is achieved through the transmitted motions of DI-S6. Before association with Cav β , AID is in a coil-type structure. The Cav β acts as a chaperone and helps AID undergo a coil to helix transition during the binding (Buraei and Yang 2013). The α -helix of AID propagates the upstream sequence of DI-S6. They form a rigid connection between the GuK domain of the Cav β and the channel pore, and mechanically transduce their binding to channel gating states (Chen, Li et al. 2004). The N-

terminus of the Cav β is anchored to the membrane, which restricts the motion and orientation of the Cav β binding to the AID and connecting the DI-S6 segment. These coupled motions help Cav β effectively regulate the gating properties of calcium channel.

Calmodulin (CaM) is a small and conserved calcium-binding messenger protein that plays an essential role in all the HVA channels. In the case of LTCCs, binding with Ca²⁺/CaM is known to pronounce calcium-dependent inhibition of the channel current. Calmodulin, being localized in the cytosolic region, detects the changes in the levels of intracellular Ca²⁺ and modulates the interaction of LTCCs with other proteins. Four EF-hand motifs distributed equally on the N- and C-terminus of the CaM works as the calcium ion sensor. Each of EF-hand motifs is composed of two alpha helices and is connected by a flexible loop with the Ca²⁺ binding site located in the middle. The Ca²⁺/CaM has a higher binding affinity to LTCC and therefore associates with the LTCC complex even at low cytoplasmic Ca²⁺ concentrations. The IQ domain and the pre-IQ domain, upstream sequence of the IQ domain, refer to the first two amino acid, isoleucine (commonly) and glutamine. And they serve as the binding site for the calmodulin (CaM). CaM is known to play a regulatory role in the calcium-dependent inactivation of LTCCs. However, the trafficking function of Ca²⁺/CaM remains controversial, due to inconsistent results in different expression systems (Bourdin, Marger et al. 2010). In hippocampal neurons, Cav1.2 trafficking to the distal dendrites is accelerated by the presence of Ca²⁺/CaM, and not by the apo-CaM (Stroffekova 2008).

From 2005 to 2012, several structures containing a short polypeptide from Cav1.1 or Cav1.2 and calcium-bound calmodulin (Ca²⁺/CaM) were determined. In 2005, three structures of the Cav1.2 IQ domain bound to the hydrophobic pocket of the Ca²⁺/CaM protein were resolved (Fallon, Halling et al. 2005, Van Petegem, Chatelain et al. 2005). In those complexes, Ca²⁺/CaM

exists in a 2:1 ratio with the IQ domain (Kim, Rumpf et al. 2010). The IQ domain engages itself in the hydrophobic pockets, present in the N-terminal and C-terminal $\text{Ca}^{2+}/\text{CaM}$ lobes, through sets of conserved ‘aromatic anchors’. In the $\text{Cav}1.2$, three residues (Tyr1627, Phe1628, and Phe1631) downstream of IQ domain bind the hydrophobic Ca^{2+}/C lobe pockets. The three upstream residues (Phe1618, Tyr1619, and Phe1622) bind the Ca^{2+}/N lobe pockets (Van Petegem, Chatelain et al. 2005). The lengths of $\text{Cav}1.2\alpha_1$ IQ domains vary among the resolved structures. For example, the 3D structures of human IQ domain have been resolved with 37 residues (PDB ID: 2BE6), and 21 residues (PDB ID: 2F3Z) and 21 residues from *Cavia porcellus* IQ domain, (PDB ID: 2F3Y) were also resolved previously. In 2009, Fallon et al. resolved the extended structure of IQ domain to include the pre-IQ domain, which comprised of 77 residues from human $\text{Cav}1.2$ C-terminus (PDB ID: 3G43) (Fallon, Baker et al. 2009). In the same year, a 21-residue IQ domain from human $\text{Cav}1.1$ was determined in complex with the $\text{Ca}^{2+}/\text{CaM}$ at 1.94 Å resolution (PDB ID: 2VAY) (Halling, Georgiou et al. 2009). In 2010, the structure of PreIQ and IQ domain from human $\text{Cav}1.2$ containing 78 residues (PDB ID: 3OXQ) was crystallized in complex with $\text{Ca}^{2+}/\text{CaM}$ at 2.55 Å resolution (Kim, Rumpf et al. 2010). In 2012, Liu and Vogel reported a novel-binding motif (NSCaTE) from N-terminus of $\text{Cav}1.2$ and $\text{Cav}1.3$ to have a higher affinity for binding $\text{Ca}^{2+}/\text{CaM}$ when compared to that of the binding region in C-terminus (Liu and Vogel 2012). Using NMR, they reported the 3D structure of a 24-residue long NSCaTE motif in complex with the $\text{Ca}^{2+}/\text{CaM}$ (PDB ID: 2LQC). Until now, the $\text{Ca}^{2+}/\text{CaM}$ complex structure has only been resolved with $\text{Cav}1.1$ and $\text{Cav}1.2$ of the LTCCs. Although $\text{Cav}1.4$ binds to $\text{Ca}^{2+}/\text{CaM}$, their interaction has not been reported to have any functional regulation.

In 2014, the first structure of a bacterial calcium channel (CavAb) was resolved by performing specific mutations on the *Arcobacter butzleri* sodium channel (NavAb) (Tang, Gamal

El-Din et al. 2014). The quaternary structure of CavAb is a symmetrical homo-tetramer, which is similar to its NavAb prototype. Four identical domains assemble to form the main structure of the channel, with each of the domain (containing 237 residues) encompassing six transmembrane helices. The topological features of the transmembrane domain of CavAb are similar to that of the LTCC. Tang et al. performed several mutations to elucidate the structural basis of Ca²⁺ selectivity and reported the crystal structures of thirteen variants that conferred different mutations in NavAb.

Each monomer is composed of a voltage-sensing domain, S1-S4, and a pore-forming domain, S5-S6 (as **Figure 1.3.5**). Four positively charged arginine in the voltage-sensing domain detect the changes in the membrane potential. The voltage-sensor movements are transmitted to the pore-forming domain through a cytoplasmic linker that connects the S4 and S5 helices. Three negatively charged aspartate residues at the selectivity filter (Asp177, Asp178, and Asp181) were found to be essential for binding the Ca²⁺ ion and render selectivity to the channel. The paper revealed that the ion-selective mechanism is based on three Ca²⁺ binding sites, site-1 (Asp178), site-2 (Asp177, Leu176), and site-3(Thr175). A single substitution at site-177, from Glu to Asp, enhanced the calcium selectivity by 1000 times over sodium, which was sufficient to convert the sodium channel to calcium channel. Although 181D is not directly involved in Ca²⁺ coordination and lies outside of the ion-conducting pore, it generates an electronegative environment to attract the extracellular cations. Binding of one Ca²⁺ blocks the pore and prevents the entry of the monovalent cations. The entry of second Ca²⁺ induces electrostatic repulsion on the first Ca²⁺, thereby forcing it to flux into the cytoplasm. Thus, the extracellular calcium ions fluently permeate into the intracellular side in response to the concentration gradient (Tang, Gamal El-Din et al. 2014). In 2016, the same group reported the mode of binding of some of the known Cav antagonists, including amlodipine, nimodipine, Br-verapamil and two other Br-dihydropyridine

derivatives in complex with the CavAb channel at a resolution of 2.7Å (Tang, Gamal El-Din et al. 2016). The complex structures of antagonist-bound Cav were shown to be in a “pre-open” (closed-inactivated state), which confirms the inactivated-state preference of these drugs in binding the channel. A more detailed discussion on the binding mode of these antagonists is available in section 3 of this chapter.

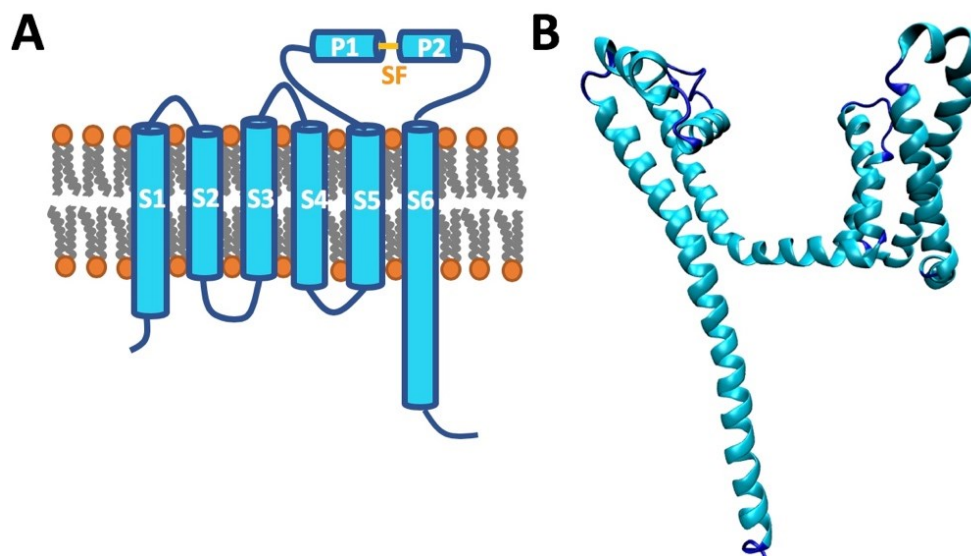


Figure 1.3.5. The homo-tetramer architecture of CavAb includes six transmembrane segments, including Voltage-Sensor Domain (VSD: S1-S4) and Pore-Forming Domain (PFD: S5-S6). The P1 helix, P-loop, and P2 helix forms the selectivity filter, which directly interacts the ions.

In 2015, Wu et al. reported the complete structure of the mammalian Cav1.1 complex at 4.2 Å resolution using the cryo-EM technique (Wu, Yan et al. 2015). Three auxiliary subunits were isolated from the rabbit skeletal muscle, the pore-forming α_1 -subunit, the extracellular $\alpha_2\delta$ -subunit, and the transmembrane γ -subunit. The fourth auxiliary subunit was included in the complex by docking the crystal structure of rat Cav β_2 (PDB ID: 1T0J) on the AID of Cav1.1 α_1 subunit. Following this complex, two rabbit Cav1.1 complexes at resolution 3.9 Å (PDB ID: 5GJW) and 3.6 Å (PDB ID: 5GJV) were reported (Wu, Yan et al. 2016). This Cav1.1 construct included 1873

amino acid residues. While the 3D coordinates of most parts of the Cav1.1 α_1 -subunit were resolved, some of the cytoplasmic (N-terminus: 1-31, DI-DII linker: 377-416, DII-DIII linker: 670-787, and C-terminus 1516-1873) and extracellular segments (DI S3-S4: 140-160, DIII S3-S4: 886-891, and DIV S3-S4: 1206-1228) were found to be missing (as **Fig.1.3.6**).

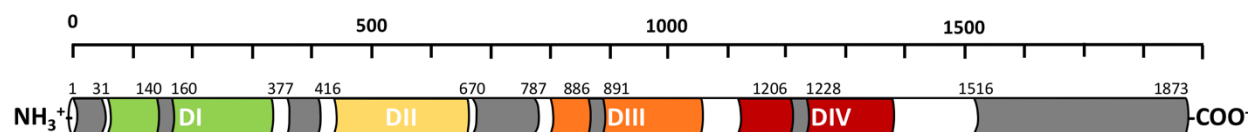


Figure 1.3.6. The missing residues in the rabbit Cav1.1 α_1 subunit (PDB ID: 5GJV) shaded in grey.

The rabbit Cav1.1 is composed of four inter-connected homologous domains, each of which includes the voltage-sensing and pore-forming domain. The S4 helix of the VSD is composed of six charged residues when compared to four residues in human Cav α s (Burashnikov, Pfeiffer et al.). Remarkably, the asymmetric pore-region of Cav1.1 is formed by the four S5, and S6 bundles and the tightly packed inner gate showcased a closed conformation and inactivated conduction-state of the Cav1.1 channel. The structure of two other auxiliary subunits, Cav $\alpha_2\delta$ and Cav γ , were also determined. The Cav α_2 subunit included four tandem cache domains and one VWA domain. The cysteine residues, Cys1074 in Cav δ and Cys406 in Cav α_2 formed a disulfide bond at the binding region between VWA domain and Cav δ . In the VWA domain, the MIDAS residues (Ser263, Ser265, Asp261, Thr333, and Asp365) and Cav α_1 DI S1-S2 residue (Asp78) are bound to a calcium ion. Both the previous and latest 3D structures identified for the Cav γ subunit included four transmembrane α -helices, however, in this Cav1.1 structure, additional extracellular β -sheets have been resolved together with the regions of the two termini. The second and third transmembrane-helices in Cav γ and DIV S3-S4 in Cav α_1 are directly involved in interactions

through hydrophobic forces. The Cryo-EM structure of the rabbit Cav1.1, have thus brought novel insights on the multi-domain structure of VGCC, especially the association of Cav with the auxiliary proteins.

Modeling Studies of LTCC

Computational modelling and simulations have been a promising technique to reveal fundamental biological mechanisms, biomolecular interactions and predicting the effects of modulators. For Cav, modeling-based studies were previously performed to understand how LTCC blockers bind to the calcium channels (Tikhonov and Zhorov 2008, Cheng, Tikhonov et al. 2009, Tikhonov and Zhorov 2009). For example, Tikhonov and Zhorov generated homology models for the open- and closed- state conformation of the pore-forming domains (S5-S6) of Cav1.2 using the crystal structure of the bacterial KvAP and KCSA channels as templates (Shaldam, Elhamamsy et al. 2014). The generated models were used to dock three types of LTCC blockers, namely, benzothiazepine, phenylalkylamine and dihydropyridine. The docking analysis showed that all three ligands bind near the S5-S6 helices of domain III and IV and the Cav residues, tyrosine in S6-DIII, tyrosine in S6-DIV, and glutamine in S5-DIII, are important for binding these ligands close to the pore domain of the channel. Since no experimentally-resolved structure of ligand-Cav was available, the in-silico docking analysis performed in this study provided useful insights for understanding ligand-binding in Cav.

Adiban et al. used the structure of the CavAb (PDB ID: 4MVQ) to model the pore-forming domain (S5-S6) of the Cav with defined charges. They performed molecular dynamics (MD) simulation to calculate the potential of mean force and showed that the affinity for Ca²⁺ in site-2 (Asp177, Leu176) is higher than that within the two other sites, site-1 (Asp178) and site-3 (Thr175). Their study also showed that, in the absence of calcium ions, the CavAb could allow the passage

of Na^+ ions, but not Cl^- ions (Adiban, Jamali et al. 2016). This study using the structure of CavAb , was helpful in understanding the structure-function relationships of the calcium channel.

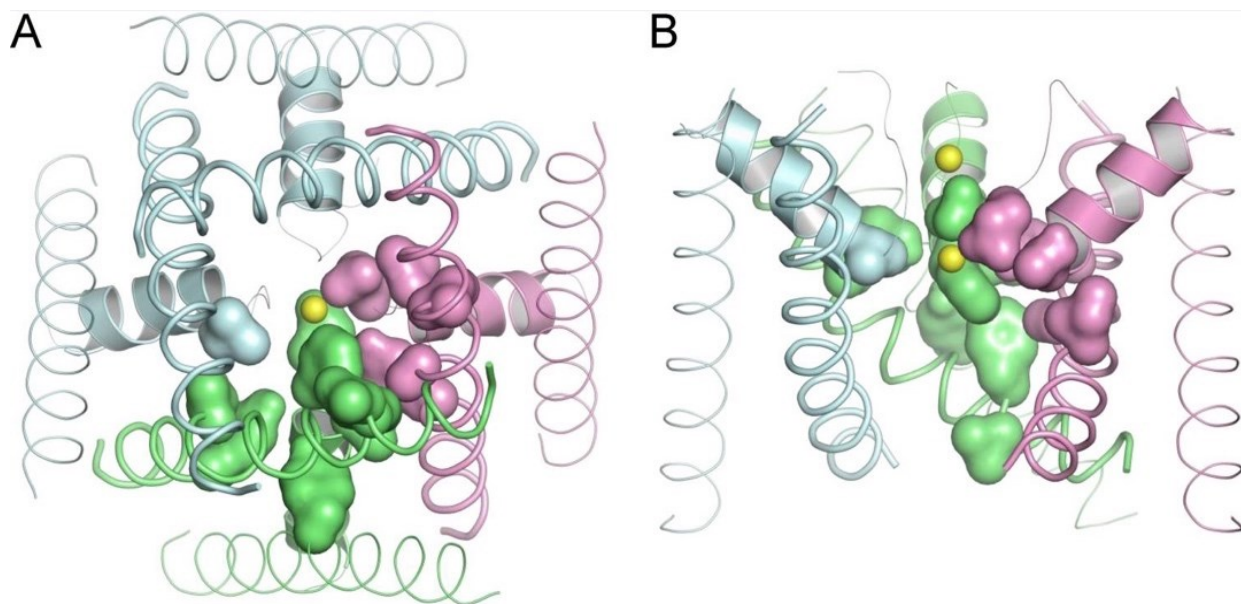


Figure 1.3.7. A) The bottom view and B) the side view of pore-forming domain (S5-S6) in the human $\text{Cav}1.2\alpha_1$ homology model. Each domain of the model is colored differently. The calcium ion has been depicted as the yellow dot.

All of the computational models built for Cav until now were based on templates with low sequence identity (< 30%). Studying molecular systems built with low-identity templates is quite challenging since the accuracy of the model is highly dependent on the similarity between the template and the target protein (Tramontano 1998). While the oligomeric structures of bacterial homologs are useful for modeling the transmembrane domains (TMDs), building the large intracellular domains that connect the TMDs using these structures is not feasible. Additionally, modeling human L-type $\text{Cav}\alpha_1$ -subunit with only the pore-forming domains (S5-S6) will eliminate the structural effects from surrounding voltage-sensor domain (S1-S4) (as **Fig. 1.3.7**). The studies on the homology model will be limited to the conformational states of template, which restricts the application of the human L-type $\text{Cav}\alpha_1$ -subunit models. With the availability of the $\text{Cav}1.1$

complex and other structural data, obtaining better quality homology-based models for the human Cav channels, especially the LTCCs, is now possible. Nevertheless, sophisticated methods and high-performance computing would be needed for modeling the multi-domain architecture of the human Cav_s. Building these models can be helpful in understanding the structure-function-dynamic properties, the Ca²⁺ influx mechanisms and effects of small molecules on these channels (Ahmed, Jalily Hasani et al. 2017, Jalily Hasani, Ganesan et al. 2018).

1.4 Human Cav1.2 Channel

Human Cav1.2 serve as the principal path for the entry of Ca²⁺ ions in cardiomyocytes and plays a significant role in vessel contractility and cardiac action potential (Hofmann, Flockerzi et al. 2014). Inhibition of Cav1.2 remains to be an established therapeutic strategy for hypertension and myocardial ischemia. Several classes of small molecules, such as dihydropyridine, benzothiazepine, and phenylalkylamine have been identified to modulate the activity of the Cav1.2 channels (Striessnig, Ortner et al. 2015). Despite the discovery of several small molecules, the mode of binding of these molecules to the Cav1.2 channel remains unclear due to the lack of a three-dimensional structure of the human Cav1.2 channel (Hering, Zangerl-Pleschl et al. 2018).

1.4.1 Cav1.2 channel complex and structure

Cav1.2 channel is a multi-subunit protein complex formed by the association of α_1 , β , and $\alpha_2\delta$ subunits, but it hasn't been found with γ -subunit. The α_1 -subunit plays the central role of calcium transfer, while the auxiliary subunits, β , and $\alpha_2\delta$, are involved in membrane-channel trafficking, anchorage and altering the biophysical properties of the channel (Hofmann, Flockerzi et al. 2014). Same as all LTCC, the α_1 -subunit of the Cav1.2 is composed of four homologous domains, and each domain is made up of six transmembrane helices (S1-S6). The first four helices

(S1-S4) in each domain form the voltage-sensing domain (VSD). The two helices (S5 and S6) and their linker (P-loop) in each domain form the pore region of the channel, known as pore-forming domain (PFD), which includes the selectivity filter (SF), the central cavity, and the internal-gate (as fig. 1.4.1) (Wu, Yan et al. 2015, Wu, Yan et al. 2016).

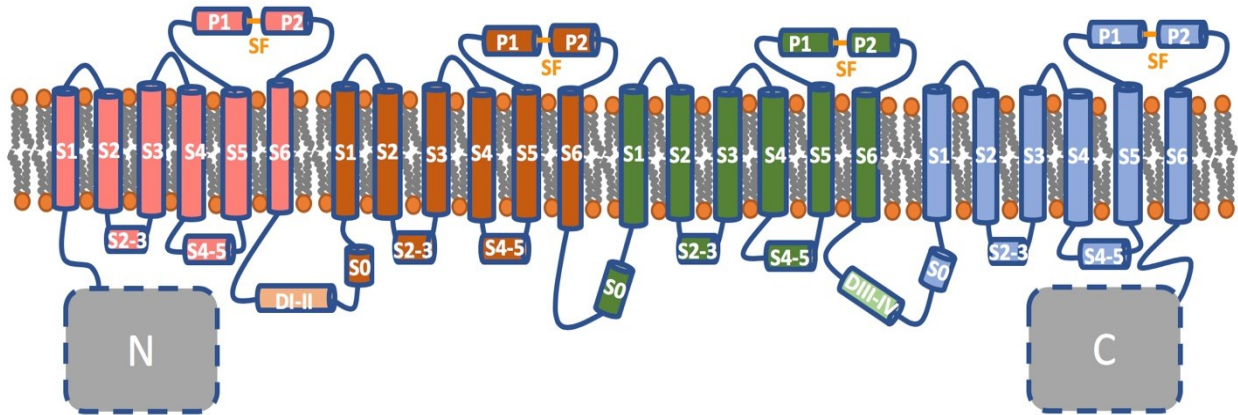


Figure 1.4.1. The secondary structure topology of the hCav1.2 α_1 -subunit. Our model includes the region between the terminal domains.

1.4.2 Cav1.2 channel regulation

Cav1.2, being a L-type calcium channel, remains mostly similar with other L-type members. The Cav1.2 is sensitive to changes in the membrane potential through the VSD (S1-S4 helices). In addition to the voltage-dependent gating mechanisms, the channel's conductivity is also dependent on the intracellular Ca^{2+} concentration, and hence, these channels are modulated by both self-regulatory and extrinsic mechanisms (Hofmann, Flockerzi et al. 2014). In addition to the voltage-dependent activation/inactivation (VDA/VDI), the Cav1.2 are also regulated by calcium-dependent mechanisms. Calcium-dependent regulation is mediated by the interactions between the Ca^{2+} /CaM and Cav pre-IQ/IQ domains. Disruption to this interaction has been known

to attenuate the calcium-dependent inactivation process. At the resting potential, apo-CaM associates with the alpha-subunit of the channel. When Ca^{2+} ions bind the CaM, the fully charged CaM with four Ca^{2+} ions allow the two polarized lobes of the CaM, the Ca^{2+} /N lobe, and the Ca^{2+} /C lobe, to envelope the alpha-binding helix. Specific interactions of two lobes with the IQ domain initiate different calcium-dependent regulations. Both these mechanisms are known to induce conformational changes on the channel gates.

The calcium-dependent channel regulation process requires the participation of multiple segments, such as the β -subunit, Ca^{2+} /CaM, CaMKII, N-terminal and C-terminal regions of the $\text{Cav}1.2\alpha_1$. Calcium-dependent inactivation serves as the auto-inhibitory control for the LTCCs to control the levels of intracellular calcium. In $\text{Cav}1.2$, CDI is caused by the interaction between the IQ domain and the Ca^{2+} /C-lobe, while CDF is facilitated by the interaction of the Ca^{2+} /N-lobe and the IQ domain (Fallon, Halling et al. 2005, Hulme, Yarov-Yarovoy et al. 2006). In contrary, the IQ domain interactions with the Ca^{2+} /N-lobe and the Ca^{2+} /C-lobe in the $\text{Cav}2.1$ channel, lead to CDF and CDI, respectively (Kim, Rumpf et al. 2008, Mori, Vander Kooi et al. 2008).

Ferreira et al. reported that calcium-dependent mechanisms could speed up the inactivation process (Ferreira, Yi et al. 1997). They used barium in the place of calcium ion and found that the channels undergo rapid activation and slow inactivation due to the lack of intracellular calcium. Their result showed that voltage-dependent mechanisms alone in the absence of calcium-dependent mechanisms would lead to slower inactivation (Lipscombe, Helton et al. 2004, Hulme, Yarov-Yarovoy et al. 2006). While CaM promotes calcium-dependent inactivation, the Ca^{2+} /calmodulin-dependent protein kinase II (CaMKII) counteracts the above process and helps in the re-activation of the channel in a calcium-dependent way. CaMKII phosphorylates the $\text{Cav}\beta$ subunit and the C-terminus of $\text{Cav}1.2\alpha_1$ at their specific phosphorylation sites, resulting in the

disruption of CaM-Cav channel interactions. Increase in the intracellular calcium ion level activates the CaMKII and reduces the effects of CDI (Abiria and Colbran 2010, Hofmann, Flockerzi et al. 2014). CaMKII enables the channel gates to be frequently left in the open state for a long time thus, prolonging the plateau phase of the action potential at high frequency.

RATIONALE, HYPOTHESIS, AND OBJECTIVES

RATIONALE

The human Cav1.2 ion channel is essential for normal cardiac and neuronal functions. It is, therefore, important to understand the different structural and dynamical events taking place within this channel at the atomic level. These events include ion conduction, gating states and the effects of drug binding on ion permeation. These complicated functions rely on two domains within the channel, namely the voltage sensor domain (VSD) and the pore-forming domain (PFD). Understanding the dynamical interactions between these two domains can reveal the different mechanisms adopted by Cav1.2 to conduct its functions. However, these conformational changes and structural mechanisms are very hard to reveal through traditional structural analysis (*e.g.* x-ray crystallography and NMR spectroscopy) and, therefore, modelling can be used to provide a fine image of these events. For this reason, this thesis aimed at building a dynamic model for the Cav1.2 channel. The model described in this work builds and improves upon the earlier models and has been validated through the reported experimental data.

HYPOTHESIS

There are three major hypotheses for this thesis:

- 1) The selectivity towards calcium ion relies on the residues and binding sites at the selectivity filter of human Cav1.2.
- 2) The gating states of Cav1.2 rely on the relative position of its VSD and PFD as well as on the bending angle of the VSD and PFD connector.
- 3) A strong Cav1.2 blocker can bind to a site close to the selectivity filter, allowing it to block the ion influx through the channel.

OBJECTIVES

To provide a clear investigation of these three hypotheses, this thesis focused on the following objectives:

- 1) To build a reliable atomistic homology model for the Cav1.2 α_1 -subunit.
- 2) To study the transitional conformations between the closed and open states of Cav1.2.
- 3) To study the mechanisms of calcium ions' permeation through Cav1.2.
- 4) To study the effects of known calcium channel blockers (CCBs) on ions' permeation.

CHAPTER 2: MODELING THE CARDIAC CA_V1.2 ION CHANNEL²

2.1 Introduction

Computational homology-based modeling has been recognized as a powerful technique for building the unknown structure of proteins, including ion channels. Furthermore, homology models of the Cav1.2 pore domain, have been previously reported using the structure of potassium channel, K_V1.2 (Stary, Shafrir et al. 2008), K_VAP (Tikhonov and Zhorov 2008), and KCSA (Tikhonov and Zhorov 2009), and sodium channels, NachBac (Martinez-Ortiz and Cardozo 2018). In 2014, the three-dimensional structures of the calcium channel from bacteria (*Arcobacter butzleri*), the CavAb, were resolved using X-ray crystallography technique (Tang, Gamal El-Din et al. 2014). This structure shows homo-tetramer architecture for the calcium channel with four copies of the same polypeptide forming the channel pore. Although this architecture is not similar to that of the Cav1.2, whose pore is formed by four non-identical repeats, the CavAb structures resolved in complex with known antagonists gave valuable insights on small molecule binding interactions (Tang, Gamal El-Din et al. 2016). Similarly, in 2015, the structure of the first mammalian VGCC (rabbit Cav1.1) in the closed conformation and complex with the β auxiliary subunit was resolved using the cryo-electron microscopy technique (PDB: 3JBR) at 4.2Å resolution (Wu, Yan et al. 2015). Later, a refined complex of Cav1.1 α_1 with the β subunit was reported at 3.9 Å (PDB: 5GJW) resolution (Wu, Yan et al. 2016). The Cav1.1 α_1 -subunit share higher sequence identity, ~65% (sequence similarity ~80%), with that of the Cav1.2 α_1 -subunit

² A version of Chapter 2 has been published as a research article: Tianhua Feng, Aravindhan Ganesan, Subha Kalyanamoorthy, and Khaled Barakat. "Atomistic modeling and molecular dynamics analysis of human Ca_V1.2 channel using external electric field and ion pulling simulations." *Biochim Biophys Acta Gen Subj.* 2019 Jun;1863(6):1116-1126.

(Table 2.1.1). With the advent of technologies and better templates (more homologous calcium channels), it is possible to build more complete and accurate models of the Cav1.2.

	Percent Identity Matrix			
	Human Ca _v 1.2	Rabbit Ca _v 1.1	Eel Na _v 1.4	Bac Ca _v Ab
Human Ca _v 1.2	100%	65.08%	18.26%	13.80%
Rabbit Ca _v 1.1	65.08%	100%	20.79%	16.10%
Eel Na _v 1.4	18.26%	20.79%	100%	16.10%
Bac Ca _v Ab	13.80%	16.10%	16.10%	100%

Table 2.1.1. The amino acid sequence comparison among human Cav1.2 α_1 -subunit, rabbit Cav1.1 α_1 -subunit, Eel Nav1.2 α_1 -subunit, and bacteria CavAb channel

A recent study by Martinez-Ortiz et al. reported an improved and optimized rabbit Cav1.1 cryo-EM structure (Martinez-Ortiz and Cardozo 2018). The rabbit Cav1.1 share high sequence similarity with that of the human Cav1.2 and possesses identical topological components in the transmembrane domain. In this study, we report a comprehensive homology-based model of the transmembrane region together with the interlinking intracellular subunits of the Cav1.2 channel built using the recent cryo-EM structure of the Cav1.1 α_1 -subunit as the template. We performed different molecular dynamic simulations methods, including the classical, external electric field and steered molecular dynamics to understand the structure-function and gating process of the Cav1.2 channel. We also report a near-open conformation (NOC) of the hCav1.2 channel obtained using our simulations and list the critical residues involved in ion conduction and gating changes. To understand the differences between our model and an open model, we also generated a hCav1.2 model based on the open conformation of Eel Nav1.4 (PDB: 5XSY) (Yan, Zhou et al. 2017). The work described here depicts the dynamics associated with ion permeation at the atomistic level.

We hope that the generated models can be used to further understand the mechanisms of drug binding and blockade to the human Cav1.2 channel (hCav1.2).

2.2 Homology Modeling of Human Cav1.2 Alpha Subunit

The three-dimensional (3D) structure of the transmembrane domain comprising of 1417 amino acid residues (corresponding to the residue numbers, 111 to 1517) was modeled using the I-Tasser molecular modeling package (as figure 2.2.1). The structure modeling was carried out in different stages as described in the methods section. Five models of the human Cav1.2 α_1 transmembrane domain was built using the recent cryo-EM resolved structure of rabbit Cav1.1 α_1 as the primary template. Since, the structure of rabbit Cav1.1 α_1 conform to the closed (or resting) state of the channel, where the internal gate is narrow, the homology models of Cav1.2 α_1 built from this template also conforms to the closed state of the Cav1.2 α_1 channel (Wu, Yan et al. 2016).

Model	C-score [#]	No. of Cluster [#]	Density [#]	PROCHECK [#] (G-factor Value)	Ramachandran Plot (%)			WHATCHECK*			
					Favoured	Allowed	Disallowed	Side Chain Planarity	Omega Angle Restraints	Bond Lengths	Bond Angle
No.1	-1.61	336	0.0239	-0.48	77.3	19.3	3.4	0.794	2.592	1.233	1.415
No.2	-1.50	357	0.0265	-0.29	79.7	17.1	3.2	1.068	1.621	1.164	1.320
No.3	-1.49	303	0.0268	-0.46	77.7	19.6	2.6	0.862	2.424	0.982	1.338
No.4	-1.81	243	0.0195	-0.57	74.1	22.4	3.5	0.991	2.735	1.149	1.455
No.5	-2.51	110	0.0097	-0.44	75.7	21.7	2.6	0.850	2.515	0.752	1.206

“*” – RMS Z-scores should be close to 1.0

“#” – Higher value indicates better quality

Table 2.2.1. Structural quality scores of five hCav1.2 homology models estimated based on overall stereochemical quality of PROCHECK and the side chain planarity, omega angle restraints, bond length, and bond angle score of WHATCHECK program.

```

CAC1C_HUMAN      1 NPIRRACISIVWKPFEIIILLTIPANCVALAIYIPFPEDDSNATNSNLE
CAC1S_RABIT      1 -----IPANCVALAVYLPMPEDDNNLSNLE
CAC1C_HUMAN     51 RVEYFLFIIFTVEAFLKVIAYGLLPHNPAYLRNGWNLDFIIVVGLFSA
CAC1S_RABIT     28 KLEYFFLTVFSIEAAMKIIAYGFLPHQDAYLRSQWNLDFIIVFLGVFTA
CAC1C_HUMAN    101 ILEQATKADGANA-LGGKAGFDVKALRAFVLRPLRLVSGVPSLQVVLN
CAC1S_RABIT     78 ILEQVNVIQSNTPAMSSKAGLDVKALRAFVLRPLRLVSGVPSLQVVLN
CAC1C_HUMAN    150 SIKAMVPLLHIALLVLFVIIYAIIGLELPMGKMHKTCY--NQEGIADV
CAC1S_RABIT    128 SIFKAMLPFHIALLVLFMVIIYAIIGLELPMGKMHKTCYIIGTDIVATV
CAC1C_HUMAN    198 PAEDDPSPCALETHGRCQCC-NGTVCVKPGWDGPKHGITNFNFAPAMLTV
CAC1S_RABIT    178 ENE-KPSPCA-RTGSGRPTINGSECRGWPNGHITHFDFNFGFSLTV
CAC1C_HUMAN    247 FQCIIMEGWTDVLYWVNDVAVGRDWPNIYFVTLLIIGSFFVLNLVGLVSG
CAC1S_RABIT    226 YQCIIMEGWTDVLYWVNDVAVGRDWPNIYFVTLLIIGSFFVLNLVGLVSG
CAC1C_HUMAN    297 EFSKEREKAKARCDPQKLRKQQL EEDLKG YLDWITQAEIDDPENEDEGM
CAC1S_RABIT    276 EFKERERKAKSRCTPQKLRKQQL EEDLRG YMSWITQGEVMDVEDLREG-
CAC1C_HUMAN    347 DEEKPRNMSPT--SETESVNTENVAGGDIEGECNGARLAHRISKSKFSR
CAC1S_RABIT    325 -----KLSLEEGGSDTESLY-----EIEGLN-----KIIQPIR
CAC1C_HUMAN    395 YWRRNRFRCRRKRAAVKSNVFWLVIPLVFLNPLTIASEHYNQPNWLTE
CAC1S_RABIT    353 HWRQWNRVFRWKCHDLVKSRVFWLVLIVLALNTLSIASEHNNQPLWLTH
CAC1C_HUMAN    445 VQDTANKALLALFTAEMLLKMYSLGLQAYVSLFNRFDFCVVCGGILETI
CAC1S_RABIT    403 LQDIANRVLLSLFTIEMLLKMYGLQLRQYFMSIFNRFDFCVVCGGILELL
CAC1C_HUMAN    495 LVETKIMSPGLGISVLRVRLRIFKITYRWNSLSNLVSLNSVRSIASL
CAC1S_RABIT    453 LVESGAMTPLGISVLRIRLRLRFKITYRWNSLSNLVSLNSVRSIASL
CAC1C_HUMAN    545 LLLFLFIIIFSLGMQLFGCKNFDEMQTRRSTFDNFPQSLTTFVQILT
CAC1S_RABIT    503 LLLFLFIIIFALLGMQLFGGRYDFEDTEVRRSNFDNFPQALISVFQVLT
CAC1C_HUMAN    595 GEDWNSVMYDGMAYGGPSFPGMLVCIYFIIILFICGNYILLNVFLAIAVD
CAC1S_RABIT    553 GEDWNSVMYNGIMAYGGPSYPGVLVCIYFIIILFVCGNYILLNVFLAIAVD
CAC1C_HUMAN    645 NLADAESL TSAQKEEEERKRLARTASPEKKQELVEKPAVGESKEEKI
CAC1S_RABIT    603 NLAEAESL TSAQKAEERKRRKMSR-GLPDKTEE--EKSVMAKLEKQ-
CAC1C_HUMAN    695 ELKSITADGESPPAT-KINMDDLQPNENEDKSPYPNPETTGEDEEPEEM
CAC1S_RABIT    649 -----PKGEGIPTTAKLKVDFESVNEVKDPYPSADFPGDDEDEPEI
744 PVGPRRPLSELHLKEKAVMPPEASAFFIFSSNNRFRLOCHRIVNDTIFT
693 PVSRRRPLAELQLKEKAVPIPEASSFFIFSPTKNVRVLRCHRIVNATWFT
794 NLILFFILLSSISLAAEDPVQHTSFRNHILFYDFIVFTTIFTIEIALKIL
743 NFILLFILLSSAALAAEDPIRAESVRNQLGLGYFDI-----
844 GNADYVFTS IPTLEIILKMTAYGAPLHKGSFCRNYFNLDLVLVSVSLIS
778 -----AFTSVFTVEIVLKMTTYGAPLHKGSFCRNYFNLDLVLVAVSLIS
894 FGIQSSAINVVKILRVLRLRPLRAINRAKGLKHEVQCVFVAIRTIGNIV
823 MGLSSTISVVKILRVLRLRPLRAINRAKGLKHEVQCVFVAIRTIGNIV
944 IVTTLLOFMFACIGVQLFKGKLYTCSSSKQTEACEKNYITKYGDEVDH
873 LVTTLLOFMFACIGVQLFKGKFCNLSKMTTEECRCGYIYVVKDGDPTQ
994 PIQPRSWENSKFDFDNLAAAMLFTVSTFEGWPELLYRSIDSHTDKG
923 MELRFRQWVHNDHFDFNLVLSAMSLFVSTFEGWPELLYRAIDSNEEDMG
1044 PIYNRVVEISIFPIIYIIIAFFMNNIFVGFVIVTFQEGQEQEYKNCELD
973 PVYNNRVEMAIFPIIYIILIAFFMNNIFVGFVIVTFQEGQETEKNCELD
1094 KNQRQCEVYALKARPLRRYIPKNOHQYKVVYVNVNSTYFEYLMFVILLNT
1023 KNQRQCVQYALKARPLRCYIPKPNYQVQVYVVTSSYFEYLMFALIMLNT
1144 ICLAMQHYGQSCLPKIAMNINLMLFTGLPTVEMILKLIAPFKPGYSDPW
1073 ICLGMQHYHQSEEMNHISDILNVAFTIIPFTLEMILKLIAPKARGYFGDPW
1194 NVDFFLIVIGSIIDVILSETNHYPDCAWNTFDALIVVGSIVDIAITEVNP
1123 NVDFFLIVIGSIIDVILSEIDTFGLASS----GGYCLGG-----
1244 AEHTQCSPSMNAENSRISITPFRFRVVMRLVKLLSRGEGIRTLWTFIK
1158 ----GCG-NVDPDESARISSAFFRFRVVMRLIKLKSRAEGVRTLWTFIK
1294 SFQALPYVALLIVMLFFIYAVIGMQVFGKIALNDTTEINRNNNFQTFPQA
1203 SFQALPYVALLIVMLFFIYAVIGMQVFGKIALVDGTQINRNNNFQTFPQA
1344 VLLFRCATGEAWQDIMALCMPGKKAPESE--PSNSTEGETPCGSSFAV
1253 VLLFRCATGEAWQELLACSYKLCDPESDYPAGE----EYTCGTNFAY
1392 FYFISFYMLCAFLIINLFAVIMDNF-----
1299 YFISFYMLCAFLIINLFAVIMDNFDYLRDWSILGPHLDEFKAIWAE

```

Figure 2.2.1. The sequence alignment between Human Cav1.2 α_1 (111-1527) and Rabbit Cav1.1 α_1 . The solid line, two dots, and one dot indicate the same, high similarity, and low similarity amino acids based on the physiochemical properties.

To evaluate the quality of the generated models and to choose the best model for further analysis, we performed a Ramachandran plot analysis on the five I-Tasser models (Roy, Kucukural et al. 2010, Yang, Yan et al. 2015). Analysis of Ramachandran plots of these five models, which were obtained from the PROCHECK module, indicate that 90% of the amino acid residues are found in the favored and allowed regions (as fig. 2.2.2 & fig.2.2.3). Additionally, in all of the five models, < 5% of the residues were found to be in the unfavorable regions of the Ramachandran

plots. The top four models show similar and acceptable C-score, a confidence score for estimating the quality of predicted models by I-TASSER. Table 2.2.1 provides the individual scores for the five models obtained from different structure quality assessment programs. The stereochemical quality assessment based on the Ramachandran plot shows that model 2 has the highest percentage of residues placed in the favorable and allowed region. The G-factor scores from the PROCHECK also confirm that model 2 has better stereochemical properties compared to other models (Laskowski, Macarthur et al. 1993). Further, the quality of the non-bonded interactions between the atoms was assessed using the ERRAT server, which showed that model 2 has a better quality compared to the other models .

The structural alignment between the rabbit Cav1.1 template and model 2 returns a root-mean-square-deviation (RMSD) value of 0.373 Å. The transmembrane regions were mostly conserved between the two proteins and had also been resolved in the rabbit Cav1.1 EM-cryo structure. To assess the accuracy of the models in areas that are not available in the template, we performed a sequence-based secondary structure prediction of the target sequence (i.e., the hCav1.2). Since most of the missing (unresolved) regions in the template were located on the extracellular and cytoplasmic regions, we focused on analyzing the consistency of secondary structures between the sequence-based prediction and the built models.

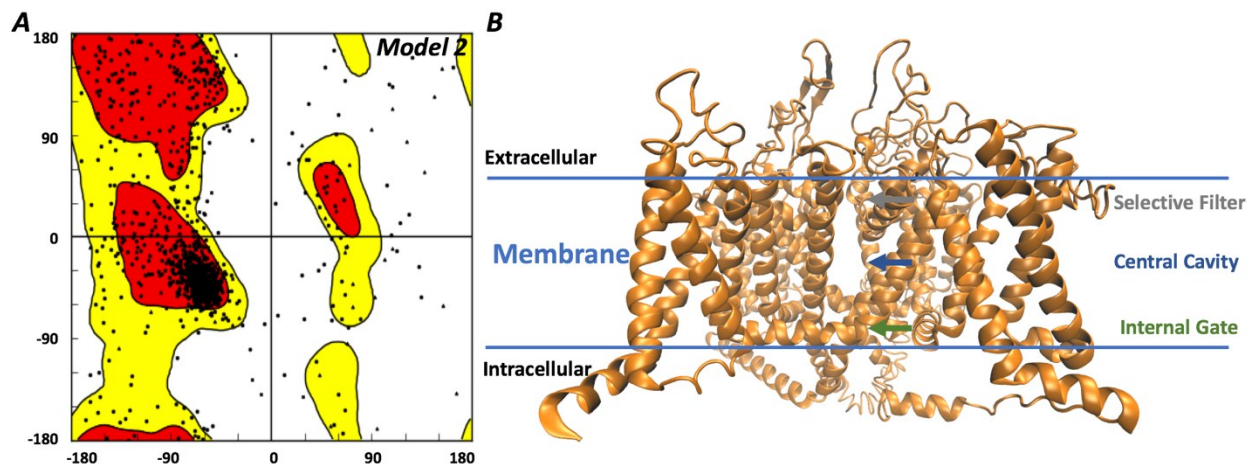


Figure 2.2.2. A) The Ramachandran plot, and B) the structure of second hCav1.2 α_1 -subunit model.

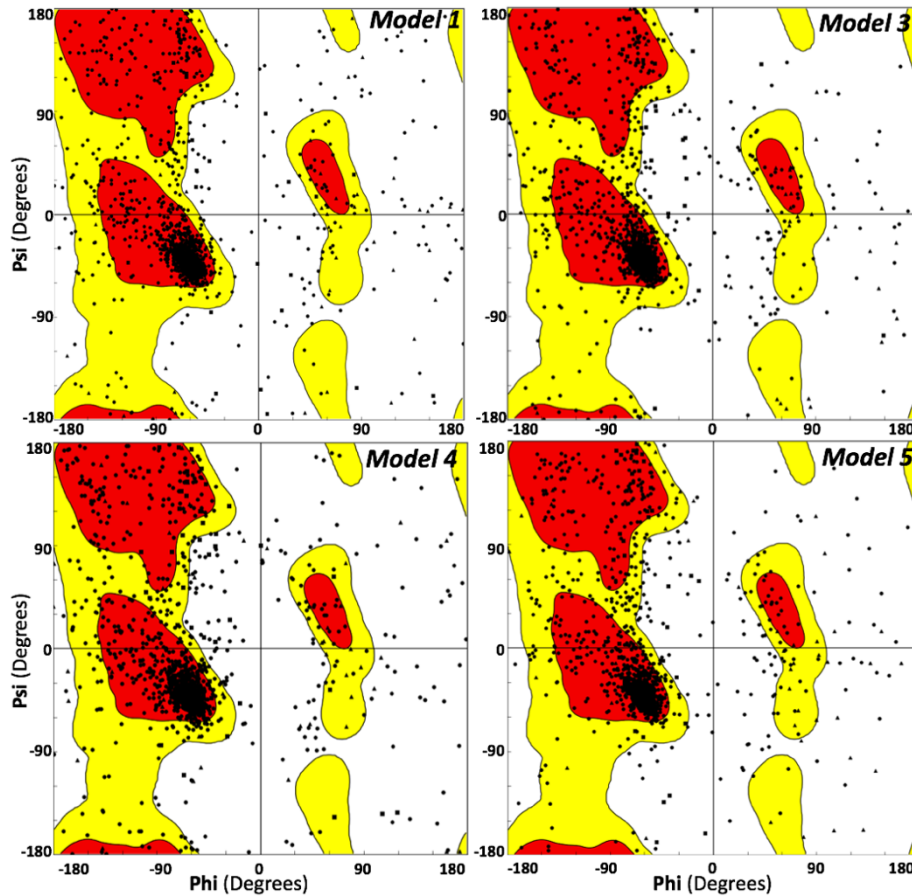


Figure 2.2.3. The Ramachandran plots on hCav1.2 α_1 -subunit first, third, fourth, and fifth models.

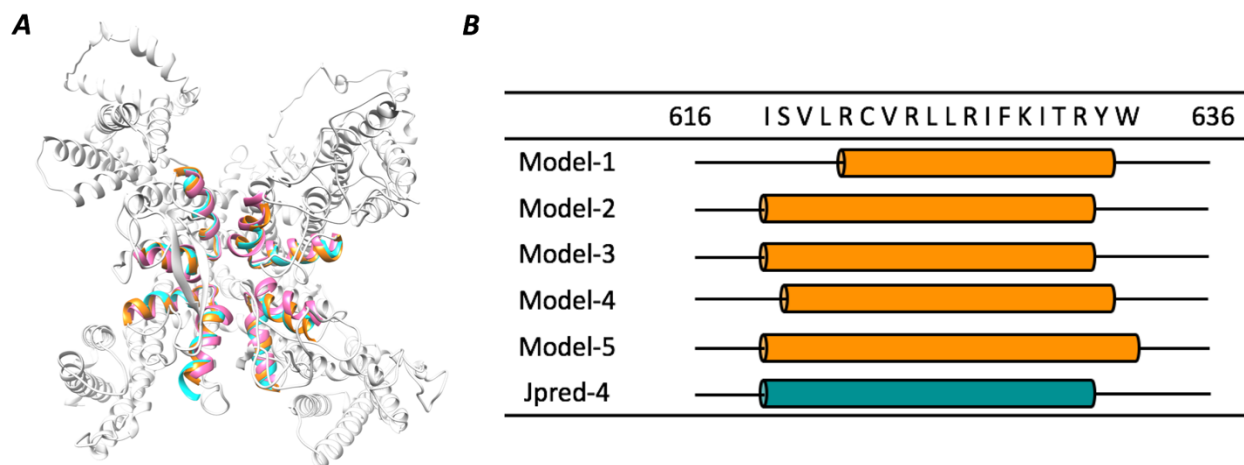


Figure 2.2.4. A) Overlapping the selectivity filter of rabbit Cav1.1 (Cyan), CavAb (Pink), and the hCav1.2 model (Orange). B) Comparing the secondary structure of S4 helix in transmembrane domain II with the Jpred-4 prediction.

The secondary structural elements of the models were found to be mostly in agreement with the sequence-based predictions. However, we found that the transmembrane helices, S4 and S6 of DII, had inconsistencies in the helix-spanning residue range. For example, except for model 2 and model 3, all the other models had different lengths of the S4 helix from what is expected, which is the helix corresponding to residues I616 to W634 (as fig. 2.2.4). In general, the secondary structural elements of models 2 and 3 are in good agreement with the sequence-based prediction when compared to the other three models. However, we found that few regions in model 3 were not properly oriented, e.g., the residues LYS460–GLU485, ILE805–LEU865, and ASP1335–PRO1361 corresponding to the cytoplasmic region were placed in proximity to the transmembrane region, which might interfere with the palmitoyl-oleoyl-phosphatidylcholine (POPC) membrane when building the system (as fig. 2.2.5).

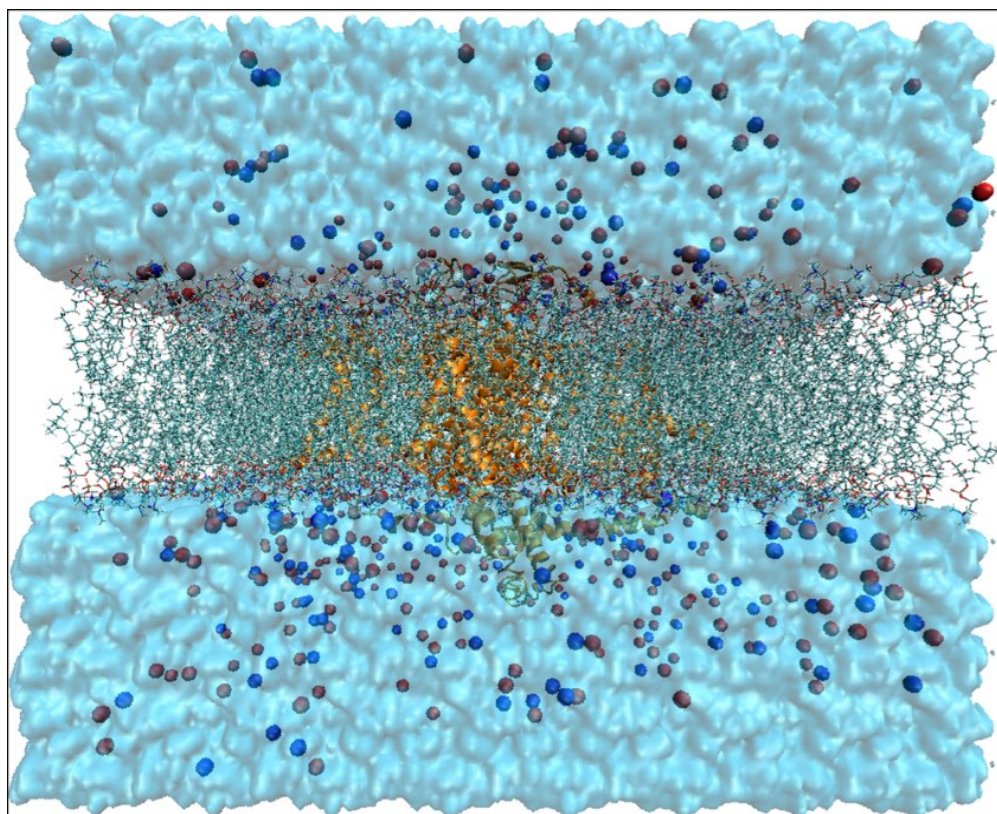


Figure 2.2.5. Classical MD simulation system on hCav1.2 channel, including solvent, ions, lipid bilayers, and transmembrane domain of human Cav1.2 channel.

Also, two crystal structures of the human Cav1.2 segment, the Alpha Interacting Domain (AID), have been resolved (PDB: 1T0J, 4DEY) previously (Van Petegem, Clark et al. 2004, Almagor, Chomsky-Hecht et al. 2012). This 18-residue long polypeptide forms an intracellular α -helix and interacts with the α -subunit to mediate calcium-dependent activation of the Cav (Buraei and Yang 2013). Among our five models, we found that model 2 accurately recovers the secondary structure and relative position of AID segment (as fig.2.2.5). However, other models are lacking this long α -helix or found to be missing or adding non-AID residues to the helical segment. Thus, we selected model 2 as our preferred model for building the lipid-embedded molecular system. Subsequently, model 2 was prepared for membrane-embedded protein simulation (see fig. 2.2.4)

with CHARMM-GUI, as mentioned earlier. The system was then subjected to molecular dynamics (MD) simulation for ~100 ns. The MD simulation also helps improve the quality of Model 2.

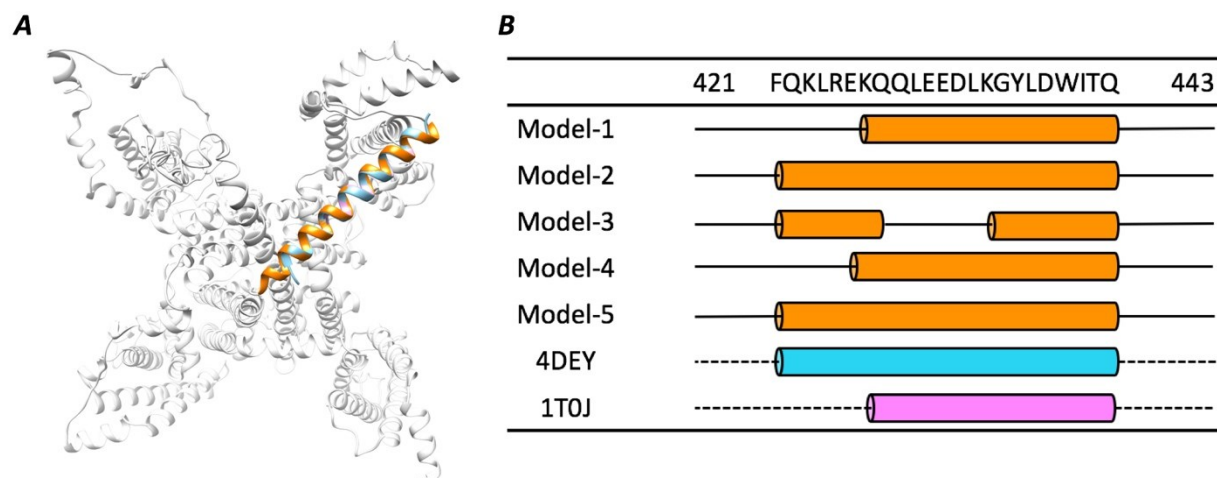


Figure 2.2.6. A) The structure and position of the AID segment (orange) in the hCav1.2 model superimposed with the AID segment from rabbit Cav1.2 (cyan-PDB: 4DEY) and the (partial) AID segment from hCav1.2 (pink-PDB: 1T0J). **B)** Comparing the secondary structure of intracellular linkers of domain II and domain III with the AID of rabbit Cav1.2 (PDB: 4DEY) and partial segment of human Cav1.2 AID (PDB: 1T0J)

2.3 Molecular Dynamic Simulations on Human Cav1.2

All production molecular dynamics simulations were carried out using the CHARMM36 force field parameters and were implemented using the NAMD-2.9 software package. The simulations were performed under periodic boundary conditions, and particle-mesh Ewald method with a grid spacing of at least 1 per Å was used for calculating the long-range electrostatic interactions. A cut-off of 12 Å was used for the van der Waals and short-range electrostatic interactions with a switching distance of 10 Å. The system was maintained at ~303.15 K temperature and 1atm pressure using the Langevin thermostat and piston. The restrained system was initially energy-minimized and equilibrated in six steps. NVT dynamics were performed in

the first two-steps using 1fs time step, followed by four-stages of NPT dynamics with different force restraints applied were performed at 2 fs time step. A 100-ns classical molecular dynamics simulation was performed without any restrictions.

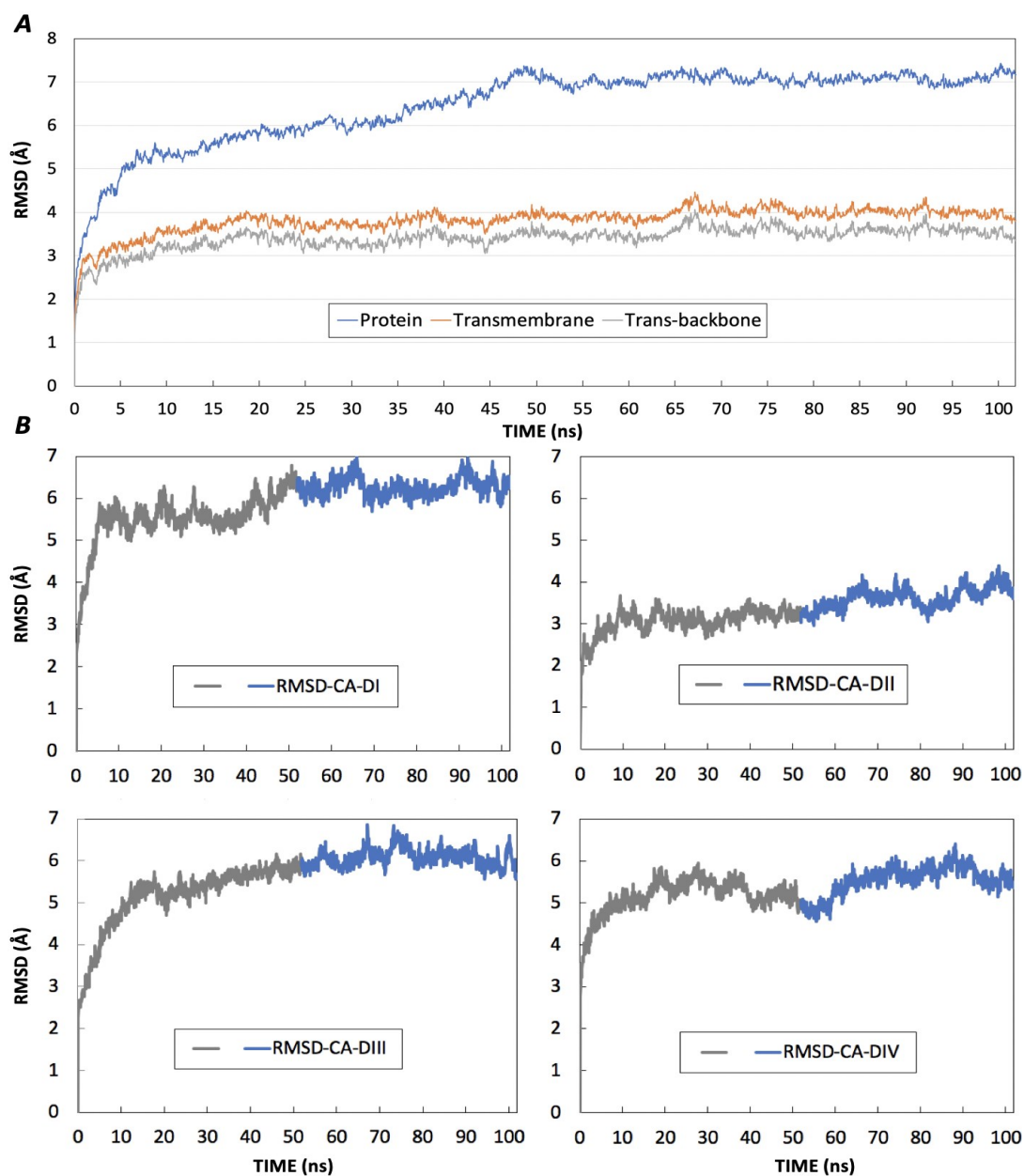


Figure 2.3.1. A) RMSD of ~100 ns length classical molecular dynamic of human calcium channel with 1) all-atom, 2) transmembrane helix, and 3) backbone of transmembrane helix. B) The CA-RMSD of four transmembrane domains, DI, DII, DIII, and DIV from the last 50 ns of the simulation is shown in blue.

A 100 ns classical molecular dynamics simulation was performed on the hCav1.2 model system. The RMSD plot of protein C α (CA), backbone (BB), and all-atom (NoH) shows the system RMSD is stable after 50 ns of the MD simulation (as fig.2.3.1). All analysis on the simulation was therefore performed on the last 50 ns of the MD trajectory. The all-atom RMSDs of the 100 ns-classical simulation stabilized at around 7 Å from the starting model. Among the four transmembrane regions, domain II has the lower average deviation of 3.63 Å, while all the other domains I, III, and IV had higher deviations with an average RMSD of 6.27 Å, 6.08 Å, and 5.53 Å respectively. All transmembrane domains stabilized quickly, within the first 20 ns of the simulation. The root-mean-square-fluctuations (RMSF) analysis (as fig. 2.3.2) shows that residues in the cytoplasmic linkers that connect the domains I and II and domains II and III, respectively are highly dynamic. On the other hand, the selectivity filter residues are quite stable with an RMSF value less than 2 Å. The extracellular loops that link the S3-S4 helices of DI (residue 210 - 232) and S3-S4 helices of DIV (residue 1322 - 1372) exhibit higher flexibility when compared to the extracellular regions of domains II and III (residue 607 – 615 and 1007-1013).

Since our initial model corresponds to closed pore architecture, we did not observe any ion passage during our classical MD simulation. It is important to note that previous MD studies conducted on the VGCCs by other groups, also reported no rapid and spontaneous penetration of calcium through the selectivity filter without the application of a biasing potential. Nevertheless, during our simulation, we observed continued occupancy of few calcium ions on the outer side of the SF region of the channel (as fig.2.3.3). Two calcium ions (CAL53, and CAL76) were found to be in close contact with two negatively charged aspartic acid residues (ASP604, and ASP1036) for at least 80% of the simulation time. We also observed a third calcium ion (CAL161) to be moving close to ASP1358 residue located on the outer side of the selectivity filter. These

negatively charged residues might, therefore, function as a pre-filter by forming a negative shield on the outer region of the pore, thus contributing to the significant selectivity of VGCC toward cations (Ca^{2+}) over anions (Cl^-) (Tang, Gamal El-Din et al. 2014, Adiban, Jamali et al. 2016).

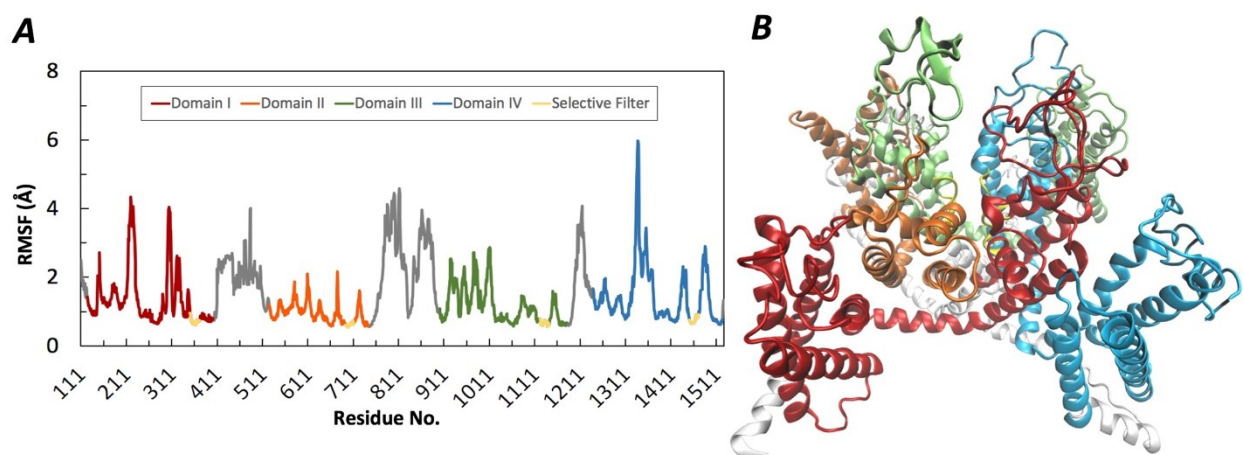


Figure 2.3.2. A) The RMSF and B) the structure of human Cav1.2 α_1 -subunit with different colored domains and selectivity filter.

We also observed that the selectivity filter on the initial model to be too narrow, however following the equilibration and MD protocol, we saw an extension in the pore diameter along the selectivity filter region (as fig.2.3.4). In order to validate our results, we also constructed an open-pore Cav1.2 model using an open-pore Eel Nav1.4 cryo-EM structure as the template. We employed the same protocol for constructing the open-Cav1.2 model. The pore-diameter after the classical MD simulation was in similar range to the pore diameter of an open-state model. The increased pore-space at the selectivity filter enabled the exchange of water molecules through the pore to the central cavity (as fig.2.3.4). On the contrary, we did not observe any increase in the diameter at the internal gate region of the channel. Given the stability of the internal gate region and that there was no passage of ions through the selectivity filter, studying the channel gating and ion conduction mechanisms in classical MD simulation would require several microseconds of

simulation. Therefore, we applied an external electric field to the membrane to enhance the conformational sampling of the channel, and to monitor ion binding/passage through the channel.

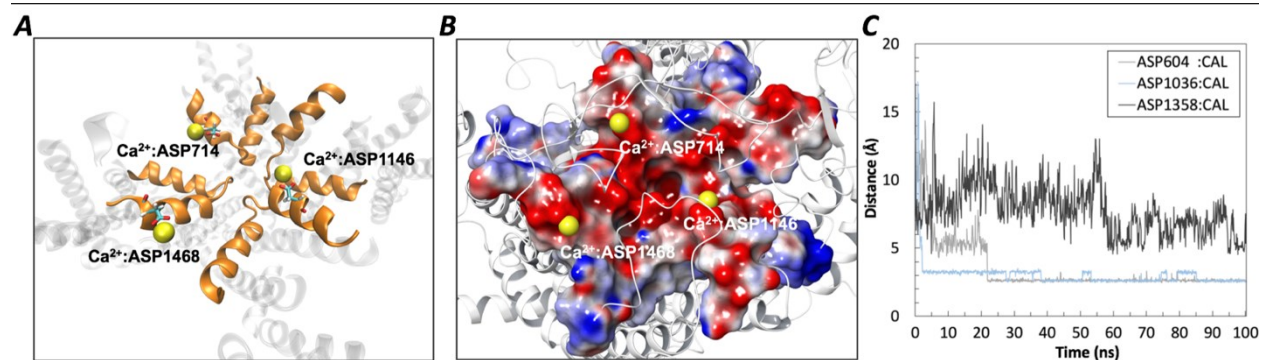


Figure 2.3.3. A) Three calcium ions (yellow) located close to the negatively charged ASP residues on the outer vestibule of the selectivity filter, B) Three calcium ions (yellow) on protein electrostatic surface (negatively charged shown as red, vice versa), and C) Distance between the three calcium ions and the corresponding carboxyl oxygen of the ASP residues.

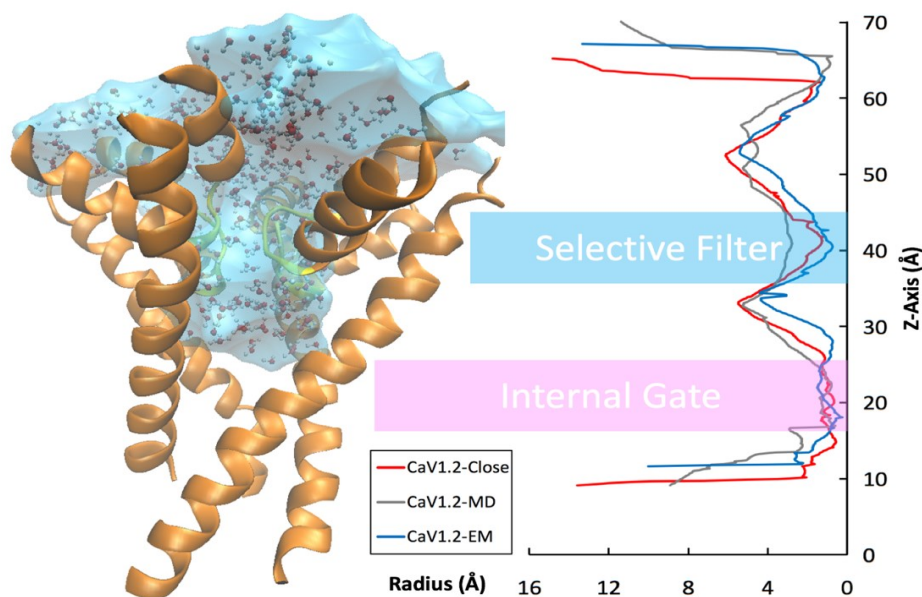


Figure 2.3.4. Water molecules permeated into the central cavity through the SF after 100 ns cMD and the pore-radius of hCaV1.2 at different stages of cMD.

2.4 External Electric Field MD Simulation on Human Cav1.2

The external electric MD method allows molecular dynamics simulations of biomembrane systems under realistic ionic gradients and asymmetric salt concentrations, while maintaining the conventional periodic boundary conditions required to minimize finite-size effects in an all-atom explicit solvent model (Khalili-Araghi, Ziervogel et al. 2013). We have simulated the human voltage-gated Cav1.2 embedded in a POPC lipid bilayer surrounded by CaCl₂ solutions at an ionic concentration of 150 mM, which has been used to equilibrate the system and accelerate the ion permeation (Adiban, Jamali et al. 2016). Electrostatic potential of -40 mV is applied across the membrane to mimic the initiation potential of human Cav1.2 (Hering, Zangerl-Plessl et al. 2018). We chose the potential similar to the activation potential of the channel to see if this can help in the spontaneous passage of the Calcium ions down the selectivity filter and to check the dynamics of the positively charged S4-residues. The membrane-embedded system and the electrostatic potential along Z-axis passing through the membrane are shown in figure 2.4.1.

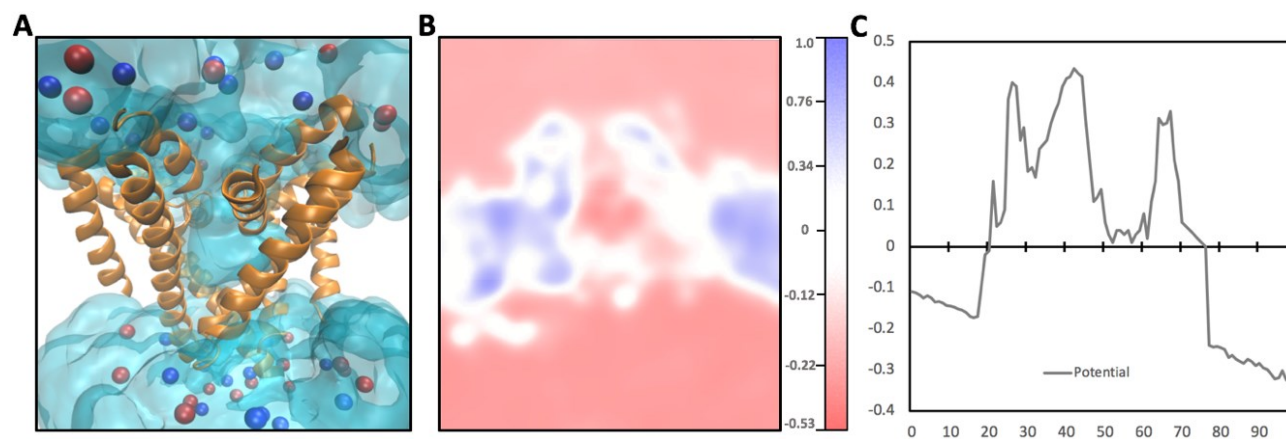


Figure 2.4.1. A) The pore domain of hCav1.2 embedded in the membrane showing water permeation through the channel and ions present on the upper and lower side of the channel. B) Electrostatic potential map over the cross section of the system and averaged over the last 5 ns of the EE-MD simulation trajectory. C) Average electrostatic potential values along the Z-axis.

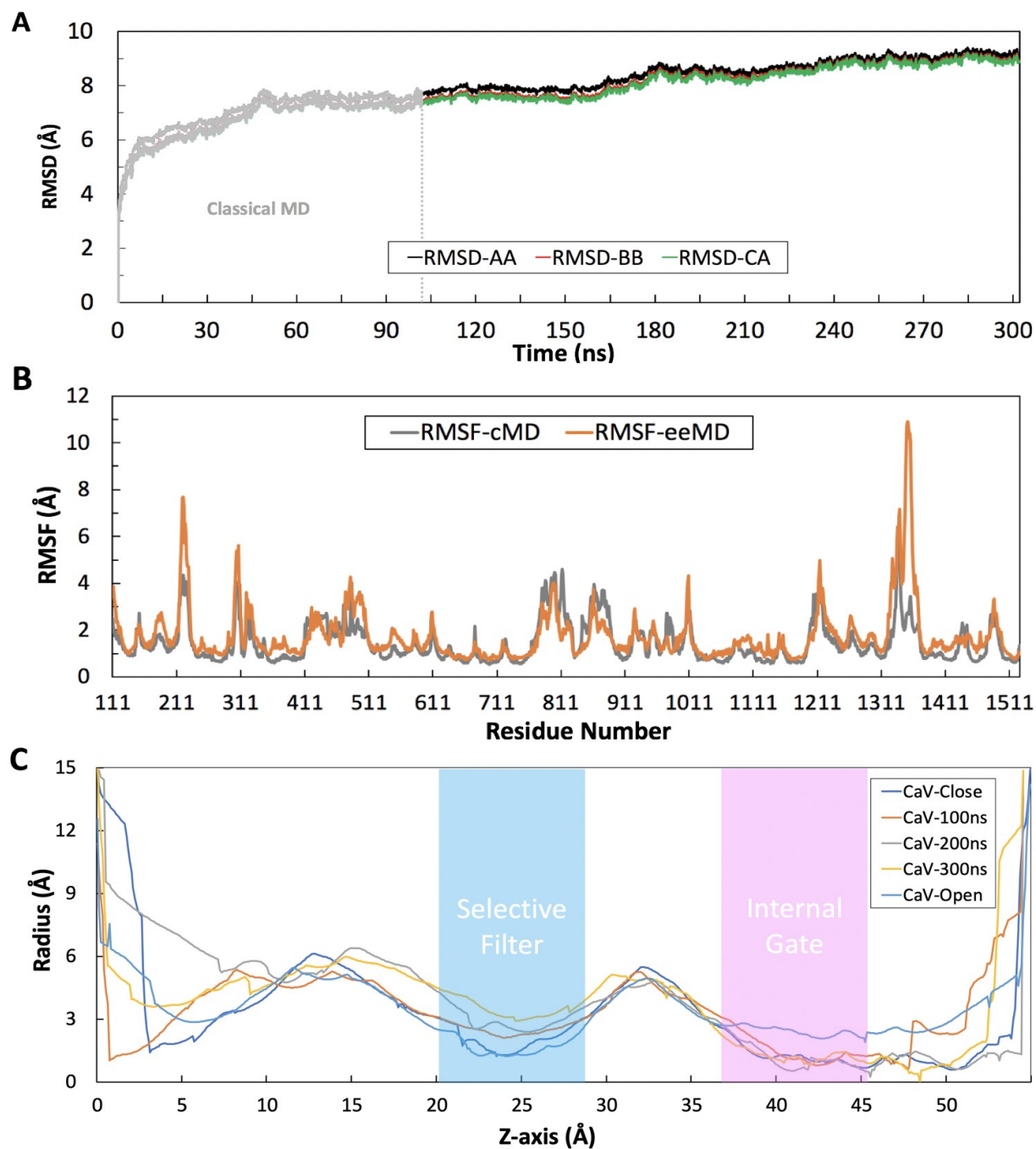


Figure 2.4.2. A) Overall ~300 ns-length RMSD plot, including ~100 ns of classical MD and 200 ns EE-MD. B) 200 ns-length RMSD plot of EE-MD referred on the last frame of MD. C) RMSF of residues in cMD and EE-MD. D) Pore-radius along ~300 ns simulation comparing with Cav open.

The well-equilibrated system was simulated for another 200 ns under the influence of the external electric field. We observed a slight increase in the RMSD of the system after 75 ns of the external electric field application (as Fig. 2.4.2A). The RMSF analysis in figure 2.4.2B shows a similar trend in the flexibility of the residues. However, the extracellular loops that link the S3-S4 helices of DI (residue 210 - 232), the S5-SF helices of DI (residue 291 - 350), and S3-S4 helices of DIV (residue 1322 - 1372) exhibit a higher flexibility. Throughout the 200 ns external field simulation we did not observe any ion passage through the selectivity filter region. Further, after 75 ns of EE-MD, we observed broadening of the selectivity filter resulting in increased pore-diameter at this region (as Fig. 2.4.2C). On the other hand, the internal gate region showed a slight expansion and did not undergo any further conformational change. Thus, we used only the first 50 ns of the EE-MD trajectory for further analysis. Since no spontaneous ion passage was observed in the EE-MD, we adopted the steered molecular dynamics method for studying the ion conduction mechanisms in the Cav1.2 channel.

2.5 Conformational States of Human Cav1.2

The dominant conformations of the Cav1.2 channel was sampled by performing RMSD-based clustering on the last 50 ns of the classical MD simulation and the external electric MD simulation. The optimal number of clusters was selected by using the elbow criterion on the ratio between a sum of squares regression (SSR) to the total sum of squares (SST) and the coinciding local-minima on the Davies-Bouldin index (DBI) metric (as Fig.2.5.1 A). The heat maps showing the RMSDs between the 25 cluster representatives are given in figure 2.5.1. A 2.3 Å threshold was used to re-filter and remove the highly similar conformations. Ten conformations in total from both the classical MD and external electric field MD was selected for the SMD simulations.

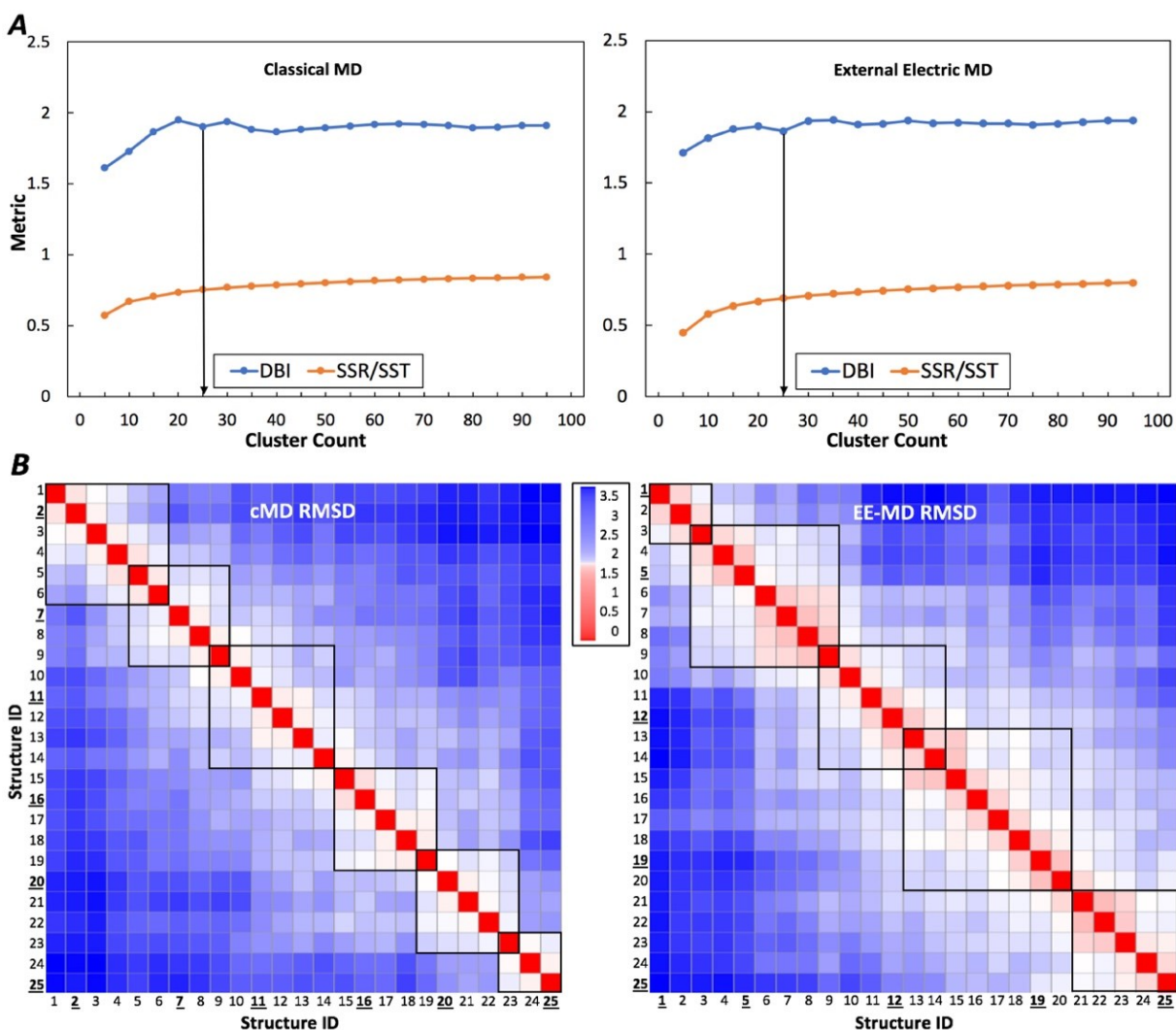


Figure 2.5.1. A) Clustering analysis for the classical MD (left) and external electric MD (right) trajectories. An optimal clustering number is predicted when a plateau in SSR/SST coincides with a local minimum in the DBI metric. B) Heatmap based on the RMSD of classical (left) and external electric (right) MD clustered conformations. During the refinement, eleven clusters from all trajectory are selected from previously selected clusters.

Clustering was performed on the last 50 ns of the classical MD (cMD) trajectory and the first 50 ns of the external electric field MD (EE-MD) trajectory (Ahmed, Jalily Hasani et al. 2017). Figure 2.5.1 A shows the clustering analysis for the two 50 ns trajectories of classical and external electric MD simulations. By varying the number of clusters from 5 to 95 while observing the two-clustering metrics DBI and SSR/SST, one can expect a high-quality clustering when an elbow on

the SSR/SST coincides with the local minimum for the DBI. Based on the SSR/SST and DBI metrics twenty-five clusters were extracted for each 50 ns trajectory. We further performed an RMSD analysis on fifty clusters and constructed the symmetrical heatmap plots (as Fig.2.5.1 B), which showed groups of similar structures with $<2.5 \text{ \AA}$ variations (marked as boxes in the heatmap) (Ahmed, Jalily Hasani et al. 2017). We chose one structure from each group as a representative/replica, which resulted in Six and five replicas from the cMD and EE-MD trajectories, respectively. Overall eleven replicas, representing significant conformations of human Cav1.2 using the cMD and EE-MD simulations were taken for the ion-pulling simulations.

2.6 Steered MD Simulation on Cav1.2

Steered molecular dynamics (SMD) method was employed to study the calcium ion influx mechanisms from the partly open and equilibrated conformations of the Cav1.2 channel. The selected representatives obtained from the external electric field simulations and the classical molecular dynamics simulations were used as replicas for the ion pulling simulations. During the SMD, a calcium ion located on the extracellular side and positioned above the selectivity filter was pulled with a constant velocity ($v = 0.00004 \text{ \AA/fs}$), by a virtual spring with spring constant ($k = 4 \text{ kcal/mol/\AA}$), in the 'Z' direction. The force required to pull the ion was calculated using the formula,

$$F(t) = k \times [Vt - (r_i - r_0)] \times Z \quad (1)$$

where t is the time, ' r_i and r_0 ' are the current and previous positions of the ion, respectively. In SMD, the relative position of the ion at every time step determines the force required to pull the ion, for example, when the ion position remains unchanged, the force required to move the ion would be increased. Thus, the force recorded for each step from the pulling simulations would be useful to identify the significant ion binding sites and the barriers along the pulling direction.

Force constraints were added to the C-alpha atom of the four residues (ILE58, ALA455, LEU856, and LEU1167) in the S1 helices of the four transmembrane domains to restrain the movement of the protein during the pulling process. The ion from the extracellular side is pulled ~ 60 Å towards the intracellular side in 3 ns time scale, and force profiles are corresponding to the pulling were generated using the Tcl scripts.

2.7 Ion Permeation

The steered molecular dynamics method was employed to study the calcium ion conduction mechanism through the Cav1.2 channel. SMD simulations were performed for all 11 replicas, named as R0-R10, which we obtained from our clustering analysis. A calcium ion (CAL76) positioned on the outer region of the selectivity filter close to the Asp residues, was manually moved along a vector (Tang, Gamal El-Din et al.) to position it on top of the SF. The calcium ion was pulled through the channel pore with a constant velocity, $v = 0.00004$ Å/fs and spring constant, $k = 4$ kcal/mol/Å along the Z-direction to cover a distance of about 60 Å. Figure 2.7.1 show the ion passage through the Cav1.2 channel pore using the SMD simulation.

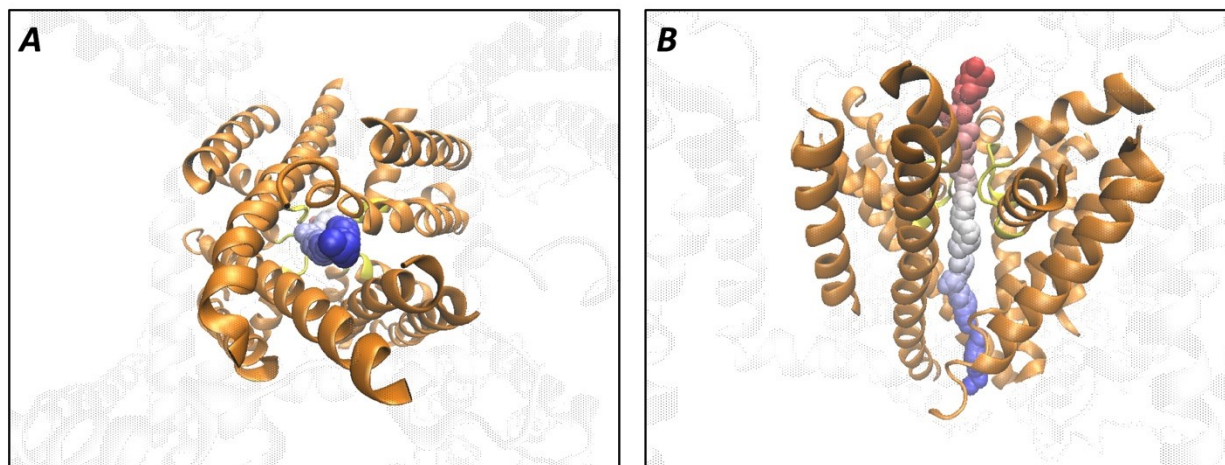


Figure 2.7.1. Calcium ion permeation pathway as seen in the SMD simulation of R6 replica A) Intracellular view and B) Z-axis view.

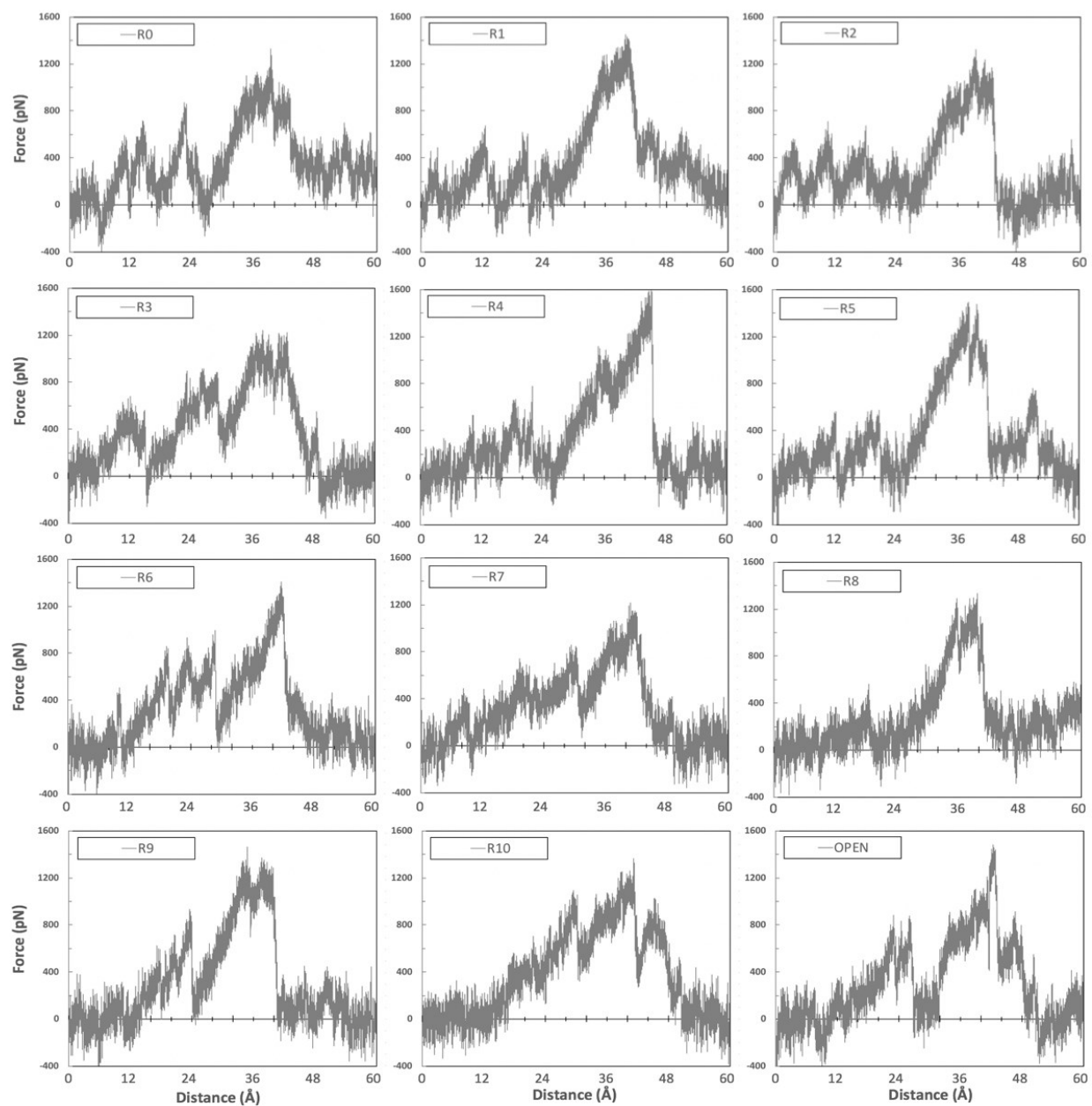


Figure 2.7.2. The force profile of SMD trajectories from R0 to R10 and the open Cav model.

The unbinding force profiles for all the 11 replicas are given in figure 2.7.2. Since the internal gate region of the model is narrow, the ion passing through all 11 replicas showed a huge barrier (or higher force) when it reached the internal gate region of the channel. Similarly, it is known that the calcium ion has three potential binding sites in the selectivity filter region and therefore the SMD simulations were expected to show higher force when passing through the

selectivity filter region of the channel. However, the R8 and R10 replicas are missing some peaks corresponding to the selectivity filter. Thus, we ignored these two replicas from the analysis, as they are unlikely to mimic the physiological calcium influx mechanism. Nevertheless, the unbinding mechanism through other replicas revealed different characteristics of the channel and the selectivity filter region. The unbinding force profiles of other replicas included one to three peaks corresponding to the selectivity filter region. For example, replica R4 had only one peak in the selectivity filter region, while replica R5 had two peaks in the selectivity filter region of the channel (Tang, Gamal El-Din et al. 2014, Adiban, Jamali et al. 2016, Ahmed, Jalily Hasani et al. 2017). Replicas R0, R1, R2, and R6 had three peaks in the SF region recording different unbinding forces of 600-900 pN. Particularly, the replica R6, which included three peaks with force values of ~900 pN, revealed the characteristics of the three binding sites in the selectivity filter region. The calcium ion encountered the first barrier when it reached the site 1 of the selectivity filter formed by four Glu residues (Glu363 (DI), Glu706 (DII), Glu1135 (DIII), and Glu1464 (DIV)) from the four transmembrane domains. The carboxylate groups of the Glu residues (Glu253 and Glu596) lie close to the calcium ion (~3 Å) and help in binding/stabilizing the ion in site 1 (Wu, Yan et al. 2015, Wu, Yan et al. 2016). The second peak is formed when the ion reaches site 2, where it is coordinated by one of the Glu residues from site 1 and a Thr residue from site 3. The third peak is formed when the ion moves to site 3, which is surrounded by four Thr residues (Thr361 (DI), Thr704 (DII), Thr1133 (DIII), and Thr1462 (DIV)). The site 1 Glu residues and the site 3 Thr residues are conserved among the different LTCCs. Previous studies in CavAb have shown that the calcium ion binds with three key residues Thr175, Asp177, Asp178 present in the SF region. Our simulation with the Cav1.2 model revealed a similarly positioned Thr residue (TTTT-ring) and a negatively charged “Glu” residue (EEEE-ring in the place of Asp177 to be involved in

calcium binding (as fig.2.7.3 A). It has been shown that these residues are essential for conferring the calcium selectivity in the mammalian VGCC over sodium and other cations. Mutating these residues to alanine completely abolished the selectivity of the channel. The position of the ion and distance to the surrounding residues are given in figure 2.7.3 B.

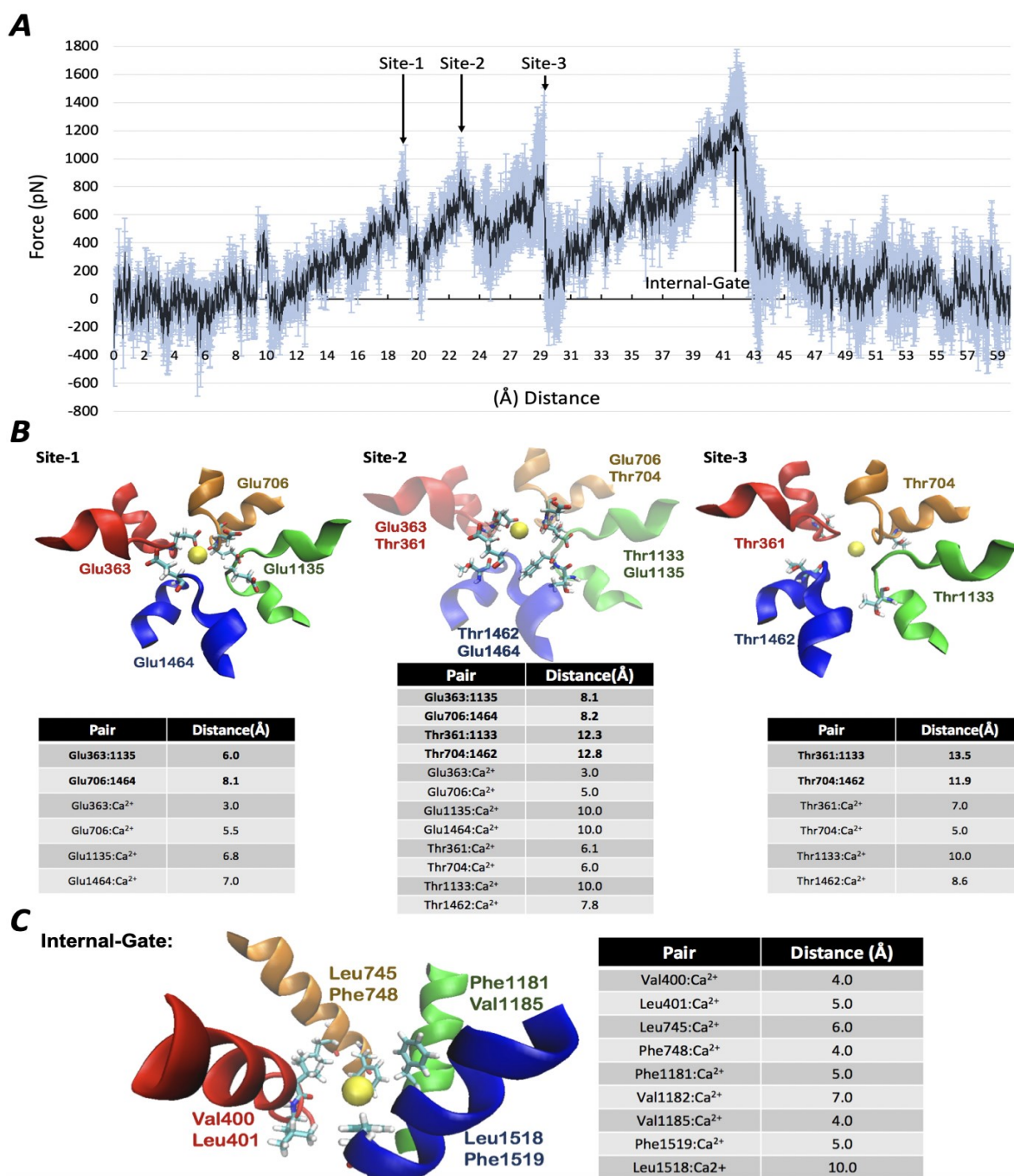


Figure 2.7.3. A) Force profile with error bar of SMD on R6 align with key residues in three SF-sites and internal-gate. B) Key residues in three SF-sites, site-1(left), site-2(middle), and site-3(right) of NOC simulation. Distances of residues and ion-residue pairs are showing the table below. C) Key residues in the internal-gate, and distance between Ca^{2+} and surrounding residues.

After passing through the site 3, the ion enters the water-filled central cavity and traverses quickly towards the internal gate region. The narrow edges of the S6 helices (DI to DIV) are lined by hydrophobic residues, such as Val400, Leu401, Leu635, Phe748, Phe1181, Val1182, Phe1185, Leu1518, and Phe1519 (as Fig.2.7.3 C). The ion exerts a maximum force of ~ 1400 pN when passing through the hydrophobic internal gate region of the channel (Fowler and Sansom 2013). The calcium ion regained its' water-coordination number after it released into the intracellular bulk solvent. The force profile dropped down to a plateau after the ion passed the internal gate and remained low and flat in the bulk solvent environment. The unbinding force profiles revealed three calcium-binding sites in most of the replicas, which suggests the affinity for the calcium ion in this region. Nevertheless, the distance between the calcium ion and the coordinating atoms at S3 site were mostly > 3 Å, which implies the lack of direct contacts with these residues.

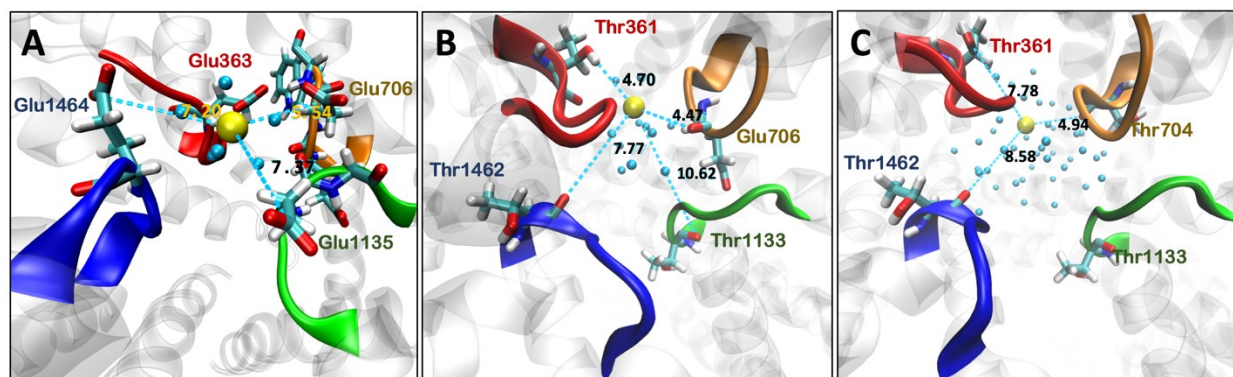


Figure. 2.7.4 Water molecules and calcium ion forms H-bond with residues at the three SF sites. A) In the site-1, the calcium ion form H-bonds with carboxyl of Glu706, Glu1135, and Glu1464 through water molecules. B) In the site-2, the calcium ion form H-bonds with carboxyl of Thr361

Glu706, and Thr1462 through water molecules. C) In the site-3, the calcium ion form H-bonds with carboxyl of Thr361 and Thr704 through water molecules. However, the Glu363 in domain-I directly interact with Ca^{2+} through electrostatic interaction. Thr1133 and Thr1462 interact with calcium ion through multiple water molecules.

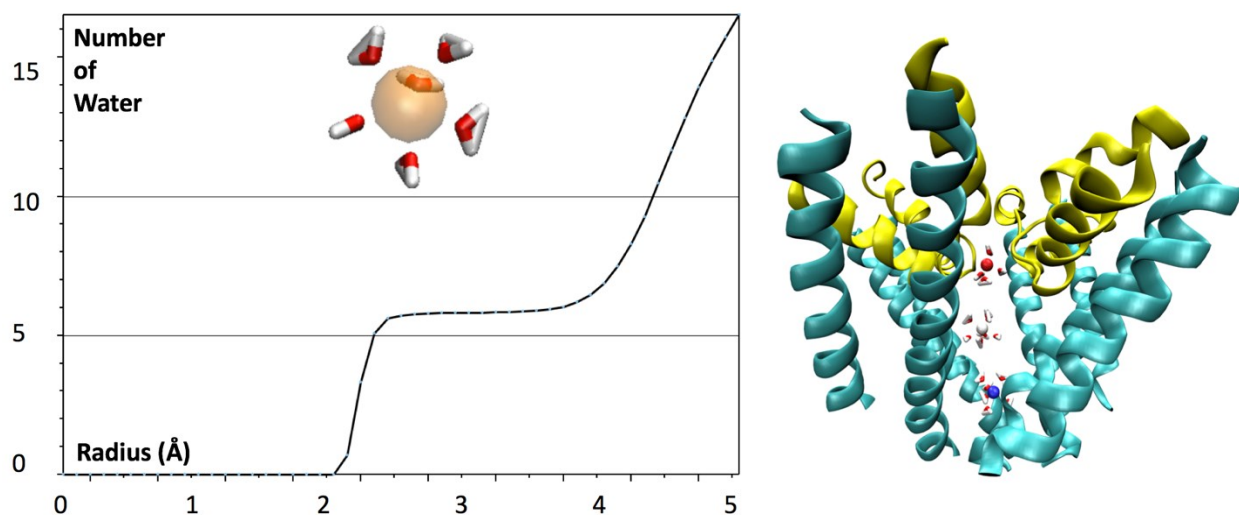


Figure. 2.7.5. The water molecules within 3.5\AA of Ca^{2+} in the selectivity filter, central cavity, and internal gate of NOC.

We observed that water played a significant role in ion permeation during the SMD simulations. On an average, six water molecules interacted with the calcium ion (within 3\AA distance) in the first hydration shell (as Fig.2.7.4 & Fig.2.7.5), which agrees well with the calcium coordination reported previously (Tang, Gamal El-Din et al. 2014, Adiban, Jamali et al. 2016). While the water molecules in the first coordination shell remained almost intact, the number of water molecules in the second hydration shell ($\sim 3\text{-}5\text{\AA}$ distance from the ion) dropped significantly whenever the pulled ion crossed an energetic barrier during SMD simulations. For example, the number of water molecules in the second hydration shell of the pulled calcium ion dropped to < 6 when it moved across the selectivity filter and the internal gate region that have been identified as potential barriers in ion permeation during SMD simulations. Whereas, when the ion is free of

barriers (i.e., in bulk water or in the central cavity region), the number of waters in the second hydration shell increased $\sim 15-18$. This clearly suggests that hydration of ion plays a significant role in the permeation processes. Although previous studies using the bacterial CavAb have shown that the Ca^{2+} is hydrated inside the SF of the channel, however, the dynamics of the hydration have not been discussed (Tang, Gamal El-Din et al. 2014, Adiban, Jamali et al. 2016). Thus, our SMD simulation provides insights into the role(s) of hydration dynamics in ion permeation in hCav1.2 channel.

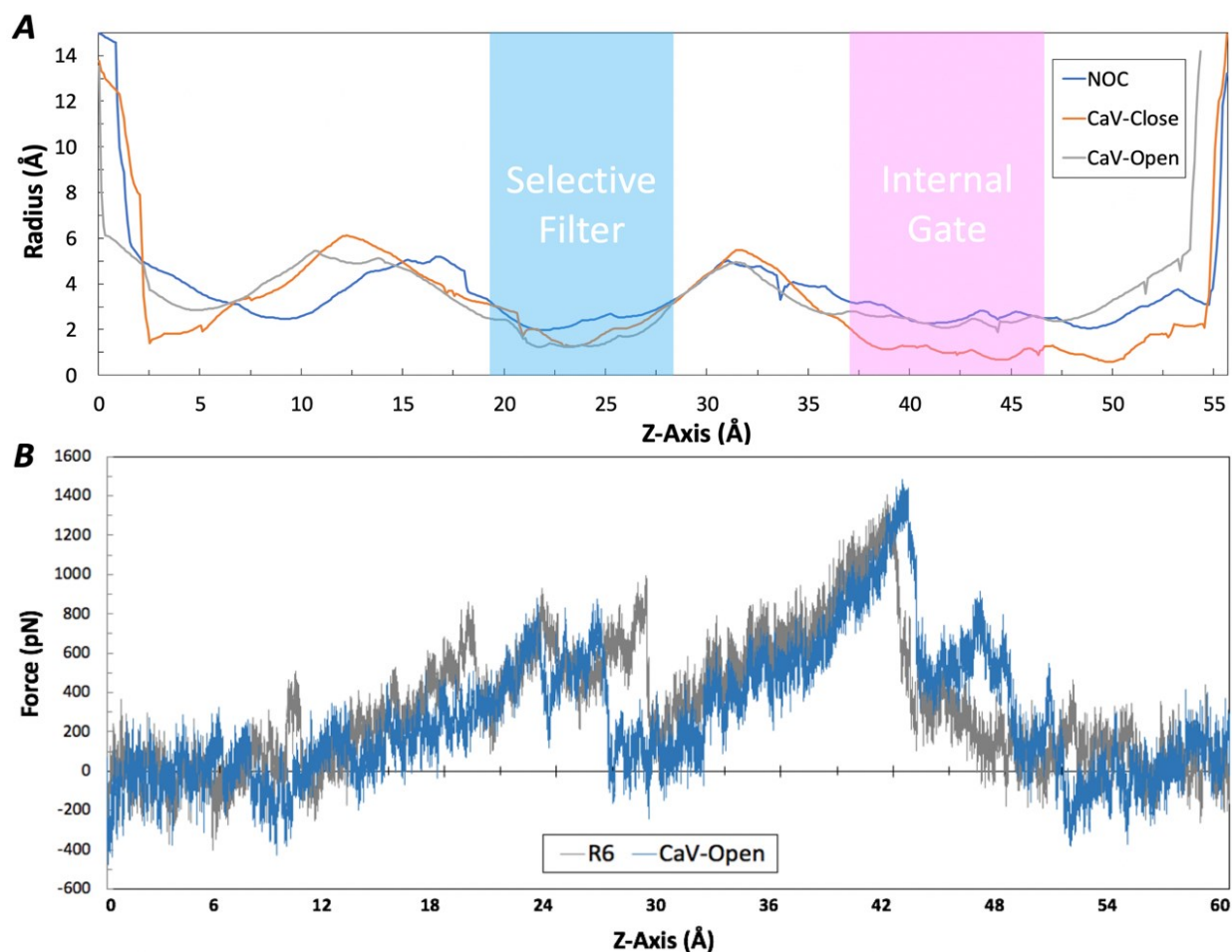


Figure 2.8.1. A) Pore radius along Z-axis of NOC, Rabbit-based close and Eel-based open hCav1.2. B) Force profile of rabbit-based R6 align with eel-based open-state hCav1.2

2.8 Open-State Conformation Cav1.2

The resulting model after the ion is released into the bulk solvent shows an expanded internal gate diameter. In order to understand this conformational state of the channel, we constructed an open-state model of the hCav1.2 using the Eel open state Nav1.4 structure using homology modeling approach and refined it through 100 ns long MD simulations. Later we compared the structures of this (refined) open hCav1.2 model and the post-SMD simulation of closed hCav1.2. We found that the pore radius in both the structures were $> 2 \text{ \AA}$ (see fig. 2.8.1A & 2.8.2), which is much wider than that was seen in the closed hCav1.2 before the SMD simulations ($\sim 1 \text{ \AA}$). In addition, the voltage sensor domain (VSD) was also found to have moved upward relative to the selectivity filter position, which is an attribute of an open-state conformation of hCav channel (Yan, Zhou et al. 2017) (as fig. 2.8.3). Further, the S5 helical bend angles in the DII and DIII domains in our post-SMD closed-state hCav1.2 channel and open-state model were very in a similar range of $1\text{-}2.5^\circ$. However, their S5 helical-bend angles from DI and DIV exhibited a variation of $\sim 8^\circ$ and $\sim 4^\circ$, respectively. These analyses confirm that the SMD simulations have resulted in a conformation of hCav1.2 channel that is partially open particularly at the pore forming domains along the pulling pathway in SMD. Therefore, we ascertain the post-SMD structure of hCav1.2 model as a probable saddle point towards complete opening, and we call this state as a ‘near open conformation’ or NOC. Finally, we performed SMD simulations on the equilibrated open state hCav1.2 model that we built using the Eel Nav1.4 structure. The resultant calcium influx force profile for the open state model shows a good agreement with that of the unbinding force profile of the ‘NOC’ conformation. This shows that our SMD simulations have been able to capture the most important barriers and the corresponding gate-keeping residues in the ion permeation pathway along the hCav1.2 channel.

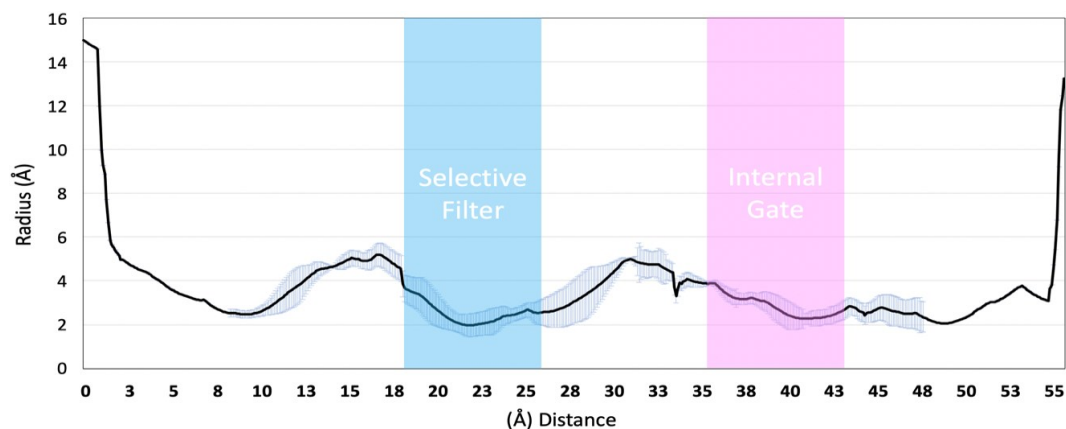


Figure 2.8.2. The pore-radius plot based on the last frame of three SMD simulations (black) with error bars (light blue).

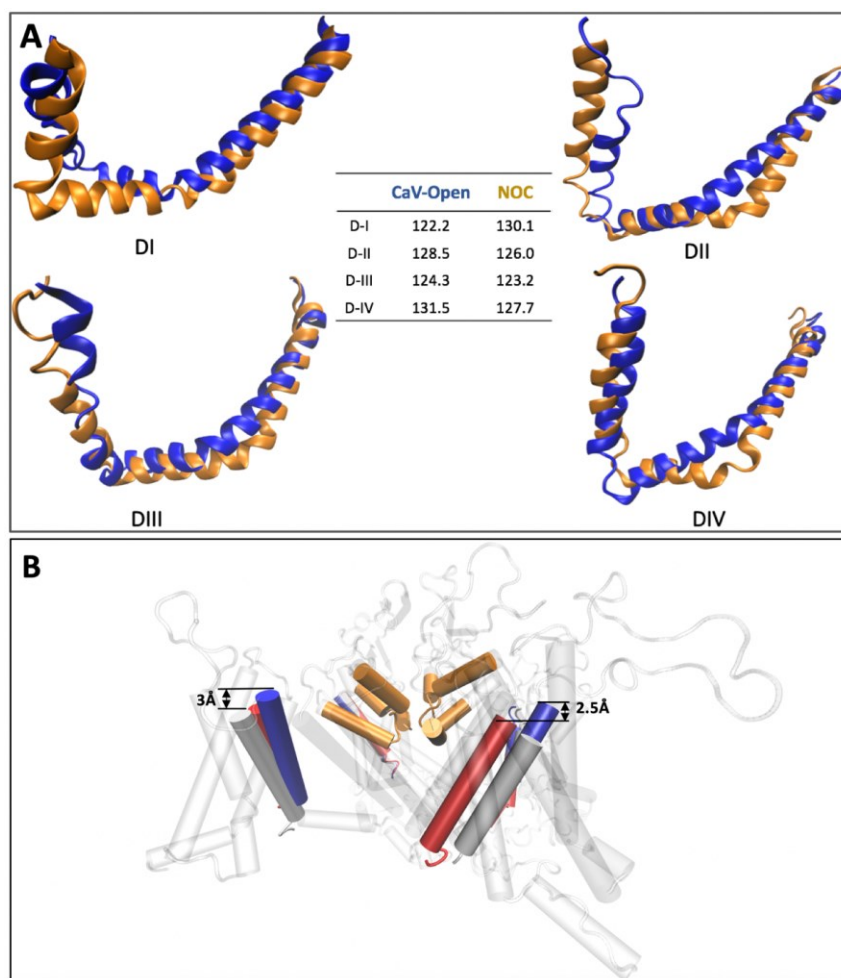


Figure. 2.8.3. A) Comparison of bending angles in the NOC (orange) and Eel-based (blue) open-state hCav1.2 model. B) The selectivity filter (orange) and S4 helix before cMD (red), after cMD (white) and NOC (blue).

2.9 Conclusion

In this work we report, for the first time, the atomistic modeling and molecular dynamics analysis of the α -subunit of the human Cav1.2 model built from a closely related rabbit Cav1.1 α_1 -subunit template. Our model and simulations show the structural flexibility and the pore characteristics of the hCav1.2 channel. Our cMD simulation did not encounter any ion permeation through the channel pore; however, we identified a plausible pre-filtering mechanism for calcium selectivity from our cMD that included the distribution of negatively charged ASP residues on the outer vestibule of the SF region.

On applying an external electric field of -40 mV, corresponding to the activation potential of the channel, we noticed slight upward movements in the VSD of the channel and widening of the selectivity filter region to enable calcium ion influx. Despite applying the electric field for 200 ns, we did not observe any calcium ion permeation through the channel pore. Therefore, in order to understand the ion flux mechanism, we collected replicas from our MD trajectories and performed a steered MD protocol to pull a calcium ion along the Z-axis through the channel pore. We identified several key residues that govern the calcium ion binding (list residues-SF) and channel gating (list residues-internal gate) process. Our ion influx mechanism also revealed an alternating cycle of hydration and dehydration of calcium ion while permeating from the extracellular to intracellular side of the channel. We analyzed the conformation (called NOC), following the ion release into the intracellular side, and noted that this conformation resembled the open state of the Cav1.2 channel. To further characterize the NOC conformation, we modeled the Cav1.2 channel with an open state template (Eel Nav1.4) and equilibrated the model with 100 ns cMD protocol. The pore radius, S5 helix bend and ion unbinding force profiles of the NOC agreed

well with the equilibrated open model. Thus, our MD protocol and NOC conformation could be useful for understanding the open-state characteristics of the channel, such as drug binding.

CHAPTER 3: SMALL MOLECULES DOCKING WITHIN HUMAN CAV1.2 CHANNEL³

3.1 Introduction

L-type calcium channels (LTCCs) play a key role in forming the membrane potential in cells (Hofmann, Flockerzi et al. 2014, Feng, Kalyaanamoorthy et al. 2018). They are involved in various physiological functions, including maintaining a regular cardiac action potential (Striessnig, Pinggera et al. 2014), muscular contraction (Benedetti, Tuluc et al. 2015), and neurotransmission (Feng, Kalyaanamoorthy et al. 2018). Of all LTCCs subtypes, the Cav1.2 ion channel is essential for the normal function of cardiac myocytes and vascular smooth muscles. Cav1.2 is a multi-subunit protein complex formed by the association of α_1 and other auxiliary subunits. The α_1 -subunit plays the central role of calcium transfer. The human Cav1.2 α_1 -subunit consists of four connected domains, DI-DIV, which contain six transmembrane segments, S1-S6, in each repeat. The S1-S4 segments form a voltage sensor domain (VSD) that can detect the changes of membrane potential and initiate the following conformational changes of the channel. The S5-S6 segments are the pore-forming domain (PFD), which directly interact with the permeation ions (Wu, Yan et al. 2015, Wu, Yan et al. 2016, Feng, Kalyaanamoorthy et al. 2019). A dysfunctional Cav1.2 channel is usually associated with multiple cardiovascular diseases, such as vasodilation (Striessnig, Bolz et al. 2010), angina (Berger and Bartsch 2014), and hypotension (Zamponi, Striessnig et al. 2015). Modulating the activity of Cav1.2 has been established as a promising therapeutic strategy for the treatment of hypertension and myocardial ischemia.

³ A version of this chapter has been submitted as a research article to the Journal of Molecular Modeling as *Feng Tianhua and Khaled Barakat. "Effects of Drug Binding on The Ion Permeation Through The Human Cav1.2 Ion Channel: A Computational Study"*.

Several Cav1.2 antagonists are used to treat cardiovascular disorders. The most commonly used drugs are mainly derivatives of 1,4-dihydropyridine (1,4-DHPs) and phenylalkylamines (PAAs) and a few examples are listed in Table 3.1.1. They usually stabilize the inactivated state of the channel and block its ability to induce calcium influx (Tang, Gamal El-Din et al. 2016, Xu, Li et al. 2016). The history of these antagonists goes back to Fleckenstein, who first showed that phenylalkylamines (PAAs) specifically inhibit the calcium current (Fleckenstein 1983, Dolphin 2006). Following that, dihydropyridines (DHPs) were also found to block Cav1.2 (Fleckenstein 1983, Felix 2005). Most current calcium channel blockers (CCB) are structurally related to the 1,4-DHP scaffold and block calcium permeation through Cav1.2 (See Table 3.1.1). These 1,4-DHP derivatives possess a similar pharmacological profile, manifested by their high-affinity frequency-dependent blockade (Kang, Cooper et al. 2012, Zamponi, Striessnig et al. 2015). Examples of DHP-derived drugs include amlodipine and nimodipine, which are used for the treatment of cardiac diseases, such as angina and hypotension (Tikhonov and Zhorov 2009, Xu, Li et al. 2016). They also help in improving the outcomes of neurological treatments (Berger and Bartsch 2014, Ortner and Striessnig 2016). The phenylalkylamine (PAA)-type of compound is another class of calcium channel blocker. These drugs most likely bind to the inactivated state of human Cav1.2. This is evident by their ability to block different conduction states of the channel. Verapamil, for example, is a widely used drug from the PAA class that is currently available for clinical use. It has been widely used for the treatment of hypertension (Elkayam, Shotan et al. 1993, DeWitt and Waksman 2004) and its binding to Cav1.2 prevents the channel from recovery from the repolarization state (Cheng, Tikhonov et al. 2009, Tang, Gamal El-Din et al. 2016).

Although many Cav inhibitors are clinically used drugs, CCBs account for > 65% of deaths from cardiovascular medications (DeWitt and Waksman 2004, Godfraind 2017). For example,

Mibefradil is a L-type calcium channel blocker to treat hypertension and chronic stable angina. However, Mibefradil was withdrawn from the market because of potentially dangerous in combination with other cardiac drugs (Mullins, Horowitz et al. 1998, Po and Zhang 1998). Additionally, the commonly used CCBs, nifedipine and diltiazem, have been also reported cause incidences of heart failure following long-term treatments (Elkayam 1998). Therefore, reducing the cardiotoxicity associated with CCB is now a major task for the treatment of cardiac diseases. This requires an in-depth understanding of the structural-based and binding mechanisms of these compounds.

Over the last few years, many mechanistic studies were performed to understand how these compounds work. For example, in 2009, Tikhonov and Zhorov investigated the binding poses of 1,4-DHP, PAA derivatives in the open and closed states of human $\text{Ca}_v1.2$ using homology modelling (Template: prokaryotic K_vAP potassium channel) (Tikhonov and Zhorov 2008, Cheng, Tikhonov et al. 2009, Tikhonov and Zhorov 2009). However, the templates used in their studies share a low sequence similarity with human $\text{Ca}_v1.2$ channel (< 30% sequence identity). Furthermore, their human $\text{Ca}_v1.2$ homology model comprised only two helices in the pore-forming domain (i.e. S5 and S6), lacking four other helices (S1 to S4), which limited the accurate predictions of the conformational dynamics in the voltage-sensing domain. A recent study in 2015 co-crystallized the structure of the bacteria Ca_vAb channel with a CCB, confirming the binding sites of PAA and DHP blockers (Tang, Gamal El-Din et al. 2016). Although this co-crystalized complex explained how these compounds interact within the pore-forming domain in bacteria, understanding this binding in human $\text{Ca}_v1.2$ and studying the effects of these compounds on the inward calcium current in human is still unclear. Lacking a human Ca_v structure limits the ability to understand this process (Dolphin 2006). Recently, our group reported the structure of human

Ca_v1.2 α_1 model, which includes the transmembrane region together with the interlinking intracellular and extracellular domains (Feng, Kalyaanamoorthy et al. 2019). This computational homology model was based on the cryo-EM structure of the rabbit Ca_v1.1 α_1 -subunit (in the closed conformation). The template we used in our earlier study is superior to the earlier models of Tikhonov and Zhorov, with more than 65% sequence identity with human Ca_v1.2 and was used to explore the different states of the channel, leading to a near-open conformation (NOC).

Drug	Drug Class	Binding Region	IC ₅₀	Reference
Amlodipine	1,4-DHP	CaV α 1 IIIS5-S6, IVS6	IC ₅₀ = 0.057 μ M	(Elkayam 1998, Ritz, Rhodes et al. 2010, Striessnig, Ortner et al. 2015, Tang, Gamal El-Din et al. 2016)
Clevidipine	1,4-DHP	CaV α 1 IIIS5-S6, IVS6	IC ₅₀ = 0.22 μ M	(Dahl, Conner et al. 2016)
Isradipine	1,4-DHP	CaV α 1 IIIS5-S6, IVS6	IC ₅₀ = 0.013 μ M	(Striessnig, Murphy et al. 1991, Striessnig, Grabner et al. 1998, Baumann, Gerstner et al. 2004, Huster, Frei et al. 2010, Senatore, Boone et al. 2011, Pinggera, Mackenroth et al. 2017)
Nicardipine	1,4-DHP	CaV α 1 IIIS5-S6, IVS6	IC ₅₀ = 0.194 μ M	(Elkayam, Shotan et al. 1993, Elkayam 1998, Nachman-Clewner, St Jules et al. 1999)
Nifedipine	1,4-DHP	CaV α 1 IIIS5-S6, IVS6	IC ₅₀ = 0.022 μ M	(Fleckenstein 1983, Hess, Lansman et al. 1984, Xu and Lipscombe 2001)
Nimodipine	1,4-DHP	CaV α 1 IIIS5-S6, IVS6	IC ₅₀ = 0.060 μ M	(Fleckenstein 1983, Hess, Lansman et al. 1984, Xu and Lipscombe 2001)
Nisoldipine	1,4-DHP	CaV α 1 IIIS5-S6, IVS6	IC ₅₀ = 0.066 μ M	(Elkayam, Shotan et al. 1993, Artalejo, Adams et al. 1994, Welling, Ludwig et al. 1997, Elkayam 1998)
Verapamil	PAA	CaV α 1 IIS6, IIIS6, IVS6	IC ₅₀ = 0.25 μ M	(Fleckenstein 1983, Elkayam, Shotan et al. 1993, Mullins, Horowitz et al. 1998, DeWitt and Waksman 2004, Cheng, Tikhonov et al. 2009, Tang, Gamal El-Din et al. 2016)

Table 3.1.1. Common L-type calcium channel antagonists. The list of drugs and their 2D structures are obtained from the Drugbank database.

The current study employed our published NOCs human Ca_v1.2 to generate an ensemble of several conformational states of Ca_v1.2 and study the mode of binding of CCBs using Rosetta flexible docking (Feng, Kalyaanamoorthy et al. 2018, Feng, Kalyaanamoorthy et al. 2019). The

ensemble docking outcomes were filtered for the best binding modes of DHP-type and PAA-type derivatives. We picked eight small molecules from those derivatives for the docking analysis. The docking outcomes were also used to identify several human Cav1.2 residues that stabilize the binding poses of these compounds and analyze their electrostatic and VDW interactions. The binding poses were clustered and ranked based on the docking score and MM-GBSA binding energy. We selected one representative complex from the best-ranking cluster for each compound. The complex has been embedded in the membrane system and performed a short energy minimization and followed by 10 ns length classical MD simulations. Re-scoring the eight complexes by MD-based MM-GBSA provide us a good ranking. Overall, we picked three DHPs-type compounds, nifedipine, nimodipine, and clevidipine, and two PAA-type compounds, verapamil, and Br-verapamil, with different binding strength. Additionally, we employed steered molecular dynamics (SMD) to pull a calcium ion through the pore domain in the presence and absence of CCBs to investigate the effects of these compounds on calcium ion permeation. With these comparisons, we can see the different binding mechanism of DHP-type and PAA-type compounds.

Our results revealed interesting findings on how these compounds interact with Cav1.2. For example, although both 1,4-DHPs and PAAs block the human Cav1.2, their blocking mechanism is different. PAAs bind in the centre cavity of the pore and physically block the ion pathway. PAAs interact with domain-II S6 helix (DII-S6) ASN631 and domain-III S6 helix (DIII) DIII-S6 MET1068 residues via hydrophobic and electrostatic forces. On the other hand, the binding site of DHPs extends from the penetration between DIII-S6 and DIV-S6 segments into the pockets under the SF region in DIII and DIV. The binding of DHPs increases the energy barrier of the selectivity filter and prevents calcium ions from passing the pore domain. Our results show

the structural basis for binding of DHP and PAA at their distinct receptor sites on human Cav1.2 channels and offer key insights into their fundamental mechanisms of action and differential therapeutic uses in cardiovascular diseases.

3.2 Methods

3.2.1 Ligand Preparation for Docking

The current study builds upon our earlier work (Feng, Kalyaanamoorthy et al. 2018, Feng, Kalyaanamoorthy et al. 2019) and employs the two Cav1.2 partially open conformations, which we identified earlier, namely NOC2 and NOC6. The objective here is to take our Cav1.2 published model one step further and use it understand the interaction of Cav1.2 with CCBs. To achieve that, we select there eight small molecule compounds, comprising derivatives from the two CCBs classes, DHP and PAA (as fig. 3.2.1) (Roy, Kucukural et al. 2010, Yang, Yan et al. 2015). The DHP scaffolds involves a pyridine core and derivatives from this class are widely used as L-type calcium channel blockers. Six DHP derivatives are selected, including amlodipine, clevidipine, felodipine, isradipine, nicardipine, nimodipine and Nisoldipine. On the other hand, the PAA pharmacophore involves two aromatic rings connected by a flexible chain with a nitrile substituent. Only two compounds are selected from this class and they include verapamil, and Br-verapamil. Prior to docking, all selected eight compounds are prepared using the ligprep utility from the Schrodinger software package (Schrödinger Release 2017-2: Ligprep, Schrödinger, LLC, New York, NY, 2017). The ligand protonation states and tautomeric states are assigned at neutral pH. The geometry of the ligands is optimized through the OPLS_2015 force field. Multiple conformations for each compound are generated using Ligprep and all conformers are sampled through the minimization methods using the OPLS force field as implemented in Schrödinger.

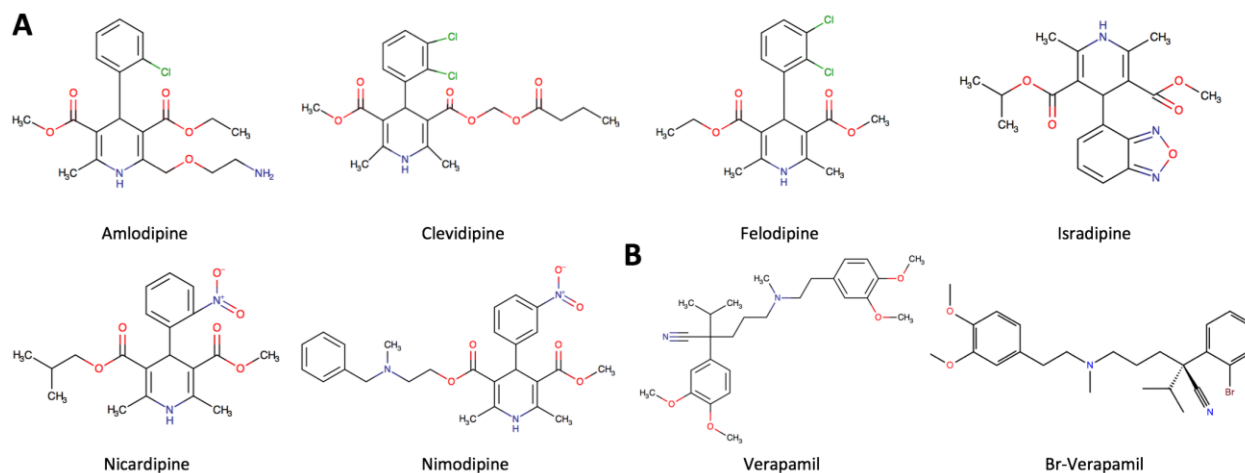


Figure 3.2.1. The chemical structures of representative DHP and PAA calcium channel blockers. A) representative DHP antagonists. B) Representative PAA antagonists.

3.2.2 Flexible Docking

Docking calculations are carried out using the most recent version of ROSETTA 3.2, which offers a better control over docking and scoring parameters. For DHP derivatives, the docking search space within Cav1.2 is centered on the fenestration formed by the DIII-S5, DIII-S6 and DIV-S6 domains. For PAA derivatives, the search space is focusing on the fenestration sites between the DIII-S6 and DIV-S6 domains as well as the central cavity in the pore-forming area. The size of the docking space for both cases comprises the three-dimensional box (XYZ: $42 \text{ \AA} \times 42 \text{ \AA} \times 36 \text{ \AA}$). The docking method allows the flexibility of all surrounding residues within 5 \AA from the center of docking box. 5000 docking poses are obtained and scored using Rosetta Flexible Docking (Lemmon and Meiler 2012), for each of the two Cav1.2 conformations (i.e. NOC2 and NOC6 (Feng, Kalyaanamoorthy et al. 2018, Feng, Kalyaanamoorthy et al. 2019)). That is 10,000 binding poses generated for each of the eight tested compounds.

The binding poses of each compound are clustered into different groups using their RMSD (2 \AA) from a reference structure. All resulting clusters are ranked based on their population sizes

and the top five clusters for each Cav1.2 conformation (i.e. ten clusters for each compound) are selected for further analysis. A representative compound-protein complex is selected from each for binding energy calculations.

3.2.3 MM-GBSA Scoring

The selected ten complexes are rescored in two-steps using the generalized Born and surface area continuum solvation (MM-GBSA) method (Genheden and Ryde 2015). The first step uses a rapid calculation using the MM-GBSA module in Schrödinger software to evaluate the interactions for each complex resulted from the docking simulation. During this initial step, these interactions between a compound and residue within a 5 Å distance from the compound. The complex with the highest scoring from this step is used as a starting point for a more comprehensive MD-based MM-GBSA calculation. In general, MM-GBSA calculates the binding free energy between a receptor and a ligand using the following equations:

$$\Delta G_{\text{bind}} = G_{\text{complex}} - G_{\text{receptor}} - G_{\text{ligand}} \quad (1)$$

$$\Delta G_{\text{bind}} = \Delta H - T\Delta S \approx \Delta E_{\text{gas}} + \Delta G_{\text{sol}} - T\Delta S \quad (2)$$

$$\Delta E_{\text{gas}} = \Delta E_{\text{int}} + \Delta E_{\text{ELE}} + \Delta E_{\text{VDW}} \quad (3)$$

$$\Delta G_{\text{sol}} = \Delta G_{\text{GB}} + \Delta G_{\text{Surf}} \quad (4)$$

The binding free energy (ΔG_{bind}) is decomposed into different energy terms. Because the structures of the complex, receptor, and ligand are extracted from the same trajectory, the internal energy change (ΔE_{int}) is usually canceled. Thus, the gas-phase interaction energy (ΔE_{gas}) between the receptor and the ligand is the sum of electrostatic (ΔE_{ELE}) and van der Waals (ΔE_{VDW}) interaction energies. The solvation free energy (ΔG_{sol}) is divided into polar and non-polar energy terms. Polar solvation energy (ΔG_{GB}) is calculated by using the GB model. The non-

polar contribution is calculated based on the solvent-accessible surface area (ΔG_{Surf}). The calculated binding free energy (ΔG_{bind}) is the sum of the gas-phase interaction energy and solvation free energy.

3.2.4 Classical MD Simulations: Parameters and Protocol

MD simulations are used for multiple purposes throughout this study. They are used to study the stability of the docked poses, prepare a trajectory for MM-GBSA calculations and select a starting conformation for steered MD (SMD) simulations. All complexes are prepared in the membrane environment prior to any MD simulations using the membrane builder of CHARMM-GUI (Jo, Kim et al. 2008). Each system is embedded in a cellular bilayer membrane, composed of 570 POPC molecules. The systems are further hydrated using a water buffer of 20 Å on the upper and lower leaflets. The membrane-embedded systems are fully solvated above and below with 66951 TIP3P water molecules and are ionized using 195 Ca^{2+} and 369 Cl^- ions to achieve an ionic concentration of 150mM. The fully assembled systems comprise a range of around 300,000 atoms. Protein, lipids, and ionic parameters are assigned using the CHARMM36m force field (Tang, Gamal El-Din et al. 2016). The NAMD package on the CEDAR supercomputer from Compute Canada is employed to run the simulations. All systems simulate under a short energy minimization, followed by 10 ns classical MD simulations. The initial energy minimization step involves 100,000 iterations, in which the protein and the lipid heads are restrained whereas the lipid tails, water and ions are free to relax. This step is essential to remove any existing steric clashes as a result of the improper packing of the membrane around the protein. Following that, The MD simulation protocol employs two consecutive NVT and NPT equilibration steps for 250ps, each. All MD simulations are performed using an integration time step of 2 fs, under periodic boundary conditions. The Langevin dynamics are adopted for temperature (310 K) and pressure

control (1 bar). Bonded interactions compute everyone timestep, short-range non-bonded interactions every two timesteps, and long-range electrostatic interactions every four-time steps. A cut-off of 12 Å is used for the Van der Waals interactions and short-range electrostatic interactions, with a switching function starting at 10 Å for van der Waals interactions to ensure a smooth cut-off. The simulations are performed under periodic boundary conditions; long-range electrostatic interactions are calculated by using the particle-mesh Ewald (PME) method. The unit cells are large enough that adjacent copies of the protein are never close enough for short-range interactions to apply. The trajectory frames are written to a file every 200 ps.

For each complex, the root means square deviation (RMSD) is calculated using the whole 10 ns-length trajectories. To assess the flexibility of the different residues, we calculate the root mean square fluctuation (RMSF) on each residue in the Cav1.2 channel using the last 3 ns of the trajectory. Hydrogen bond analyses evaluate every potential H-bond based on their bond length and angle during the MD simulation. Neighbouring water molecules within 5 Å of the bound compounds are also evaluated for their ability to bridge any H-bond interactions with the surrounding residues and are visualized using the MOE software for the final conformation.

3.2.5 MD-based MM-PBSA

As described above, the MD trajectories are used to restore the binding free energy for each complex. To do that, we use snapshots from the final 3 ns trajectory of the MD simulations, which include 150 frames for each complex. Each trajectory is processed using the MM-PBSA module as implemented in AMBERTOOLS of AMBER18 (Case, Cheatham et al. 2005). The same utility is used to carry out a binding energy decomposition among the different residues involving in the binding reaction. The contribution from each residue is further decomposed into electrostatic and VDW portions. Based on these calculations, we finally select five complexes to go forward for

SMD simulations. The final selection involves three DHP derivatives (a strong blocker, nicardipine; a medium blocker, nimodipine; and a weak blocker, clevidipine) and two PAA derivatives (a strong blocker, verapamil; and a weak blocker, Br-verapamil).

3.2.6 Steered Molecular Dynamics Simulations

For each of the final five selected complexes, the starting conformation for SMD simulations is obtained from the last frame of the classical MD systems, using the same membrane environment. SMD simulations are performed using NAMD 2.9 package, with a non-bonded cutoff of 13.5 Å (Kale, Skeel et al. 1999). The temperature is controlled through a velocity reassignment approach once per picosecond at a temperature of 310 K. An external force of 4 kcal/mol/Å is applied on a calcium ion to pull the ion from the extracellular region, through the selectivity filter and finally toward the intracellular region of the channel into intracellular water with a constant velocity ($v = 0.00004$ Å/fs). This force applies along the Z-axis vector and points from the initial pulling position of the calcium ion toward the intracellular side. During this simulation, the C α atoms of residues GLY392, GLY740, ALA1174, and ALA1512, locate in S6 helices in the four subunits are constrained along the Z-direction with a force constant of 1 kcal/mol. This is done to prevent any structural drifts in the protein and to prevent its dislocation from the membrane while the calcium ion was being pulled. With this setting, the center of mass movement limits to a maximum of 0.5 Å. The direction and magnitude of all applied forces are held constant during the simulations. The channel is experiencing no appreciable drift in the plane of the membrane; therefore, the applied forces may be considered to be radial at all points in the simulations.

3.2.7 Visualization and Analysis

Visualized analysis of simulation trajectories is performed using VMD, Chimera, and MOE software suites. Pore radius profiles are calculated using the HOLE2.0 program. Plots are generated using Gnuplot and GraphPad Prism version 6.0. Protein-Ligand interaction maps are generated using the MOE software suite.

3.3 Results and Discussion

Calcium channel blockers (CCBs) reduce the calcium influx into the cytoplasm by blocking calcium channels in the membrane. These agents are widely used for the treatment of various cardiovascular diseases including hypertension, angina and supraventricular tachycardias. CCBs reported to date target mostly the L-type calcium channels with more specificity toward the Cav1.2 channel. The current work was focused on studying two of the most commonly prescribed CCBs, namely, phenylalkylamines (PAA; e.g. verapamil) and dihydropyridines (DHP; e.g., nifedipine). Earlier work suggests that PAAs blockade is a use-dependent, requiring Cav1.2 to open first for the drug to work and implying a role for the activation gate in mediating this blockade (Striessnig, Grabner et al. 1998). On the other hand, DHPs are not use-dependent and their affinity to the Cav1.2 is enhanced by the membrane depolarization (Sanguinetti and Kass 1984). Thus, despite being leading to the same blocking effect, their mechanism of action on Cav1.2 is different. Understanding these differences at the atomistic level is required for their safe use and to help design better CCBs. Both classes bind to the α_1 subunit of Cav1.2, however, each class seems to interact with a distinct site. Their binding sites have been reported to be partially overlapping and to be located within the S5 and S6 at the fenestration between DIII and DIV and are allosterically related to each other (DeWitt and Waksman 2004, Tang, Gamal El-Din et al. 2016, Nguyen, DeMarco et al. 2019). Since most DHPs are lipophilic, they tend to bind at the outer surface of the channel, facing the lipid molecules and forming interactions with the S5 and S6 helix in domains

DIII and DIV (Tikhonov and Zhorov 2009, Godfraind 2017, Nguyen, DeMarco et al. 2019). The co-crystallized structure of the bacterial CavAb channel with phenylalkylamine shows clearly that the drug binds in the central cavity of the pore domain at the intracellular side of the selectivity filter (Cheng, Tikhonov et al. 2009, Tang, Gamal El-Din et al. 2016). These findings were further refined in the recently published Cryo-EM complexes which compared the binding sites for PAAs and DHPs within the rabbit Cav1.1 channel (Wu, Yan et al. 2016, Zhao, Huang et al. 2019). According to these structures, DHPs bind at a lower and closer position toward the central cavity compared to PAAs (Zhao, Huang et al. 2019). This data is contradicting with the earlier findings from bacterial CavAb structure and consequently contradicts with the earlier modelling studies that were based on this bacterial channel.

The main objective of the current study was to build upon these earlier findings and to evaluate the effects of CCBs on the calcium ion permeation in Cav1.2. To accomplish that, docking studies were employed to predict the most probable binding locations and binding modes for the DHPs and PAAs classes, using their suggested sites as the initial docking search space. To assess the effects of their structural variations we decided to include a range of DHP and PAA derivatives to understand the reasons behind gaining/losing the blocking activity of these derivatives and how this is reflected in the ion passage through the selectivity filter towards the pore of the channel. Initially, eight compounds were selected from the literature and docked within Cav1.2. The objective at this stage was to confirm the accuracy of our docking protocol in ranking these compounds and in predicting their binding to Cav1.2. At the later stages of the current study, we focused on five compounds; three DHPs (*i.e.* nifedipine, nimodipine and clevidipine) and two PAAs (*i.e.* verapamil and Br-verapamil). Each group comprised a range of strong to weak analogues (Elkayam, Shotan et al. 1993, Striessnig, Ortner et al. 2015, Tang, Gamal El-Din et al.

2016). For example, nifedipine and clevidipine have been reported to be the relatively strong and weak DHP derivatives, respectively (Elkayam, Shotan et al. 1993, Elkayam 1998, Nachman-Clewner, St Jules et al. 1999, Dahl, Conner et al. 2016). On the other hand, verapamil and Br-verapamil were selected as the strongest and weakest PAAs, respectively (Fleckenstein 1983, Striessnig, Grabner et al. 1998, Cheng, Tikhonov et al. 2009, Tang, Gamal El-Din et al. 2016). The current work continues our earlier work on Cav1.2 and founded on the hypothesis that, regardless of the binding mode and binding location of a compound, a strong blocker would be able to intercept the ion passage and increase the energy barrier for the ion to pass and exit the channel. On the other hand, a weaker blocker would have a reduced effect on ion passage. To study this hypothesis, we used steered molecular dynamics (SMD) simulations to calculate the force profile of pulling a calcium ion through the channel in the absence and presence of each compound. Results described below provide the details for each calculation step we performed and reveal how each compound interacted with and affected the Cav1.2 channel at the atomistic level.

3.3.1 Rosetta Flexible Docking

As described above, docking simulations were used to place each compound within the channel and to predict its most probable binding mode. Two protein conformations were used from our earlier study on Cav1.2 (Feng, Kalyaanamoorthy et al. 2019). The two structures represent a near open conformation (NOC) of the channel and provide a suitable environment to study CCBs. As reported in the literature, we focused the docking search space for DHPs at the fenestration cavity formed by the DIII-S5, DIII-S6 and DIV-S6 domains. On the other hand, for PAAs, the search space was focused on the fenestration sites between the DIII-S6 and DIV-S6 domains as well as on the central cavity in the pore-forming area. To allow the full flexibility for each compound, all possible conformers of the tested eight CCBs (see Figure 3.2.1) have been

considered and used during the docking simulations. To further account for the flexibility of the binding site, we used Rosette flexible docking (Lemmon and Meiler 2012) and allowed the flexibility of all surrounding residues within 5 Å from the center of the docking box. The docking simulations resulted in 10,000 binding poses for each of the eight tested compounds (Lemmon and Meiler 2012) using the two Cav1.2 conformations as targets (i.e. NOC2 and NOC6 (Feng, Kalyaanamoorthy et al. 2018, Feng, Kalyaanamoorthy et al. 2019)). All docking poses explored the whole space of the proposed binding area. To select the representative conformations, we clustered the 10,000 binding poses in complexes and the top-ten conformational clusters were used for further analysis using the best scoring complex for each cluster as a representative complex.

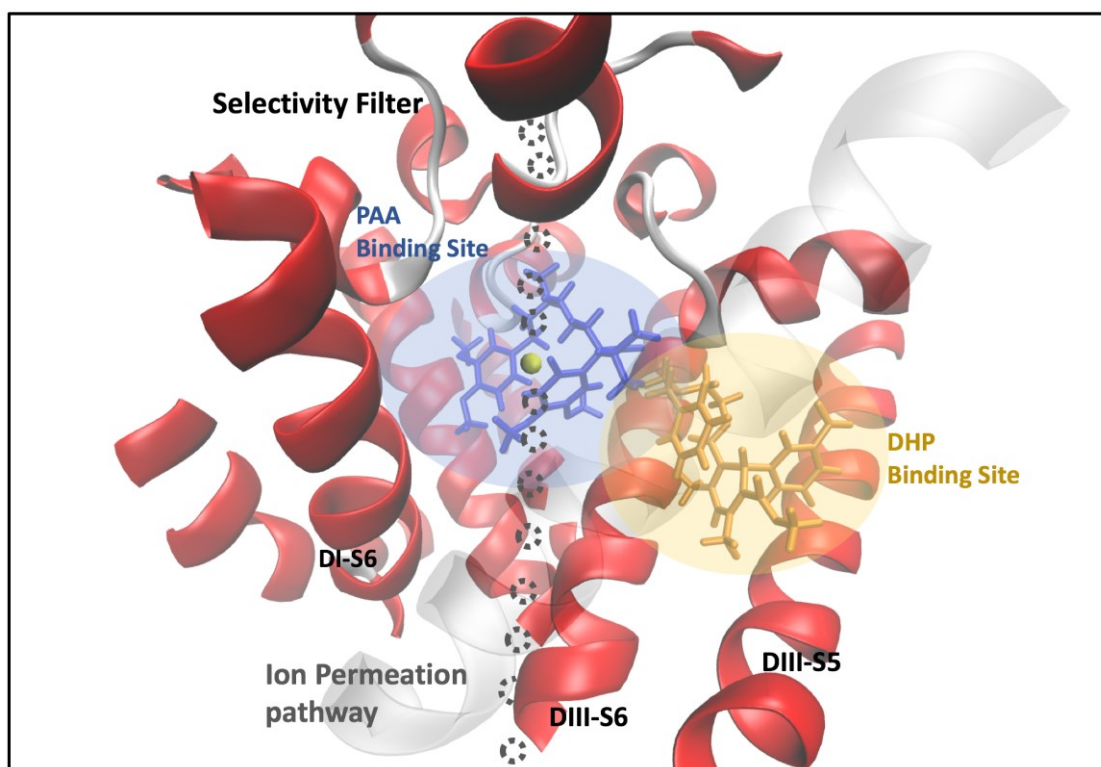


Figure 3.3.1. The permeation pathway (grey) of Cav1.2 with calcium ion (yellow), nicardipine (blue), and verapamil (Orange). The binding sites of DHPs and PAAs shade in blue and orange.

Cluster	Amlodipine	Clevidipine	Isradipine	Nicardipine	Nifedipine	Nimodipine	Verapamil	Br-Verapamil
C0	-1398	-1400	-1394	-1406	-1388	-1394	-1480	-1402
C1	-1405	-1403	-1405	-1394	-1401	-1404	-1379	-1402
C2	-1388	-1402	-1402	-1398	-1402	-1401	-1493	-1389
C3	-1388	-1383	-1403	-1401	-1399	-1383	-1465	-1399
C4	-1387	-1405	-1399	-1367	-1385	-1388	-1398	-1405
C5	-1722	-1732	-1735	-1707	-1726	-1732	-1720	-1733
C6	-1731	-1715	-1730	-1740	-1735	-1719	-1760	-1736
C7	-1743	-1725	-1727	-1730	-1731	-1734	-1663	-1740
C8	-1730	-1737	-1733	-1738	-1729	-1728	-1795	-1725
C9	-1729	-1712	-1735	-1742	-1724	-1713	-1787	-1805

Table 3.3.1. The scores of Rosetta flexible docking between small molecules and human Ca_v1.2.

Compound	Pose 1 (kcal/mol)	Pose 2 (kcal/mol)	Pose 3 (kcal/mol)	Pose 4 (kcal/mol)	Pose 5 (kcal/mol)
Amlodipine	-56	-47	-41	-45	-45
Clevidipine	-41	-46	-44	-39	-47
Isradipine	-41	-40	-48	-40	-37
Nicardipine	-47	-56	-55	-54	-49
Nifedipine	-41	-38	-42	-37	-33
Nimodipine	-49	-40	-48	-43	-35
Verapamil	-46	-47	-49	-53	-51
Br-Verapamil	-47	-33	-46	-48	-33

Table 3.3.2. The MM-GBSA binding free energy of complexes, between small molecules and human Ca_v1.2.

Our docking results revealed that DHPs did not directly interfere with the ion permeation pathway. The dihydropyridine rings in nicardipine, nimodipine, and clevidipine occupied the same location within the polarized residues in DIII-S5. In all three small molecules, the phenyl rings are aligned on the same plate with minor relative rotations. On the other hand, PAAs seem to directly

interfere with the ion permeation pathway (as figure 3.3.1). The hydrophobic residues close to the phenylalkylamine interact with DII-S6 and DIII-S6. Furthermore, there is a well-defined electrostatic interaction between verapamil and polarized residue in selectivity filter. Although the docking studies illustrated important details about how each class would interact with the channel, the ranking of the ten clusters for each compound was not very different and did not correlate very well with the published experimental data. For example, the Rosetta score are more correlating with the conformations. The docking clusters of the NOC2 are all around 1400, which are lower than the NOC5 (~1700) (as Table 3.3.1). To rescore these representative conformations, we used the *MM-GBSA* binding energy method as implemented in the Schrödinger software (Schrödinger Release 2017-2: Ligprep, Schrödinger, LLC, New York, NY, 2017) as a rapid tool to select a single representative complex for each compound. Given that most of the predicted top ranked poses from docking had similar modes of binding, the objective was to reduce the computational resources in subsequent analysis (e.g. MD simulations and SMD) by focusing on the best pose for each compound.

Table 3.3.2 lists the top representative complexes for each compound based on their Schrödinger MM-GBSA energies. The best ranking for each compound (out of its top five docking poses listed in table 3.3.2) correlates well with the published in vitro IC_{50} blocking activity for each compound (DeWitt and Waksman 2004, Genheden and Ryde 2015, Tang, Gamal El-Din et al. 2016). Although the docking ranking of blockers with comparable strengths (e.g. amlodipine and nifedipine) cannot be fully discriminated according to this data, compounds with well-separated activities (e.g. nifedipine, nimodipine, and verapamil) are well ranked. Next, a Pearson product-moment correlation coefficient was computed to assess the relationship between the scores calculated from the docking poses of the ligands against the Cav1.2 protein, and the IC_{50} of

the compounds. Overall, there is a positive correlation (~ 0.78 , with an empirical range from 0.7 to 0.9) between the two variables (Mukaka 2012), indicating that our model has been successful in discriminating blockers of variable activity (as Figure 3.3.2).

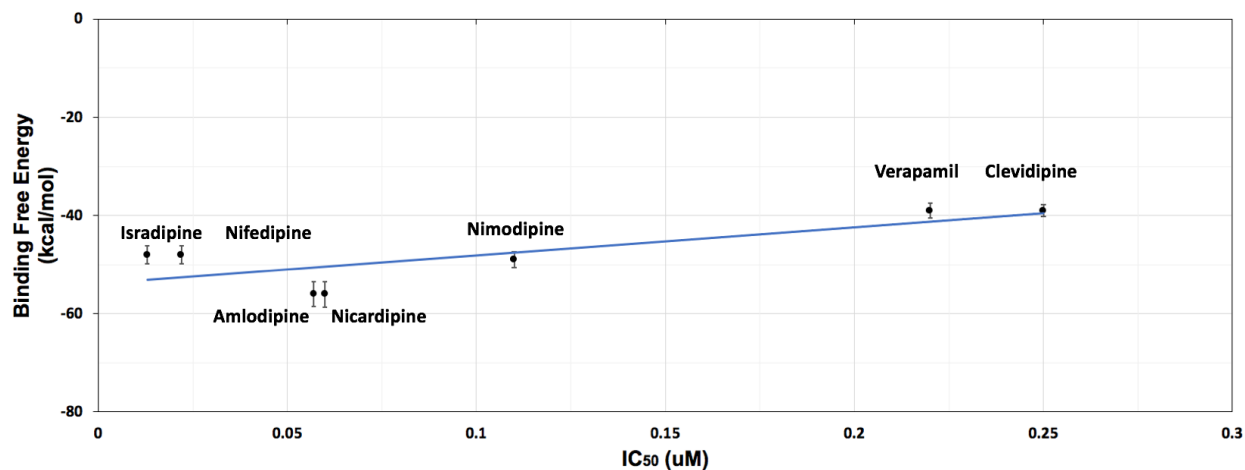


Figure 3.3.2. The correlation between MM-GBSA binding energy and experimental binding affinity (IC_{50}) of amlodipine, nicardipine, isradipine, nifedipine, nimodipine, and verapamil, shows a strong positive correlation ($R_{\text{person}} = 0.78$). The error bar is calculated based on the top five representative conformations of each compounds.

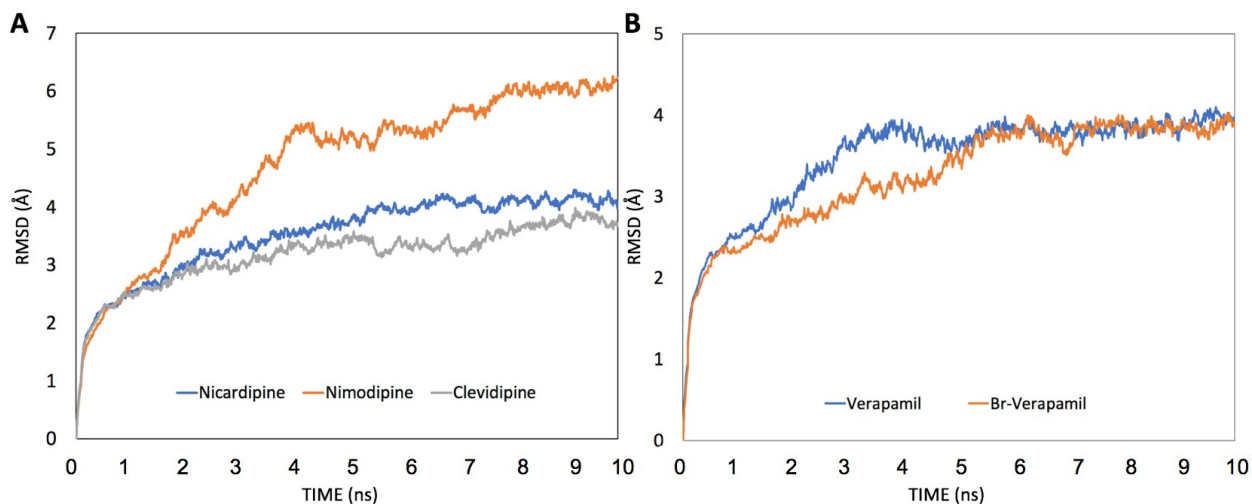


Figure 3.3.3. The RMSD value of human Cav1.2 complex with calcium channel blockers, A) nicardipine, nimodipine, and clevidipine, and B) verapamil and Br-verapamil, calculate along the ~ 10 ns length classical MD trajectory based on the initial conformation of the complex.

With some limitations, the combined docking - Schrödinger MM-GBSA results show that our model was successful in discriminating strong from weak CCBs, nonetheless, it was unable to rank compounds with similar activities (see fig.3.3.2). Consequently, these docking results are not sufficient to explain the detailed reasons behind the blocking activity for each compound, particularly in the case of DHPs, where our docking results show that that this class of compounds interacts in a way that is not directly interfering with the ion passage. A possible mechanism for DHPs' blocking activity can be explained through an allosteric interference with ions. This cannot be observed in the context of docking simulations, where no flexibility beyond the binding site is allowed and most of the protein residues are treated as rigid entities. An allosteric modulation can involve significant dynamics in the channel core, which may not be only limited to side chains' movements and may require backbone dynamics from far regions relative to the ion passage route. To account for the full flexibility of both the compounds and the channel, we decided to study each compound-protein system using MD simulations. To efficiently use our computational resources and to remove any redundant information from docking simulations, we decided to focus on the best pose only for each compound, rather than running the same simulations on very similar poses. We decided also to focus only on five compounds representing a wide range of activity for CCBs from strong CCBs (e.g. nifedipine and verapamil) to weak CCBs (e.g. clevidipine and Br-verapamil) (Fleckenstein 1983, Elkayam, Shotan et al. 1993, Striessnig, Grabner et al. 1998, Cheng, Tikhonov et al. 2009, Striessnig, Ortner et al. 2015, Tang, Gamal El-Din et al. 2016). Our selection also comprised compounds from the two CCBs classes (i.e. DHPs and PAAs). The five selected compounds are bold in table 3.3.2 and the trajectories from the simulations for of these compounds were used for a comprehensive MM-PBSA free energy calculation to re-rank their binding activity and to study the effects of the different Cav1.2 residues on the binding to each compound.

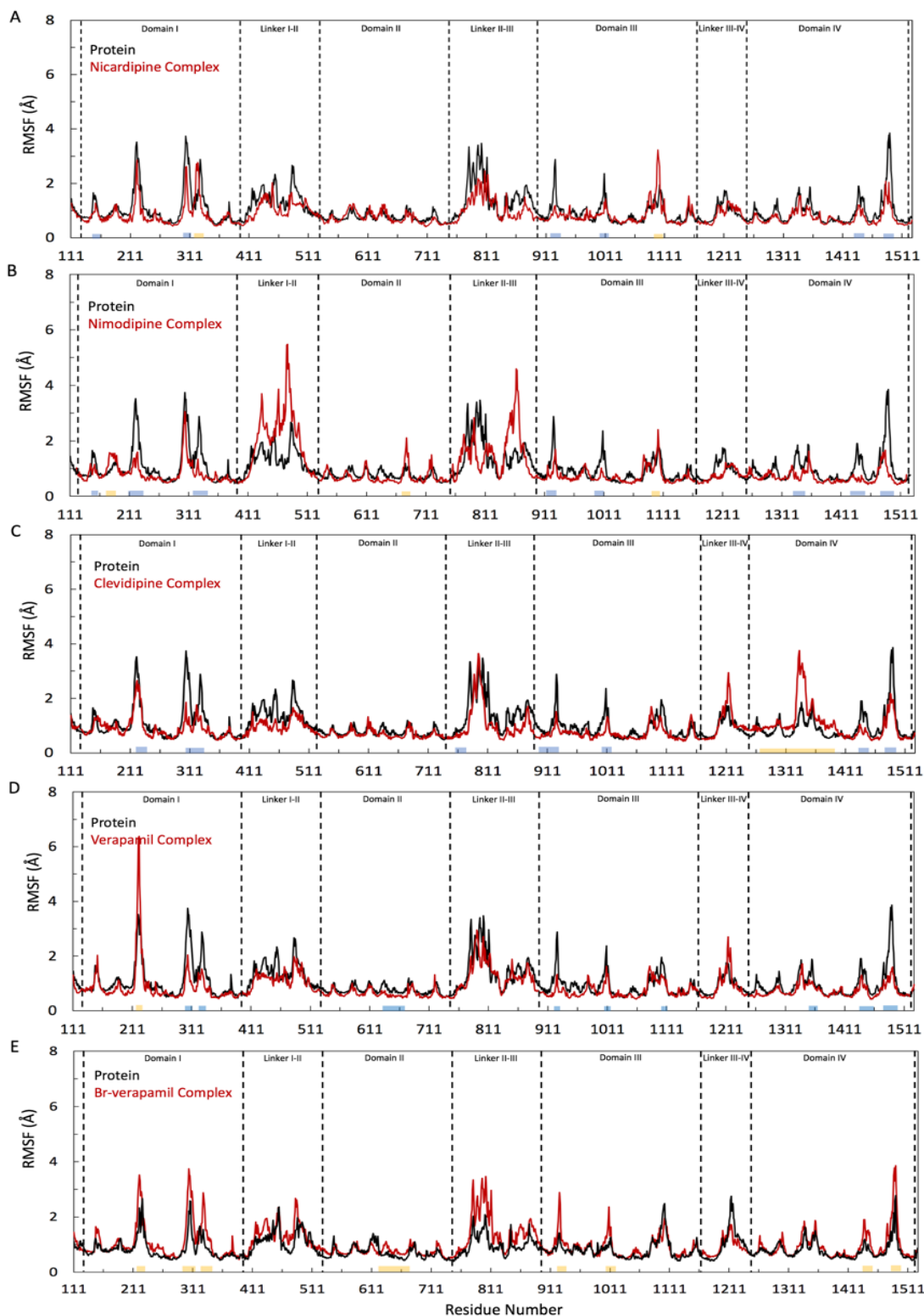


Figure 3.3.4. The comparison of RMSF value between protein (black) and complex (red), A) nicardipine, B) nimodipine. C) clevidipine, D) verapamil, and E) Br-verapamil. The underline indicates the region in complex are more flexible (yellow) or stable (blue) during the simulation.

3.3.2 Classical MD Studies

Each simulated compound-protein system was modeled at physiological conditions in which the bound complex was imbedded in a membrane environment and submerged in explicit water. Modelling these systems at these explicit conditions was important to study any water/lipid-mediated interactions and to provide a natural environment in which these binding interactions can occur. Each system was simulated up to 10 ns of simulation time and the stability of each system was assessed by calculating the all-atom root-mean-square-deviations (NoH-RMSDs) over the total simulation time. Figure 3.3.3 shows the RMSDs for the five tested compounds.

For all compounds, the initial conformations obtained from their docking simulations were used as references and their stable RMSDs averaged over a range from 3 Å to 5 Å, with the most flexibility observed in the nimodipine case and the least for Br-Verapamil. The observed flexibility in RMSDs is normal for ion channels' simulations (Feng, Kalyaanamoorthy et al. 2019) and can be mainly attributed to the loops within the channel. To confirm that and to evaluate the effects of each compound on the flexibility of the different parts of the channel, we used the last 3 ns from each simulation to calculate the root-mean-square-fluctuation (RMSF) values for each residue in the absence and presence of a compound. Our RMSF calculations in the absence of the compounds revealed interesting data (see fig.3.3.4). Most of the channel's residues remained relatively nonflexible, with the significant differences observed in the cytoplasmic and extracellular loops, as expected. Regions with extreme flexibility included the extracellular loop between S5 and S6 in each domain and the cytoplasmic loops between Domain II and Domain III. On the other hand, the selectivity filter residues seem to be quite stable through the simulations. It is important to note that the observed highly flexible regions are located at the connections of the transmembrane helices, which are exposed to bulk water and not at the core of the channel. The effect of

compounds' binding was greatly observed in specific regions in the channel. These regions had very limited flexibility/rigidity in the absence of the compounds and their movements were clearly transformed upon the compounds' binding. For instance, the S5-S6 helices of DIII (residues 1052 to 1181) and S5-S6 helices of DIV (residues 1250 to 1360) exhibit higher flexibility upon the binding of DHPs. Although the three DHPs affected almost the same regions, their effects were not identical. For example, while nicardipine decreased the flexibility of residues 411 to 510, nimodipine seems to significantly enhance the flexibility of the same region and clevidipine interacts almost similarly to nicardipine on these residues. Furthermore, the three compounds interacted differently on residues 760 to 900, where nicardipine reduced their flexibility, nimodipine reduced the flexibility of residues 760 to 800 and enhanced the flexibility of residues 830 to 870, and clevidipine had almost no effect on these residues.

3.3.3 MM-PBSA analysis

Further to calculating the binding affinities and as suggested by RMSFs calculations, which highlighted important residues to study, we decomposed the binding affinities into residue contributions. The compounds using the MD-based MM-PBSA energy analysis confirmed the binding strength of three DHP derivatives and two PAA derivatives. Using the trajectories from MD simulations and calculating the binding energies different snapshots from these simulations can provide the detailed energy decomposition, which decomposes the energy contribution from each residue as electrostatic and VDW terms. The MD-based MM-PBSA energy analysis was performed on trajectories from the last 3 ns of the MD simulations.

Figure 3.3.5 provides heatmaps for this energy decomposition analysis into electrostatics and Van der Waals breakdown. These heatmaps correlates with the observations from the RMSFs calculations and explain these data from an energy perspective. For example, DHPs show strong

electrostatic interactions with residues from S6 in DIII, including ILE1046 VAL1053 GLN1060 MET1177 ILE1180 PHE1181. Similarly, these compounds seem to interact with S6 residues in DIV, such as TYR1508, MET1509, ALA1512, ILE1516, which submerge DHPs CCBs in a hydrophobic environment. A similar situation was observed for PAAs, where most of the interactions took place with the hydrophobic residues spreading over the central cavity of the pore region. These residues interact with the PAA analogues through the VDW interactions, such as S6 helix in Domain II: GLY705 and PHE737; S6 helix in Domain III: ILE1170, PHE1134, and MET1177; S6 helix in Domain IV: MET1509 and ALA1512. It is important to note that the same residues interact with both DHPs and PAAs, which emphasises the partially overlapped binding sites for both classes of CCBs. In addition to these PAAs' VDW interactions, it is worth noting that the only polar interaction for verapamil is involving residue ASN741 in DII-S6 through the tertiary amine group in verapamil. Furthermore, both verapamil and Br- verapamil directly interact with residues from the selectivity filter, which helps these compounds block the entrance of calcium ions through the channel.

3.3.4 Modes of binding

MD simulations provided stable conformations for each compound, in which water, ions and lipids were allowed to mediate the interactions between the channel and the bound compounds. These conformations offer a wealth of structural data to study the modes of binding of the five tested compounds and compare their interactions with the different residues of human $Ca_v1.2$. One aspect to study these interactions is to analyze the hydrogen bonds network associated with each compound, which can help understand the mechanism by which each compound can block the channel. Figure 3.3.6 shows the predicted binding modes and the hydrogen bonds' analysis of nicardipine, nimodipine, clevidipine, verapamil, and Br-verapamil.

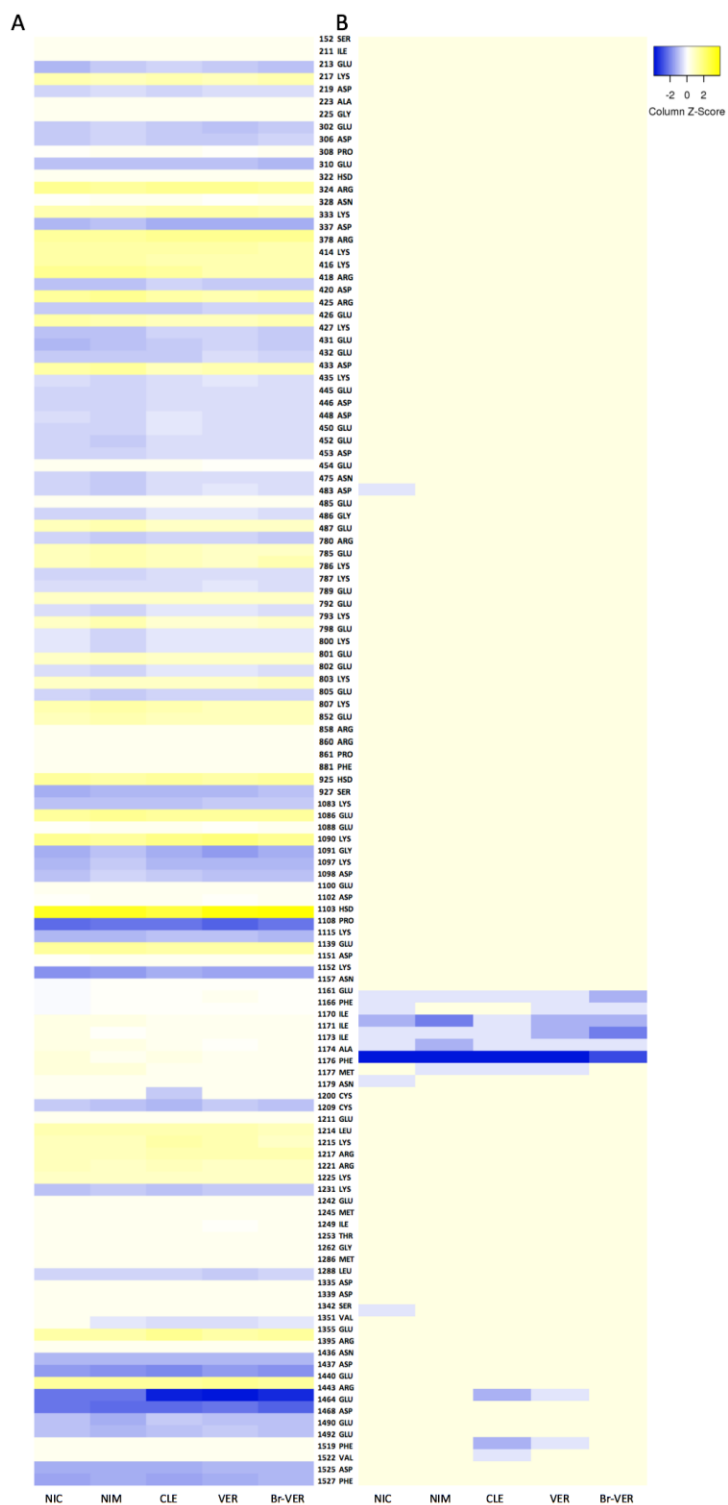
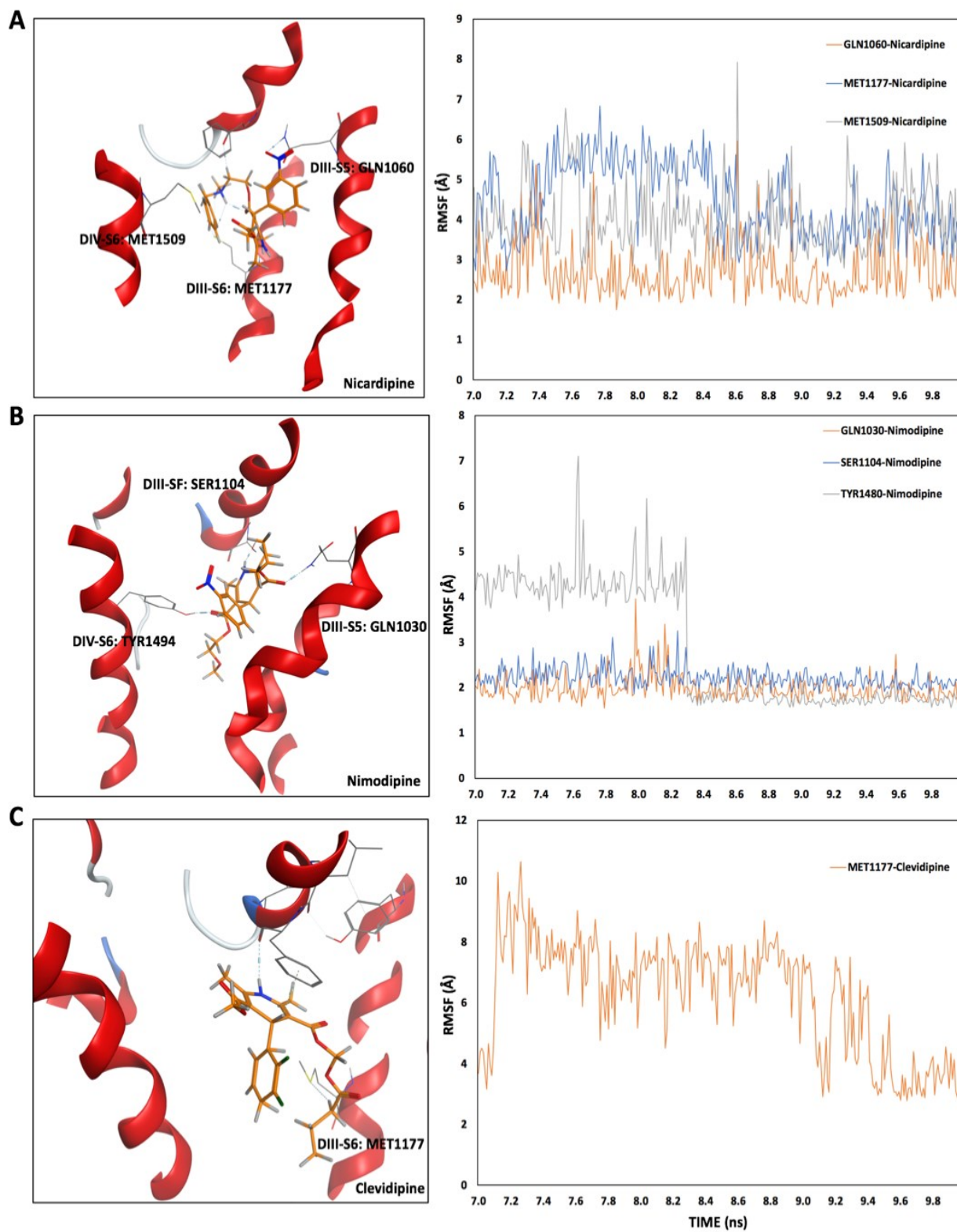


Figure 3.3.5. The heatmap of residues in A) electrostatic interaction and B) Van der Waals interaction in DHP-binding complex, nicardipine, nimodipine, and clevidipine, and PAA-binding complex, verapamil and Br-verapamil.



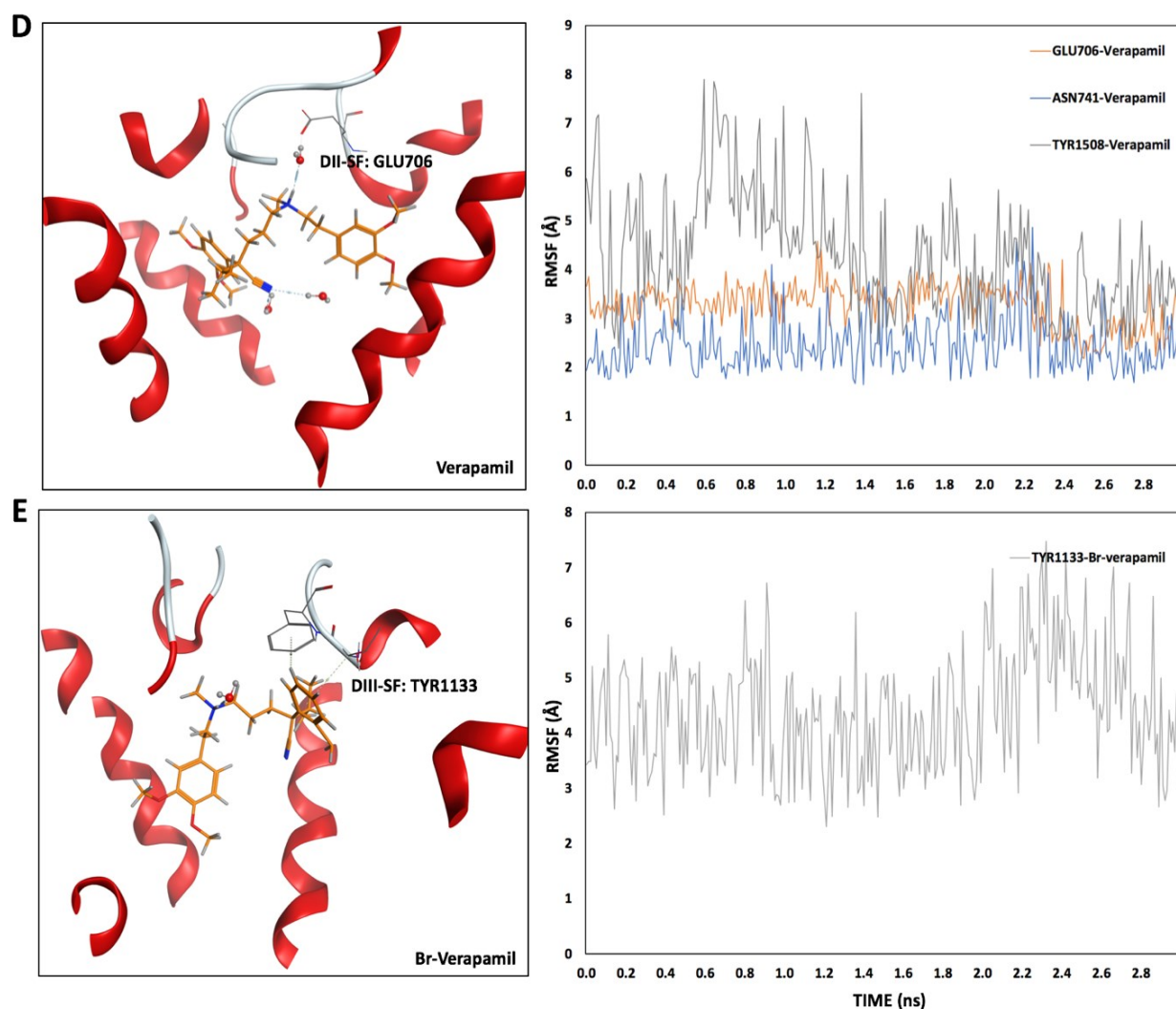


Figure 3.3.6. The H-bond (left) and the distance (right) between residues and ligand in the DHP-type complex, including A) nicardipine, B) nimodipine, and C) clevidipine, and PAA-type complex, D) verapamil and E) Br-verapamil.

Nicardipine forms multiple H-bonds with the surrounding residues (see fig. 3.3.6A), which stabilize nicardipine's binding to the channel. The strongest hydrogen bond is formed between GLN1060 with an average distance of 3 Å. A weaker hydrogen bond is formed with MET1509, which fluctuated around 4 Å. The weakest hydrogen bond for nicardipine is formed with GLN1177 with around 50% occupation and fluctuating around 4.5 Å at the final half of the simulation time. Furthermore, VDW interactions play a role in nicardipine binding to the channel and PHE1129

seem to interact strongly with the hydrophobic chain of the compound with an average distance of 2.5 Å. A similar but stronger hydrogen bond network was observed for nimodipine. These hydrogen bonds include a bond between the nitrogen atom in pyridine ring of nimodipine and the oxygen atom of SER1008 (Tang, Gamal El-Din et al. 2016) and two bonds between the negatively charged oxygen of nimodipine carboxylic group and GLN1030 and TYR1480. The two hydrogen bonds between nimodipine and SER1008 and GLN1030 are much stronger compared to that with TYR1480 (see fig. 3.3.6B), with distances averaged around 2 Å. Much weaker interactions were observed for clevidipine. There are no stable hydrogen bonds for clevidipine, and VDW interactions seem to be dominating its binding to the channel. Similar to nicardipine, clevidipine is interacting strongly with a phenylalanine residue, namely PHE1129. A weaker interaction for clevidipine is observed with MET1177. Altogether, these binding data for DHPs indicate that nicardipine has the strongest interactions with the binding site. These interactions are mediated by hydrogen bonds and VDW interactions (as fig.3.3.6C). On the other hand, clevidipine has the lowest number of interactions with the binding site, which involve only a VDW interaction with PHE1129 and no stable hydrogen bonds to enhance these interactions.

As the binding location of PAAs is slightly distinctive from DHPs binding site and the nature of their scaffolds is also different, PAAs are expected to interact with Cav1.2 differently from DHPs. For example, as the two main functional groups of verapamil are located at each side of the compound, these functional groups are expected to mediate more favourable interactions. This is clearly illustrated in figure 3.3.6D, where four negatively charged oxygen atoms interact through hydrogen bonding with the amine group of DII-S6 ASN741 and the S-methyl thioether side chain of DIII-S6 MET1178. There is also a weak electrostatic interaction between verapamil and TYE150. A water-mediated H-bond is also formed between the GLU706. Compared to

verapamil, Br-verapamil has two ether groups one side of the molecule, with the other side is lacking these groups. The interaction of Br-verapamil and the surrounding residues is very weak, deficient from any stable hydrogen bonds throughout the simulation time. Although the energy decomposition analysis suggests the presence of electrostatic interactions of Br-verapamil and THR704, PHE1134, and THR1508, these interactions seem to involve very weak hydrogen bonds (see fig. 3.3.6E).

Although the binding modes mentioned above reveal how each compound interacts with Cav1.2, these binding conformations cannot fully explain the ion blocking mechanisms for these compounds. One way to directly assess that is to pull a calcium ion through the selectivity filter in the absence and presence of the compound and evaluate the energetic barriers for ion passage due to the binding of the compound. Furthermore, by comparing these energy barriers between strong and weak blockers, one can understand the reasons behind their ion blocking variations and develop a method to rank these compounds more accurately. To accomplish that, the abovementioned modes of binding were used as a starting point to carry out steered MD (SMD) simulations.

3.3.5 Steered MD studies

Steered molecular dynamics (SMD) is a nonequilibrium MD method (Adiban, Jamali et al. 2017, Jalily Hasani, Ganesan et al. 2018). It is usually used to accelerate ligand dissociation from a receptor and can be applied to a single atom. In a constant velocity SMD, for instance, the time taken for this ion/ligand to be pulled out of the receptor is constant and SMD can hence provide a quantitatively tool to evaluate the dissociation resistance faced by the pulled ion through the channel. In SMD an external force is applied to the individual ion and the response of the system to this external force is measured in relation to the displacement of the pulled ion. In our

case, the pulled ion is expected to face at least one energy barrier corresponding to its passage through the selectivity filter. Furthermore, the presence of a strong CCB is expected to introduce additional energy barriers against the ion passage, which can explain the mechanism of its blocking activity. A weak CCB, however, may not add significant barriers against the passing ion. In this context, SMD becomes a valuable tool to study the mechanism of ion blockade by CCBs and to rank their inhibitory strength quantitatively.

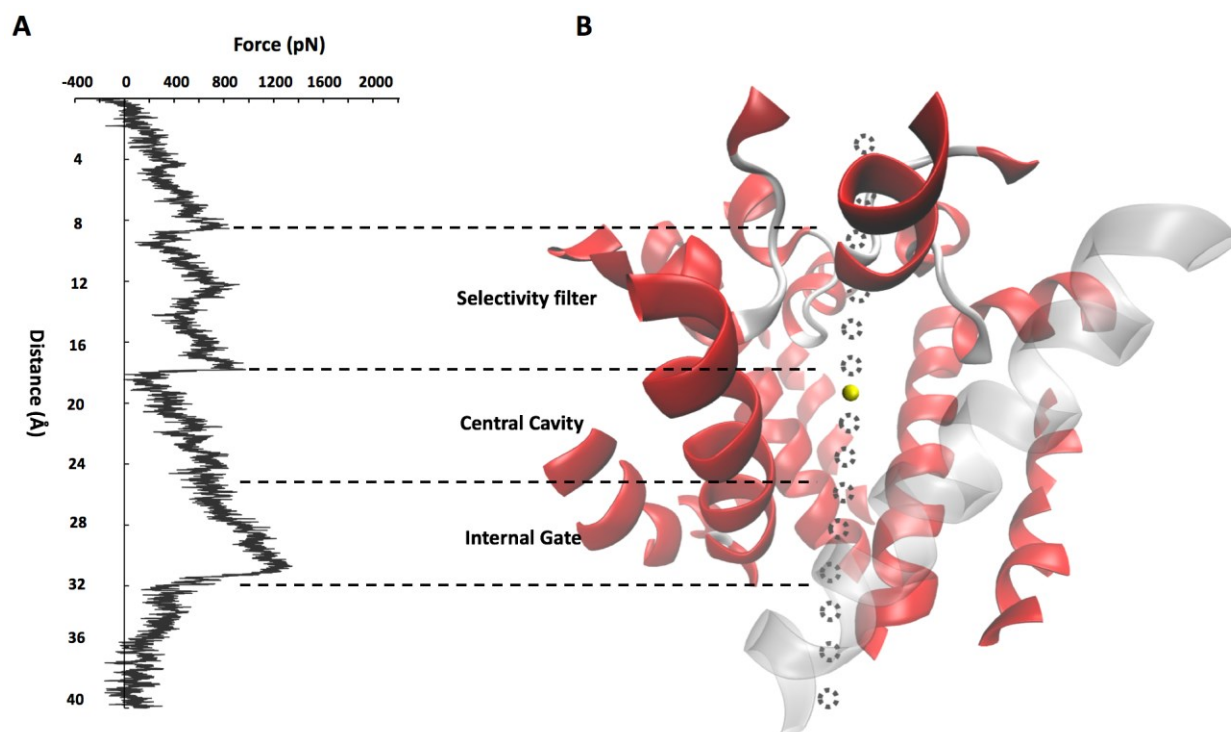


Figure 3.3.7. A) The force profiles of SMD on human Cav1.2, and B) The NOC conformation of human Cav1.2 channel. The force profile and structure align on the Z-axis direction. The calcium ion passed through the selectivity filter, central cavity, and internal gate.

Figure 3.3.7 shows the force profile for an ion pulling SMD simulation in the absence of any bound CCB. This force profile is our reference to understand the effects of CCBs on the ion passage. Along the ion permeation pathway, the range from 8 Å to 17 Å corresponds to the selectivity filter, and the range from 26 Å to 32 Å corresponds to the internal gate. To understand the

significance of the observed peaks in these profiles, one should keep in mind the correspondence of the shown distances in the x-axis with the different locations within the channel. At the beginning of the ion journey, the force profile is fluctuating around zero N, indicating no barriers against the ion to pass through this region. This allowed zone for the ion represents the distance from outside of the channel up to the beginning of the selectivity filter.

Following that, the ion started to feel the presence of the selectivity filter, which is reflected by the appearance of three small ramps with peaks at 8Å, 12Å, and 17Å, representing three calcium binding sites within the selectivity filter. These sites are important to attract calcium ions from outside the channel towards the pore of the channel (Tang, Gamal El-Din et al. 2014, Adiban, Jamali et al. 2016, Tang, Gamal El-Din et al. 2016, Wu, Yan et al. 2016, Feng, Kalyaanamoorthy et al. 2019). Site-1 is formed by four deprotonated glutamine residues (Glu363 (DI), Glu706 (DII), Glu1135 (DIII), and Glu1464 (DIV)) located within the four transmembrane domains. The carboxylate groups of these glutamine residues (Glu253 and Glu596) lie close to the calcium ion (~ 3 Å) and mediates its binding to site-1. Site-2 is formed by one of the glutamine residues from site-1 and a threonine residue from site 3. The third peak is formed when the ion moves to site-3, which is formed by four threonine residues (Thr361 (DI), Thr704 (DII), Thr1133 (DIII), and Thr1462 (DIV)). It is important to note that the glutamine residues forming site-1 and the threonine residues forming site-3 are conserved among all different LTCCs (Wu, Yan et al. 2015, Wu, Yan et al. 2016). Following these three peaks appears a major peak at 30Å from the initial position, corresponding to the hydrophobic internal gated area, which dehydrate the calcium ion from bulk water associated with the ion from the central cavity (Feng, Kalyaanamoorthy et al. 2019). After passing through this last barrier the force profile is reduced again to zero, indicating another free zone for the ion to exit the channel.

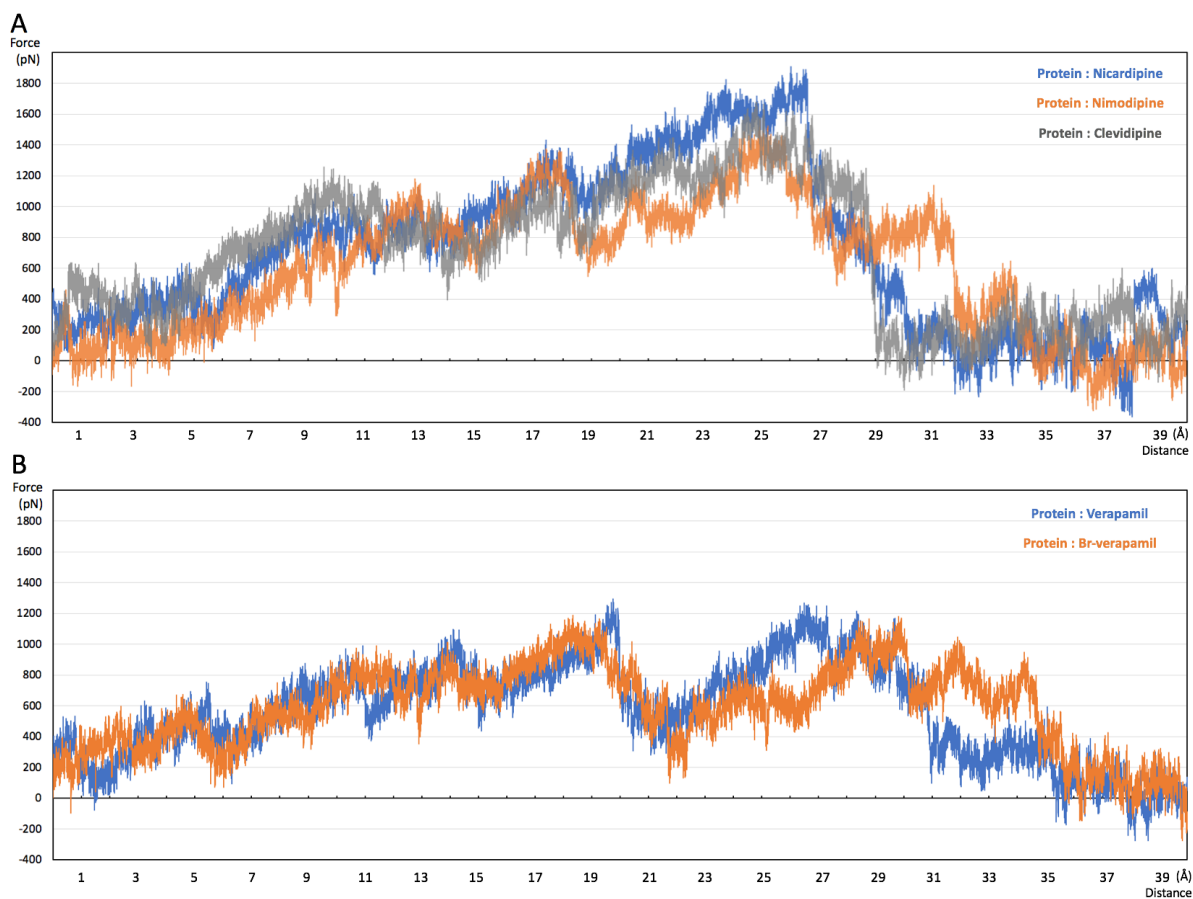


Figure 3.3.8. The force profiles of SMD simulations on **A)** DHP-type inhibitors, including nicardipine (Orange), nimodipine (Blue), and clevidipine (Grey) **B)** PHE-type inhibitors, including Br-verapamil (Orange) and verapamil (Blue).

Comparing the effects of the presence of CCBs bound to Cav1.2 reveals interesting findings. Figure 3.3.8A illustrates the force profiles for DHPs. The strength relativity of the three DHP derivatives is clear. While the three peaks corresponding to the calcium binding sites within the selectivity filter are reproducible for each compound, the main difference lies in final peak attributed to ion dehydration at the hydrophobic internal gate within the channel. The highest energy barrier is created by nicardipine, particularly at 27Å from the beginning of the ion trajectory and forming ~1800pN barrier, adding ~600pN barrier on top what the ion is facing at the final calcium binding site at the selectivity filter (*i.e.* Site-3). This constitute a significant barrier for the

ion to pass and this barrier can explain why nifedipine can be ranked as a strong blocker from the DHP class of CCBs. On the other hand, while nimodipine, and clevidipine have very similar effect regarding the three peaks corresponding to the calcium site at the selectivity filter, which can indicate similar blocking activity for the two compounds, there is a major difference at 31A shown as what appears to be a new peak for nimodipine. While the resistance at this site is around ~ 800 pN, which is relatively lower compared to the observed peaks for the selectivity filter, this additional peak can explain why nimodipine is relatively stronger compared to clevidipine. On average, there is an increase of 100-200 pN force barrier at the selectivity filter sites for three DHP derivatives compared to the apo-Cav1.2 force profile. This force increase can be attributed to the asymmetrical modes of binding for the three compounds and the to the formed hydrogen bond network between the compounds and the polarized residues discussed above. Overall, the force profiles shown in Figure 3.3.8A suggest a blocking ranking for the three DHPs in which nifedipine is the strongest and clevidipine is the weakest, which correlates very well with the ranking reported in the literature (Zhao, Huang et al. 2019).

Figure 3.3.8B shows the force profiles for the PAA derivatives. The overall effects of PAA on ion passage reveals a weaker effect compared to DHPs. Given that PAAs bind within the central cavity of the channel and their interactions with the residues below the selectivity filter are mediated mainly by VDW forces (see fig. 3.3.8D&E), their binding is directly affecting the selectivity filter. PAAs prevent the calcium ion from passing through the channel by increasing the energy barriers at the selectivity filter. On The binding of PAAs adds an average 100 pN force at three binding sites (Site-1: ~ 900 pN, Site-2: ~ 1000 pN, and Site-3: ~ 1100 pN), compared to the apo channel. Despite slight differences between verapamil and Br-verapamil effects at the internal gate, there is no significant change from the apo channel force profile in this region. It is worth

noting that one extra electrostatic interaction exists between the amine group in DII-S6 ASN731 and two negatively charged oxygen atoms in verapamil. This maintains the stability of bound verapamil and seems to generate a slightly higher peak corresponding to site-3 in the selectivity filter. This missing electrostatic interaction can explain why a calcium ion can easily cross br-verapamil to enter the bulk water of the central cavity. Based on this data, verapamil is predicted to be a stronger blocker compared to br-verapamil, which also agrees with the available experimental data (Tang, Gamal El-Din et al. 2014, Tang, Gamal El-Din et al. 2016).

3.4 Conclusion

Calcium channel blockers (CCBs) are widely used for the treatment of various cardiovascular diseases including hypertension and angina. The current work was focused on studying two of the most commonly prescribed CCBs, namely, phenylalkylamines (PAA; e.g. verapamil) and dihydropyridines (DHP; e.g., nifedipine). Both classes bind to the α subunit of Cav1.2, however, each class seems to interact with the channel via a distinct site. The objective of the current study was to evaluate the effects of CCBs on the calcium ion permeation in Cav1.2. To accomplish that, docking studies were employed to predict the most probable binding locations and binding modes for DHPs and PAAs. Our results confirm earlier findings and show that while the binding sites for the two CCB classes are distinct, their binding locations are partially overlapping.

To understand the mode of binding of the two classes, we used molecular dynamics simulations and free binding energy calculation studies. Ion pulling studies using steered molecular dynamics (SMD) was also used to study the atomistic details for the effects of each class on the ion passage through the channel. During these simulations a calcium ion was pulled through the

channel in the absence presence of the bound blocker and the force profiles in both cases were compared. Overall, our findings show that DHPs seem to have a stronger effect on ion passage compared to PAAs. While DHPs increase the energy barriers for the ions to pass in both the selectivity filter and hydrophobic inner gate of the channel, the dominant effects of PAAs are found within the selectivity filter. Our results provide dynamical and structural perspectives to explain drug mediated blocking mechanisms in calcium ion channels.

CHAPTER 4: GENERAL DISCUSSION

The human Cav1.2 ion channel belongs to the large family of voltage-gated calcium channels. Cav1.2 is the dominant L-type calcium channel expressed in the human heart (Zamponi and Snutch 2013, Hofmann, Flockerzi et al. 2014). The depolarized potential of the membrane activates Cav1.2, generating the inward calcium current (I_{Ca}), which extends the cardiac repolarization and helps define the shape of the action potential in cardiac and smooth muscles (Fleckenstein 1983, Bers 2002, Grant 2009). The importance of I_{Ca} is evident from the number of pathophysiological conditions that can result from mutations affecting the biophysical and regulatory properties of the Cav1.2. An example of such conditions is the induction of long QT syndrome (LQTS), where the QT interval of the cardiac action potential is prolonged, a condition that causes heart arrhythmias and may lead to sudden cardiac death (SCD)(Burashnikov, Pfeiffer et al. 2010, Kim 2014, Giudicessi and Ackerman 2016, Rougier and Abriel 2016). The Timothy Syndrome (TS), is an extremely rare multisystem LQTS subtype, that is mainly caused by dysfunctions in LTCCs and Ca^{2+} handling proteins (Striessnig, Bolz et al. 2010, Napolitano and Antzelevitch 2011, Cohen-Kutner, Yahalom et al. 2012).

Understanding the mechanisms of ion conduction and ligand binding in Cav1.2 has been the focus of several studies over the last few years. This included the emergence of new crystal structures for calcium channels, including the bacterial CavAb (Tang, Gamal El-Din et al. 2014, Tang, Gamal El-Din et al. 2016) and the rabbit Cav1.1 channels (Wu, Yan et al. 2015, Wu, Yan et al. 2016). These emerging experimental structures offered valuable resources to build accurate structural models for Cav1.2 (Adiban, Jamali et al. 2016, Hering, Zangerl-Plessl et al. 2018, Martinez-Ortiz and Cardozo 2018, Feng, Kalyaanamoorthy et al. 2019). Although these experimental and computational studies provided a breakthrough the schematic representation of

Cav, there are still many unanswered questions, particularly when one tries to address these mechanisms associated with the channel at the resolution of a single ion.

Thus, this thesis studied the structural and functional properties of human Cav1.2 and focused on modelling the α_1 -subunit of the channel, which maintains the ion permeation functions and is the target of many calcium channel blockers (CCBs). Our aim was to establish a high-resolution dynamical study investigating how ions pass through the channel? What are the atomistic determinants that control this process? And how the binding of a channel blocker affect this passage. To our knowledge, this thesis represents the first comprehensive attempt to answer these important questions at this level of details. Towards this goal, we combined several advanced computational tools and techniques while incorporating the latest experimental data to construct a reliable model for the human Cav1.2.

The thesis was presented in the following order. The first chapter laid the foundation of this thesis and provided the essential background on voltage-gated calcium channels, in general, and on the human Cav1.2 channel, in particular. Chapter 2 presented the details of constructing a human Cav1.2 model and explained the structural basis for the calcium selectivity and ion permeation mechanisms. Chapter 3 utilized the model generated in chapter 2 to answer a more sophisticated question; that is, how a CCB affect the ions' permeation through the channel. In this chapter, the ions' passage phenomena was investigated in the presence and absence of small molecule blockers and the force profiles and energy barriers associated with ions' passage was calculated and compared at different levels. Appendix A provided a general overview on the methods used to predict druggable binding sites in proteins. Finally, appendix B summarized the theories behind the molecular dynamic simulations methods used to study Cav1.2.

In chapter 2 a structural model for human Cav1.2 channel was constructed, while fitting the model to all available experimental data in the literature (Feng, Kalyaanamoorthy et al. 2019). The final refined Cav1.2 model had an excellent correlation with the reported experimental data. This included the exposure of certain residues to the lipid environment and secondary structure of important protein segments. The generated Cav1.2 homology model was refined using a substantially long classical MD simulation for ~100 ns. This long MD simulation was conducted for two reasons. First, MD simulations allowed the relaxation of the protein and the removal of structural clashes that can otherwise lead to further imprecisions in the desired results. Secondly, for a complete human Cav1.2 channel generation, an ensemble of Cav1.2 conformations were required. After reaching equilibration, we used external electric field MD (EEMD) simulations to accelerate and explore the sampling of the Cav1.2 conformational space. EEMD is one of the main techniques to involve the depolarized potential and accelerate transitions of proteins conformations. We took advantage of the ability of the EEMD method to change the positions of the voltage sensor domain (VSD), which initiates the activation of the channel. A 200 ns length trajectory was collected from the EEMD simulation. Overall, a 300-ns trajectory was clustered to sample eleven representative conformations, which composed the conformational ensemble of human Cav1.2 channel. Subsequently, we employed steered molecular dynamics (SMD) to understand calcium ion permeation in hCav1.2. Our SMD simulations on the model revealed four important barriers for ion permeation: these included three calcium binding sites formed by the EEEE- and TTTT-rings within the selectivity filter region and a large barrier representing the hydrophobic internal gate of the channel. Our modeling study clearly demonstrated the specific structural changes and residues which play important roles in controlling the channel's ion transport mechanisms. Our results also revealed that the first hydration shell of calcium remained intact throughout the

simulations, thus playing an important role in ion permeation in hCav1.2. Our results have provided important mechanistic insights into the structure, dynamics and ion permeation in hCav1.2. The significant barriers for ion permeation formed by the four phenylalanine residues at the internal gate region suggested that this site is important for channel activation and may be a target site for small-molecule-based modulation.

Chapter 3 focused on the mechanism of channel blockage by small molecules and their effects on ion permeation. Calcium channel antagonists are widely used in the treatment of cardiovascular disorders. As explained in chapter 3, they are mainly limited to 1,4-dihydropyridine (1,4-DHPs) and phenylalkylamines (PAAs) derivatives and are used primarily for the treatment of hypertension, angina pectoris, and cardiac arrhythmias. Despite their well-established efficiency, the structural basis behind their activity is not very clear. Through this study, we investigated the binding of a set of known calcium channel blockers using flexible docking simulations. The compounds consisted of eight derivatives from DHPs and PAAs, representing a broad range of activity. The selection of these compounds was to validate our model and to test its competence in predicting the differential blocking effect of drug molecules. Using the model generated in chapter 2, chapter 3 examined the mode of binding of these antagonists within the pore domain as well as the fenestration of the pore-forming domains. The protein-ligand interactions occurred in a well-defined pocket right below the selectivity filter, as was reported before in previous mutational studies in the literature.

Following the placement of the blockers within their suitable modes of binding within the channel, we examined the effects of these drugs on ions' permeation. To do that, we used steered molecular dynamics (SMD) simulations and ion pulling studies. Further analysis of the pore topology allowed us to understand the effect of the blockers on the physical characteristics of the

channel pore. The calcium ions passing through the Cav1.2 channel in complex with different drug molecules revealed two dominate modes of interactions. For the PAA derivatives, the VDW interactions played an important role in the binding with surrounding residues of S6 helix in each domain and helped discriminate the strength of their blockage. For the DHP derivatives, both the VDW and electrostatic interactions were involved in their binding with DIV-S6 and DIII-S6 respectively. Although the strong, medium, and weak DHP blockers shared the same binding site of Cav1.2, their blockage strength on the pore are determined by the existing H-bonds with the DIII-S6 helix. These in-depth structural analyses suggested that small molecules can effectively block the Cav1.2 ion channel as long as they interact similarly to key residues within the pore. Therefore, assessment of drugs for cardiotoxicity should involve close examination and investigations on the channel residues and ion interactions with the ligands. These ligand interaction studies represent novel and very interesting findings. It showed that regardless of the binding location of a CCB, a strong blocker has to alter the hydrogen bond network surrounding the selectivity filter to block the ions from moving through the channel. This blockade can either result from a direct interaction with the selectivity filter (*e.g.* DHPs) or through allosteric binding within the channel pore (*e.g.* PAAs). In both cases, the energy barriers throughout the ions' permeation pathway is altered, with more penalties added at the three ionic binding sites within the selectivity filter as well as at the internal gate of the channel. These findings represent the major outcomes of the current thesis and can provide new suggestions to rationally design a new generation of CCBs targeting the Cav1.2 channel.

The results combined from the two parts of this thesis, presented in Chapters 2 and 3, shed light on the conformational transitions and the effect of different binding sites in the ion permeation pathway within the hCav1.2 channel. These data are significant from both a drug design point of

view as well as to understand the mechanisms of drug-mediated cardiotoxicity effects in ion channels. The structural details from our studies has revealed key residues related to the normal permeation of calcium ions and essential non-bonding interactions existing between calcium channel blocker and the channel. This information may open new ways for drug design strategies to overcome the barriers that disrupt the passage of ions. Additionally, the unintentional blockage of Cav1.2 ion channels are one of the main causes of drug-mediated cardiotoxicity. Our ion permeation studies using the DHP and PAAs scaffolds and their effects on ions' permeation, revealed important mechanisms related to this process.

Overall, the findings from this thesis are important and investigated novel aspects of the Cav1.2 channel. However, one should look into this thesis as a good starting point for further studies to investigate different drug scaffolds and different mechanisms by which they can affect ion permeation in human Cav1.2 channels. It can be also a good starting point to apply the same techniques adopted in this thesis to model other cardiac ion channels and combine these models to reproduce the cardiac rhythm and understand the effect of drugs on this important phenomenon.

CHAPTER 5: FUTURE PERSPECTIVES

The approach presented in this thesis provides the methods to accelerate and sample various conformations from the transition states of human Cav1.2. The partially opened conformations of the human Cav1.2 provide dynamical and structural perspectives to explain the conformational changes of calcium ion channels. However, available structures of calcium channels are all limited to the inactivated state. In this thesis we tried to induce a transition from this closed state to an open state using external electric field simulations, which led to a partially open conformation for the Cav1.2 channel. This can be extended further to completely open the channel and to also understand how this transition from a closed to an open state take place. Understanding this transition can help designing new Cav1.2 modulators that can restrain the channel at a transition state. This can also help design compounds that can act as Cav1.2 activators, favoring the binding to the open active confirmation of the channel.

It is also worth noting that the human Cav1.2 channel is a multiple subunits complex, involving the cytoplasmic β -subunit, extracellular $\alpha_2\delta$ -subunit, and transmembrane γ -subunit (Arikkath and Campbell 2003, Dolphin 2003). Including all these auxiliary subunits in a single model can be the second possible future direction. Building the multi-subunit hCav1.2 will bring the different physiological properties into the channel, such as the extrinsic regulation mechanisms and calcium-dependent channel regulation. This study may also include the differential ion permeation pathways with the effects of auxiliary subunits. This will allow us to test the effects of auxiliary subunits on the ion permeation pathway and understand how they affect the binding of calcium channel blockers. Additionally, druggable binding sites exist on the surface of the $\alpha_2\delta$ -subunit, which can be used to investigate the binding modes and the effects of pregabalin and gabapentin (Taylor, Angelotti et al. 2007, Bannister, Adebiyi et al. 2009, Offord and Isom 2015).

The results of our ion permeation studies provided the molecular basis for ion permeation and drug binding effects. Multiple essential interactions determine the binding and strength of calcium channel blockers. A long-term goal of this project is to use these data to optimize the binding affinity of available calcium channel blockers. To achieve this, a combination of computational and in-depth experimental structural data is required to provide detailed validation of the computational data.

BIBLIOGRAPHY:

- [1] Abiria, S.A. and R.J. Colbran, *CaMKII associates with CaV1.2 L-type calcium channels via selected beta subunits to enhance regulatory phosphorylation*. J Neurochem, 2010. **112**(1): p. 150-61 DOI: 10.1111/j.1471-4159.2009.06436.x.
- [2] Abriel, H. and R.S. Kass, *Regulation of the voltage-gated cardiac sodium channel Nav1.5 by interacting proteins*. Trends Cardiovasc Med, 2005. **15**(1): p. 35-40 DOI: 10.1016/j.tcm.2005.01.001.
- [3] Abriel, H., J.S. Rougier, and J. Jalife, *Ion channel macromolecular complexes in cardiomyocytes: roles in sudden cardiac death*. Circ Res, 2015. **116**(12): p. 1971-88 DOI: 10.1161/CIRCRESAHA.116.305017.
- [4] Adapala, R.K., et al., *Activation of mechanosensitive ion channel TRPV4 normalizes tumor vasculature and improves cancer therapy*. Oncogene, 2016. **35**(3): p. 314-22 DOI: 10.1038/onc.2015.83.
- [5] Adiban, J., Y. Jamali, and H. Rafii-Tabar, *Modeling ion permeation through a bacterial voltage-gated calcium channel CaVAb using molecular dynamics simulations*. Mol Biosyst, 2016. **13**(1): p. 208-214 DOI: 10.1039/c6mb00690f.
- [6] Arien, H., et al., *Syntaxin 1A modulates the voltage-gated L-type calcium channel (Ca_v)1.2 in a cooperative manner*. J Biol Chem, 2003. **278**(31): p. 29231-9 DOI: 10.1074/jbc.M301401200.
- [7] Artalejo, C.R., M.E. Adams, and A.P. Fox, *Three types of Ca²⁺ channel trigger secretion with different efficacies in chromaffin cells*. Nature, 1994. **367**(6458): p. 72-6 DOI: 10.1038/367072a0.
- [8] Ash, W.L., et al., *Computer simulations of membrane proteins*. Biochim Biophys Acta, 2004. **1666**(1-2): p. 158-89 DOI: 10.1016/j.bbamem.2004.04.012.
- [9] Adiban, J., Y. Jamali, and H. Rafii-Tabar, *Modeling ion permeation through a bacterial voltage-gated calcium channel Ca(V)Ab using molecular dynamics simulations*. Molecular Biosystems, 2017. **13**(1): p. 208-214 DOI: 10.1039/c6mb00690f.
- [10] Almog, M. and A. Korngreen, *Is realistic neuronal modeling realistic?* J Neurophysiol, 2016. **116**(5): p. 2180-2209 DOI: 10.1152/jn.00360.2016.
- [11] Aviner, B., et al., *Selective pressure modulation of synaptic voltage-dependent calcium channels-involvement in HPNS mechanism*. J Cell Mol Med, 2016. **20**(10): p. 1872-88 DOI: 10.1111/jcmm.12877.
- [12] Ayton, G.S., W.G. Noid, and G.A. Voth, *Multiscale modeling of biomolecular systems: in serial and in parallel*. Curr Opin Struct Biol, 2007. **17**(2): p. 192-8 DOI: 10.1016/j.sbi.2007.03.004.
- [13] Ball, S.L., et al., *Role of the beta(2) subunit of voltage-dependent calcium channels in the retinal outer plexiform layer*. Invest Ophthalmol Vis Sci, 2002. **43**(5): p. 1595-603.
- [14] Bannister, J.P., et al., *The voltage-dependent L-type Ca²⁺ (CaV1.2) channel C-terminus fragment is a bi-modal vasodilator*. J Physiol, 2013. **591**(12): p. 2987-98 DOI: 10.1113/jphysiol.2013.251926.
- [15] Bannister, J.P., et al., *The voltage-dependent L-type Ca²⁺ (Ca(V))1.2 channel C-terminus fragment is a bi-modal vasodilator*. Journal of Physiology-London, 2013. **591**(12): p. 2987-2998 DOI: 10.1113/jphysiol.2013.251926.
- [16] Bannister, J.P., et al., *Ca(V)1.2 channel N-terminal splice variants modulate functional surface expression in resistance size artery smooth muscle cells*. J Biol Chem, 2011. **286**(17): p. 15058-66 DOI: 10.1074/jbc.M110.182816.

- [17] Benedetti, B., et al., *Physiological and pharmacological modulation of the embryonic skeletal muscle calcium channel splice variant CaV1.1e*. Biophys J, 2015. **108**(5): p. 1072-80 DOI: 10.1016/j.bpj.2015.01.026.
- [18] Berger, S.M. and D. Bartsch, *The role of L-type voltage-gated calcium channels Cav1.2 and Cav1.3 in normal and pathological brain function*. Cell Tissue Res, 2014. **357**(2): p. 463-76 DOI: 10.1007/s00441-014-1936-3.
- [19] Bers, D.M., *Cardiac excitation-contraction coupling*. Nature, 2002. **415**(6868): p. 198-205 DOI: 10.1038/415198a.
- [20] Bertin, S., et al., *The TRPA1 ion channel is expressed in CD4+ T cells and restrains T-cell-mediated colitis through inhibition of TRPV1*. Gut, 2016 DOI: 10.1136/gutjnl-2015-310710.
- [21] Best, J.M. and T.J. Kamp, *Different subcellular populations of L-type Ca²⁺ channels exhibit unique regulation and functional roles in cardiomyocytes*. J Mol Cell Cardiol, 2012. **52**(2): p. 376-87 DOI: 10.1016/j.yjmcc.2011.08.014.
- [22] Blaich, A., et al., *Mutation of the calmodulin binding motif IQ of the L-type Ca(v)1.2 Ca²⁺ channel to EQ induces dilated cardiomyopathy and death*. J Biol Chem, 2012. **287**(27): p. 22616-25 DOI: 10.1074/jbc.M112.357921.
- [23] Brandmayr, J., et al., *Deletion of the C-terminal phosphorylation sites in the cardiac beta-subunit does not affect the basic beta-adrenergic response of the heart and the Ca(v)1.2 channel*. J Biol Chem, 2012. **287**(27): p. 22584-92 DOI: 10.1074/jbc.M112.366484.
- [24] Buraei, Z. and J. Yang, *The ss subunit of voltage-gated Ca²⁺ channels*. Physiol Rev, 2010. **90**(4): p. 1461-506 DOI: 10.1152/physrev.00057.2009.
- [25] Burashnikov, E., et al., *Mutations in the cardiac L-type calcium channel associated with inherited J-wave syndromes and sudden cardiac death*. Heart Rhythm, 2010. **7**(12): p. 1872-82 DOI: 10.1016/j.hrthm.2010.08.026.
- [26] Burgess, D.L., et al., *beta subunit reshuffling modifies N- and P/Q-type Ca²⁺ channel subunit compositions in lethargic mouse brain*. Mol Cell Neurosci, 1999. **13**(4): p. 293-311 DOI: 10.1006/mcne.1999.0748.
- [27] Calderon-Rivera, A., et al., *Identification of a disulfide bridge essential for structure and function of the voltage-gated Ca(2+) channel alpha(2)delta-1 auxiliary subunit*. Cell Calcium, 2012. **51**(1): p. 22-30 DOI: 10.1016/j.ceca.2011.10.002.
- [28] Capener, C.E., et al., *Homology modeling and molecular dynamics simulation studies of an inward rectifier potassium channel*. Biophys J, 2000. **78**(6): p. 2929-42 DOI: 10.1016/S0006-3495(00)76833-0.
- [29] Carosati, E., et al., *Synthesis and L-type calcium channel blocking activity of new chiral oxadiazolothiazinones*. Eur J Med Chem, 2015. **92**: p. 481-9 DOI: 10.1016/j.ejmech.2014.12.044.
- [30] Castillo, J.P., et al., *beta1-subunit-induced structural rearrangements of the Ca²⁺- and voltage-activated K⁺ (BK) channel*. Proc Natl Acad Sci U S A, 2016. **113**(23): p. E3231-9 DOI: 10.1073/pnas.1606381113.
- [31] Catterall, W.A., *Voltage-gated calcium channels*. Cold Spring Harb Perspect Biol, 2011. **3**(8): p. a003947 DOI: 10.1101/cshperspect.a003947.
- [32] Catterall, W.A. and T.M. Swanson, *Structural Basis for Pharmacology of Voltage-Gated Sodium and Calcium Channels*. Mol Pharmacol, 2015. **88**(1): p. 141-50 DOI: 10.1124/mol.114.097659.

- [33] Chattipakorn, N., et al., *Calcium channels and iron uptake into the heart*. World J Cardiol, 2011. **3**(7): p. 215-8 DOI: 10.4330/wjc.v3.i7.215.
- [34] Chen, R. and S.H. Chung, *Complex structures between the N-type calcium channel (CaV2.2) and omega-conotoxin GVIA predicted via molecular dynamics*. Biochemistry, 2013. **52**(21): p. 3765-72 DOI: 10.1021/bi4003327.
- [35] Chen, X., et al., *Structure of the full-length Shaker potassium channel Kv1.2 by normal-mode-based X-ray crystallographic refinement*. Proc Natl Acad Sci U S A, 2010. **107**(25): p. 11352-7 DOI: 10.1073/pnas.1000142107.
- [36] Cohen-Kutner, M., et al., *Calcineurin Controls Voltage-Dependent-Inactivation (VDI) of the Normal and Timothy Cardiac Channels*. Sci Rep, 2012. **2**: p. 366 DOI: 10.1038/srep00366.
- [37] Colovos, C. and T.O. Yeates, *Verification of Protein Structures - Patterns of Nonbonded Atomic Interactions*. Protein Science, 1993. **2**(9): p. 1511-1519 DOI: DOI 10.1002/pro.5560020916.
- [38] Dahl, G.P., et al., *High affinity complexes of pannexin channels and L-type calcium channel splice-variants in human lung: Possible role in clevidipine-induced dyspnea relief in acute heart failure*. EBioMedicine, 2016. **10**: p. 291-7 DOI: 10.1016/j.ebiom.2016.06.027.
- [39] DeWitt, C.R. and J.C. Waksman, *Pharmacology, pathophysiology and management of calcium channel blocker and beta-blocker toxicity*. Toxicol Rev, 2004. **23**(4): p. 223-38.
- [40] Doerner, J.F., M. Delling, and D.E. Clapham, *Ion channels and calcium signaling in motile cilia*. Elife, 2015. **4** DOI: 10.7554/eLife.11066.
- [41] Domes, K., et al., *Truncation of murine CaV1.2 at Asp-1904 results in heart failure after birth*. J Biol Chem, 2011. **286**(39): p. 33863-71 DOI: 10.1074/jbc.M111.252312.
- [42] Eisenberg, D., R. Luthy, and J.U. Bowie, *VERIFY3D: assessment of protein models with three-dimensional profiles*. Methods Enzymol, 1997. **277**: p. 396-404.
- [43] Elinder, F., J. Nilsson, and P. Arhem, *On the opening of voltage-gated ion channels*. Physiol Behav, 2007. **92**(1-2): p. 1-7 DOI: 10.1016/j.physbeh.2007.05.058.
- [44] Enes, J., et al., *Electrical activity suppresses axon growth through Ca(v)1.2 channels in adult primary sensory neurons*. Curr Biol, 2010. **20**(13): p. 1154-64 DOI: 10.1016/j.cub.2010.05.055.
- [45] Faggioni, M. and B.C. Knollmann, *Arrhythmia Protection in Hypokalemia: A Novel Role of Ca²⁺-Activated K⁺ Currents in the Ventricle*. Circulation, 2015. **132**(15): p. 1371-3 DOI: 10.1161/CIRCULATIONAHA.115.018874.
- [46] Feldkamp, M.D., L. Yu, and M.A. Shea, *Structural and energetic determinants of apo calmodulin binding to the IQ motif of the Na(V)1.2 voltage-dependent sodium channel*. Structure, 2011. **19**(5): p. 733-47 DOI: 10.1016/j.str.2011.02.009.
- [47] Felix, R., *Molecular regulation of voltage-gated Ca²⁺ channels*. J Recept Signal Transduct Res, 2005. **25**(2): p. 57-71 DOI: 10.1081/RRS-200068102.
- [48] Feng, T., S. Kalyaanamoorthy, and K. Barakat, *L-Type Calcium Channels: Structure and Functions*, in *Ion Channels in Health and Sickness*. 2018 DOI: 10.5772/intechopen.77305.
- [49] Feng, T., et al., *Atomistic modeling and molecular dynamics analysis of human CaV1.2 channel using external electric field and ion pulling simulations*. Biochim Biophys Acta Gen Subj, 2019. **1863**(6): p. 1116-1126 DOI: 10.1016/j.bbagen.2019.04.006.
- [50] Fernandez-Tenorio, M., et al., *Short communication: genetic ablation of L-type Ca²⁺ channels abolishes depolarization-induced Ca²⁺ release in arterial smooth muscle*. Circ Res, 2010. **106**(7): p. 1285-9 DOI: 10.1161/CIRCRESAHA.109.213967.

- [51] Fernandez-Tenorio, M., et al., *Metabotropic regulation of RhoA/Rho-associated kinase by L-type Ca²⁺ channels: new mechanism for depolarization-evoked mammalian arterial contraction*. Circ Res, 2011. **108**(11): p. 1348-57 DOI: 10.1161/CIRCRESAHA.111.240127.
- [52] Fleckenstein, A., *History of calcium antagonists*. Circ Res, 1983. **52**(2 Pt 2): p. I3-16.
- [53] Fleishman, S.J., V.M. Unger, and N. Ben-Tal, *Transmembrane protein structures without X-rays*. Trends Biochem Sci, 2006. **31**(2): p. 106-13 DOI: 10.1016/j.tibs.2005.12.005.
- [54] Fowler, P.W. and M.S.P. Sansom, *The pore of voltage-gated potassium ion channels is strained when closed*. Nature Communications, 2013. **4** DOI: ARTN 1872
10.1038/ncomms2858.
- [55] Fox, A.P., *Voltage-dependent inactivation of a calcium channel*. Proc Natl Acad Sci U S A, 1981. **78**(2): p. 953-6.
- [56] Frost, A., V.M. Unger, and P. De Camilli, *The BAR domain superfamily: membrane-molding macromolecules*. Cell, 2009. **137**(2): p. 191-6 DOI: 10.1016/j.cell.2009.04.010.
- [57] Fu, Y., et al., *Deletion of the distal C terminus of CaV1.2 channels leads to loss of beta-adrenergic regulation and heart failure in vivo*. J Biol Chem, 2011. **286**(14): p. 12617-26 DOI: 10.1074/jbc.M110.175307.
- [58] Fukuyama, M., et al., *L-Type Calcium Channel Mutations in Japanese Patients With Inherited Arrhythmias*. Circulation Journal, 2013. **77**(7): p. 1799-1806 DOI: 10.1253/circj.CJ-12-1457.
- [59] Fuller, M.D., et al., *Molecular mechanism of calcium channel regulation in the fight-or-flight response*. Sci Signal, 2010. **3**(141): p. ra70 DOI: 10.1126/scisignal.2001152.
- [60] Genheden, S. and U. Ryde, *The MM/PBSA and MM/GBSA methods to estimate ligand-binding affinities*. Expert Opin Drug Discov, 2015. **10**(5): p. 449-61 DOI: 10.1517/17460441.2015.1032936.
- [61] Gifford, J.L., M.P. Walsh, and H.J. Vogel, *Structures and metal-ion-binding properties of the Ca²⁺-binding helix-loop-helix EF-hand motifs*. Biochem J, 2007. **405**(2): p. 199-221 DOI: 10.1042/BJ20070255.
- [62] Giudicessi, J.R. and M.J. Ackerman, *Calcium Revisited: New Insights Into the Molecular Basis of Long-QT Syndrome*. Circ Arrhythm Electrophysiol, 2016. **9**(7) DOI: 10.1161/CIRCEP.116.002480.
- [63] Goebel, A., *Autoantibody pain*. Autoimmun Rev, 2016. **15**(6): p. 552-7 DOI: 10.1016/j.autrev.2016.02.011.
- [64] Gomes, B., et al., *Lymphocyte calcium signaling involves dihydropyridine-sensitive L-type calcium channels: facts and controversies*. Crit Rev Immunol, 2004. **24**(6): p. 425-47.
- [65] Goonasekera, S.A., et al., *Decreased cardiac L-type Ca(2)(+) channel activity induces hypertrophy and heart failure in mice*. J Clin Invest, 2012. **122**(1): p. 280-90 DOI: 10.1172/JCI58227.
- [66] Grant, A.O., *Cardiac ion channels*. Circ Arrhythm Electrophysiol, 2009. **2**(2): p. 185-94 DOI: 10.1161/CIRCEP.108.789081.
- [67] Gregg, R.G., et al., *Absence of the beta subunit (cchb1) of the skeletal muscle dihydropyridine receptor alters expression of the alpha 1 subunit and eliminates excitation-contraction coupling*. Proc Natl Acad Sci U S A, 1996. **93**(24): p. 13961-6.
- [68] Gumbart, J., et al., *Molecular dynamics simulations of proteins in lipid bilayers*. Curr Opin Struct Biol, 2005. **15**(4): p. 423-31 DOI: 10.1016/j.sbi.2005.07.007.

- [69] Hamshere, M.L., et al., *Genome-wide significant associations in schizophrenia to ITIH3/4, CACNA1C and SDCCAG8, and extensive replication of associations reported by the Schizophrenia PGC*. Mol Psychiatry, 2013. **18**(6): p. 708-12 DOI: 10.1038/mp.2012.67.
- [70] Hansen, P.B., *Functional importance of T-type voltage-gated calcium channels in the cardiovascular and renal system: news from the world of knockout mice*. Am J Physiol Regul Integr Comp Physiol, 2015. **308**(4): p. R227-37 DOI: 10.1152/ajpregu.00276.2014.
- [71] Hasani, H.J., M. Ahmed, and K. Barakat, *A comprehensive structural model for the human KCNQ1/KCNE1 ion channel*. Journal of Molecular Graphics & Modelling, 2017. **78**: p. 26-47 DOI: 10.1016/j.jmkgm.2017.09.019.
- [72] Hess, P., J.B. Lansman, and R.W. Tsien, *Different modes of Ca channel gating behaviour favoured by dihydropyridine Ca agonists and antagonists*. Nature, 1984. **311**(5986): p. 538-44.
- [73] Hill-Eubanks, D.C., et al., *Calcium signaling in smooth muscle*. Cold Spring Harb Perspect Biol, 2011. **3**(9): p. a004549 DOI: 10.1101/cshperspect.a004549.
- [74] Hofmann, F., et al., *L-type CaV1.2 calcium channels: from in vitro findings to in vivo function*. Physiol Rev, 2014. **94**(1): p. 303-26 DOI: 10.1152/physrev.00016.2013.
- [75] Huang, J. and A.D. MacKerell, Jr., *CHARMM36 all-atom additive protein force field: validation based on comparison to NMR data*. J Comput Chem, 2013. **34**(25): p. 2135-45 DOI: 10.1002/jcc.23354.
- [76] Hughes, M.A., M.J. Shipston, and A.F. Murray, *Towards a 'siliconeural computer': technological successes and challenges*. Philos Trans A Math Phys Eng Sci, 2015. **373**(2046) DOI: 10.1098/rsta.2014.0217.
- [77] Huster, M., et al., *A complex of Ca(V)1.2/PKC is involved in muscarinic signaling in smooth muscle*. FASEB J, 2010. **24**(8): p. 2651-9 DOI: 10.1096/fj.09-149856.
- [78] Iossifov, I., et al., *De novo gene disruptions in children on the autistic spectrum*. Neuron, 2012. **74**(2): p. 285-99 DOI: 10.1016/j.neuron.2012.04.009.
- [79] Isralewitz, B., M. Gao, and K. Schulten, *Steered molecular dynamics and mechanical functions of proteins*. Current Opinion in Structural Biology, 2001. **11**(2): p. 224-230 DOI: Doi 10.1016/S0959-440x(00)00194-9.
- [80] Jaeger, D. and R. Jung, 2015 DOI: 10.1007/978-1-4614-6675-8.
- [81] Jalily Hasani, H., M. Ahmed, and K. Barakat, *A comprehensive structural model for the human KCNQ1/KCNE1 ion channel*. J Mol Graph Model, 2017. **78**: p. 26-47 DOI: 10.1016/j.jmkgm.2017.09.019.
- [82] Jeon, D., et al., *Observational fear learning involves affective pain system and Cav1.2 Ca²⁺ channels in ACC*. Nat Neurosci, 2010. **13**(4): p. 482-8 DOI: 10.1038/nn.2504.
- [83] Jorgensen, W.L., D.S. Maxwell, and J. TiradoRives, *Development and testing of the OPLS all-atom force field on conformational energetics and properties of organic liquids*. Journal of the American Chemical Society, 1996. **118**(45): p. 11225-11236 DOI: DOI 10.1021/ja9621760.
- [84] Kahm, M. and M. Kschischo, *Mathematical Modelling of Cation Transport and Regulation in Yeast*. Adv Exp Med Biol, 2016. **892**: p. 291-305 DOI: 10.1007/978-3-319-25304-6_12.
- [85] Kale, L., et al., *NAMD2: Greater scalability for parallel molecular dynamics*. Journal of Computational Physics, 1999. **151**(1): p. 283-312 DOI: DOI 10.1006/jcph.1999.6201.
- [86] Kalia, J., et al., *From foe to friend: using animal toxins to investigate ion channel function*. J Mol Biol, 2015. **427**(1): p. 158-75 DOI: 10.1016/j.jmb.2014.07.027.

- [87] Kang, S., et al., *CaV1.3-selective L-type calcium channel antagonists as potential new therapeutics for Parkinson's disease*. Nat Commun, 2012. **3**: p. 1146 DOI: 10.1038/ncomms2149.
- [88] Kaur, G., et al., *A Polybasic Plasma Membrane Binding Motif in the I-II Linker Stabilizes Voltage-gated CaV1.2 Calcium Channel Function*. J Biol Chem, 2015. **290**(34): p. 21086-100 DOI: 10.1074/jbc.M115.645671.
- [89] Kobayashi, T., et al., *Regulation of CaV1.2 Current: Interaction With Intracellular Molecules*. Journal of Pharmacological Sciences, 2007. **103**(4): p. 347-353 DOI: 10.1254/jphs.CR0070012.
- [90] Koval, O.M., et al., *CaV1.2 beta-subunit coordinates CaMKII-triggered cardiomyocyte death and afterdepolarizations*. Proc Natl Acad Sci U S A, 2010. **107**(11): p. 4996-5000 DOI: 10.1073/pnas.0913760107.
- [91] Kutzner, C., et al., *Computational electrophysiology: the molecular dynamics of ion channel permeation and selectivity in atomistic detail*. Biophys J, 2011. **101**(4): p. 809-17 DOI: 10.1016/j.bpj.2011.06.010.
- [92] Laasch, N., et al., *Small molecule ligand docking to genotype specific bundle structures of hepatitis C virus (HCV) p7 protein*. Comput Biol Chem, 2016. **64**: p. 56-63 DOI: 10.1016/j.compbiolchem.2016.04.010.
- [93] Laskowski, R.A., et al., *Procheck - a Program to Check the Stereochemical Quality of Protein Structures*. Journal of Applied Crystallography, 1993. **26**: p. 283-291 DOI: Doi 10.1107/S0021889892009944.
- [94] Lee, A.S., et al., *Forebrain elimination of cacna1c mediates anxiety-like behavior in mice*. Mol Psychiatry, 2012. **17**(11): p. 1054-5 DOI: 10.1038/mp.2012.71.
- [95] Lemmon, G. and J. Meiler, *Rosetta Ligand docking with flexible XML protocols*. Methods Mol Biol, 2012. **819**: p. 143-55 DOI: 10.1007/978-1-61779-465-0_10.
- [96] Leo, M.D. and J.H. Jaggar, *Ion Channel Trafficking and Control of Arterial Contractility*. 2016: p. 153-168 DOI: 10.1007/978-3-319-29635-7_7.
- [97] Li, L., et al., *Up-regulation of Cavbeta3 subunit in primary sensory neurons increases voltage-activated Ca²⁺ channel activity and nociceptive input in neuropathic pain*. J Biol Chem, 2012. **287**(8): p. 6002-13 DOI: 10.1074/jbc.M111.310110.
- [98] Li, Q., et al., *Structural mechanism of voltage-dependent gating in an isolated voltage-sensing domain*. Nat Struct Mol Biol, 2014. **21**(3): p. 244-52 DOI: 10.1038/nsmb.2768.
- [99] Li, Z., et al., *A single amino acid change in Ca(v)1.2 channels eliminates the permeation and gating differences between Ca(2+) and Ba(2+)*. J Membr Biol, 2010. **233**(1-3): p. 23-33 DOI: 10.1007/s00232-009-9221-1.
- [100] Lindahl, E. and M.S. Sansom, *Membrane proteins: molecular dynamics simulations*. Curr Opin Struct Biol, 2008. **18**(4): p. 425-31 DOI: 10.1016/j.sbi.2008.02.003.
- [101] Long, S.B., et al., *Atomic structure of a voltage-dependent K⁺ channel in a lipid membrane-like environment*. Nature, 2007. **450**(7168): p. 376-82 DOI: 10.1038/nature06265.
- [102] Louch, W.E., S. Land, and S.A. Niederer, *Strange bedfellows: biologists and mathematical modelers tie the knot on cardiomyocyte calcium homeostasis*. Drug Discovery Today: Disease Models, 2014. **14**: p. 11-16 DOI: 10.1016/j.ddmod.2014.05.001.
- [103] Lupala, C.S., et al., *Using molecular dynamics for the refinement of atomistic models of GPCRs by homology modeling*. Journal of Biomolecular Structure & Dynamics, 2018. **36**(9): p. 2436-2448 DOI: 10.1080/07391102.2017.1357503.

- [104] Luzhkov, V.B., et al., *Computational modelling of the open-state Kv1.5 ion channel block by bupivacaine*. Biochimica et Biophysica Acta (BBA) - Proteins and Proteomics, 2003. **1652**(1): p. 35-51 DOI: 10.1016/j.bbapap.2003.08.006.
- [105] Ma, H., et al., *Excitation-transcription coupling in sympathetic neurons and the molecular mechanism of its initiation*. Neurosci Res, 2011. **70**(1): p. 2-8 DOI: 10.1016/j.neures.2011.02.004.
- [106] Ma, Z., et al., *Calcium homeostasis modulator (CALHM) ion channels*. Pflugers Arch, 2016. **468**(3): p. 395-403 DOI: 10.1007/s00424-015-1757-6.
- [107] Mahapatra, S., et al., *Equal sensitivity of Cav1.2 and Cav1.3 channels to the opposing modulations of PKA and PKG in mouse chromaffin cells*. J Physiol, 2012. **590**(20): p. 5053-73 DOI: 10.1113/jphysiol.2012.236729.
- [108] Marshall, M.R., et al., *Functional roles of a C-terminal signaling complex of CaV1 channels and A-kinase anchoring protein 15 in brain neurons*. J Biol Chem, 2011. **286**(14): p. 12627-39 DOI: 10.1074/jbc.M110.175257.
- [109] Martinez-Ortiz, W. and T.J. Cardozo, *An Improved Method for Modeling Voltage-Gated Ion Channels at Atomic Accuracy Applied to Human Cav Channels*. Cell Rep, 2018. **23**(5): p. 1399-1408 DOI: 10.1016/j.celrep.2018.04.024.
- [110] Matthews, E.A., et al., *The Cav2.3 calcium channel antagonist SNX-482 reduces dorsal horn neuronal responses in a rat model of chronic neuropathic pain*. Eur J Neurosci, 2007. **25**(12): p. 3561-9 DOI: 10.1111/j.1460-9568.2007.05605.x.
- [111] Meissner, M., et al., *Moderate calcium channel dysfunction in adult mice with inducible cardiomyocyte-specific excision of the cacnb2 gene*. J Biol Chem, 2011. **286**(18): p. 15875-82 DOI: 10.1074/jbc.M111.227819.
- [112] Mim, C., et al., *Structural basis of membrane bending by the N-BAR protein endophilin*. Cell, 2012. **149**(1): p. 137-45 DOI: 10.1016/j.cell.2012.01.048.
- [113] Mim, C. and V.M. Unger, *Membrane curvature and its generation by BAR proteins*. Trends Biochem Sci, 2012. **37**(12): p. 526-33 DOI: 10.1016/j.tibs.2012.09.001.
- [114] Minor, D.L., Jr. and F. Findeisen, *Progress in the structural understanding of voltage-gated calcium channel (CaV) function and modulation*. Channels (Austin), 2010. **4**(6): p. 459-74 DOI: 10.4161/chan.4.6.12867.
- [115] Mirams, G.R., et al., *Prediction of Thorough QT study results using action potential simulations based on ion channel screens*. J Pharmacol Toxicol Methods, 2014. **70**(3): p. 246-54 DOI: 10.1016/j.vascn.2014.07.002.
- [116] Moczydlowski, E.G., *On the Natural and Unnatural History of the Voltage-Gated Na(+)-Channel*. Curr Top Membr, 2016. **78**: p. 3-36 DOI: 10.1016/bs.ctm.2016.06.002.
- [117] Morton, R.A. and C.F. Valenzuela, *Further characterization of the effect of ethanol on voltage-gated Ca(2+) channel function in developing CA3 hippocampal pyramidal neurons*. Brain Res, 2016. **1633**: p. 19-26 DOI: 10.1016/j.brainres.2015.12.023.
- [118] Murakami, M., et al., *Conserved smooth muscle contractility and blood pressure increase in response to high-salt diet in mice lacking the beta3 subunit of the voltage-dependent calcium channel*. J Cardiovasc Pharmacol, 2000. **36 Suppl 2**: p. S69-73.
- [119] Murphy, T.H., P.F. Worley, and J.M. Baraban, *L-type voltage-sensitive calcium channels mediate synaptic activation of immediate early genes*. Neuron, 1991. **7**(4): p. 625-35.
- [120] Namkung, Y., et al., *Targeted disruption of the Ca2+ channel beta3 subunit reduces N- and L-type Ca2+ channel activity and alters the voltage-dependent activation of P/Q-type Ca2+ channels in neurons*. Proc Natl Acad Sci U S A, 1998. **95**(20): p. 12010-5.

- [121] Napolitano, C. and C. Antzelevitch, *Phenotypical manifestations of mutations in the genes encoding subunits of the cardiac voltage-dependent L-type calcium channel*. *Circ Res*, 2011. **108**(5): p. 607-18 DOI: 10.1161/CIRCRESAHA.110.224279.
- [122] Narayanan, A. and M.P. Jacobson, *Computational studies of protein regulation by post-translational phosphorylation*. *Curr Opin Struct Biol*, 2009. **19**(2): p. 156-63 DOI: 10.1016/j.sbi.2009.02.007.
- [123] Natchimuthu, V., et al., *Design, synthesis and computational evaluation of a novel intermediate salt of N-cyclohexyl-N-(cyclohexylcarbamoyl)-4-(trifluoromethyl) benzamide as potential potassium channel blocker in epileptic paroxysmal seizures*. *Comput Biol Chem*, 2016. **64**: p. 64-73 DOI: 10.1016/j.compbiolchem.2016.05.003.
- [124] Nguyen, P.T., et al., *Structural basis for antiarrhythmic drug interactions with the human cardiac sodium channel*. *Proc Natl Acad Sci U S A*, 2019. **116**(8): p. 2945-2954 DOI: 10.1073/pnas.1817446116.
- [125] Nichols, C.B., et al., *Sympathetic stimulation of adult cardiomyocytes requires association of AKAP5 with a subpopulation of L-type calcium channels*. *Circ Res*, 2010. **107**(6): p. 747-56 DOI: 10.1161/CIRCRESAHA.109.216127.
- [126] Oliveria, S.F., et al., *Localized calcineurin confers Ca²⁺-dependent inactivation on neuronal L-type Ca²⁺ channels*. *J Neurosci*, 2012. **32**(44): p. 15328-37 DOI: 10.1523/JNEUROSCI.2302-12.2012.
- [127] Ortner, N.J. and J. Striessnig, *L-type calcium channels as drug targets in CNS disorders*. *Channels (Austin)*, 2016. **10**(1): p. 7-13 DOI: 10.1080/19336950.2015.1048936.
- [128] Osterberg, F. and J. Aqvist, *Exploring blocker binding to a homology model of the open hERG K⁺ channel using docking and molecular dynamics methods*. *FEBS Lett*, 2005. **579**(13): p. 2939-44 DOI: 10.1016/j.febslet.2005.04.039.
- [129] Pantazis, A., et al., *Functional heterogeneity of the four voltage sensors of a human L-type calcium channel*. *Proc Natl Acad Sci U S A*, 2014. **111**(51): p. 18381-6 DOI: 10.1073/pnas.1411127112.
- [130] Paulsen, C.E., et al., *Structure of the TRPA1 ion channel suggests regulatory mechanisms*. *Nature*, 2015. **520**(7548): p. 511-7 DOI: 10.1038/nature14367.
- [131] Payandeh, J. and D.L. Minor, Jr., *Bacterial voltage-gated sodium channels (BacNa(V)s) from the soil, sea, and salt lakes enlighten molecular mechanisms of electrical signaling and pharmacology in the brain and heart*. *J Mol Biol*, 2015. **427**(1): p. 3-30 DOI: 10.1016/j.jmb.2014.08.010.
- [132] Plank, G., et al., *From mitochondrial ion channels to arrhythmias in the heart: computational techniques to bridge the spatio-temporal scales*. *Philos Trans A Math Phys Eng Sci*, 2008. **366**(1879): p. 3381-409 DOI: 10.1098/rsta.2008.0112.
- [133] Pontius, J., J. Richelle, and S.J. Wodak, *Deviations from standard atomic volumes as a quality measure for protein crystal structures*. *Journal of Molecular Biology*, 1996. **264**(1): p. 121-136 DOI: DOI 10.1006/jmbi.1996.0628.
- [134] Poomvanicha, M., et al., *Facilitation and Ca²⁺-dependent inactivation are modified by mutation of the Ca(v)1.2 channel IQ motif*. *J Biol Chem*, 2011. **286**(30): p. 26702-7 DOI: 10.1074/jbc.M111.247841.
- [135] Poulsen, M.H., et al., *Binding of ArgTX-636 in the NMDA receptor ion channel*. *J Mol Biol*, 2015. **427**(1): p. 176-89 DOI: 10.1016/j.jmb.2014.05.017.

- [136] Prakash, S., et al., *Electrokinetic transport of monovalent and divalent cations in silica nanochannels*. *Microfluidics and Nanofluidics*, 2016. **20**(1) DOI: 10.1007/s10404-015-1667-0.
- [137] Protti, D.A. and O.D. Uchitel, *Transmitter release and presynaptic Ca²⁺ currents blocked by the spider toxin omega-Aga-IVA*. *Neuroreport*, 1993. **5**(3): p. 333-6.
- [138] Qu, Y., et al., *Perinatal and postnatal expression of Cav1.3 alpha1D Ca(2)(+) channel in the rat heart*. *Pediatr Res*, 2011. **69**(6): p. 479-84 DOI: 10.1203/PDR.0b013e318217a0df.
- [139] RamaKrishnan, A.M. and K. Sankaranarayanan, *Understanding autoimmunity: The ion channel perspective*. *Autoimmun Rev*, 2016. **15**(7): p. 585-620 DOI: 10.1016/j.autrev.2016.02.004.
- [140] Ramsey, I.S., et al., *An aqueous H⁺ permeation pathway in the voltage-gated proton channel Hv1*. *Nat Struct Mol Biol*, 2010. **17**(7): p. 869-875 DOI: 10.1038/nsmb.1826.
- [141] Raval, A., et al., *Refinement of protein structure homology models via long, all-atom molecular dynamics simulations*. *Proteins*, 2012. **80**(8): p. 2071-9 DOI: 10.1002/prot.24098.
- [142] Romero, L., et al., *In silico screening of the impact of hERG channel kinetic abnormalities on channel block and susceptibility to acquired long QT syndrome*. *J Mol Cell Cardiol*, 2014. **72**: p. 126-37 DOI: 10.1016/j.yjmcc.2014.02.018.
- [143] Rosati, B., et al., *Robust L-type calcium current expression following heterozygous knockout of the Cav1.2 gene in adult mouse heart*. *J Physiol*, 2011. **589**(Pt 13): p. 3275-88 DOI: 10.1113/jphysiol.2011.210237.
- [144] Rougier, J.S. and H. Abriel, *Cardiac voltage-gated calcium channel macromolecular complexes*. *Biochim Biophys Acta*, 2016. **1863**(7 Pt B): p. 1806-12 DOI: 10.1016/j.bbamcr.2015.12.014.
- [145] Roux, B., et al., *Theoretical and computational models of biological ion channels*. *Quarterly Reviews of Biophysics*, 2004. **37**(1): p. 15-103 DOI: 10.1017/s0033583504003968.
- [146] Roux, B. and K. Schulten, *Computational studies of membrane channels*. *Structure*, 2004. **12**(8): p. 1343-51 DOI: 10.1016/j.str.2004.06.013.
- [147] Rudy, Y. and J.R. Silva, *Computational biology in the study of cardiac ion channels and cell electrophysiology*. *Q Rev Biophys*, 2006. **39**(1): p. 57-116 DOI: 10.1017/S0033583506004227.
- [148] Saad, M., et al., *Ranolazine in Cardiac Arrhythmia*. *Clin Cardiol*, 2016. **39**(3): p. 170-8 DOI: 10.1002/clc.22476.
- [149] Sanguinetti, M.C. and M. Tristani-Firouzi, *hERG potassium channels and cardiac arrhythmia*. *Nature*, 2006. **440**(7083): p. 463-9 DOI: 10.1038/nature04710.
- [150] Satake, A., G. Sakurai, and T. Kinoshita, *Modeling strategies for plant survival, growth and reproduction*. *Plant Cell Physiol*, 2015. **56**(4): p. 583-5 DOI: 10.1093/pcp/pcv041.
- [151] Schierberl, K., et al., *Cav1.2 L-type Ca(2)(+) channels mediate cocaine-induced GluA1 trafficking in the nucleus accumbens, a long-term adaptation dependent on ventral tegmental area Ca(v)1.3 channels*. *J Neurosci*, 2011. **31**(38): p. 13562-75 DOI: 10.1523/JNEUROSCI.2315-11.2011.
- [152] Schlick, B., B.E. Flucher, and G.J. Obermair, *Voltage-activated calcium channel expression profiles in mouse brain and cultured hippocampal neurons*. *Neuroscience*, 2010. **167**(3): p. 786-98 DOI: 10.1016/j.neuroscience.2010.02.037.

- [153] Schramm, C.A., et al., *Knowledge-based potential for positioning membrane-associated structures and assessing residue-specific energetic contributions*. Structure, 2012. **20**(5): p. 924-35 DOI: 10.1016/j.str.2012.03.016.
- [154] Senatore, A., et al., *Mapping of dihydropyridine binding residues in a less sensitive invertebrate L-type calcium channel (LCa v 1)*. Channels (Austin), 2011. **5**(2): p. 173-87 DOI: 10.4161/chan.5.2.15141.
- [155] Shaldam, M.A., et al., *1,4-Dihydropyridine Calcium Channel Blockers: Homology Modeling of the Receptor and Assessment of Structure Activity Relationship*. ISRN Medicinal Chemistry, 2014. **2014**: p. 1-14 DOI: 10.1155/2014/203518.
- [156] Singh, A., et al., *Modulation of voltage- and Ca²⁺-dependent gating of CaV1.3 L-type calcium channels by alternative splicing of a C-terminal regulatory domain*. J Biol Chem, 2008. **283**(30): p. 20733-44 DOI: 10.1074/jbc.M802254200.
- [157] Soong, T.W. and M.X. Mori, *Post-transcriptional modifications and "Calmodulation" of voltage-gated calcium channel function: Reflections by two collaborators of David T Yue*. Channels (Austin), 2016. **10**(1): p. 14-9 DOI: 10.1080/19336950.2015.1051271.
- [158] Southern, J., et al., *Multi-scale computational modelling in biology and physiology*. Prog Biophys Mol Biol, 2008. **96**(1-3): p. 60-89 DOI: 10.1016/j.pbiomolbio.2007.07.019.
- [159] Stary, A., et al., *Molecular Dynamics and Mutational Analysis of a Channelopathy mutation in the IIS6 Helix of CaV1.2*. Channels, 2014. **2**(3): p. 216-223 DOI: 10.4161/chan.2.3.6160.
- [160] Stary, A., et al., *Structural Model of the CaV1.2 Pore*. Channels, 2008. **2**(3): p. 210-215 DOI: 10.4161/chan.2.3.6158.
- [161] Straub, C. and S. Tomita, *The regulation of glutamate receptor trafficking and function by TARPs and other transmembrane auxiliary subunits*. Curr Opin Neurobiol, 2012. **22**(3): p. 488-95 DOI: 10.1016/j.conb.2011.09.005.
- [162] Striessnig, J., H.J. Bolz, and A. Koschak, *Channelopathies in Cav1.1, Cav1.3, and Cav1.4 voltage-gated L-type Ca²⁺ channels*. Pflugers Arch, 2010. **460**(2): p. 361-74 DOI: 10.1007/s00424-010-0800-x.
- [163] Striessnig, J., et al., *L-type Ca²⁺ channels in heart and brain*. Wiley Interdiscip Rev Membr Transp Signal, 2014. **3**(2): p. 15-38 DOI: 10.1002/wmts.102.
- [164] Subramanyam, P. and H.M. Colecraft, *Ion channel engineering: perspectives and strategies*. J Mol Biol, 2015. **427**(1): p. 190-204 DOI: 10.1016/j.jmb.2014.09.001.
- [165] Suetsugu, S., K. Toyooka, and Y. Senju, *Subcellular membrane curvature mediated by the BAR domain superfamily proteins*. Semin Cell Dev Biol, 2010. **21**(4): p. 340-9 DOI: 10.1016/j.semcdb.2009.12.002.
- [166] Sun, J., et al., *Cellular Architecture Regulates Collective Calcium Signaling and Cell Contractility*. PLoS Comput Biol, 2016. **12**(5): p. e1004955 DOI: 10.1371/journal.pcbi.1004955.
- [167] Tadmouri, A., et al., *Cacnb4 directly couples electrical activity to gene expression, a process defective in juvenile epilepsy*. EMBO J, 2012. **31**(18): p. 3730-44 DOI: 10.1038/emboj.2012.226.
- [168] Tang, L., et al., *Structural basis for Ca²⁺ selectivity of a voltage-gated calcium channel*. Nature, 2014. **505**(7481): p. 56-61 DOI: 10.1038/nature12775.
- [169] Tang, L., et al., *Structural basis for inhibition of a voltage-gated Ca²⁺ channel by Ca²⁺ antagonist drugs*. Nature, 2016. **537**(7618): p. 117-121 DOI: 10.1038/nature19102.

- [170] Tikhonov, D.B. and B.S. Zhorov, *Modeling P-loops domain of sodium channel: homology with potassium channels and interaction with ligands*. Biophys J, 2005. **88**(1): p. 184-97 DOI: 10.1529/biophysj.104.048173.
- [171] Tikhonov, D.B. and B.S. Zhorov, *Molecular modeling of benzothiazepine binding in the L-type calcium channel*. J Biol Chem, 2008. **283**(25): p. 17594-604 DOI: 10.1074/jbc.M800141200.
- [172] Tramontano, A., *Homology modeling with low sequence identity*. Methods, 1998. **14**(3): p. 293-300 DOI: 10.1006/meth.1998.0585.
- [173] Treptow, W. and M. Tarek, *K⁺ conduction in the selectivity filter of potassium channels is monitored by the charge distribution along their sequence*. Biophys J, 2006. **91**(10): p. L81-3 DOI: 10.1529/biophysj.106.095992.
- [174] Trick, J.L., et al., *Voltage Gating of a Biomimetic Nanopore: Electrowetting of a Hydrophobic Barrier*. ACS Nano, 2017. **11**(2): p. 1840-1847 DOI: 10.1021/acsnano.6b07865.
- [175] Tuluc, P., et al., *A CaV1.1 Ca²⁺ channel splice variant with high conductance and voltage-sensitivity alters EC coupling in developing skeletal muscle*. Biophys J, 2009. **96**(1): p. 35-44 DOI: 10.1016/j.bpj.2008.09.027.
- [176] Tuluc, P., et al., *Molecular Interactions in the Voltage Sensor Controlling Gating Properties of CaV Calcium Channels*. Structure, 2016. **24**(2): p. 261-71 DOI: 10.1016/j.str.2015.11.011.
- [177] Tveito, A., et al., *Computing rates of Markov models of voltage-gated ion channels by inverting partial differential equations governing the probability density functions of the conducting and non-conducting states*. Math Biosci, 2016. **277**: p. 126-35 DOI: 10.1016/j.mbs.2016.04.011.
- [178] UniProt, C., *UniProt: a hub for protein information*. Nucleic Acids Res, 2015. **43**(Database issue): p. D204-12 DOI: 10.1093/nar/gku989.
- [179] Wallner, B. and A. Elofsson, *Can correct protein models be identified?* Protein Science, 2003. **12**(5): p. 1073-1086 DOI: 10.1110/ps.0236803.
- [180] Waxman, S.G. and G.W. Zamponi, *Regulating excitability of peripheral afferents: emerging ion channel targets*. Nat Neurosci, 2014. **17**(2): p. 153-63 DOI: 10.1038/nn.3602.
- [181] Weiss, S., et al., *Regulation of cardiac L-type Ca²⁺(+) channel CaV1.2 via the beta-adrenergic-cAMP-protein kinase A pathway: old dogmas, advances, and new uncertainties*. Circ Res, 2013. **113**(5): p. 617-31 DOI: 10.1161/CIRCRESAHA.113.301781.
- [182] Weissgerber, P., et al., *Reduced cardiac L-type Ca²⁺ current in Ca(V)beta2^{-/-} embryos impairs cardiac development and contraction with secondary defects in vascular maturation*. Circ Res, 2006. **99**(7): p. 749-57 DOI: 10.1161/01.RES.0000243978.15182.c1.
- [183] Welling, A., et al., *Alternatively spliced IS6 segments of the alpha 1C gene determine the tissue-specific dihydropyridine sensitivity of cardiac and vascular smooth muscle L-type Ca²⁺ channels*. Circ Res, 1997. **81**(4): p. 526-32.
- [184] Wheeler, D.G., et al., *Ca(V)1 and Ca(V)2 channels engage distinct modes of Ca²⁺ signaling to control CREB-dependent gene expression*. Cell, 2012. **149**(5): p. 1112-24 DOI: 10.1016/j.cell.2012.03.041.
- [185] Wu, J., et al., *Structure of the voltage-gated calcium channel Ca(v)1.1 at 3.6 Å resolution*. Nature, 2016. **537**(7619): p. 191-196 DOI: 10.1038/nature19321.

- [186] Xu, L., et al., *Alterations of L-type calcium current and cardiac function in CaMKII δ knockout mice*. *Circ Res*, 2010. **107**(3): p. 398-407 DOI: 10.1161/CIRCRESAHA.110.222562.
- [187] Xu, M., et al., *Enhanced expression of L-type Cav1.3 calcium channels in murine embryonic hearts from Cav1.2-deficient mice*. *J Biol Chem*, 2003. **278**(42): p. 40837-41 DOI: 10.1074/jbc.M307598200.
- [188] Xu, W.F. and D. Lipscombe, *Neuronal Ca(v)1.3 alpha(1) L-type channels activate at relatively hyperpolarized membrane potentials and are incompletely inhibited by dihydropyridines*. *Journal of Neuroscience*, 2001. **21**(16): p. 5944-5951.
- [189] Yan, Z., et al., *Structure of the Nav1.4-beta1 Complex from Electric Eel*. *Cell*, 2017. **170**(3): p. 470-482 e11 DOI: 10.1016/j.cell.2017.06.039.
- [190] Yang, J., et al., *The I-TASSER Suite: protein structure and function prediction*. *Nat Methods*, 2015. **12**(1): p. 7-8 DOI: 10.1038/nmeth.3213.
- [191] Yarov-Yarovoy, V., T.W. Allen, and C.E. Clancy, *Computational Models for Predictive Cardiac Ion Channel Pharmacology*. *Drug Discov Today Dis Models*, 2014. **14**: p. 3-10 DOI: 10.1016/j.ddmod.2014.04.001.
- [192] Yarov-Yarovoy, V., D. Baker, and W.A. Catterall, *Voltage sensor conformations in the open and closed states in ROSETTA structural models of K(+) channels*. *Proc Natl Acad Sci U S A*, 2006. **103**(19): p. 7292-7 DOI: 10.1073/pnas.0602350103.
- [193] Yarov-Yarovoy, V., et al., *Structural basis for gating charge movement in the voltage sensor of a sodium channel*. *Proc Natl Acad Sci U S A*, 2012. **109**(2): p. E93-102 DOI: 10.1073/pnas.1118434109.
- [194] Yesylevskyy, S.O., et al., *Polarizable water model for the coarse-grained MARTINI force field*. *PLoS Comput Biol*, 2010. **6**(6): p. e1000810 DOI: 10.1371/journal.pcbi.1000810.
- [195] Zamponi, G.W., et al., *The Physiology, Pathology, and Pharmacology of Voltage-Gated Calcium Channels and Their Future Therapeutic Potential*. *Pharmacol Rev*, 2015. **67**(4): p. 821-70 DOI: 10.1124/pr.114.009654.
- [196] Zemzemi, N., et al., *Computational assessment of drug-induced effects on the electrocardiogram: from ion channel to body surface potentials*. *Br J Pharmacol*, 2013. **168**(3): p. 718-33 DOI: 10.1111/j.1476-5381.2012.02200.x.
- [197] Zhang, Q., et al., *The molecular mechanism of the effect of sulfur dioxide inhalation on the potassium and calcium ion channels in rat aortas*. *Hum Exp Toxicol*, 2016. **35**(4): p. 418-27 DOI: 10.1177/0960327115591375.
- [198] Zhang, Y., *Protein structure prediction: when is it useful?* *Curr Opin Struct Biol*, 2009. **19**(2): p. 145-55 DOI: 10.1016/j.sbi.2009.02.005.
- [199] Zhang, Y., et al., *The beta subunit of voltage-gated Ca²⁺ channels interacts with and regulates the activity of a novel isoform of Pax6*. *J Biol Chem*, 2010. **285**(4): p. 2527-36 DOI: 10.1074/jbc.M109.022236.
- [200] Zhu, W., Z. Varga, and J.R. Silva, *Molecular motions that shape the cardiac action potential: Insights from voltage clamp fluorometry*. *Prog Biophys Mol Biol*, 2016. **120**(1-3): p. 3-17 DOI: 10.1016/j.pbiomolbio.2015.12.003.
- [201] Ahern, C.A., et al., *Modulation of L-type Ca²⁺ current but not activation of Ca²⁺ release by the gamma1 subunit of the dihydropyridine receptor of skeletal muscle*. *BMC Physiol*, 2001. **1**: p. 8.

- [202] Ahmed, M., et al., *Modeling the human Nav1.5 sodium channel: structural and mechanistic insights of ion permeation and drug blockade*. Drug Des Devel Ther, 2017. **11**: p. 2301-2324 DOI: 10.2147/DDDT.S133944.
- [203] Almagor, L., et al., *The role of a voltage-dependent Ca²⁺ channel intracellular linker: a structure-function analysis*. J Neurosci, 2012. **32**(22): p. 7602-13 DOI: 10.1523/JNEUROSCI.5727-11.2012.
- [204] Anantharaman, V. and L. Aravind, *Cache - a signaling domain common to animal Ca²⁺ channel subunits and a class of prokaryotic chemotaxis receptors*. Trends in Biochemical Sciences, 2000. **25**(11): p. 535-537 DOI: Doi 10.1016/S0968-0004(00)01672-8.
- [205] Andranovits, S., et al., *Key role of segment IS4 in Cav1.2 inactivation: link between activation and inactivation*. Pflugers Arch, 2017 DOI: 10.1007/s00424-017-2038-3.
- [206] Arikath, J. and K.P. Campbell, *Auxiliary subunits: essential components of the voltage-gated calcium channel complex*. Current Opinion in Neurobiology, 2003. **13**(3): p. 298-307 DOI: 10.1016/s0959-4388(03)00066-7.
- [207] Bähring, R. and M. Covarrubias, *Mechanisms of closed-state inactivation in voltage-gated ion channels*. J Physiol, 2011. **589**(Pt 3): p. 461-79 DOI: 10.1113/jphysiol.2010.191965.
- [208] Bannister, J.P., et al., *Smooth muscle cell alpha2delta-1 subunits are essential for vasoregulation by CaV1.2 channels*. Circ Res, 2009. **105**(10): p. 948-55 DOI: 10.1161/CIRCRESAHA.109.203620.
- [209] Baumann, L., et al., *Functional characterization of the L-type Ca²⁺ channel Cav1.4alpha1 from mouse retina*. Invest Ophthalmol Vis Sci, 2004. **45**(2): p. 708-13.
- [210] Berrow, N.S., et al., *Antisense depletion of beta-subunits modulates the biophysical and pharmacological properties of neuronal calcium channels*. J Physiol, 1995. **482** (Pt 3): p. 481-91.
- [211] Bertet, C., L. Sulak, and T. Lecuit, *Myosin-dependent junction remodelling controls planar cell intercalation and axis elongation*. Nature, 2004. **429**(6992): p. 667-71 DOI: 10.1038/nature02590.
- [212] Bidaud, I., et al., *Voltage-gated calcium channels in genetic diseases*. Biochim Biophys Acta, 2006. **1763**(11): p. 1169-74 DOI: 10.1016/j.bbamcr.2006.08.049.
- [213] Black, J.L., et al., *The voltage-gated calcium channel gamma subunit family: Electrophysiology, association with AMPA receptors and association with memory function*. Biological Psychiatry, 2003. **53**(8): p. 148s-148s.
- [214] Bock, G., et al., *Functional properties of a newly identified C-terminal splice variant of Cav1.3 L-type Ca²⁺ channels*. J Biol Chem, 2011. **286**(49): p. 42736-48 DOI: 10.1074/jbc.M111.269951.
- [215] Bourdin, B., et al., *Molecular determinants of the CaVbeta-induced plasma membrane targeting of the CaV1.2 channel*. J Biol Chem, 2010. **285**(30): p. 22853-63 DOI: 10.1074/jbc.M110.111062.
- [216] Briot, J., et al., *Three-Dimensional Architecture of the L-Type Calcium Channel: Structural Insights into the CaValpha2delta1 Auxiliary Protein*. Biochemistry & Molecular Biology Journal, 2016. **02**(03) DOI: 10.21767/2471-8084.100025.
- [217] Bruhova, I. and B.S. Zhorov, *A homology model of the pore domain of a voltage-gated calcium channel is consistent with available SCAM data*. J Gen Physiol, 2010. **135**(3): p. 261-74 DOI: 10.1085/jgp.200910288.

- [218] Brunet, S., et al., *Phosphorylation sites in the Hook domain of CaVbeta subunits differentially modulate CaV1.2 channel function*. J Mol Cell Cardiol, 2015. **87**: p. 248-56 DOI: 10.1016/j.yjmcc.2015.08.006.
- [219] Buonarati, O.R., et al., *Proteolytic processing of the L-type Ca (2+) channel alpha 11.2 subunit in neurons*. F1000Res, 2017. **6**: p. 1166 DOI: 10.12688/f1000research.11808.1.
- [220] Buraei, Z. and J. Yang, *Structure and function of the beta subunit of voltage-gated Ca(2)(+) channels*. Biochim Biophys Acta, 2013. **1828**(7): p. 1530-40 DOI: 10.1016/j.bbamem.2012.08.028.
- [221] Butcher, A.J., et al., *The importance of occupancy rather than affinity of Ca(V)beta subunits for the calcium channel I-II linker in relation to calcium channel function*. Journal of Physiology-London, 2006. **574**(2): p. 387-398 DOI: 10.1113/jphysiol.2006.109744.
- [222] Canti, C., et al., *The metal-ion-dependent adhesion site in the Von Willebrand factor-A domain of alpha2delta subunits is key to trafficking voltage-gated Ca2+ channels*. Proc Natl Acad Sci U S A, 2005. **102**(32): p. 11230-5 DOI: 10.1073/pnas.0504183102.
- [223] Carbone, E. and H.D. Lux, *A low voltage-activated, fully inactivating Ca channel in vertebrate sensory neurones*. Nature, 1984. **310**(5977): p. 501-2.
- [224] Catterall, W.A., et al., *International Union of Pharmacology. XLVIII. Nomenclature and structure-function relationships of voltage-gated calcium channels*. Pharmacol Rev, 2005. **57**(4): p. 411-25 DOI: 10.1124/pr.57.4.5.
- [225] Chen, R.S., et al., *Calcium channel gamma subunits: a functionally diverse protein family*. Cell Biochemistry and Biophysics, 2007. **47**(2): p. 178-186 DOI: 10.1007/s12013-007-0002-0.
- [226] Chen, Y.H., et al., *Structural basis of the alpha1-beta subunit interaction of voltage-gated Ca2+ channels*. Nature, 2004. **429**(6992): p. 675-80 DOI: 10.1038/nature02641.
- [227] Cheng, R.C., D.B. Tikhonov, and B.S. Zhorov, *Structural model for phenylalkylamine binding to L-type calcium channels*. J Biol Chem, 2009. **284**(41): p. 28332-42 DOI: 10.1074/jbc.M109.027326.
- [228] Chu, P.J., H.M. Robertson, and P.M. Best, *Calcium channel gamma subunits provide insights into the evolution of this gene family*. Gene, 2001. **280**(1-2): p. 37-48 DOI: Doi 10.1016/S0378-1119(01)00738-7.
- [229] Davies, A., et al., *Functional biology of the alpha(2)delta subunits of voltage-gated calcium channels*. Trends Pharmacol Sci, 2007. **28**(5): p. 220-8 DOI: 10.1016/j.tips.2007.03.005.
- [230] De Waard, M., C.A. Gurnett, and K.P. Campbell, *Structural and functional diversity of voltage-activated calcium channels*. Ion Channels, 1996. **4**: p. 41-87.
- [231] De Waard, M., et al., *Identification of critical amino acids involved in alpha1-beta interaction in voltage-dependent Ca2+ channels*. FEBS Lett, 1996. **380**(3): p. 272-6.
- [232] Di Virgilio, F., et al., *Voltage-dependent activation and inactivation of calcium channels in PC12 cells. Correlation with neurotransmitter release*. J Biol Chem, 1987. **262**(19): p. 9189-95.
- [233] Dolphin, A.C., *Beta subunits of voltage-gated calcium channels*. J Bioenerg Biomembr, 2003. **35**(6): p. 599-620.
- [234] Dolphin, A.C., *beta subunits of voltage-gated calcium channels*. Journal of Bioenergetics and Biomembranes, 2003. **35**(6): p. 599-620 DOI: DOI 10.1023/B:JOB.0000008026.37790.5a.
- [235] Dolphin, A.C., *A short history of voltage-gated calcium channels*. Br J Pharmacol, 2006. **147 Suppl 1**: p. S56-62 DOI: 10.1038/sj.bjp.0706442.

- [236] Dolphin, A.C., *Calcium channel diversity: multiple roles of calcium channel subunits*. *Curr Opin Neurobiol*, 2009. **19**(3): p. 237-44 DOI: 10.1016/j.conb.2009.06.006.
- [237] Dolphin, A.C., *Calcium channel auxiliary alpha2delta and beta subunits: trafficking and one step beyond*. *Nat Rev Neurosci*, 2012. **13**(8): p. 542-55 DOI: 10.1038/nrn3311.
- [238] Dolphin, A.C., *The alpha(2)delta subunits of voltage-gated calcium channels*. *Biochimica Et Biophysica Acta-Biomembranes*, 2013. **1828**(7): p. 1541-1549 DOI: 10.1016/j.bbamem.2012.11.019.
- [239] Dolphin, A.C., *Voltage-gated calcium channels and their auxiliary subunits: physiology and pathophysiology and pharmacology*. *Journal of Physiology-London*, 2016. **594**(19): p. 5369-5390 DOI: 10.1113/Jp272262.
- [240] Elkayam, U., et al., *Calcium-Channel Blockers in Heart-Failure*. *Journal of the American College of Cardiology*, 1993. **22**(4): p. A139-A144 DOI: Doi 10.1016/0735-1097(93)90478-J.
- [241] Eroglu, C., et al., *Gabapentin receptor alpha2delta-1 is a neuronal thrombospondin receptor responsible for excitatory CNS synaptogenesis*. *Cell*, 2009. **139**(2): p. 380-92 DOI: 10.1016/j.cell.2009.09.025.
- [242] Etemad, S., et al., *Differential neuronal targeting of a new and two known calcium channel beta4 subunit splice variants correlates with their regulation of gene expression*. *J Neurosci*, 2014. **34**(4): p. 1446-61 DOI: 10.1523/JNEUROSCI.3935-13.2014.
- [243] Fallon, J.L., et al., *Crystal structure of dimeric cardiac L-type calcium channel regulatory domains bridged by Ca²⁺center dot calmodulins*. *Proceedings of the National Academy of Sciences of the United States of America*, 2009. **106**(13): p. 5135-5140 DOI: 10.1073/pnas.0807487106.
- [244] Fallon, J.L., et al., *Structure of calmodulin bound to the hydrophobic IQ domain of the cardiac Ca(v)1.2 calcium channel*. *Structure*, 2005. **13**(12): p. 1881-6 DOI: 10.1016/j.str.2005.09.021.
- [245] Fang, K. and H.M. Colecraft, *Mechanism of auxiliary beta-subunit-mediated membrane targeting of L-type (Ca(V)1.2) channels*. *J Physiol*, 2011. **589**(Pt 18): p. 4437-55 DOI: 10.1113/jphysiol.2011.214247.
- [246] Ferreira, G., et al., *Ion-dependent inactivation of barium current through L-type calcium channels*. *Journal of General Physiology*, 1997. **109**(4): p. 449-461 DOI: DOI 10.1085/jgp.109.4.449.
- [247] Findeisen, F., et al., *Stapled Voltage-Gated Calcium Channel (CaV) alpha-Interaction Domain (AID) Peptides Act As Selective Protein-Protein Interaction Inhibitors of CaV Function*. *ACS Chem Neurosci*, 2017. **8**(6): p. 1313-1326 DOI: 10.1021/acchemneuro.6b00454.
- [248] Flavell, S.W. and M.E. Greenberg, *Signaling mechanisms linking neuronal activity to gene expression and plasticity of the nervous system*. *Annu Rev Neurosci*, 2008. **31**: p. 563-90 DOI: 10.1146/annurev.neuro.31.060407.125631.
- [249] Gao, T., et al., *C-terminal fragments of the alpha 1C (CaV1.2) subunit associate with and regulate L-type calcium channels containing C-terminal-truncated alpha 1C subunits*. *J Biol Chem*, 2001. **276**(24): p. 21089-97 DOI: 10.1074/jbc.M008000200.
- [250] Godfraind, T., *Discovery and Development of Calcium Channel Blockers*. *Front Pharmacol*, 2017. **8**: p. 286 DOI: 10.3389/fphar.2017.00286.

- [251] Gomez-Ospina, N., et al., *The C terminus of the L-type voltage-gated calcium channel Ca(V)1.2 encodes a transcription factor*. Cell, 2006. **127**(3): p. 591-606 DOI: 10.1016/j.cell.2006.10.017.
- [252] Gong, H.C., et al., *Tissue-specific expression and gabapentin-binding properties of calcium channel alpha2delta subunit subtypes*. J Membr Biol, 2001. **184**(1): p. 35-43.
- [253] Gutman, G.A., et al., *International Union of Pharmacology. LIII. Nomenclature and molecular relationships of voltage-gated potassium channels*. Pharmacol Rev, 2005. **57**(4): p. 473-508 DOI: 10.1124/pr.57.4.10.
- [254] Haase, H., et al., *Expression of Ca(2+) channel subunits during cardiac ontogeny in mice and rats: identification of fetal alpha(1C) and beta subunit isoforms*. J Cell Biochem, 2000. **76**(4): p. 695-703.
- [255] Halling, D.B., et al., *Determinants in CaV1 channels that regulate the Ca2+ sensitivity of bound calmodulin*. J Biol Chem, 2009. **284**(30): p. 20041-51 DOI: 10.1074/jbc.M109.013326.
- [256] Hansen, J.P., et al., *Calcium channel gamma6 subunits are unique modulators of low voltage-activated (Cav3.1) calcium current*. J Mol Cell Cardiol, 2004. **37**(6): p. 1147-58 DOI: 10.1016/j.yjmcc.2004.08.005.
- [257] Hendrich, J., et al., *Pharmacological disruption of calcium channel trafficking by the alpha2delta ligand gabapentin*. Proc Natl Acad Sci U S A, 2008. **105**(9): p. 3628-33 DOI: 10.1073/pnas.0708930105.
- [258] Hering, S., et al., *Calcium channel gating*. Pflugers Arch, 2018. **470**(9): p. 1291-1309 DOI: 10.1007/s00424-018-2163-7.
- [259] Hetzenauer, A., et al., *Brain activation pattern induced by stimulation of L-type Ca(2+)-channels: Contribution of Ca(v)1.3 and Ca(v)1.2 isoforms*. Neuroscience, 2006. **139**(3): p. 1005-1015 DOI: 10.1016/j.neuroscience.2006.01.059.
- [260] Hetzenauer, A., et al., *Brain activation pattern induced by stimulation of L-type Ca2+-channels: contribution of Ca(V)1.3 and Ca(V)1.2 isoforms*. Neuroscience, 2006. **139**(3): p. 1005-15 DOI: 10.1016/j.neuroscience.2006.01.059.
- [261] Hockerman, G.H., et al., *Molecular determinants of drug binding and action on L-type calcium channels*. Annu Rev Pharmacol Toxicol, 1997. **37**: p. 361-96 DOI: 10.1146/annurev.pharmtox.37.1.361.
- [262] Hullin, R., et al., *Calcium channel beta subunit heterogeneity: functional expression of cloned cDNA from heart, aorta and brain*. EMBO J, 1992. **11**(3): p. 885-90.
- [263] Hulme, J.T., et al., *Autoinhibitory control of the CaV1.2 channel by its proteolytically processed distal C-terminal domain*. J Physiol, 2006. **576**(Pt 1): p. 87-102 DOI: 10.1113/jphysiol.2006.1111799.
- [264] Jalily Hasani, H., et al., *Effects of protein-protein interactions and ligand binding on the ion permeation in KCNQ1 potassium channel*. PLoS One, 2018. **13**(2): p. e0191905 DOI: 10.1371/journal.pone.0191905.
- [265] Jay, S.D., et al., *Structural characterization of the dihydropyridine-sensitive calcium channel alpha 2-subunit and the associated delta peptides*. J Biol Chem, 1991. **266**(5): p. 3287-93.
- [266] Jo, S., et al., *CHARMM-GUI: a web-based graphical user interface for CHARMM*. J Comput Chem, 2008. **29**(11): p. 1859-65 DOI: 10.1002/jcc.20945.
- [267] Jones, S.W., *Calcium channels: unanswered questions*. J Bioenerg Biomembr, 2003. **35**(6): p. 461-75.

- [268] Kang, M.G. and K.P. Campbell, *gamma Subunit of voltage-activated calcium channels*. Journal of Biological Chemistry, 2003. **278**(24): p. 21315-21318 DOI: 10.1074/jbc.R300004200.
- [269] Khalili-Araghi, F., et al., *Molecular dynamics simulations of membrane proteins under asymmetric ionic concentrations*. Journal of General Physiology, 2013. **142**(4): p. 465-475 DOI: 10.1085/jgp.201311014.
- [270] Kim, E.Y., et al., *Structures of CaV2 Ca²⁺/CaM-IQ domain complexes reveal binding modes that underlie calcium-dependent inactivation and facilitation*. Structure, 2008. **16**(10): p. 1455-67 DOI: 10.1016/j.str.2008.07.010.
- [271] Kim, E.Y., et al., *Multiple C-terminal tail Ca(2+)/CaMs regulate Ca(V)1.2 function but do not mediate channel dimerization*. EMBO J, 2010. **29**(23): p. 3924-38 DOI: 10.1038/emboj.2010.260.
- [272] Lacinova, L. and N. Klugbauer, *Modulation of gating currents of the Ca(v)3.1 calcium channel by alpha 2 delta 2 and gamma 5 subunits*. Arch Biochem Biophys, 2004. **425**(2): p. 207-13 DOI: 10.1016/j.abb.2004.03.010.
- [273] Liang, H., et al., *Unified mechanisms of Ca²⁺ regulation across the Ca²⁺ channel family*. Neuron, 2003. **39**(6): p. 951-60.
- [274] Liao, P. and T.W. Soong, *CaV1.2 channelopathies: from arrhythmias to autism, bipolar disorder, and immunodeficiency*. Pflügers Archiv - European Journal of Physiology, 2009. **460**(2): p. 353-359 DOI: 10.1007/s00424-009-0753-0.
- [275] Liao, P. and T.W. Soong, *Understanding alternative splicing of Cav1.2 calcium channels for a new approach towards individualized medicine*. J Biomed Res, 2010. **24**(3): p. 181-6 DOI: 10.1016/S1674-8301(10)60027-9.
- [276] Liao, P., et al., *Splicing for alternative structures of Cav1.2 Ca²⁺ channels in cardiac and smooth muscles*. Cardiovasc Res, 2005. **68**(2): p. 197-203 DOI: 10.1016/j.cardiores.2005.06.024.
- [277] Liao, P., et al., *Smooth muscle-selective alternatively spliced exon generates functional variation in Cav1.2 calcium channels*. J Biol Chem, 2004. **279**(48): p. 50329-35 DOI: 10.1074/jbc.M409436200.
- [278] Lipscombe, D., A. Andrade, and S.E. Allen, *Alternative splicing: Functional diversity among voltage-gated calcium channels and behavioral consequences*. Biochimica Et Biophysica Acta-Biomembranes, 2013. **1828**(7): p. 1522-1529 DOI: 10.1016/j.bbamem.2012.09.018.
- [279] Lipscombe, D., T.D. Helton, and W. Xu, *L-type calcium channels: the low down*. J Neurophysiol, 2004. **92**(5): p. 2633-41 DOI: 10.1152/jn.00486.2004.
- [280] Lipscombe, D., T.D. Helton, and W.F. Xu, *L-type calcium channels: The low down*. Journal of Neurophysiology, 2004. **92**(5): p. 2633-2641 DOI: 10.1152/jn.00486.2004.
- [281] Liu, X., et al., *Molecular simulations study of novel 1,4-dihydropyridines derivatives with a high selectivity for Cav3.1 calcium channel*. Protein Sci, 2015. **24**(11): p. 1737-47 DOI: 10.1002/pro.2763.
- [282] Liu, Z. and H.J. Vogel, *Structural basis for the regulation of L-type voltage-gated calcium channels: interactions between the N-terminal cytoplasmic domain and Ca(2+)-calmodulin*. Front Mol Neurosci, 2012. **5**: p. 38 DOI: 10.3389/fnmol.2012.00038.
- [283] Loll, B., et al., *Loss of recognition by cross-reactive T cells and its relation to a C-terminus-induced conformational reorientation of an HLA-B*2705-bound peptide*. Protein Sci, 2011. **20**(2): p. 278-90 DOI: 10.1002/pro.559.

- [284] Lyu, L., et al., *A new interaction between proximal and distal C-terminus of Cav1.2 channels*. J Pharmacol Sci, 2017. **133**(4): p. 240-246 DOI: 10.1016/j.jphs.2017.03.002.
- [285] Mangoni, M.E., et al., *Functional role of L-type Cav1.3 Ca²⁺ channels in cardiac pacemaker activity*. Proc Natl Acad Sci U S A, 2003. **100**(9): p. 5543-8 DOI: 10.1073/pnas.0935295100.
- [286] Mangoni, M.E., et al., *Bradycardia and slowing of the atrioventricular conduction in mice lacking CaV3.1/alpha1G T-type calcium channels*. Circ Res, 2006. **98**(11): p. 1422-30 DOI: 10.1161/01.RES.0000225862.14314.49.
- [287] McDonald, T.F., et al., *Regulation and modulation of calcium channels in cardiac, skeletal, and smooth muscle cells*. Physiol Rev, 1994. **74**(2): p. 365-507 DOI: 10.1152/physrev.1994.74.2.365.
- [288] Mori, M.X., et al., *Crystal structure of the CaV2 IQ domain in complex with Ca²⁺/calmodulin: high-resolution mechanistic implications for channel regulation by Ca²⁺*. Structure, 2008. **16**(4): p. 607-20 DOI: 10.1016/j.str.2008.01.011.
- [289] Mould, J., et al., *The alpha2delta auxiliary subunit reduces affinity of omega-conotoxins for recombinant N-type (Cav2.2) calcium channels*. J Biol Chem, 2004. **279**(33): p. 34705-14 DOI: 10.1074/jbc.M310848200.
- [290] Movafagh, S., L. Cleemann, and M. Morad, *Regulation of cardiac Ca(2+) channel by extracellular Na(+)*. Cell Calcium, 2011. **49**(3): p. 162-73 DOI: 10.1016/j.ceca.2011.01.008.
- [291] Nachman-Clewner, M., R. St Jules, and E. Townes-Anderson, *L-type calcium channels in the photoreceptor ribbon synapse: localization and role in plasticity*. J Comp Neurol, 1999. **415**(1): p. 1-16.
- [292] Nakayama, H., et al., *Identification of 1,4-dihydropyridine binding regions within the alpha 1 subunit of skeletal muscle Ca²⁺ channels by photoaffinity labeling with diazepam*. Proc Natl Acad Sci U S A, 1991. **88**(20): p. 9203-7.
- [293] Namkung, Y., et al., *Requirement for the L-type Ca(2+) channel alpha(1D) subunit in postnatal pancreatic beta cell generation*. J Clin Invest, 2001. **108**(7): p. 1015-22 DOI: 10.1172/JCI13310.
- [294] Obermair, G.J., et al., *The Ca²⁺ channel alpha2delta-1 subunit determines Ca²⁺ current kinetics in skeletal muscle but not targeting of alpha1S or excitation-contraction coupling*. J Biol Chem, 2005. **280**(3): p. 2229-37 DOI: 10.1074/jbc.M411501200.
- [295] Offord, J. and L.L. Isom, *Drugging the undruggable: gabapentin, pregabalin and the calcium channel alpha2delta subunit*. Crit Rev Biochem Mol Biol, 2015. **51**(4): p. 246-56 DOI: 10.3109/10409238.2016.1173010.
- [296] Olson, P.A., et al., *G-protein-coupled receptor modulation of striatal CaV1.3 L-type Ca²⁺ channels is dependent on a Shank-binding domain*. J Neurosci, 2005. **25**(5): p. 1050-62 DOI: 10.1523/JNEUROSCI.3327-04.2005.
- [297] Opatowsky, Y., et al., *Structural analysis of the voltage-dependent calcium channel beta subunit functional core and its complex with the alpha 1 interaction domain*. Neuron, 2004. **42**(3): p. 387-399 DOI: Doi 10.1016/S0896-6273(04)00250-8.
- [298] Perez-Reyes, E., et al., *Cloning and expression of a cardiac/brain beta subunit of the L-type calcium channel*. J Biol Chem, 1992. **267**(3): p. 1792-7.
- [299] Perez-Reyes, E., et al., *Molecular diversity of L-type calcium channels. Evidence for alternative splicing of the transcripts of three non-allelic genes*. J Biol Chem, 1990. **265**(33): p. 20430-6.

- [300] Pfaff, M., et al., *Integrin beta cytoplasmic domains differentially bind to cytoskeletal proteins*. J Biol Chem, 1998. **273**(11): p. 6104-9.
- [301] Pinggera, A., et al., *New gain-of-function mutation shows CACNA1D as recurrently mutated gene in autism spectrum disorders and epilepsy*. Human Molecular Genetics, 2017. **26**(15): p. 2923-2932 DOI: 10.1093/hmg/ddx175.
- [302] Pitt, G.S., *Calmodulin and CaMKII as molecular switches for cardiac ion channels*. Cardiovasc Res, 2007. **73**(4): p. 641-7 DOI: 10.1016/j.cardiores.2006.10.019.
- [303] Pragnell, M., et al., *Calcium channel beta-subunit binds to a conserved motif in the I-II cytoplasmic linker of the alpha 1-subunit*. Nature, 1994. **368**(6466): p. 67-70 DOI: 10.1038/368067a0.
- [304] Qin, N., et al., *Molecular cloning and characterization of the human voltage-gated calcium channel alpha(2)delta-4 subunit*. Mol Pharmacol, 2002. **62**(3): p. 485-96.
- [305] Reid, C.A., J.D. Clements, and J.M. Bekkers, *Nonuniform distribution of Ca²⁺ channel subtypes on presynaptic terminals of excitatory synapses in hippocampal cultures*. J Neurosci, 1997. **17**(8): p. 2738-45.
- [306] Ritz, B., et al., *L-type calcium channel blockers and Parkinson disease in Denmark*. Ann Neurol, 2010. **67**(5): p. 600-6 DOI: 10.1002/ana.21937.
- [307] Rosenfeld, M.R., et al., *Cloning and characterization of a Lambert-Eaton myasthenic syndrome antigen*. Ann Neurol, 1993. **33**(1): p. 113-20 DOI: 10.1002/ana.410330126.
- [308] Simms, B.A. and G.W. Zamponi, *Trafficking and stability of voltage-gated calcium channels*. Cell Mol Life Sci, 2012. **69**(6): p. 843-56 DOI: 10.1007/s00018-011-0843-y.
- [309] Spedding, M. and R. Paoletti, *Classification of calcium channels and the sites of action of drugs modifying channel function*. Pharmacol Rev, 1992. **44**(3): p. 363-76.
- [310] Striessnig, J., et al., *Structural basis of drug binding to L Ca²⁺ channels*. Trends Pharmacol Sci, 1998. **19**(3): p. 108-15.
- [311] Striessnig, J., B.J. Murphy, and W.A. Catterall, *Dihydropyridine receptor of L-type Ca²⁺ channels: identification of binding domains for [3H](+)-PN200-110 and [3H]azidopine within the alpha 1 subunit*. Proc Natl Acad Sci U S A, 1991. **88**(23): p. 10769-73.
- [312] Striessnig, J., N.J. Ortner, and A. Pinggera, *Pharmacology of L-type Calcium Channels: Novel Drugs for Old Targets?* Curr Mol Pharmacol, 2015. **8**(2): p. 110-22.
- [313] Stroffekova, K., *Ca²⁺/CaM-dependent inactivation of the skeletal muscle L-type Ca²⁺ channel (Cav1.1)*. Pflugers Arch, 2008. **455**(5): p. 873-84 DOI: 10.1007/s00424-007-0344-x.
- [314] Takahashi, S.X., S. Mittman, and H.M. Colecraft, *Distinctive modulatory effects of five human auxiliary beta2 subunit splice variants on L-type calcium channel gating*. Biophys J, 2003. **84**(5): p. 3007-21 DOI: 10.1016/S0006-3495(03)70027-7.
- [315] Tan, G.M.Y., et al., *Alternative Splicing at C Terminus of Ca(V)1.4 Calcium Channel Modulates Calcium-dependent Inactivation, Activation Potential, and Current Density*. Journal of Biological Chemistry, 2012. **287**(2): p. 832-847 DOI: 10.1074/jbc.M111.268722.
- [316] Taylor, C.P., T. Angelotti, and E. Fauman, *Pharmacology and mechanism of action of pregabalin: the calcium channel alpha2-delta (alpha2-delta) subunit as a target for antiepileptic drug discovery*. Epilepsy Res, 2007. **73**(2): p. 137-50 DOI: 10.1016/j.eplepsyres.2006.09.008.

- [317] Temme, S.J. and G.G. Murphy, *The L-type voltage-gated calcium channel CaV1.2 mediates fear extinction and modulates synaptic tone in the lateral amygdala*. *Learn Mem*, 2017. **24**(11): p. 580-588 DOI: 10.1101/lm.045773.117.
- [318] Teng, J., et al., *Ion-channel blocker sensitivity of voltage-gated calcium-channel homologue Cchl in Saccharomyces cerevisiae*. *Microbiology*, 2008. **154**(Pt 12): p. 3775-81 DOI: 10.1099/mic.0.2008/021089-0.
- [319] Tikhonov, D.B. and B.S. Zhorov, *Structural model for dihydropyridine binding to L-type calcium channels*. *J Biol Chem*, 2009. **284**(28): p. 19006-17 DOI: 10.1074/jbc.M109.011296.
- [320] Torri Tarelli, F., et al., *Presynaptic localization of omega-conotoxin-sensitive calcium channels at the frog neuromuscular junction*. *Brain Res*, 1991. **547**(2): p. 331-4.
- [321] Van Petegem, F., F.C. Chatelain, and D.L. Minor, Jr., *Insights into voltage-gated calcium channel regulation from the structure of the CaV1.2 IQ domain-Ca²⁺/calmodulin complex*. *Nat Struct Mol Biol*, 2005. **12**(12): p. 1108-15 DOI: 10.1038/nsmb1027.
- [322] Van Petegem, F., et al., *Structure of a complex between a voltage-gated calcium channel beta-subunit and an alpha-subunit domain*. *Nature*, 2004. **429**(6992): p. 671-5 DOI: 10.1038/nature02588.
- [323] Wang, H.G., et al., *Ca²⁺/calmodulin regulates trafficking of Ca(V)1.2 Ca²⁺ channels in cultured hippocampal neurons*. *Journal of Neuroscience*, 2007. **27**(34): p. 9086-9093 DOI: 10.1523/Jneurosci.1720-07.2007.
- [324] Wellman, G.C. and M.T. Nelson, *Signaling between SR and plasmalemma in smooth muscle: sparks and the activation of Ca²⁺-sensitive ion channels*. *Cell Calcium*, 2003. **34**(3): p. 211-29.
- [325] Wu, J., et al., *Structure of the voltage-gated calcium channel Cav1.1 complex*. *Science*, 2015. **350**(6267): p. aad2395 DOI: 10.1126/science.aad2395.
- [326] Wycisk, K.A., et al., *Structural and functional abnormalities of retinal ribbon synapses due to Cacna2d4 mutation*. *Investigative Ophthalmology & Visual Science*, 2006. **47**(8): p. 3523-3530 DOI: 10.1167/iovs.06-0271.
- [327] Xu, L., et al., *Binding mechanisms of 1,4-dihydropyridine derivatives to L-type calcium channel Cav1.2: a molecular modeling study*. *Mol Biosyst*, 2016. **12**(2): p. 379-90 DOI: 10.1039/c5mb00781j.
- [328] Yang, J., et al., *Molecular determinants of Ca²⁺ selectivity and ion permeation in L-type Ca²⁺ channels*. *Nature*, 1993. **366**(6451): p. 158-61 DOI: 10.1038/366158a0.
- [329] Yasuda, T., et al., *Auxiliary subunit regulation of high-voltage activated calcium channels expressed in mammalian cells*. *Eur J Neurosci*, 2004. **20**(1): p. 1-13 DOI: 10.1111/j.1460-9568.2004.03434.x.
- [330] Zamponi, G.W., *Targeting voltage-gated calcium channels in neurological and psychiatric diseases*. *Nat Rev Drug Discov*, 2016. **15**(1): p. 19-34 DOI: 10.1038/nrd.2015.5.
- [331] Zamponi, G.W. and T.P. Snutch, *Advances in voltage-gated calcium channel structure, function and physiology*. *Biochim Biophys Acta*, 2013. **1828**(7): p. 1521 DOI: 10.1016/j.bbamem.2013.03.014.
- [332] Zamponi, G.W. and T.P. Snutch, *Advances in voltage-gated calcium channel structure, function and physiology*. *Biochimica Et Biophysica Acta-Biomembranes*, 2013. **1828**(7): p. 1521-1521 DOI: 10.1016/j.bbamem.2013.03.014.
- [333] Zuhlke, R.D., et al., *Calmodulin supports both inactivation and facilitation of L-type calcium channels*. *Nature*, 1999. **399**(6732): p. 159-162.

- [334] Zvejniece, L., et al., *R-phenibut binds to the alpha2-delta subunit of voltage-dependent calcium channels and exerts gabapentin-like anti-nociceptive effects*. *Pharmacol Biochem Behav*, 2015. **137**: p. 23-9 DOI: 10.1016/j.pbb.2015.07.014.
- [335] Mukaka, M. M. (2012). "Statistics Corner: A guide to appropriate use of Correlation coefficient in medical research." Malawi Medical Journal **24**(3): 69-71.

APPENDIX A: PREDICTION OF DRUGGABLE BINDING SITES⁴

A.1 Introduction

Although using an automated approach to predict the ‘druggability’ of a binding site is still difficult, computational methods are becoming more promising in this aspect. These computational methods are usually composed of two subsequent stages, namely, identifying the binding site and, subsequently, characterizing its druggability. The site identification phase aims at analyzing the distribution of all hot spots on the target and employs both structure-based methods and sequence-based methods. On the other hand, the druggability of a binding site can be characterized different druggability indexes, as described below.

In general, binding sites can be classified into three major types. The first includes catalytic sites or enzymatic binding sites. These binding sites usually possess specific catalytic functions, allowing it to interact with a substrate and execute chemical reactions, transforming the substrate into a new product. The second class comprises allosteric binding sites, which are not inducing any catalytic activity, however, interacting with these sites can indirectly impact the function, dynamics, or distribution of conformations of the target, which can indirectly modulate its activity. The third and the most complicated class of binding sites are usually termed as cryptic binding sites. They are almost hidden and rarely can appear on the surface of the protein. They usually occupy a small portion of the conformational ensemble of the target and are only partly detectable in the unbound target. Identifying cryptic sites may require a great deal of structural and conformational analysis of the target (as fig.A.1.1).

⁴ A version of this appendix has been published as a book chapter: *Tianhua Feng and Khaled Barakat. "Molecular Dynamics Simulation and Prediction of Druggable Binding Sites." Methods Mol Biol. Springer, 2018;1762:87-103.*

Binding site recognition methods can hardly identify all potential binding sites, especially, if the search process involves only a single static structure. An experimental crystal structure is an average in time and space of protein dynamics. A binding site can be easily hidden in a crystal structure and can be only identified when its dynamical properties are taken into account. In this context, the flexibility of the target plays a significant role in binding site formation and identification and studying these conformational dynamics is an essential step in this process. One way to study and reveal these dynamics is to use molecular dynamics (MD) simulations. The snapshots extracted from the MD trajectory represent multiple conformers of the protein structure, involving both backbone and side chain dynamics. These extracted conformations can reveal hidden spots within a crystal structure.

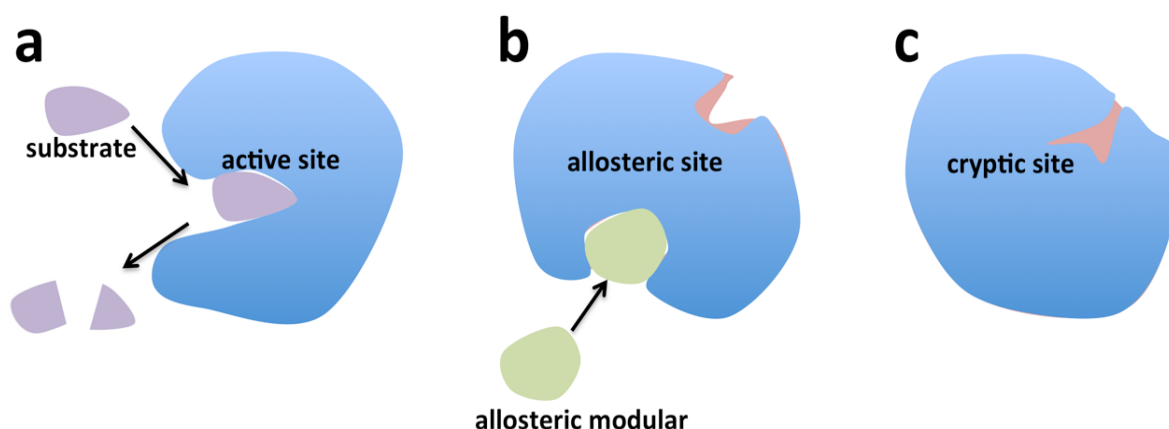


Figure. A.1.1 Different types of binding sites include the active site (a), allosteric site (b), which can change their conformation before (pink) and after (blue) binding with allosteric modular, and cryptic binding site(c), which keep in continuous changing (blue and pink).

This chapter will focus on binding site identification approaches, with an emphasis on structure-based methods. It will also discuss the use of MD simulations in identifying these sites, understanding their dynamicity and evaluating their druggability. Finally, a few case studies will

be summarized, followed by a summary and conclusion of our findings. We hope this chapter shed light on recent advances in this hot area and be of a wide use by interested researchers.

A.2 Binding Site Identification and Druggability Evaluation

As mentioned above, the prediction of druggable binding sites involves two stages. Firstly, one should identify all potential binding sites within and on the surface of the target structure. This is followed by the ranking of these in terms of their druggability.

A.2.1 Binding site identification methods

The last few years witnessed the development of a few reliable structure-based methods to identify binding sites. These structural methods can be categorized into two main classes, geometric-based methods (e.g. PASS, POCKET, LigSite), and energy-based methods (e.g. GRID, Q-SiteFinder). Several reviews comprehensively describe these two approaches, however, they will be briefly summarized below.

Geometric-based methods

Geometric-based methods recognize a binding site based on its geometric parameters. Two example parameters that are commonly used in this aspect are the depth and surface area of the binding site. In this context, Hajduk et al. defined a term, called pocket compactness, as the ratio of the pocket volume to the pocket surface area. The optimal value for this parameter is usually in the range of 0.4. Larger values correspond to more spherical shaped pockets and smaller values represent more elongated shaped pockets. The residual composition of a binding site, which includes polarization, charges, and H-bonds, are also important geometrical parameters to characterize binding sites. By using these various parameters one can identify potential binding sites and provide further druggability assessment (as fig.A.2.1).

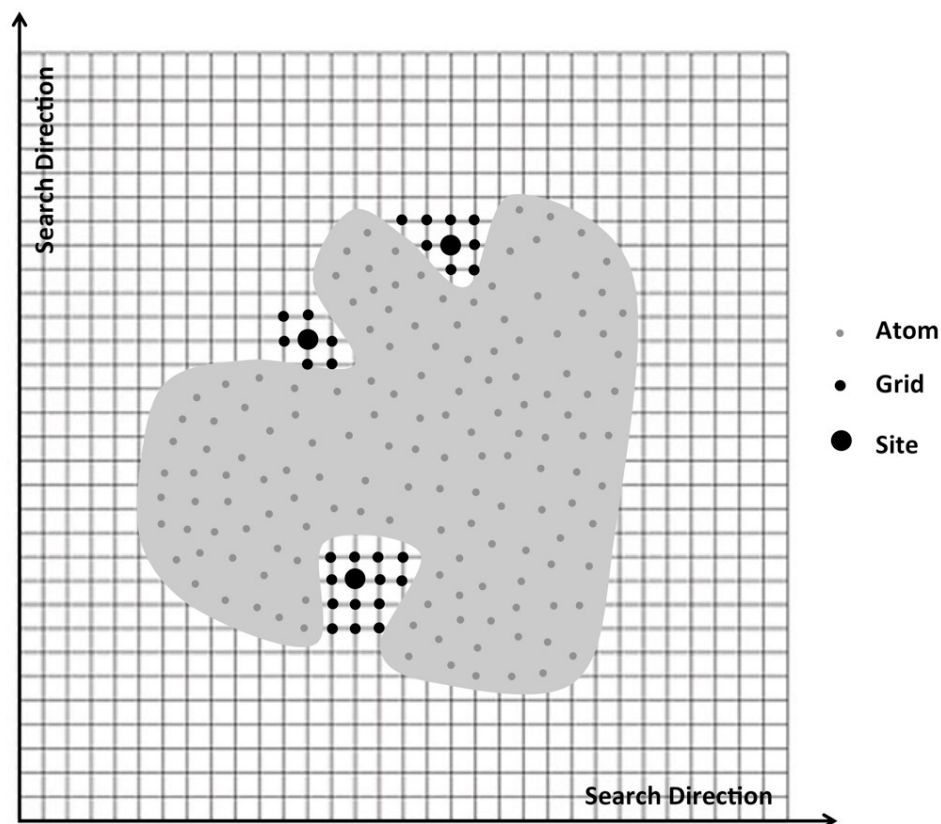


Figure A.2.1 Geometric-based binding site identification mechanism. The methods scan the grid points outside the protein for protein-solvent-protein and surface-solvent-surface events.

For protein-protein interactions (PPIs), the geometric descriptors are usually smaller compared to those of catalytic/active sites, which are usually formed by major, large and deep binding clefts. An important study in this regard is the work by Bourgeas et al. They extracted the best descriptors, geometrical parameters, and residue properties for PPIs, and used this information to guide their search for binding sites in heterodimer complexes (Bourgeas, Basse et al. 2010). The 2P2I database gather geometry information of interfaces, which comes from known druggable PPIs' interfaces. They summarize several different properties of these interfaces after compared with general PPI interfaces. The druggable PPIs' interfaces are smaller, more hydrophobic and

composed by fewer pockets. What's more, the druggable have less salt bridges and charged residues, but more hydrogen bonds at the interface (Bourgeas, Basse et al. 2010).

Energy-based methods

Energy-based methods employ molecular docking as the main tool to identify and characterize the binding sites on proteins. These methods dock multiple probes to potential pockets and calculate their binding free energies. These predicted energies reflect the strength of the interactions of these probes within the target (Ivetac and McCammon 2010). Fragment-based mapping algorithm (FTMAP) is a popular energy-based method. FTMAP was a developed version of its predecessor, Computational Solvent Mapping (CS-map)(Landon, Lancia et al. 2007).

FTMAP uses a diverse library of 16 small organic molecules as probes to search the whole target protein surface for potential binding sites (Bakan, Nevins et al. 2012, Miao, Nichols et al. 2014). These small organic probes have different hydrophobicity and hydrogen bond capacities, allowing them to interact with many parts on the protein surface. A fast Fourier transform correlation approach is implemented to sample millions of receptor-probe complexes. These complexes are clustered within the same probe type, and the generated clusters are ranked based on their binding energies. The method extracts top-ranking clusters from different types of probe and regroups them again. The consensus sites (CSs) represent putative hot spots, where multiple probes congregate. The CSs containing the largest number of probe clusters are considered the main hot spots (as fig. A.2.2) (Ivetac and McCammon 2010). The FTMAP method has been developed as web server, which is linked to the protein data bank (PDB) and generates a file containing the CSs and their congregated probes for a given target (Kozakov, Grove et al. 2015).

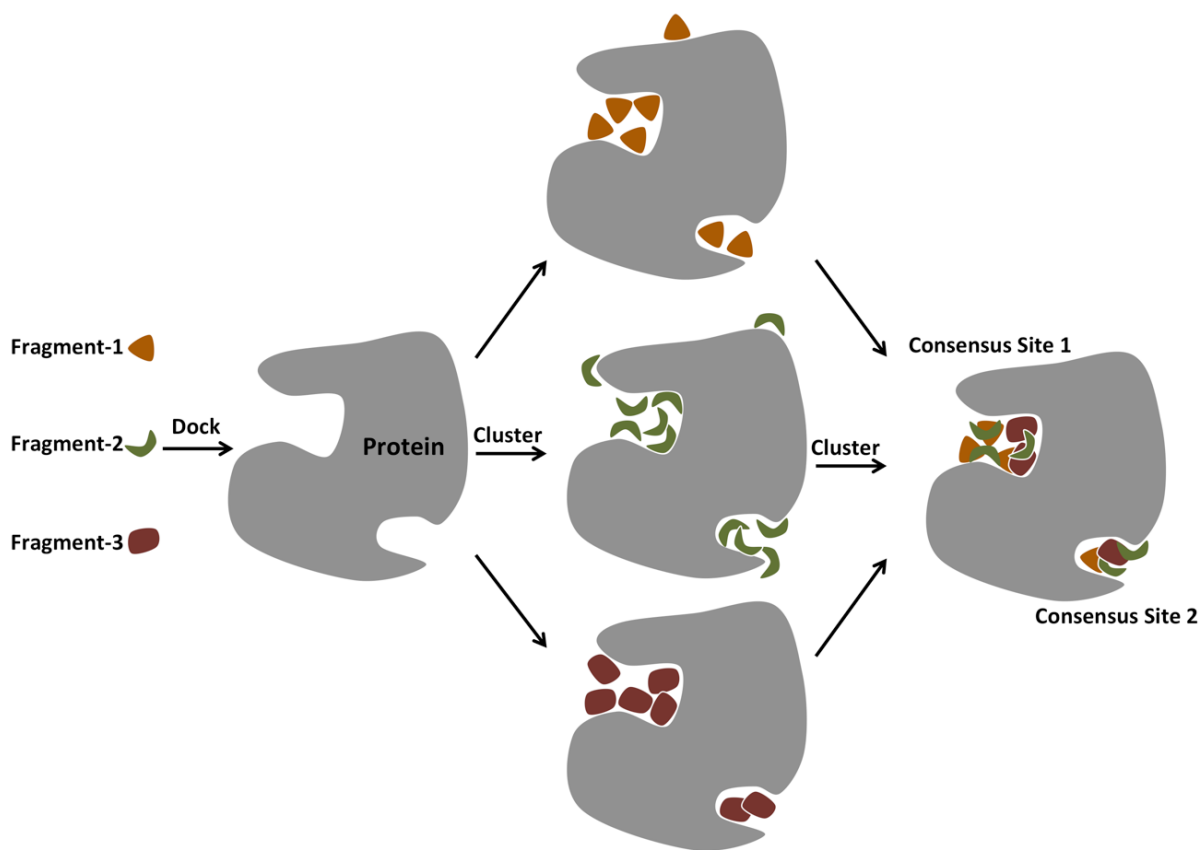


Figure A.2.2 Energy-based binding site identification mechanism. Different types of drug-like fragments dock on the protein surface. And, after two turns of cluster process, multiple fragments are gathering around the Consensus Sites.

A.2.2 Druggability evaluation methods

Once a binding site is identified, the next stage focuses on the evaluation of its druggability. In general, this is usually accomplished by analyzing the binding site using various geometrical descriptors and binding free energy analysis. All these calculations are summarized in what is termed as a druggability index. A druggability index, I_D , provides a measure of the potential of a given binding site to accommodate a small-molecule candidate drug.

Most of the current methods search for a binding site using a static protein structure and the calculated values of the various geometrical descriptors contribute to the final value of the druggability index. Typical I_D values are in the range of -3.0 to 0.0 (Brown and Hajduk 2006). Binding pockets with an I_D greater than -1.0 are having a high potential for being druggable, whereas pockets with an I_D less than -1.5 are having a low potential for small-molecule druggability (Brown and Hajduk 2006). The druggability index can be calculated using the equation (1):

$$I_D = \sum_{i=1}^N [a_i X_i + b_i \log(X_i)] \quad (1)$$

Where N is the number of the active-site descriptors used, X_i is the i^{th} descriptor, and a_i and b_i are coefficients (obtained from fitting to experimental data) for the linear and logarithmic terms of the i^{th} parameter, respectively (Brown and Hajduk 2006).

Cheng et al. defined the terms, “curvature” and “lipophilicity”, which reflect the shape of the binding site and its hydrophobicity, respectively. These two parameters indicate the maximal binding affinity for drug-like compounds (Cheng, Coleman et al. 2007, Makley and Gestwicki 2013). Other binding sites’ identification methods use different geometrical descriptors. An example is the Dscore method, which forms a linear function of three pocket properties: size, enclosure (akin to an average degree of buriedness), and hydrophilicity (Halgren 2009, Craig, Pflieger et al. 2011). Another druggability evaluation method, which originated from NMR-Based fragment screening, try to mimic the hit rates concept, This hit rate method relies on the assumption that sites that bind with a higher proportion of fragments are also more likely to deliver high-affinity, noncovalent drug-like leads (Hajduk, Huth et al. 2005). The FTMAP is an example of such methods and it can estimate the maximal binding affinity, while evaluating the druggability of a given target toward a particular compound.

A.3 Importance of Protein Flexibility

All the methods described above do not take the protein flexibility into account, making them very limited in identifying and studying complicated and hidden binding sites. For example, many studies have shown that the druggability index can vary significantly, when calculating the same index for the same target, but for a different state (i.e. free vs. bound structures)(Brown and Hajduk 2006). This is clearly demonstrated in highly dynamical proteins (Yang and Wang 2011). For example, the unbound Bcl-xL protein cannot accommodate the Bak peptide, which is normally associated with a low druggability index (ID=-2.0). On the contrary, the bound conformation is much wider and deeper, which is reflected by a much higher druggability index (ID=-0.5) (as fig. A.3.1)(Brown and Hajduk 2006, Wysoczanski, Mart et al. 2012).

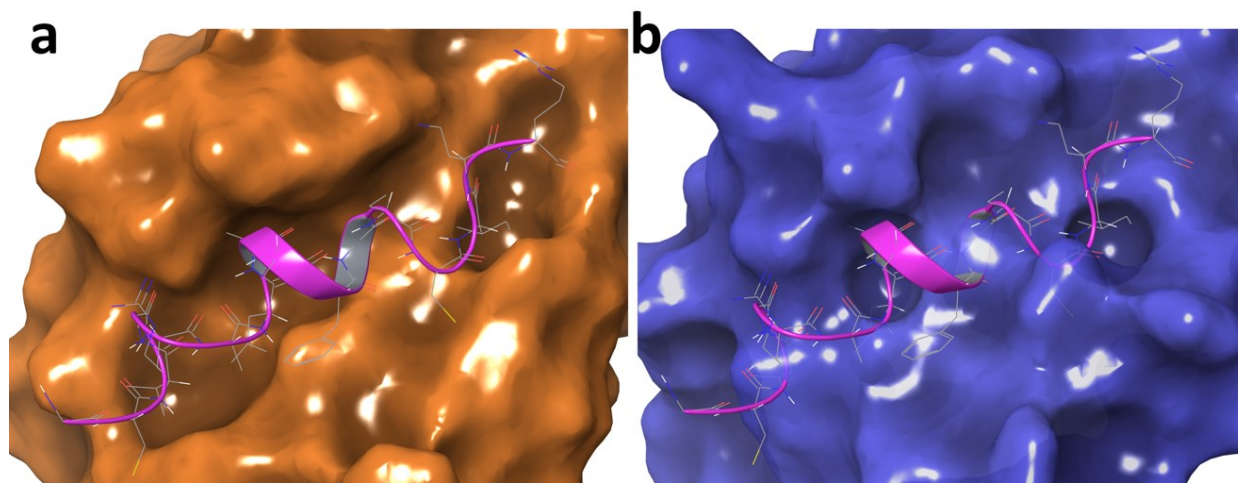


Figure A.3.1 Surface representation of Bcl-xL in unbound and bound conformation. Based on the geometric feature, the binding site can be recognized as high druggability A) in bound conformation with Bak peptide. However, the same binding site of B) unbound Bcl-xL is identified as low druggability.

A more complicated example is the discovery of a hidden trench in HIV integrase, which is not accessible within the available crystal structure (Schames, Henchman et al. 2004). Other

examples include the identification of uncharacterized binding sites on the Cruzain, a therapeutic target for Chagas' disease (Durrant, Keranen et al. 2010) and the identification of novel transient allosteric binding sites in Ras proteins, a hallmark of diverse cancers (Grant, Lukman et al. 2011). All these examples emphasize the importance of introducing protein flexibility in the search process for a binding site.

A.3.1 Generation of Conformation Ensemble

A conformational ensemble is a group of structures from the same target with different conformations, reflecting the flexibility of the backbone and side chains. In the early 1990s, Pang and Kozikowski made the first attempt to extract multiple conformations of the acetylcholinesterase enzyme from MD trajectories. Since this moment, MD simulations become the most common way to generate such structural ensembles (De Vivo, Masetti et al. 2016). The depth and the shape of a given protein pocket can be assessed during the simulation and transient cavities can be identified and explored (Grove, Hall et al. 2013).

The generation of a conformational ensemble involves two steps. First is to run an MD simulation on the target structure to generate a trajectory. This atomic trajectory can be either a single extensive trajectory, coming from a single simulation, or multiple trajectories combined together to form a single long trajectory (Perot, Sperandio et al. 2010). The two approaches can lead to different outcomes, and it seems that using multiple simulations can provide more improved conformational sampling over the use of a single MD trajectory (Ivetac and McCammon 2010).

The next step, involves the clustering of the long trajectory obtained from the simulation. This clustering step not only identifies representative conformations for the target protein, but is also used to reduce the computational time in subsequent binding site evaluation steps (Craig, Pflieger et al. 2011). The most common way for clustering protein conformations is using RMSD-based

methods. Other methods may also involve principal component analysis (PCA) (Lukman, Nguyen et al. 2017), non-negative matrix factorization (NMF) (Lee and Seung 1999), and independent component analysis (ICA) (Hyvarinen and Oja 2000, Lukman, Nguyen et al. 2017).

A.3.2 Cosolvent Molecular Dynamics Simulations

Flooding a protein structure with different probes during MD simulations emerged as a new way to detect binding sites while taking into account their flexibility. A promising example of such methods is the cosolvent MD simulation approach. In this method, the protein structure is soaked in different concentrations of different explicit solvents, allowing these solvent molecules to diffuse and interact with hot spots on the protein surface. In this way, cosolvent MD simulations have two major advantages over the traditional binding site recognition methods, described above. First, cosolvent MD simulations does not require a training set to run. Meaning that, the method can be applied to all types of protein structures, without a prior knowledge about similar protein structures or potential binding sites (Li, Kasam et al. 2014). The second and, perhaps, the most important feature of cosolvent MD simulations is that it fully accommodates protein flexibility, solvent effects and many other parameters during the simulation.

The used organic solvents can have different chemical properties and shapes, allowing the study of different possible interactions with the protein and also helping in predicating the maximum binding affinity for any identified binding site (Seco, Luque et al. 2009, Henrich, Salo-Ahen et al. 2010, Bakan, Nevins et al. 2012, Nisius, Sha et al. 2012). During a typical simulation the different solvent molecule is spontaneously distributed and concentrated around possible binding sites. The elapsed time for solvent molecules to occupy the binding site is directly related to its druggability (Seco, Luque et al. 2009). In this context, the identified binding sites are ranked by the occupation time and the increase in the local density of the interacting organic molecules.

The druggability is also assessed by the maximum binding affinity as predicted from these interactions (Cheng, Coleman et al. 2007). The maximum binding affinity can be obtained by calculating the associated free energy, ΔG_i . It counts the number of times the different solvents are attracted to a given hot spot and compares with expected value.

$$\Delta G_i = -k_B T \ln(N_i/N_o) \quad (2)$$

In equation (2), k_B is the Boltzmann constant, T is the temperature, N_i represents the observed solvent population, while N_o represents the expected value.

Different studies using the cosolvent MD simulation technique helped in identifying new binding sites and identified the limitations of the method. For example, in 2009, Seco et al. performed MD simulations on five different proteins, dissolved in explicit binary solvents, 20% Isopropanol/water (volume/volume). They were able to identify the binding sites on the target proteins and evaluate their druggability (Seco, Luque et al. 2009). However, they also pointed out to the effect of the simulation time as well as the low diffusion rate of the solvents on the binding site prediction. In particular, they concluded that a low diffusion rate can limit solvent exchange and can also prevent the solvent probes from diffusing into cavities and gaps within the protein structure (Seco, Luque et al. 2009, Alvarez-Garcia and Barril 2014).

A.3.3 Site Identification by ligand competitive Saturation

Guvench et al. developed a more refined MD-based method, namely the Site Identification by ligand competitive Saturation (SILCS). The method uses explicit ternary solvents, comprising benzene, isopropanol and water. The objective of combining these different solvent molecules was to provide a precise division of affinity properties among hydrophobic groups, aromatic groups, hydrogen bond donors and hydrogen bond acceptors (Guvench and MacKerell 2009, Lexa and

Carlson 2011). They validated the SILCS method using a full flexible simulation for Bcl-6. While including different solvent molecules improved the prediction of interaction energies, it did not overcome the diffusions' limitation (Makley and Gestwicki 2013). Raman et al brought up an improvement to the SILCS method in 2013, where more diverse solvent molecules were used (Raman, Yu et al. 2013).

A related approach, with some distinct technical details, is called MixMD and involved an explicitly binary solvent, 50% Acetonitrile/Water (weight/weight). In enhanced method, Lexa et al. also add isopropanol into the MixMD approach and tested on five proteins. They indicated multiple short MD simulations might be more efficient in sampling binding sites than few but long MD simulations (Lexa and Carlson 2011). These two methods have been successfully applied to ligand design and reproducing crystallographic binding sites of small organic molecules (Alvarez-Garcia and Barril 2014).

A similar method, named MDmix, employed two binary solvent systems, 20% Acetonitrile/water and 20% Isopropanol/water (volume/volume). Two proteins were tested, namely, the heat shock protein 90 N-terminal domain (Hsp90) and the HIV-1 protease (HIVpr). MDmix method showed more accurate interaction map and provided affordable water displaceability predictions compared with normal energy-based methods, such as Grid (Goodford 1985, Alvarez-Garcia and Barril 2014).

A.3.4 WaterMap

WaterMap is another MD-based approach for binding site identification. The method employs explicit water as the only solvent molecules interacting with the protein. WaterMap relies on the tendency for druggable binding sites to have a higher density of thermodynamic unstable

hydration sites. Accordingly, the method uses statistical analysis techniques to identify these locations within a given target (Beuming, Che et al. 2012).

A.4 Cases Studies

Following the description of the different MD-based methods for binding site identification, the next section will provide recent case studies from the literature.

A.4.1 A catalytic site problem: Viral Neuraminidase

As mentioned above, catalytic active sites are the primary type of druggable targets in drug development and they always have significant geometric features over allosteric sites. Neuraminidase enzymes represent an example of such targets and are usually targeted as the antigenic determinants on the surface of the influenza virus. Neuraminidase has one catalytic site that cleaves sialic acid and promotes new virus particles release (Masukawa, Kollman et al. 2003). Oseltamivir and zanamivir are both effective orthosteric inhibitors that bind to the active site (Fig. 4.1.1).

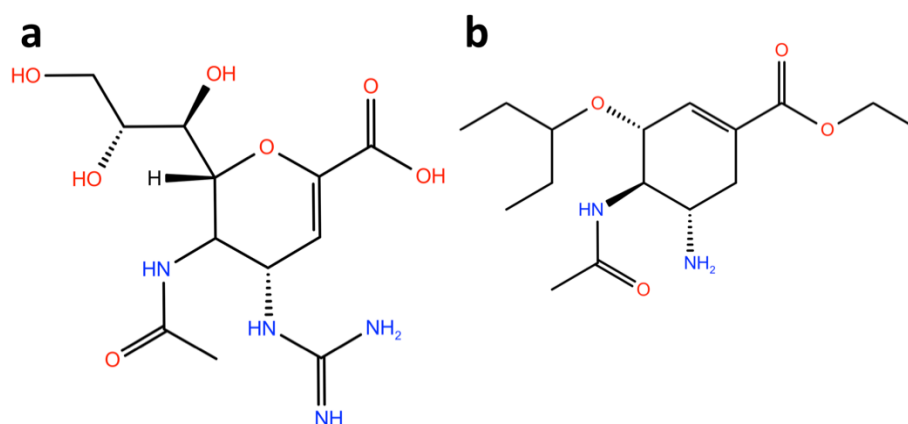


Figure A.4.1 2D chemical structure of Oseltamivir(a) and Zanamivir(b). They are both orthosteric inhibitors bind to the active site of Neuraminidase. Generated by Maestro.

Neuraminidase exhibits a high degree of selectivity among structurally similar compounds. The N1 subtype specifically binds with Tamiflu and mutations at the binding site can cause resistance against the drug. Therefore, enhancing drug selectivity and searching for novel binding sites are important research areas for influenza treatment. In the search for new binding sites in Neuraminidase for the H5N1 strain, Landon et al. combined extended explicit solvent molecular dynamics (MD) and computational solvent mapping (CS-Map) techniques to identify putative 'hot-spots' within flexible binding regions of N1 neuraminidase. They used representative conformations of the N1 binding region as extracted from the clustering of 40 ns MD trajectories. They then employed CS-Map to assess the ability of small solvent-sized molecules to bind close to the sialic acid binding region. Mapping analyses of the dominant MD conformations revealed the presence of additional hot spot around binding region. Hot spot analysis provided further support for the feasibility of developing high-affinity inhibitors that were capable of binding to these regions, which appeared to be unique to the N1 strain(Landon, Amaro et al. 2008). Furthermore, MD simulations also revealed the function of crystal water molecules in the active site. Interestingly, Landon et al. found that more potent ligands did not interact strongly with these co-crystallized water molecules (Masukawa, Kollman et al. 2003). They were also able to study the effects of mutations on the interactions with these compounds. (Shu, Lin et al. 2011).

A.4.2 An allosteric site problem: G-Protein Coupled Receptor (GPCR)

G-Protein Coupled Receptors (GPCRs) are major targets for drug development(Dror, Pan et al. 2011). They are associated with approximately 30% of current drugs and are linked to many diseases related to cancer, cardiovascular and central nervous systems (Overington, Al-Lazikani et al. 2006, Ivetac and McCammon 2010, Dror, Pan et al. 2011, Miao, Nichols et al. 2014). GPCRs are transmembrane proteins with a conservative topology composition, comprising of seven

transmembrane alpha-helices, and highly dynamics structure (Miao, Nichols et al. 2014, Kappel, Miao et al. 2015). Ivetac and McCammon used an ensemble-based approach combined with the FTMAP algorithm to study binding sites in two different GPCRs, namely, the β_1 (β_1 AR) and the β_2 (β_2 AR) adrenergic receptors. They used Coarse-Grain MD simulations to rapidly assemble the protein-lipid complexes. Then, they extracted a conformational ensemble for the proteins from six independent 40 ns long conventional MD simulations for each complex. The final protein structures involved 14 dominant conformations, representing the whole 240 ns MD simulation. Five allosteric binding sites, four of which are conserved within the two complexes were detected through this investigation. Site-1 and Site-4 were located at the extracellular and intracellular mouth of the proteins and were exposed to the solvent environment. On the other hand, the protein-lipid interface contained site-2, site-3, and site-5. Site-5 was observed only in the β_2 AR structure, which emphasized its value as a selective β_2 AR-targeted pocket (Ivetac and McCammon 2010).

A.4.3 A cryptic site problem: Bcl-xL protein

As discussed above, a cryptic site is defined as a hidden binding site when the protein is in the free/unbound state (Eyrisch and Helms 2007, Oleinikovas, Saladino et al. 2016). Cimermancic et al. used machine learning to predict new cryptic sites based on the features of available cryptic sites (Cimermancic, Weinkam et al. 2016). These features included their amino acid sequences, structures and dynamical attributes. Their major finding was that cryptic sites tend to be as conserved in evaluation as traditional binding pockets but are also less hydrophobic and more flexible (Cimermancic, Weinkam et al. 2016). Oleinikovas et al. characterized several additional characteristics for cryptic sites. They concluded that the appearance of a cryptic site does not correspond to a local minimum in the computed conformational free energy landscape. They also found that temperature-based enhanced sampling approaches, such as Parallel Tempering, do not

improve the situation, as the entropic term does not help in the opening of these sites. Interestingly, They found that a conventional MD simulation can occasionally lead to the opening of a cryptic site (Seco, Luque et al. 2009, Oleinikovas, Saladino et al. 2016).

As the Bcl-2 family of proteins, Bcl-xL is a key regulator of programmed cell death(Petros, Olejniczak et al. 2004). MD simulations was performed on the apo-Bcl-xL structure in water and in cosolvent to detect binding sites on the protein. In water, the binding site of the apo-Bcl-xL had relatively minor conformational changes. Simulations of three holo-Bcl-xL structures in water, however, showed that the protein exhibited significant dynamic transition of conformations, including burying of several solvent exposed hydrophobic residues in the binding groove. In contrast, the apo-Bcl-xL in cosolvent, the hydrophobic surface tends to exposing itself to the interface, which is similar to the tendency in the crystal complex of Bcl-xL. However, the free energy differences of the Bcl-xL conformations obtained from both solution methods were small, which indicates the perturbation of cosolvent molecules is acceptable to Bcl-xL structure in relatively short MD simulations(Lexa and Carlson 2011). Furthermore, the novel binding hot spots that were revealed by cosolvent MD simulation did not find in the co-crystallized complex (Yang and Wang 2011). Taken together, this study suggested that cosolvent is very capable method in identifying cryptic sites, particularly, for flexible and hydrophobic targets.

A.5 Conclusion

The surface of a protein target encompasses many hot spots. These spots are essential in mediating the interactions between the target protein and other proteins as well as small molecule drugs. A binding site is formed by the grouping of these hot spots within the surface of the protein. There are many types of such sites. The most complicated ones include cryptic and allosteric sites.

Both types do not induce direct effects on the activity of the target protein, however, they indirectly influence the activity by inducing conformational changes within the protein structure.

Identifying these sites and evaluating their druggability is very complicated. Current tools employ both geometrical-based and energy-based approaches to identify a binding site and assess its druggability. While these methods can easily study catalytic sites, they can poorly identify and study more complicated sites. This is mainly due to the fact that they rely on a static structure of the target protein., while an accurate prediction of these sites requires the accommodation of protein flexibility during the binding site search process. It also requires studying the structural dynamics of the different hot spots for a protonated time scale.

This chapter focused on overviewing the different methods used to identify and evaluate binding sites within a given target. It also highlighted the importance of incorporating protein flexibility within the search process. So, in the following section, we will discuss the applications of MD simulation.

A.6 References

- [1] Nisius, B., F. Sha, and H. Gohlke, *Structure-based computational analysis of protein binding sites for function and druggability prediction*. J Biotechnol, 2012. **159**(3): p. 123-34 DOI: 10.1016/j.jbiotec.2011.12.005.
- [2] Wells, J.A. and C.L. McClendon, *Reaching for high-hanging fruit in drug discovery at protein-protein interfaces*. Nature, 2007. **450**(7172): p. 1001-9 DOI: 10.1038/nature06526.
- [3] Hajduk, P.J., J.R. Huth, and C. Tse, *Predicting protein druggability*. Drug Discovery Today, 2005. **10**(23-24): p. 1675-1682 DOI: 10.1016/s1359-6446(05)03624-x.
- [4] Barakat, K.H., J.Y. Mane, and J.A. Tuszynski, *Virtual Screening: An Overview on Methods and Applications*, in *Handbook of Research on Computational and Systems Biology*, L.A.L.e. al., Editor. 2011, IGI Global: NY. p. 28-60 DOI: 10.4018/978-1-60960-491-2.ch002.
- [5] Ahmed, M., et al., *Targeting the Achilles heel of the hepatitis B virus: a review of current treatments against covalently closed circular DNA*. Drug Discov Today, 2015 DOI: 10.1016/j.drudis.2015.01.008.
- [6] Barakat, K., *Editorial: Computer-Aided Drug Design*. J Pharma Care Health Sys, 2014. **1**(4): p. 1000e113.
- [7] Bakan, A., et al., *Druggability Assessment of Allosteric Proteins by Dynamics Simulations in the Presence of Probe Molecules*. J Chem Theory Comput, 2012. **8**(7): p. 2435-2447 DOI: 10.1021/ct300117j.
- [8] Brown, S.P. and P.J. Hajduk, *Effects of conformational dynamics on predicted protein druggability*. ChemMedChem, 2006. **1**(1): p. 70-2 DOI: 10.1002/cmdc.200500013.
- [9] Seco, J., F.J. Luque, and X. Barril, *Binding site detection and druggability index from first principles*. J Med Chem, 2009. **52**(8): p. 2363-71 DOI: 10.1021/jm801385d.
- [10] Henrich, S., et al., *Computational approaches to identifying and characterizing protein binding sites for ligand design*. J Mol Recognit, 2010. **23**(2): p. 209-19 DOI: 10.1002/jmr.984.
- [11] Halgren, T.A., *Identifying and characterizing binding sites and assessing druggability*. J Chem Inf Model, 2009. **49**(2): p. 377-89 DOI: 10.1021/ci800324m.
- [12] Barakat, K.H., et al., *Detailed computational study of the active site of the hepatitis C viral RNA polymerase to aid novel drug design*. J Chem Inf Model, 2013. **53**(11): p. 3031-43 DOI: 10.1021/ci4003969.
- [13] Viricel, C., M. Ahmed, and K. Barakat, *Human PD-1 binds differently to its human ligands: A comprehensive modeling study*. J Mol Graph Model, 2015. **57C**: p. 131-142 DOI: 10.1016/j.jmgm.2015.01.015.
- [14] Ahmed, M. and K. Barakat, *Baby Steps Toward Modelling The Full human Programmed Death-1 (PD-1) Pathway*. Receptors & Clinical Investigation, 2015. **2**(3).
- [15] Barakat, K.H., et al., *A computational model for overcoming drug resistance using selective dual-inhibitors for aurora kinase A and its T217D variant*. Mol Pharm, 2013. **10**(12): p. 4572-89 DOI: 10.1021/mp4003893.
- [16] Gajewski, M., et al., *Interactions of laulimalide, peloruside, and their derivatives with the isoforms of β -tubulin*. Canadian Journal of Chemistry, 2013. **91**(7): p. 511-517.
- [17] Gentile, F., J.A. Tuszynski, and K.H. Barakat, *New design of nucleotide excision repair (NER) inhibitors for combination cancer therapy*. J Mol Graph Model, 2016. **65**: p. 71-82 DOI: 10.1016/j.jmgm.2016.02.010.

- [18] Hu, G., et al., *Human structural proteome-wide characterization of Cyclosporine A targets*. *Bioinformatics*, 2014. **30**(24): p. 3561-6 DOI: btu581 [pii] 10.1093/bioinformatics/btu581.
- [19] McClendon, C.L., et al., *Quantifying Correlations Between Allosteric Sites in Thermodynamic Ensembles*. *J Chem Theory Comput*, 2009. **5**(9): p. 2486-2502 DOI: 10.1021/ct9001812.
- [20] Eyrisch, S. and V. Helms, *Transient pockets on protein surfaces involved in protein-protein interaction*. *J Med Chem*, 2007. **50**(15): p. 3457-64 DOI: 10.1021/jm070095g.
- [21] Oleinikovas, V., et al., *Understanding Cryptic Pocket Formation in Protein Targets by Enhanced Sampling Simulations*. *J Am Chem Soc*, 2016. **138**(43): p. 14257-14263 DOI: 10.1021/jacs.6b05425.
- [22] Ganesan, A., M.L. Coote, and K. Barakat, *Molecular dynamics-driven drug discovery: leaping forward with confidence*. *Drug Discov Today*, 2017. **22**(2): p. 249-269 DOI: 10.1016/j.drudis.2016.11.001.
- [23] Perot, S., et al., *Druggable pockets and binding site centric chemical space: a paradigm shift in drug discovery*. *Drug Discov Today*, 2010. **15**(15-16): p. 656-67 DOI: 10.1016/j.drudis.2010.05.015.
- [24] Brady, G.P., Jr. and P.F. Stouten, *Fast prediction and visualization of protein binding pockets with PASS*. *J Comput Aided Mol Des*, 2000. **14**(4): p. 383-401.
- [25] Levitt, D.G. and L.J. Banaszak, *POCKET: a computer graphics method for identifying and displaying protein cavities and their surrounding amino acids*. *J Mol Graph*, 1992. **10**(4): p. 229-34.
- [26] Hendlich, M., F. Rippmann, and G. Barnickel, *LIGSITE: automatic and efficient detection of potential small molecule-binding sites in proteins*. *J Mol Graph Model*, 1997. **15**(6): p. 359-63, 389.
- [27] Goodford, P.J., *A computational procedure for determining energetically favorable binding sites on biologically important macromolecules*. *J Med Chem*, 1985. **28**(7): p. 849-57.
- [28] Laurie, A.T. and R.M. Jackson, *Q-SiteFinder: an energy-based method for the prediction of protein-ligand binding sites*. *Bioinformatics*, 2005. **21**(9): p. 1908-16 DOI: 10.1093/bioinformatics/bti315.
- [29] Villoutreix, B.O., et al., *Drug-Like Protein-Protein Interaction Modulators: Challenges and Opportunities for Drug Discovery and Chemical Biology*. *Mol Inform*, 2014. **33**(6-7): p. 414-437 DOI: 10.1002/minf.201400040.
- [30] Bourgeas, R., et al., *Atomic analysis of protein-protein interfaces with known inhibitors: the 2P2I database*. *PLoS One*, 2010. **5**(3): p. e9598 DOI: 10.1371/journal.pone.0009598.
- [31] Ivetac, A. and J.A. McCammon, *Mapping the druggable allosteric space of G-protein coupled receptors: a fragment-based molecular dynamics approach*. *Chem Biol Drug Des*, 2010. **76**(3): p. 201-17 DOI: 10.1111/j.1747-0285.2010.01012.x.
- [32] Landon, M.R., et al., *Identification of hot spots within druggable binding regions by computational solvent mapping of proteins*. *J Med Chem*, 2007. **50**(6): p. 1231-40 DOI: 10.1021/jm061134b.
- [33] Miao, Y., S.E. Nichols, and J.A. McCammon, *Mapping of allosteric druggable sites in activation-associated conformers of the M2 muscarinic receptor*. *Chem Biol Drug Des*, 2014. **83**(2): p. 237-46 DOI: 10.1111/cbdd.12233.

- [34] Kozakov, D., et al., *The FTMap family of web servers for determining and characterizing ligand-binding hot spots of proteins*. Nat Protoc, 2015. **10**(5): p. 733-55 DOI: 10.1038/nprot.2015.043.
- [35] Cheng, A.C., et al., *Structure-based maximal affinity model predicts small-molecule druggability*. Nat Biotechnol, 2007. **25**(1): p. 71-5 DOI: 10.1038/nbt1273.
- [36] Makley, L.N. and J.E. Gestwicki, *Expanding the number of 'druggable' targets: non-enzymes and protein-protein interactions*. Chem Biol Drug Des, 2013. **81**(1): p. 22-32 DOI: 10.1111/cbdd.12066.
- [37] Fauman, E.B., B.K. Rai, and E.S. Huang, *Structure-based druggability assessment--identifying suitable targets for small molecule therapeutics*. Curr Opin Chem Biol, 2011. **15**(4): p. 463-8 DOI: 10.1016/j.cbpa.2011.05.020.
- [38] Craig, I.R., et al., *Pocket-space maps to identify novel binding-site conformations in proteins*. J Chem Inf Model, 2011. **51**(10): p. 2666-79 DOI: 10.1021/ci200168b.
- [39] Yang, C.Y. and S. Wang, *Hydrophobic Binding Hot Spots of Bcl-xL Protein-Protein Interfaces by Cosolvent Molecular Dynamics Simulation*. ACS Med Chem Lett, 2011. **2**(4): p. 280-4 DOI: 10.1021/ml100276b.
- [40] Schames, J.R., et al., *Discovery of a novel binding trench in HIV integrase*. J Med Chem, 2004. **47**(8): p. 1879-81 DOI: 10.1021/jm0341913.
- [41] Durrant, J.D., et al., *Computational identification of uncharacterized cruzain binding sites*. PLoS Negl Trop Dis, 2010. **4**(5): p. e676 DOI: 10.1371/journal.pntd.0000676.
- [42] Grant, B.J., et al., *Novel allosteric sites on Ras for lead generation*. PLoS One, 2011. **6**(10): p. e25711 DOI: 10.1371/journal.pone.0025711.
- [43] Schmidtke, P., et al., *MDpocket: open-source cavity detection and characterization on molecular dynamics trajectories*. Bioinformatics, 2011. **27**(23): p. 3276-85 DOI: 10.1093/bioinformatics/btr550.
- [44] Grove, L.E., et al., *FTFlex: accounting for binding site flexibility to improve fragment-based identification of druggable hot spots*. Bioinformatics, 2013. **29**(9): p. 1218-9 DOI: 10.1093/bioinformatics/btt102.
- [45] De Vivo, M., et al., *Role of Molecular Dynamics and Related Methods in Drug Discovery*. J Med Chem, 2016. **59**(9): p. 4035-61 DOI: 10.1021/acs.jmedchem.5b01684.
- [46] Lukman, S., et al., *Discovery of Rab1 binding sites using an ensemble of clustering methods*. Proteins, 2017. **85**(5): p. 859-871 DOI: 10.1002/prot.25254.
- [47] Lee, D.D. and H.S. Seung, *Learning the parts of objects by non-negative matrix factorization*. Nature, 1999. **401**(6755): p. 788-91 DOI: 10.1038/44565.
- [48] Hyvarinen, A. and E. Oja, *Independent component analysis: algorithms and applications*. Neural Netw, 2000. **13**(4-5): p. 411-30.
- [49] Ortiz-Sanchez, J.M., et al., *Identification of potential small molecule binding pockets on Rho family GTPases*. PLoS One, 2012. **7**(7): p. e40809 DOI: 10.1371/journal.pone.0040809.
- [50] Sugita, Y. and Y. Okamoto, *Replica-exchange multicanonical algorithm and multicanonical replica-exchange method for simulating systems with rough energy landscape*. Chemical Physics Letters, 2000. **329**(3-4): p. 261-270 DOI: Doi 10.1016/S0009-2614(00)00999-4.
- [51] Voter, A.F., *Hyperdynamics: Accelerated molecular dynamics of infrequent events*. Physical Review Letters, 1997. **78**(20): p. 3908-3911 DOI: DOI 10.1103/PhysRevLett.78.3908.
- [52] Kerrigan, J.E., *Molecular dynamics simulations in drug design*. Methods Mol Biol, 2013. **993**: p. 95-113 DOI: 10.1007/978-1-62703-342-8_7.

- [53] Mortier, J., et al., *The impact of molecular dynamics on drug design: applications for the characterization of ligand-macromolecule complexes*. Drug Discov Today, 2015. **20**(6): p. 686-702 DOI: 10.1016/j.drudis.2015.01.003.
- [54] Zhao, H. and A. Caflisch, *Molecular dynamics in drug design*. Eur J Med Chem, 2015. **91**: p. 4-14 DOI: 10.1016/j.ejmech.2014.08.004.
- [55] Li, H., et al., *Computational method to identify druggable binding sites that target protein-protein interactions*. J Chem Inf Model, 2014. **54**(5): p. 1391-400 DOI: 10.1021/ci400750x.
- [56] Alvarez-Garcia, D. and X. Barril, *Molecular simulations with solvent competition quantify water displaceability and provide accurate interaction maps of protein binding sites*. J Med Chem, 2014. **57**(20): p. 8530-9 DOI: 10.1021/jm5010418.
- [57] Guvench, O. and A.D. MacKerell, Jr., *Computational fragment-based binding site identification by ligand competitive saturation*. PLoS Comput Biol, 2009. **5**(7): p. e1000435 DOI: 10.1371/journal.pcbi.1000435.
- [58] Lexa, K.W. and H.A. Carlson, *Full protein flexibility is essential for proper hot-spot mapping*. J Am Chem Soc, 2011. **133**(2): p. 200-2 DOI: 10.1021/ja1079332.
- [59] Raman, E.P., et al., *Inclusion of multiple fragment types in the site identification by ligand competitive saturation (SILCS) approach*. J Chem Inf Model, 2013. **53**(12): p. 3384-98 DOI: 10.1021/ci4005628.
- [60] Beuming, T., et al., *Thermodynamic analysis of water molecules at the surface of proteins and applications to binding site prediction and characterization*. Proteins, 2012. **80**(3): p. 871-83 DOI: 10.1002/prot.23244.
- [61] Masukawa, K.M., P.A. Kollman, and I.D. Kuntz, *Investigation of neuraminidase-substrate recognition using molecular dynamics and free energy calculations*. J Med Chem, 2003. **46**(26): p. 5628-37 DOI: 10.1021/jm030060q.
- [62] Landon, M.R., et al., *Novel druggable hot spots in avian influenza neuraminidase H5N1 revealed by computational solvent mapping of a reduced and representative receptor ensemble*. Chem Biol Drug Des, 2008. **71**(2): p. 106-16 DOI: 10.1111/j.1747-0285.2007.00614.x.
- [63] Shu, M., et al., *Molecular dynamics simulation of oseltamivir resistance in neuraminidase of avian influenza H5N1 virus*. J Mol Model, 2011. **17**(3): p. 587-92 DOI: 10.1007/s00894-010-0757-x.
- [64] Dror, R.O., et al., *Pathway and mechanism of drug binding to G-protein-coupled receptors*. Proc Natl Acad Sci U S A, 2011. **108**(32): p. 13118-23 DOI: 10.1073/pnas.1104614108.
- [65] Overington, J.P., B. Al-Lazikani, and A.L. Hopkins, *Opinion - How many drug targets are there?* Nature Reviews Drug Discovery, 2006. **5**(12): p. 993-996 DOI: 10.1038/nrd2199.
- [66] Kappel, K., Y. Miao, and J.A. McCammon, *Accelerated molecular dynamics simulations of ligand binding to a muscarinic G-protein-coupled receptor*. Q Rev Biophys, 2015. **48**(4): p. 479-87 DOI: 10.1017/S0033583515000153.
- [67] Cimermancic, P., et al., *CryptoSite: Expanding the Druggable Proteome by Characterization and Prediction of Cryptic Binding Sites*. J Mol Biol, 2016. **428**(4): p. 709-719 DOI: 10.1016/j.jmb.2016.01.029.
- [68] Petros, A.M., E.T. Olejniczak, and S.W. Fesik, *Structural biology of the Bcl-2 family of proteins*. Biochim Biophys Acta, 2004. **1644**(2-3): p. 83-94 DOI: 10.1016/j.bbamcr.2003.08.012.

APPENDIX B: MOLECULAR DYNAMIC SIMULATIONS⁵⁵

B.1 Introduction

Multiple MD simulations methods engaged in this thesis and discussed in Chapter 2 and 3. Therefore, the current chapter serves as an introduction to these techniques. The applications of Molecular Dynamic Simulations, both classical and advanced ones, have been widely used in understanding the structure and function of molecules (e.g. proteins, membrane, water, ions). Molecular biology techniques such as X-ray crystallography, Nuclear Magnetic Resonance (NMR) spectroscopy and Cryo-electron microscopy (cryo-EM) have been quite successful in providing high-resolution atomic structures for these molecules (Jorgensen, Maxwell et al. 1996, MacKerell, Bashford et al. 1998, Huang and MacKerell 2013). These structures provided the molecular details to understand the structure-function mechanism. However, these molecular structures are limited by their static properties. Proteins, especially transmembrane proteins, are highly dynamic molecular entities, which contains multiple conformational states and interacts with other molecules, such as signalling molecules, transporters, catalysts, sensors, and mechanical effectors (MacKerell, Bashford et al. 1998). Exploring these conformational states has become an essential task to deeply understand the molecular mechanism of protein (Xu, Li et al. 2016). Revealing all information from a static protein structure is not possible. With the help of advanced computational resources, molecular dynamics can be a powerful method to calculate the movement of molecules.

The molecular dynamics (MD) simulation is a promising method to study the dynamical behaviour, structure-function connection, and molecular interaction mechanism (Schmidtke, Bidon-Chanal et

⁵ A version of this appendix has been published as a book chapter: *Tianhua Feng and Khaled Barakat. "Molecular Dynamics Simulation and Prediction of Druggable Binding Sites." Methods Mol Biol. Springer, 2018;1762:87-103.*

al. 2011, Grove, Hall et al. 2013). These simulations can be carried out in the context of the solvent, ions and various physiological conditions. The method became very popular in studying protein structures and in extracting conformational ensembles of the target (Roux and Schulten 2004).

This section serves as a brief description of the MD techniques used in this thesis. The basic theory of MD simulation is generally discussed. And, a brief description of classical MD and enhanced MD simulations, including external electric field MD (EE-MD) and steered MD (SMD), will be reviewed.

B.2 Classical MD Simulations

Molecular dynamics (MD) simulation is a valuable tool for studying biomolecular systems and the physical movements of atoms and molecules. Specifically, different MD techniques have allowed the exploration of the dynamic properties, structure and inaccessible events related to proteins. The main output from a simulation consists of a phase space trajectory that are determined by numerically solving Newton's equations of motion (Lindahl and Sansom 2008, Huang and MacKerell 2013). The trajectory is known as the trace of molecules to explore their conformational surface. In this trajectory, each of the atom requires parameters for every interaction, which is called force field. The basic functional term of potential energy in molecular mechanics includes bonded terms for interactions of atoms that are linked by covalent bonds, and nonbonded terms that describe the long-range electrostatic and van der Waals forces (see section 3). By using the proper force field, the MD simulation can largely reproduce the molecular movement in the experiment. Additionally, the molecular dynamics can be used to predict the multiple processes, such as protein-ligand and protein-protein interactions, protein folding, homology refinements, computational protein design, and ion permeation cross the membranes (Lindahl and Sansom 2008, Raval, Piana et al. 2012, Adiban, Jamali et al. 2016, Jalily Hasani, Ahmed et al. 2017).

To run a classical MD simulation, several basic steps need to be followed. The first step is to choose a force field and MD tools for the simulation. Each of the force field and MD tools have their specific area, which has been optimized for the area. The second step is to prepare the simulation system. For example, the protein or complex can be download from different database. These molecules may need to be solvent and ionized in vacuum, liquid, or membrane, which depends on the purpose of the simulation. The following step is performing energy minimization on built system. The ideal outcome from an energy minimization is an optimized arrangement of the atoms that possess a local minimum or less frequently a global minimum. Equilibration step is bringing equilibrium to the system. During this step, it is necessary to adjust the temperature of the system and to raise it to the desired range. This step can be divided into two major phases, which are the "isothermal-isochoric" NVT and the "isothermal-isobaric" NPT. Large conformational changes are expected to be observed in these two phases. The final MD phases is called the production. The equilibrated system is applied to simulate atomic movements, vibrations and interactions based on the force field. During MD simulation, quite different molecular conformations of the system are sampled. The output of a production run is a trajectory file that records the positions and relevant information about the system at each time step. Ideally, clustering this trajectory can provide us with multiple conformations. These conformations have been widely used to analyze and interpret the complex experiments and/or systems at a spatial resolution

B.2.1 Limitations of Classical MD

In many cases and depending on the plasticity of the target, most of protein conformations will not be observed in a short MD simulation time. For example, Susanne et al. identified transient conformation of the protein after 10 ns of MD simulation (Eyrisch and Helms 2007). However, in

most cases, conventional MD simulations cannot access these conformations and a significantly long MD simulation may be required to sample the conformational space of the target. This is mainly due to the entrapment of the protein structure in a local minimum within the energy surface and not being able to cross the high-energy barriers separating these minima (as fig.A.3.2) (Ortiz-Sanchez, Nichols et al. 2012).

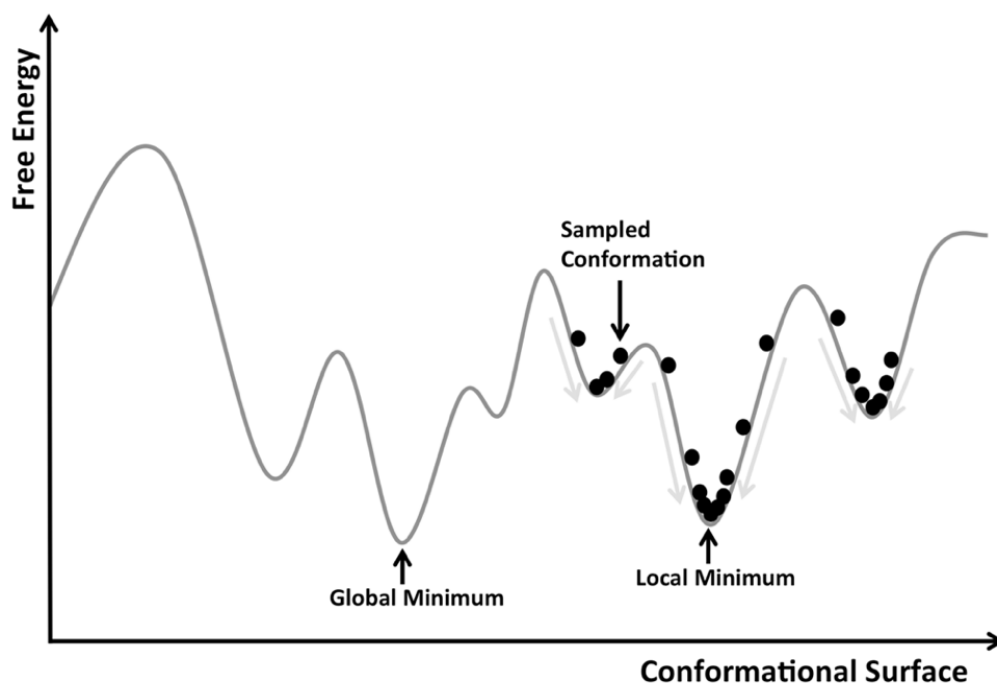


Figure. B.2.1. The free-energy surface of protein. During the MD simulation, conformations of targeted protein are sampled. The local and global minimums are separated by energy barriers.

The conformations may gather around local minimums and cannot reach global minimum, which leads to the insufficient sampling. Insufficient sampling has often been a limitation for the applicability of MD to different problems. This limitation is due to rough energy landscapes, with many local minimums separated by high-energy barriers, which govern the biomolecular motion. The sampling problem mainly refers to the fact that MD simulation does not cover all the relevant conformational states. As a result, the dynamics and function of the molecule of interest cannot be

meaningfully characterized. For example, the huge conformational changes or transitions of proteins, which are substantial to their function, may not be completely captured by classical MD simulations. Another example is transport through membrane proteins, channels and transporters that have to undergo large conformational changes to allow the influx or efflux of substances. These intricate and time-consuming processes are beyond the ability of straightforward MD simulations and enhanced sampling algorithms are needed.

B.3 Enhanced MD Simulations

Several methods have been developed to address the sampling problem and to explore events that occur on timescales, inaccessible to classical all-atom MD simulation (Ganesan, Coote et al. 2017). These include metadynamics, external electric field molecular dynamics (EEMD) (Adiban, Jamali et al. 2018, Feng, Kalyaanamoorthy et al. 2019), steered molecular dynamics (SMD) (Jalily Hasani, Ahmed et al. 2017, Feng, Kalyaanamoorthy et al. 2019), umbrella sampling and adaptive bias force steering (ABFS) (Abrams & Bussi, 2014). Here we present a brief overview of the EEMD and SMD technique, which is one of the tools employed in this thesis.

B.3.1 External Electric Field MD Simulations

Selective and controlled transport of water and ions across the cellular membrane is essential for the survival of cells and multicellular organisms. Transport of ions through membrane channels play fundamental roles in biological processes such as cell volume regulation and neuronal signalling. For instance, the action of voltage-gated ion channel relies on the membrane potential changes. The external electric field will induce a voltage across a pore-containing membrane system. This system performs classical MD simulation and equilibrates into the condition under the specific membrane potential. The method shifts the protein into the stable conformation with

the help of transmembrane potential. These conformational changes determine the ion permeation and the electrostatic properties of membrane channels.

B.3.2 Steered MD Simulations

Steered MD (SMD) simulation is another MD technique as an enhanced sampling method. It has been widely used to facilitate the phenomena related to association and disassociation of ligands to or from proteins. During the pulling, the SMD can reveal the conformational changes of biomolecules, which cannot be achieved by classical MD simulation. (Ahmed, Jalily Hasani et al. 2017, Jalily Hasani, Ahmed et al. 2017). The method is basically performing a time-dependent biased force on a selected atom, such as ion or dummy atom, to mimic its permeation. For example, SMD techniques are applied to investigate the ion permeation of the channel (Feng, Kalyaanamoorthy et al. 2019).

In general, there are two types of SMD, the constant-force SMD and the constant-velocity SMD. In the constant-force SMD, the atom is pulled with a constant amount of force. The constant-velocity SMD simulation involves pulling of the selected atom or groups of atoms at a constant velocity. The amount of force or the velocity employed depends on the type of property being studied as well as the stability of the system. The force applied on the atom is then recorded, allowing one to estimate the potential of mean force (PMF), which composed the force profile (MacKerell, Bashford et al. 1998, Adiban, Jamali et al. 2016, Ganesan, Coote et al. 2017). The force profile can indicate and locate the key residues, essential interactions, and binding sites during the SMD simulation.

B.4 References

- [1] MacKerell, A.D., et al., *All-atom empirical potential for molecular modeling and dynamics studies of proteins*. Journal of Physical Chemistry B, 1998. **102**(18): p. 3586-3616.
- [2] Huang, J. and A.D. MacKerell, Jr., *CHARMM36 all-atom additive protein force field: validation based on comparison to NMR data*. J Comput Chem, 2013. **34**(25): p. 2135-45 DOI: 10.1002/jcc.23354.
- [3] Jorgensen, W.L., D.S. Maxwell, and J. TiradoRives, *Development and testing of the OPLS all-atom force field on conformational energetics and properties of organic liquids*. Journal of the American Chemical Society, 1996. **118**(45): p. 11225-11236 DOI: DOI 10.1021/ja9621760.
- [4] Xu, L., et al., *Binding mechanisms of 1,4-dihydropyridine derivatives to L-type calcium channel Cav1.2: a molecular modeling study*. Mol Biosyst, 2016. **12**(2): p. 379-90 DOI: 10.1039/c5mb00781j.
- [5] Schmidtke, P., et al., *MDpocket: open-source cavity detection and characterization on molecular dynamics trajectories*. Bioinformatics, 2011. **27**(23): p. 3276-85 DOI: 10.1093/bioinformatics/btr550.
- [6] Grove, L.E., et al., *FTFlex: accounting for binding site flexibility to improve fragment-based identification of druggable hot spots*. Bioinformatics, 2013. **29**(9): p. 1218-9 DOI: 10.1093/bioinformatics/btt102.
- [7] Roux, B. and K. Schulten, *Computational studies of membrane channels*. Structure, 2004. **12**(8): p. 1343-51 DOI: 10.1016/j.str.2004.06.013.
- [8] Lindahl, E. and M.S. Sansom, *Membrane proteins: molecular dynamics simulations*. Curr Opin Struct Biol, 2008. **18**(4): p. 425-31 DOI: 10.1016/j.sbi.2008.02.003.
- [9] Jalily Hasani, H., M. Ahmed, and K. Barakat, *A comprehensive structural model for the human KCNQ1/KCNE1 ion channel*. J Mol Graph Model, 2017. **78**: p. 26-47 DOI: 10.1016/j.jmgm.2017.09.019.
- [10] Raval, A., et al., *Refinement of protein structure homology models via long, all-atom molecular dynamics simulations*. Proteins, 2012. **80**(8): p. 2071-9 DOI: 10.1002/prot.24098.
- [11] Adiban, J., Y. Jamali, and H. Rafii-Tabar, *Modeling ion permeation through a bacterial voltage-gated calcium channel CaVAb using molecular dynamics simulations*. Mol Biosyst, 2016. **13**(1): p. 208-214 DOI: 10.1039/c6mb00690f.
- [12] Eyrisch, S. and V. Helms, *Transient pockets on protein surfaces involved in protein-protein interaction*. J Med Chem, 2007. **50**(15): p. 3457-64 DOI: 10.1021/jm070095g.
- [13] Ortiz-Sanchez, J.M., et al., *Identification of potential small molecule binding pockets on Rho family GTPases*. PLoS One, 2012. **7**(7): p. e40809 DOI: 10.1371/journal.pone.0040809.
- [14] Ganesan, A., M.L. Coote, and K. Barakat, *Molecular dynamics-driven drug discovery: leaping forward with confidence*. Drug Discovery Today, 2017. **22**(2): p. 249-269 DOI: 10.1016/j.drudis.2016.11.001.
- [15] Feng, T., et al., *Atomistic modeling and molecular dynamics analysis of human CaV1.2 channel using external electric field and ion pulling simulations*. Biochim Biophys Acta Gen Subj, 2019. **1863**(6): p. 1116-1126 DOI: 10.1016/j.bbagen.2019.04.006.
- [16] Adiban, J., Y. Jamali, and H. Rafii-Tabar, *Simulation of the effect of an external GHz electric field on the potential energy profile of Ca(2+) ions in the selectivity filter of the CaV Ab channel*. Proteins, 2018. **86**(4): p. 414-422 DOI: 10.1002/prot.25456.

- [17] Ahmed, M., et al., *Modeling the human Nav1.5 sodium channel: structural and mechanistic insights of ion permeation and drug blockade*. *Drug Des Devel Ther*, 2017. **11**: p. 2301-2324 DOI: 10.2147/DDDT.S133944.
- [18] Ganesan, A., M.L. Coote, and K. Barakat, *Molecular dynamics-driven drug discovery: leaping forward with confidence*. *Drug Discov Today*, 2017. **22**(2): p. 249-269 DOI: 10.1016/j.drudis.2016.11.001.